

Investigations into Glass Additive Manufacturing by Selective Laser Melting and Directed Energy Deposition

By

Fiona Spirrett

Thesis

Submitted to the University of Nottingham

for the degree of

Doctor of Philosophy

Department of Engineering

Centre for Additive Manufacturing

2021

Abstract

Glass is a desirable material for many industrial applications, offering unique properties such as transparency, chemical durability, and high thermal resistance. Current production of complex glass shapes is typically achieved through the use of moulds. Customisation of glass geometries therefore often increases the production cost of bespoke glass pieces. Additive Manufacturing methods are capable of fabricating complex geometries at efficient cost for small production volumes, making customisation cost-effective. The opportunities that AM presents for glass manufacturing could be exploited for a number of applications, including fabrication of customised microfluidic devices, and bespoke décor for high value glass packaging. The potential applications for additively manufactured glass parts have driven research and industry to face the associated challenges, such as thermal stresses from high temperature gradients causing parts to crack or fracture, high transmittance in the near-infrared (NIR) range reducing laser absorption at certain wavelengths, and porosities and cracking compromising transparency.

In this thesis, research into glass processing by two AM techniques is presented: Selective Laser Melting (SLM), and powder-fed Directed Energy Deposition (DED). Investigations were carried out to define suitable processing parameters for SLM and DED of a common glass composition, soda lime silica. Investigations evaluated the effect of laser parameters and processing set ups on glass processing.

For SLM, soda lime silica was processed onto two substrates: soda lime silica glass and alumina. Different geometries were fabricated, including single walls, cubes, hollow cylinders, lattices, and text structures. Channel structures were fabricated to demonstrate the potential for customised glass continuous flow reactor (CFR) production by SLM. For on-glass processing, adhesion of parts to substrates was inspected, highlighting the impact of SLM processing on crack formation in glass substrates for the first time. The effect of substrate heating on glass SLM was also investigated, showing promising results on transparency and porosity in glass SLM. For applications requiring removal of parts from substrates, alumina discs provided suitable adhesion to glass powders during processing, and easy removal of parts post process. Energy densities between 80-110 J/mm³ are recommended for processing 3D structures on alumina substrates, and for on-glass processing energy densities above 28 J/mm² were found necessary to achieve glass consolidation.

Novel glass processing by a powder-fed DED method is presented in this work, demonstrating customisation of glass bottle packaging. Process maps are presented for powder-fed DED of soda lime silica glass onto glass substrates for the first time, evaluating the effect of laser power and scan speed on glass powder consolidation and substrate cracking. Suitable processing parameters were identified, with cracking found to associate with laser power, and consolidation of glass correlating with energy density. Parameters of laser power below 115 W and energy density above 11 J/mm² are recommended. Challenges including the transmission of laser energy through transparent feedstocks and substrates and delivery of glass powder through nozzle systems were evaluated and overcome. Darkened base plates are recommended below transparent substrates to reduce laser reflection, and a single layer of cellophane tape was used to improve glass melting and adhesion to substrates by acting as a heat source during processing.

Also highlighted in this research was the flowability of glass powder feedstocks for AM methods, and the effect of flowability on forming homogenous powder beds for SLM and achieving consistent powder delivery for DED. A case study on glass powder spheroidisation is presented, comparing methods of altering angular glass powder morphologies for improved flowability. Flame spheroidisation and plasma spheroidisation are presented as promising techniques for improving flowability of glass materials for AM, and their limitations are evaluated.

The work done during the course of this PhD contributes to understanding of glass processing by SLM and through powder-fed DED, demonstrating the potential for glass processing by these AM methods. Recommendations are made for future work to further develop these methods of glass processing, with the hopes of establishing AM as a valid technique for forming customised, complex geometries for high value applications.

Acknowledgements

I would like to thank Prof. Ruth Goodridge, my supervisor and role model, for being a source of encouragement and inspiration in a technical field dominated by men. I would also like to thank my supervisor Prof. Ian Ashcroft, for his patience and guidance whilst also pushing me out of my comfort zone. I consider myself lucky to have a supervision team with such an incredible wealth of knowledge and expertise.

I would like to thank Dr Kyriaki Datsiou and Dr Ehab Saleh for supporting my experimental research. Thanks to my wonderful sponsors at GTS: Marlin Magallanes, Chris Holcroft, Dave Eustice, and Rob Ireson. I am also grateful to Martyn Marshall and Paul Sharp for their technical support during my industrial placement.

To all of the technicians that worked by my side over the years, thank you for your support. Special thanks to Mark Hardy and Mark East in CfAM, and Stuart Branston and Alexander Jackson-Crisp in Engineering. Your contribution to my PhD is not insignificant.

Thanks to my parents, Wendy and Andy, and my sister, Caroline, for encouraging me and supporting me unconditionally. You nurtured my curiosity and inspired me to learn. I would not be who I am today if not for your love and support. To my husband, Declan, who knows more about my research than he ever wished to, thank you for always believing in me.

My thanks to everyone in the Centre for Additive Manufacturing at the University of Nottingham, for creating a wonderful environment for research and collaboration. I would like to thank the EPSRC and Glass Technology Services Ltd for funding this research.

Publications

Powder-Fed Directed Energy Deposition of Soda Lime Silica Glass on Glass Substrates -
(Submitted to Journal of the American Ceramic Society, Under Review)

Fiona Spirrett¹, Kyriaki Corinna Datsiou¹, Marlin Magallanes², Ian Ashcroft¹, Ruth Goodridge¹

Laser Powder Bed Fusion of Soda Lime Silica Glass: Optimisation of Processing Parameters and Evaluation of Part Properties – Additive Manufacturing, 2021

K.C. Datsiou¹, F. Spirrett¹, I. Ashcroft¹, M. Magallanes², S. Christie³, R. Goodridge¹

Additive Manufacturing of Glass with Laser Powder Bed Fusion - Journal of the American Ceramic Society, 2019

Kyriaki Corinna Datsiou¹, Ehab Saleh¹, Fiona Spirrett¹, Ruth Goodridge¹, Ian Ashcroft¹, Dave Eustice²

Optimising Thermoplastic Polyurethane for Desktop Laser Sintering – Proceedings of the 28th Annual International Solid Freeform Fabrication Symposium, 2017

I. P. F. Richards, T. M. N. Garabet, I. S. Bitar, F. M. Salmon

Conference Presentation

Glass Material for Directed Energy Deposition (DED) – 43rd International Conference and Exposition on Advanced Ceramics and Composites, 2019

Paper in Preparation

Selective Laser Melting of Soda Lime Silica Glass onto a Glass Substrate

Fiona Spirrett¹, Kyriaki Datsiou¹, Ehab Saleh¹, Ruth Goodridge¹, Ian Ashcroft¹, Dave Eustice²

¹ Centre for Additive Manufacturing, University of Nottingham, UK

² Glass Technology Services, Sheffield, UK

³ School of Chemistry, Loughborough University, UK

Table of Contents

ABSTRACT	I
ACKNOWLEDGEMENTS	III
PUBLICATIONS	IV
LIST OF FIGURES	IX
LIST OF TABLES	XV
ABBREVIATIONS	XVI
CHAPTER 1: INTRODUCTION	1
1.1 GLASS	1
1.2 ADDITIVE MANUFACTURING	3
CHAPTER 2: LITERATURE REVIEW	7
2.1 BACKGROUND INFORMATION: GLASS MATERIALS	7
2.1.1 <i>Glass Compositions</i>	12
2.2 CURRENT STATE OF THE ART IN GLASS ADDITIVE MANUFACTURING	15
2.3 MATERIAL EXTRUSION	16
2.4 VAT PHOTOPOLYMERISATION	21
2.5 POWDER BED FUSION	24
2.5.1 <i>Laser Sintering</i>	24
2.5.2 <i>Selective Laser Melting</i>	28
2.6 DIRECTED ENERGY DEPOSITION	38
2.6.1 <i>State of the Art in Glass DED</i>	40
2.7 CONSIDERATIONS FOR GLASS POWDER PROCESSING BY AM	45
2.8 SUMMARY	53
CHAPTER 3: AIMS & OBJECTIVES, AND RESEARCH METHODOLOGY	56
3.1 INTRODUCTION	56
3.2 GAP IN THE RESEARCH	59
3.3 AIM AND OBJECTIVES	63
3.4 RESEARCH METHODOLOGY	64
CHAPTER 4. EXPERIMENTAL MATERIALS AND PROCEDURES	66
4.1 INTRODUCTION	66
4.1.1 <i>Materials for SLM</i>	67
4.1.2 <i>Materials for DED</i>	68
4.2 FEEDSTOCK PRODUCTION	69
4.2.1 <i>Glass Fibres</i>	69
4.2.2 <i>Glass Powder Preparation</i>	69

4.3	MATERIAL CHARACTERISATION	71
4.3.1	<i>Composition Analysis</i>	71
4.3.2	<i>Morphology</i>	72
4.3.3	<i>Particle Size Analysis</i>	75
4.3.4	<i>Powder Flowability</i>	77
4.3.5	<i>Other Characterisation Methods</i>	83
4.4	CASE STUDY: GLASS FLOWABILITY	89
4.4.1	<i>Powder Rheology</i>	89
4.4.2	<i>Observation of Sample Spreading for Powder Bed Formation</i>	92
4.5	CASE STUDY: POWDER SPHEROIDISATION	94
4.5.1	<i>Flame Spheroidisation</i>	94
4.5.2	<i>Plasma Spheroidisation</i>	98
4.5.3	<i>Electron Beam Irradiation</i>	100
4.6	CONCLUSIONS	102
CHAPTER 5: SELECTIVE LASER MELTING OF GLASS		104
5.1	INTRODUCTION	104
5.1.1	<i>Experimental Set-Up</i>	105
5.1.2	<i>Substrates</i>	105
5.1.3	<i>Glass Powder Feedstocks</i>	106
5.1.4	<i>Evaluation of Processing Parameters</i>	107
5.2	PROCESS PARAMETER INVESTIGATION	108
5.2.1	<i>Energy Density</i>	108
5.2.2	<i>Hatch Spacing</i>	109
5.2.3	<i>Scanning Strategy</i>	109
5.2.4	<i>Layer Delay</i>	110
5.2.5	<i>Design Geometry</i>	110
5.3	PROCESSING GLASS ONTO ALUMINA SUBSTRATES	112
5.3.1	<i>Process Maps</i>	112
5.3.2	<i>Catalysts</i>	113
5.3.3	<i>Glass Continuous Flow Reactor Channels</i>	114
5.3.4	<i>Discussion</i>	115
5.4	EXPERIMENTAL RESULTS	119
5.4.1	<i>Energy Density</i>	119
5.4.2	<i>Hatch Spacing and Scanning Strategy</i>	123
5.5	CASE STUDY: SLM MACHINE MODIFICATION – MICROHEATER	135
5.5.1	<i>Introduction</i>	135
5.5.2	<i>Bench Testing</i>	136

5.5.3	<i>Installation</i>	137
5.5.4	<i>Experimental Description and Results</i>	139
5.5.5	<i>Discussion</i>	141
5.6	SLM DISCUSSION AND CONCLUSIONS	144
CHAPTER 6: DIRECTED ENERGY DEPOSITION OF GLASS		147
6.1	INTRODUCTION	147
6.2	DED PROCESSING SYSTEM	148
6.3	INVESTIGATING THE FEASIBILITY OF GLASS PROCESSING BY DED	150
6.3.1	<i>Introduction</i>	150
6.3.2	<i>Methods</i>	150
6.3.3	<i>Powder Study 1: Feasibility of Processing Different Glass Compositions</i>	151
6.3.4	<i>Powder Study 2: Effect of Powder Bed Thickness</i>	152
6.3.5	<i>Powder Study 3: Feasibility of Fusing Glass Powder to Glass Substrates</i>	153
6.3.6	<i>Feasibility of Glass Fibre Processing</i>	153
6.3.7	<i>Results</i>	155
6.3.8	<i>Discussion and Conclusions for Feasibility Studies</i>	162
6.4	ADAPTATION OF MACHINE SET-UP	164
6.4.1	<i>Introduction</i>	164
6.4.2	<i>Investigation of Powder Feedstock Delivery</i>	164
6.4.3	<i>The Importance of Substrates and Baseplates</i>	165
6.4.4	<i>Investigation of Experimental Variables</i>	167
6.5	OPTIMISATION OF DED PROCESS PARAMETERS	169
6.6	EXPERIMENTAL RESULTS	172
6.6.1	<i>Measurement of Feedstock Delivery Rate</i>	172
6.6.2	<i>Experimental Variables</i>	177
6.6.3	<i>Laser Processing Parameters for Glass DED</i>	181
6.6.4	<i>The Effect of Scan Design on Glass DED</i>	183
6.7	DISCUSSION AND CONCLUSIONS FOR DED INVESTIGATIONS OF GLASS PROCESSING	192
6.7.1	<i>Experimental Results</i>	192
6.7.2	<i>DED Set-Up and System</i>	194
6.7.3	<i>Conclusions</i>	196
CHAPTER 7: GENERAL DISCUSSION AND CONCLUSIONS		197
7.1	INTRODUCTION	197
7.2	EVALUATION OF GLASS PROCESSING BY SLM	198
7.3	EVALUATION OF GLASS PROCESSING BY POWDER-FED DED	201
7.4	SLM VS DED FOR GLASS PROCESSING	204
7.5	ENERGY DENSITY AS A MEASUREMENT FOR SLM AND DED	207

7.6	CONCLUSIONS	209
CHAPTER 8: RECOMMENDATIONS FOR FUTURE WORK		211
8.1	RECOMMENDATIONS FOR SLM OF GLASS	212
8.2	RECOMMENDATIONS FOR POWDER-FED DED OF GLASS	214
8.3	ADDITIONAL RECOMMENDATIONS	216
8.4	SUMMARY	218
REFERENCES		219
APPENDIX		233

List of Figures

FIGURE 1 GLASS MANUFACTURING PROCESSES IN INDUSTRY. LEFT: GLASS BLOWING. IMAGE SOURCE: CORNING MUSEUM OF GLASS ¹¹ . RIGHT: THE FLOAT GLASS PROCESS. IMAGE SOURCE: PILKINGTON ¹²	2
FIGURE 2 A: SiO ₄ TETRAHEDRAL UNIT. B: SCHEMATIC OF THE STRUCTURE OF A QUARTZ CRYSTAL, SHOWING A REGULAR REPEATING PATTERN OF SiO ₄ TETRAHEDRA. C: SCHEMATIC OF THE AMORPHOUS QUARTZ GLASS, SHOWING A RANDOM NETWORK OF SiO ₄ TETRAHEDRA. D: SCHEMATIC OF THE RANDOM ARRANGEMENT OF ATOMS IN A SODIUM SILICATE GLASS, WHERE Na ⁺ CATIONS BREAK UP BRIDGING Si-O-Si BONDS AND OCCUPY THE AVAILABLE SPACE.....	8
FIGURE 3 VOLUME/TEMPERATURE DIAGRAM FOR CRYSTALLISATION AND GLASS FORMATION. THE CURVE SHOWS THE TRANSFORMATION OF A LIQUID TO A CRYSTAL AT T _M DURING CRYSTALLISATION. THE LIQUID MAY ALSO TRANSFORM INTO A SUPERCOOLED MELT UNDER RAPID COOLING, WITH A GRADUAL DECREASE IN VOLUME TO THE GLASS TRANSFORMATION RANGE. THE INTERSECTION BETWEEN THE SUPERCOOLED LIQUID AND GLASS STATE CURVE INDICATED THE GLASS TRANSITION TEMPERATURE (T _G). THE MATERIAL SOLIDIFIES TO A GLASS BELOW THE T _G ON FURTHER COOLING.	9
FIGURE 4 ABSORPTION OF DIFFERENT MATERIALS AS A FUNCTION OF THE WAVELENGTH. GLASS SHOWS GREATER ABSORPTION IN THE ULTRAVIOLET AND LONG WAVE IR REGIONS, WITH LOW ABSORPTION AT NEAR IR WAVELENGTHS ⁴²	12
FIGURE 5 PERCENTAGE TRANSMISSION IN THE 0-5 μM WAVELENGTH REGION OF LEFT: BASE GLASS (SODA LIME SILICA), AND RIGHT: THE BASE GLASS DOPED WITH COBALT. AN ABSORPTION PEAK IS SEEN BETWEEN 1-2 μM WAVELENGTH IN THE CO DOPED GLASS ⁴⁴	12
FIGURE 6 BESPOKE FDM SET-UP FOR EXTRUSION OF MOLTEN SODA LIME SILICA GLASS. 1: CRUCIBLE, 2: HEATING ELEMENTS, 3: NOZZLE, 4: THERMOCOUPLE, 5: FEED ACCESS LID, 6: STEPPER MOTORS, 7: PRINTER FRAME, 8: PRINT ANNEALER, 9: CERAMIC PRINT PLATE, 10: Z-DRIVE TRAIN, 11: CERAMIC VIEWING WINDOW, 12: INSULATING SKIRT. ^{58,59}	16
FIGURE 7 GLASS OBJECTS PRESENTED BY KLEIN ET AL. ⁵⁸ LEFT: A COLOURED GLASS OBJECT FABRICATED BY MATERIAL EXTRUSION, WITH VISIBLY DISCERNIBLE LAYERS. RIGHT: A CLEAR GLASS FABRICATED PART DEMONSTRATING OPTICAL TRANSPARENCY.	17
FIGURE 8 A: MATERIAL EXTRUSION SET-UP USED TO PROCESS As ₄₀ S ₆₀ CHALCOGENIDE GLASS FILAMENTS, B-C: PROCESSED CHALCOGENIDE GLASS STRUCTURES WITH VISIBLY DISCERNIBLE LAYERS, AND A YELLOW COLOUR FROM SULPHIDE VAPOUR ⁶¹	19
FIGURE 9 EXAMPLES OF GLASS PARTS PRODUCED BY DIRECT INK WRITING. LEFT: HOLLOW GLASS CYLINDER OF 20WT% SILICA INK FILLED WITH LIQUID ⁶² RIGHT: EXAMPLE OF SILICA-TITANIA GLASS OPTICS WITH GRADIENT REFRACTIVE INDEX ⁶³	20
FIGURE 10 EXAMPLES OF STRUCTURES FABRICATED BY STEREO LITHOGRAPHY LEFT: 45S5 BIOACTIVE GLASS FABRICATED IN A SCAFFOLD GEOMETRY ⁶⁸ . RIGHT: WDE GLASS CERAMIC SCAFFOLD FABRICATED BY DLP AND HEAT TREATED AT 90°C ⁷⁰	21
FIGURE 11 INVESTIGATION OF GLASS PROCESSING BY KOTZ ET AL A: FUSED SILICA GLASS PART FABRICATED BY SLA ⁷³ . B: FUSED SILICA GLASS MICROFLUIDIC CHIP FABRICATED BY "LIQGLASS" LITHOGRAPHY. ⁵ C: FUSED SILICA GLASS MICROFLUIDIC SPIRAL CHANNELS FABRICATED BY SACRIFICIAL TEMPLATE REPLICATION ⁷⁴ . D: FUSED SILICA GLASS LENS FABRICATED BY TWO-PHOTON POLYMERISATION ⁷⁵	22
FIGURE 12 LEFT: FABRICATED "GREEN PART" SCAFFOLDS OF 13-93 BIOACTIVE GLASS WITH VARIOUS GEOMETRIES ⁸⁷ . RIGHT: SCAFFOLD ARCHITECTURES OF 13-93B3 BIOACTIVE GLASS ⁹²	26
FIGURE 13 LASER SINTERING OF BOROSILICATE GLASS BY KLOCKE ET AL. WITH LASER POWER INCREASING FROM LEFT TO RIGHT, WITH VISIBLE CRACKS AND ROUGH SURFACE ⁹⁴	27

FIGURE 14 SCHEMATIC OF A TYPICAL SLM/LPBF PROCESS ¹⁰¹ AND TYPICAL BUILD CHAMBER ¹⁰⁰ . A ROLLER OR WIPER MAY BE USED TO SPREAD POWDER ACROSS A BUILD PLATFORM.	29
FIGURE 15 EXAMPLES OF SLM SCAN STRATEGIES (A: UNIDIRECTIONAL SCAN, B: BI-DIRECTIONAL SCAN, C: ISLAND SCAN, D: HELIX SCAN) ¹⁰⁷ AND HATCH ROTATIONS (E: 90° ROTATION, F: 45° ROTATION, G: 67° ROTATION) ¹⁰⁵	30
FIGURE 16 INVESTIGATIONS INTO SLM OF SODA LIME GLASS BY FATERI ET AL. ^{130,132} A: A DOME GEOMETRY, B: TOOTH PROTOTYPE, C: THE EFFECT OF SCAN STRATEGY ON GLASS PART APPEARANCE, LEFT: "LINE", RIGHT: "CHECKERBOARD"	34
FIGURE 17 SLM PROCESSING OF SPODUMENE GLASS CERAMIC USING A: 50 μM LAYER THICKNESS, B: 100 μM LAYER THICKNESS, AND C: 150 μM LAYER THICKNESS. THE APPEARANCE OF THE TOP SURFACE OF PARTS SHOWS VARIATION IN TRANSPARENCY/APPEARANCE ¹⁴¹	36
FIGURE 18 EXAMPLES OF COMPLEX GEOMETRIES FABRICATED BY SLM OF A TI-BASED BULK METALLIC GLASS. PARTS WERE REPORTED TO BE FULLY GLASSY AND RELATIVELY SMOOTH.	37
FIGURE 19 SCHEMATIC OF THE DED PROCESS (FOR POWDER FEEDSTOCK) ¹⁴⁶	38
FIGURE 20 SCHEMATIC OF TWO POWDER DELIVERY NOZZLES FOR DED PROCESSING. A: COAXIAL NOZZLE, INDICATING THE STREAM OF POWDER DELIVERED THROUGH AN ANNULAR ORIFICE, COMPRESSED BY SHIELDING GAS. B: SINGLE NOZZLE FOR POWDER DELIVERY LATERALLY TO THE LASER BEAM. TAKEN FROM GIBSON, ROSEN AND STUCKER ¹⁵	40
FIGURE 21 GLASS PROCESSING BY FILAMENT-FED DED A: CONVEX SODA LIME GLASS PART ¹⁵⁶ . B: 20 MM DIAMETER HOLLOW CYLINDER OF QUARTZ GLASS ¹⁶⁰ . C: GLASS WALL BEFORE POST-PROCESS HEAT TREATMENT AND D: GLASS WALL AFTER POST PROCESS HEAT TREATMENT SHOWING REDUCTION IN RESIDUAL STRESSES ¹⁵⁷	43
FIGURE 22 A: DOWNWARD MOTION OF FT4 BLADE TO MEASURE BFE. B: UPWARD MOTION OF BLADE TO MEASURE SE.	47
FIGURE 23 SEM IMAGE OF A TYPICAL ANGULAR/IRREGULAR MORPHOLOGY OF A BALL MILLED PHOSPHATE GLASS POWDER ¹⁷⁶	48
FIGURE 24 A: SCHEMATIC OF THE FLAME SPHEROIDISATION PROCESS. B: SCHEMATIC OF THE PLASMA SPHEROIDISATION PROCESS ¹⁸⁵	49
FIGURE 25 TRANSMITTANCE SPECTRUM FOR 200 μM GLASS, HIGHLIGHTED AT CO LASER AND CO ₂ LASER WAVELENGTHS. AN INCREASE IN TRANSMITTANCE IS SEEN AT CO LASER WAVELENGTH (5.65 μM), COMPARED TO CO ₂ LASER WAVELENGTHS (9.34-11.15 μM) ¹⁹⁰	50
FIGURE 26 TRANSMISSION SPECTRA FOR A: A TYPICAL SODA LIME SILICA COMPOSITION ¹⁹¹ , B: A COMMERCIALY AVAILABLE SCHOTT BOROFLOAT® 33 COMPOSITION AT DIFFERENT GLASS THICKNESSES ¹⁹² , AND C: A CLEAN AND DOPED BIOACTIVE GLASS (45S5) COMPOSITION ¹⁹⁴	52
FIGURE 27 A-B EXAMPLE MICROFLUIDIC REACTOR DESIGN. ²⁰² EXAMPLES OF GLASS DÉCOR BY C: EMBOSsing AND D: ENGRAVING.	57
FIGURE 28 ADDITIVELY MANUFACTURED CFR STRUCTURES. A: FUSED DEPOSITION MODELLING (FDM, MATERIAL EXTRUSION) SPLIT-AND-RECOMBINE MIXER ²⁰³ , B: SLA SPLIT-AND-RECOMBINE MIXER ²⁰³ , AND C: LPBF STAINLESS STEEL REACTOR ²⁰⁰	61
FIGURE 29 RESEARCH FRAMEWORK FOR INVESTIGATING THE EFFECT OF AM PROCESS PARAMETERS ON GLASS MATERIALS, AND ULTIMATELY DEFINING PROCESSING WINDOWS FOR DED AND SLM OF GLASS.	64
FIGURE 30 OPTICAL MICROSCOPY OF DRAWN GLASS FIBRES (SLSG-FIBRE). A BUNDLE OF FIBRE ENDS (LEFT) AND A SINGLE FIBRE AT 5X MAGNIFICATION (RIGHT).	69
FIGURE 31 IMAGE OF Poured BULK GLASS (LEFT) AND MILLED AND SIEVED POWDER (RIGHT).	70
FIGURE 32 SEM IMAGES OF SEVERAL GLASS POWDER SAMPLES. A-F = GTS-1 - GTS-6 RESPECTIVELY. G: HIGHER MAGNIFICATION OF GTS-6 TO SHOW ANGULAR PARTICLES AND IRREGULARITIES.	74
FIGURE 33 PARTICLE SIZE ANALYSIS OF SPHERICAL SODA LIME SILICA GLASS POWDERS - GTS-1, GTS-2, AND GTS-6.	75

FIGURE 34 PARTICLE SIZE ANALYSIS OF ORIGINAL GLASS SAMPLES (GTS-1 - GTS-6), AN ANGULAR, DOPED SODA LIME SILICA (SLSG-Fe), AND SODA LIME SILICA BEADS CREATED IN A BEAD FURNACE (GTS-7).	76
FIGURE 35 FLOWABILITY BY HALL FLOW METER TESTING OF FOUR GLASS SAMPLES. A 0 MEASUREMENT INDICATES MATERIAL DID NOT FLOW THROUGH THE HALL FLOW METER NOZZLE.	78
FIGURE 36 BASIC FLOWABILITY ENERGY OF FIVE GLASS SAMPLE. SPHERICAL SODA LIME SILICA OF VARYING PARTICLE SIZE (GTS-1, GTS-2, GTS-6), AND ANGULAR BOROSILICATE (GTS-4), AS WELL AS ANGULAR SODA LIME SILICA (SLSG).	80
FIGURE 37 BFE AND FRI VALUES MEASURED FOR DIFFERENT GLASS SAMPLES.	82
FIGURE 38 SE AND FRI VALUES MEASURED FOR DIFFERENT GLASS SAMPLES.	82
FIGURE 39 DTA CURVES OF GTS-2 AND GTS-3 GLASS SAMPLES SHOWING TEMPERATURE VS HEAT FLOW.....	84
FIGURE 40 UV VIS ABSORPTION SPECTRA OF GTS-6 SODA LIME SILICA GLASS.	85
FIGURE 41 UV VIS ABSORPTION SPECTRA FOR TWO IRON DOPED SODA LIME SILICA COMPOSITIONS (SLSG-Fe AND SLSG-FEC).	86
FIGURE 42 XRD MEASUREMENT OF TWO Fe DOPED SODA LIME SILICA GLASSES, SLSG-Fe AND SLSG-FEC. BOTH GLASS COMPOSITION ARE AMORPHOUS.....	87
FIGURE 43 XRD MEASUREMENT OF VIRGIN SODA LIME SILICA GLASS (GTS-6) SHOWING NO CRYSTALLINITY.	87
FIGURE 44 SEM IMAGES VISUALISING THE DIFFERENT MORPHOLOGY MIXTURES OF SODA LIME SILICA A: ANGULAR, B: 50% BEADS, C: 100% BEADS.	89
FIGURE 45 FLOWABILITY OF SODA LIME SILICA WITH VARYING PERCENT SPHERICITY. GTS-6 "100 % BEADS", SLSG "ANGULAR" AND A MIX OF BOTH AT 50 WT% "50% BEADS". GRAPH INDICATES TEST CYCLES USED FOR EACH MEASUREMENT.	90
FIGURE 46 FLOW RATE INDEX (FRI) OF GLASS SAMPLES BY SPHERICITY. A FLOW RATE INDEX CLOSE TO UNITY REPRESENTS A LOW SENSITIVITY TO FLOW RATE.....	90
FIGURE 47 FLOWABILITY (BFE AND SE) OF SODA LIME SILICA GLASS SAMPLES: 100 % BEAD, 50% BEAD, AND ANGULAR.	91
FIGURE 48 GLASS POWDER SAMPLES AS SPREAD ON AN SLM BASE PLATE TO FORM A SINGLE LAYER POWDER BED. A: ANGULAR, B: 50% BEAD, C: 100% BEAD.	92
FIGURE 49 SEM IMAGES OF A: VIRGIN BOROSILICATE (BSG), B: PLASMA SPHEROIDISED BSG, C: VIRGIN DOPED SODA LIME SILICA (SLSG-Fe), AND D: PLASMA SPHEROIDISED SLSG-Fe.....	99
FIGURE 50 THE REALIZER SLM-50 MACHINE.	105
FIGURE 51 SCHEMATIC FOR SLM SCAN STRATEGY INVESTIGATIONS (ALTERNATING = BI-DIRECTIONAL).....	110
FIGURE 52 PROCESS MAP FOR 5 x 5 x 5 MM SODA LIME SILICA (GTS-6) CUBES FABRICATED ON CERAMIC SUBSTRATES.	113
FIGURE 53 RECTANGULAR GRID STRUCTURES FOR CATALYSIS AND SUPPORT STRUCTURES. LEFT: SEM MICROGRAPHS OF GTS-2 AND GTS-6 GRIDS. RIGHT: STRUCTURED CATALYSTS.	114
FIGURE 54 EXAMPLES OF CHANNEL STRUCTURES FABRICATED BY SLM A: CHANNELS ON CERAMIC SUBSTRATE WITH SUPPORT STRUCTURES, B: 2 MM DIAMETER LINEAR CHANNEL, C: 3 MM DIAMETER ANGLES CHANNEL, D: 2 MM DIAMETER U-SHAPED CHANNEL.	114
FIGURE 55 A: BEND PORTIONS OF CHANNEL STRUCTURES. B: X HATCH, C: Y HATCH, D: ALTERNATING X/Y HATCH, E: DEMONSTRATION OF CHANNEL STRUCTURE WITH MULTIPLE BENDS.	115
FIGURE 56 DEMONSTRATED GEOMETRIES FOR SLM OF SODA LIME SILICA GLASS. LEFT: LATTICE GEOMETRY. RIGHT: HOLLOW CHANNEL STRUCTURE.	117

FIGURE 57 SLM OF GTS-6 ON GLASS SUBSTRATE. ENERGY DENSITY DECREASING FRONT TO BACK, AND SCAN SPEED INCREASING LEFT TO RIGHT.	119
FIGURE 58 SEM MICROGRAPHS (x40 MAGNIFICATION) OF SLM GTS-6 ON GLASS SUBSTRATE. A: 67.5 W, 57 MM/S, B: 67.5 W, 47 MM/S, C: 67.5 W 37 MM/S, D: 75 W, 57 MM/S, E: 75 W, 47 MM/S, F: 75 W, 37 MM/S. ...	120
FIGURE 59 PROCESS MAP SHOWING SLM OF GLASS (GTS-6) AT DIFFERENT PARAMETER COMBINATIONS. EXAMPLES OF "FULL CONSOLIDATION" AND "INCOMPLETE CONSOLIDATION" HIGHLIGHTED.....	121
FIGURE 60 "3DGLASS" LOGO PROCESSED ONTO GLASS SUBSTRATES BY DIFFERENT SCAN STRATEGY OR HATCH SPACING. A: REDUCED HATCH SPACING, B: X HATCH, C: Y HATCH, D: ALTERNATING X/Y HATCH.	124
FIGURE 61 SLM MICROGRAPHS COMPARING FEATURES OF BUILT PARTS. A,C: 90° ROTATION HATCH, B,D: 67° ROTATION HATCH.....	125
FIGURE 62 CUBOID AND CYLINDER STRUCTURES ON GLASS SUBSTRATES, A: 1 x 2 x 1 MM CUBOIDS, B: 1 x 2 x 5 MM CUBOIDS, C: CYLINDERS (3 MM Ø, 2 MM Ø INTERNAL - ALTERNATING X-Y HATCH), D: CYLINDERS ALTERNATING X HATCH (3 MM Ø, 2 MM Ø INTERNAL).	126
FIGURE 63 SEM MICROGRAPHS OF A: 1 x 2 x 1 MM CUBOID ELEMENTS, AND B: 3 MM Ø CYLINDER (2 MM Ø INTERNAL) ALTERNATING X/Y HATCH (90° ROTATION).	127
FIGURE 64 CHANNEL STRUCTURES BUILT WITH 1 x 2 MM ELEMENTS ON GLASS SUBSTRATES.....	127
FIGURE 65 40X MAGNIFICATION SEM MICROGRAPHS OF CHANNEL ELEMENTS BASED ON SCANNING STRATEGY/HATCH SPACING A: 90° HATCH ROTATION, B: 67° HATCH ROTATION, C: ALTERNATING X HATCH, D: ALTERNATING Y HATCH.	128
FIGURE 66 THIN-WALLED CYLINDERS PROCESSED ON GLASS SUBSTRATES. A: TRIAL 2, B: TRIAL 3, C: TRIAL 4. HIGHLIGHTED STRUCTURES SHOWS HOLLOW CYLINDER PROCESSED USING 67° ROTATION HATCH	129
FIGURE 67 GLASS DIAMOND LATTICE PROCESSED ON A GLASS SUBSTRATE AT 87.75 J/MM ³ ENERGY DENSITY.	130
FIGURE 68 SEM IMAGE OF "3DGLASS" LOGO BUILT ON A GLASS SUBSTRATE USING X-Y ALTERNATING HATCH (90° ROTATION).....	131
FIGURE 69 A, B: 1 x 3 x 5 MM GLASS STRUCTURE (PROCESSED AT 80 W, 37 MM/S, H= 0.33 MM) REMOVED FROM GLASS SUBSTRATE. C: GLASS SUBSTRATE AFTER PART REMOVAL.	132
FIGURE 70 SEM MICROGRAPHS OF GLASS POWDER PROCESSING BY SLM A: SINGLE LAYER, B: TWO LAYERS.	133
FIGURE 71 LASER PROCESSING OF GLASS SUBSTRATE IN THE ABSENCE OF FEEDSTOCK LAYER A: PROCESSED GLASS SUBSTRATE AS SEEN B:50X MAGNIFICATION SEM, C: 100X MAGNIFICATION SEM.	133
FIGURE 72 MHI MICRO HEATER AS SUPPLIED WITH CERAMIC INSULATING DISCS.	135
FIGURE 73 BENCH TESTING OF THE SUBSTRATE HEATER (UP TO 550°C AS PROGRAMMED INTO THE HEATER CONTROLLER). THE COIL GLOWS BRIGHTLY, SUGGESTING THE ACTUAL TEMPERATURE OF THE COIL IS HIGHER THAN RECORDED BY THERMOCOUPLE.....	136
FIGURE 74 SET-UP OF MICROHEATER IN THE REALIZER SLM-50. A: POSITIONING OF HEATING ELEMENTS, B: SET UP SHOWING THERMOCOUPLE PLACEMENT C: SET-UP DURING OPERATION OF MICRO-HEATER.....	138
FIGURE 75 SINGLE LAYER SODA LIME SILICA GLASS CUBES PROCESSED BY SLM ON ALUMINA SUBSTRATE DURING HIGH TEMPERATURE SUBSTRATE HEATER TRIALS.	139
FIGURE 76 SEM MICROGRAPHS SHOWING A: SINTERING OF GLASS POWDER BED AND B: INTERFACE BETWEEN LASER PROCESSED AND UNPROCESSED GLASS POWDER DURING HIGH TEMPERATURE PROCESSING.....	140
FIGURE 77 GLASSY SLM STRUCTURES. LEFT: SLM MICROGRAPH OF SLM PROCESSED GLASS ON CERAMIC SUBSTRATE. RIGHT: OPTICAL MICROSCOPY OF SLM GLASS STRUCTURE ON CERAMIC SUBSTRATE. ARROWS INDICATE VISIBLE SCAN TRACKS.	141

FIGURE 78 LEFT: DED SCHEMATIC FOR EXPERIMENTAL SET-UP. RIGHT: EXAMPLE OF EXPERIMENTAL SET-UP A: LATERAL POWDER NOZZLE, B: LASER C: ARGON NOZZLE, D: GLASS SUBSTRATES AFFIXED TO BASE PLATE.	148
FIGURE 79 POWDER-FED DED SET-UPS LEFT: LATERAL NOZZLE, RIGHT: COAXIAL NOZZLE.	149
FIGURE 80 MACHINED ALUMINIUM BASE PLATES FOR DED FEASIBILITY STUDIES. A: 10 x 10 x 65 MM VOIDS, B: 10 x 10 x Z MM VOIDS (Z= 0.9-0.1 MM), C: 25 x 5 x 75 MM VOIDS.	151
FIGURE 81 SLSG-FIBRE PROCESSING TRIAL SET UP, WITH 1 MM WIRE FEEDER ATTACHMENT.	154
FIGURE 82 EFFECT OF ENERGY DENSITY ON DED OF SODA LIME SILICA GLASS POWDER (GTS-2). SAMPLE NUMBERS INDICATE THE PROCESS PARAMETERS DEFINED IN TABLE 1. CALCULATED ENERGY DENSITIES: 1= 30 J/MM ² , 2= 60 J/MM ² , 3= 90 J/MM ² , 4=120 J/MM ² , 5= 150 J/MM ² , 6= 180 J/MM ² , 7= 60 J/MM ² , 8= 120 J/MM ² , 9= 180 J/MM ²	155
FIGURE 83 OPTICAL MICROSCOPY OF SODA LIME SILICA (GTS-2) MELTED BY DED IRRADIATION AT 1200 W AND 400 MM/MIN.	156
FIGURE 84 FUSED SODA LIME SILICA GLASS POWDER IN POWDER BEDS OF VARYING THICKNESS (LEFT TO RIGHT: 0.1-0.9 MM).	157
FIGURE 85 FUSED SODA LIME SILICA GLASS SAMPLES PROCESSED IN POWDER BED THICKNESS OF A: 0.1 MM AND B: 0.9 MM.	158
FIGURE 86 DIMENSIONS OF FUSED SODA LIME SILICA GLASS SEGMENTS BY POWDER BED THICKNESS, WITH ERROR BARS INDICATING THE MINIMUM AND MAXIMUM MEASURED VALUES.	158
FIGURE 87 EVIDENCE OF FUSION OF SODA LIME SILICA GLASS IN A 1 MM POWDER BED ATOP A GLASS SUBSTRATE.	159
FIGURE 88 SODA LIME SILICA (GTS-2) MELTED AND DEPOSITED ONTO GLASS SUBSTRATE OF THE SAME COMPOSITION, USING PARAMETERS OF 200 W LASER POWER AND 650 MM/MIN SCAN SPEED WITH POWDER DELIVERY BY COAXIAL NOZZLE. A: TOP SURFACE OF GLASS SUBSTRATE B: BOTTOM SURFACE OF GLASS SUBSTRATE.	160
FIGURE 89 GLASS FIBRES (SLSG-FIBRE) PROCESSED ONTO A GLASS SUBSTRATE AT 150 W LASER POWER, AND 400 MM/MIN SCAN SPEED.	161
FIGURE 90 BOTTLE SUBSTRATES USED FOR INVESTIGATIONS INTO DED OF GLASS ON SUBSTRATES OF DIFFERENT THICKNESS/DIMENSIONS.	166
FIGURE 91 LASER FOCAL POSITION IN RELATION TO SUBSTRATE SURFACE AS DETERMINED BY LASER HEAD HEIGHT.	167
FIGURE 92 FOUR MAIN DESIGN GEOMETRIES SHOWING FEATURES OF INTEREST. A: SINGLE TRACKS, B: CURVED FEATURES, C: STRAIGHT FEATURES, D: COMBINATION FEATURES (TEXT).	170
FIGURE 93 AVERAGE GLASS POWDER DELIVERY (MG/S) BY COOPER SIDE NOZZLE OF SODA LIME SILICA FEEDSTOCKS OF VARYING PARTICLE SIZE DISTRIBUTION. ERROR BARS INDICATE THE MINIMUM AND MAXIMUM VALUES OF MASS DELIVERY MEASUREMENTS.	172
FIGURE 94 FEED DELIVERY RATE (MG/S) OF GTS-6 THROUGH A COPPER NOZZLE, TEFLON LINED NOZZLE, AND COAXIAL NOZZLE. ERROR BARS INDICATE THE MINIMUM AND MAXIMUM VALUES OF MASS DELIVERED.	173
FIGURE 95 PROCESSED TRACKS OF GTS-6 USING ENERGY DENSITY = 11 J/MM ² AT DIFFERENT POWDER WHEEL SPEEDS. A: 12 RPM, B: 1 RPM.	174
FIGURE 96 COMPARISON OF AVERAGE GLASS DEPOSIT HEIGHT (MM) AT 1 RPM AND 12 RPM POWDER WHEEL SPEEDS, AT 11-13 J/MM ² ENERGY DENSITY. ERROR BARS INDICATE MINIMUM AND MAXIMUM MEASURED VALUES.	175
FIGURE 97 SEM IMAGES OF DEPOSITED GLASS TRACKS AT ED= 11 J/MM ² . POWDER WHEEL SPEEDS OF A: 1 RPM, B: 12 RPM.	176
FIGURE 98 AVERAGE GLASS DEPOSIT HEIGHT BY LASER FOCAL POSITION (AT VARYING LASER POWER). SCAN SPEED = 680 MM/MIN. ERROR BARS INDICATE MINIMUM AND MAXIMUM MEASURED VALUES.	178
FIGURE 99 IMAGE SHOWING POWDER IRRADIATION AT F>0 AND F<0.	179

FIGURE 100 AVERAGE DEPOSIT HEIGHT OF 1, 2, AND 5 LAYERS OF PROCESSED SODA LIME SILICA (GTS-6) ON A GLASS MICROSCOPE SLIDE (1 MM). ERROR BARS INDICATE MINIMUM AND MAXIMUM MEASURED VALUES.	180
FIGURE 101 SEM IMAGES OF PROCESSED GLASS TRACKS ON 1 MM GLASS SUBSTRATES AT A: ROOM TEMPERATURE AND B: MODERATE HEATING (~100°C).....	181
FIGURE 102 PROCESS MAP FOR SINGLE TRACKS OF SODA LIME SILICA (GTS-6) ON A 1 MM SUBSTRATE OF THE SAME COMPOSITION. TRENDLINES DEPICT THE ENERGY DENSITY AT DIFFERENT COMBINATIONS OF LASER POWER AND SCAN SPEED.....	182
FIGURE 103 AN EXAMPLE OF A SINGLE TRACK OF PROCESSED SODA LIME SILICA (GTS-6) ON A 1 MM GLASS SUBSTRATE (ED= 11 J/MM ²).	183
FIGURE 104 XCT IMAGES OF A CROSS SECTION OF DED PROCESSED GLASS (GTS-6) ON GLASS SUBSTRATE. IMAGES SHOW CRACK FORMATION AND INTERNAL POROSITY. SAMPLE WAS PROCESSED AT 12 J/MM ² (FEED PARAMETERS: 2 RPM, 5 L/MIN).	184
FIGURE 105 XRD ANALYSIS OF DED PROCESSED GTS-6 GLASS SHOWING NO CRYSTALLINITY.	184
FIGURE 106 CURVED FEATURES DESIGN OF GTS-6 PROCESSED ONTO 1 MM GLASS SUBSTRATES AT VARYING ENERGY DENSITY. A: 8.8 J/MM ² , B: 9.24 J/MM ² , C: 9.68 J/MM ² , D: 10.12 J/MM ²	185
FIGURE 107 GTS-6 GLASS FEEDSTOCK PROCESSED ONTO A 4 MM GLASS SUBSTRATE AT 9.24 J/MM ² IN THE CURVED FEATURES DESIGN.	186
FIGURE 108 CURVED FEATURE DESIGN OF GTS-6 SUCCESSFULLY PROCESSED ONTO A GLASS BOTTLE SUBSTRATE AT 9.68 J/MM ² BY POWDER FED DED.....	186
FIGURE 109 GTS-6 GLASS PROCESSED ONTO 1 MM GLASS SUBSTRATES USING THE STRAIGHT FEATURES DESIGN AT DIFFERENT ENERGY DENSITIES A: 10.12 J/MM ² , B: 12.0 J/MM ² , C: 12.6 J/MM ² , D: 13.2 J/MM ²	188
FIGURE 110 GTS-6 FEEDSTOCK PROCESSED ONTO A 4 MM GLASS SUBSTRATE USING THE STRAIGHT FEATURES DESIGN, AT 12.6 J/MM ²	189
FIGURE 111 GTS-6 GLASS PROCESSED BY THE STRAIGHT FEATURES DESIGN ONTO A BOTTLE SUBSTRATE. ENERGY DENSITY = 13.2 J/MM ²	189
FIGURE 112 GTS-6 PROCESSED ON 1 MM SUBSTRATES BY THE COMBINED FEATURES (TEXT) DESIGN AT 100 W AND SCAN SPEEDS BETWEEN 450-650 MM/MIN.	191
FIGURE 113 TEXT FEATURES PROCESSED ON A 4 MM SUBSTRATE BETWEEN 9.2-13.3 J/MM ²	191

List of Tables

TABLE 1 SEVEN AM PROCESS CATEGORIES AS DEFINED BY ASTM, WITH EXAMPLE TECHNOLOGIES AND TYPICAL MATERIALS ^{16,21}	4
TABLE 2 COMPILED DATA FOR THE PROPERTIES OF VITREOUS SILICA, SODA LIME SILICA, BOROSILICATE (PYREX) AND 13-93 BIOACTIVE GLASS COMPOSITIONS, INCLUDING CHARACTERISTIC TEMPERATURES FOR SOFTENING, ANNEALING, AND STRAIN POINT, COEFFICIENT OF THERMAL EXPANSION, AND MECHANICAL PROPERTIES ^{30,57}	14
TABLE 3 PROCESS PARAMETERS REPORTED IN LITERATURE FOR SLM AND DED OF DIFFERENT GLASS COMPOSITIONS. ENERGY DENSITY CALCULATIONS HAVE BEEN MADE BASED ON REPORTED PARAMETERS AND THE ENERGY DENSITY EQUATIONS (1) AND (2).	46
TABLE 4 SUMMARY OF KEY POINTS FROM GLASS AM LITERATURE INCLUDING TECHNIQUE, GLASS COMPOSITIONS, APPLICATIONS, AND STRENGTHS AND WEAKNESSES.	53
TABLE 5 LIST OF GLASS MATERIALS SUPPLIED OR PRODUCED FOR THIS RESEARCH, INDICATING THE MATERIALS USED FOR CHARACTERISATION ONLY, CASE STUDIES, AND DED OR SLM EXPERIMENTAL INVESTIGATIONS.....	66
TABLE 6 GLASS MATERIALS USED IN SLM INVESTIGATIONS.	67
TABLE 7 GLASS MATERIALS USED FOR DED INVESTIGATIONS.	68
TABLE 8 GLASS COMPOSITIONS AS MEASURED BY EDX AS OXIDE WEIGHT PERCENTAGE.	71
TABLE 9 COMPARISON OF MEASURED OXIDE CONCENTRATION OF GTS-3 AND TWO Fe DOPED 13-93 GLASS COMPOSITIONS BY EDX AND XRF.	72
TABLE 10 PARTICLE SIZE ANALYSIS OF GLASS SAMPLES SHOWING PERCENTAGE VOLUME DISTRIBUTION. "SLSG" INDICATES SODA LIME SILICA COMPOSITION. "(s)" INDICATES SPHERICAL MORPHOLOGY.	76
TABLE 11 FLOWABILITY DATA FOR GLASS SAMPLES, AS MEASURED BY FT4 POWDER RHEOMETRY.	81
TABLE 12 GTS-3 POWDER PROCESSED BY FLAME SPHEROIDISATION. A: FINE PARTICLES COLLECTED IN TRAY 2, B: FINE PARTICLES COLLECTED IN TRAY 3, C: 63-136 µM PARTICLES COLLECTED IN TRAY 2, D: 63-136 µM PARTICLES COLLECTED IN TRAY 3.	96
TABLE 13 SEM MICROGRAPHS OF GLASS FEEDSTOCKS BEFORE AND AFTER ELECTRON BEAM IRRADIATION.	100
TABLE 14 SEM IMAGES OF 1 X 3 X 6 MM STRUCTURES AFTER REMOVAL FROM GLASS SUBSTRATES. IMAGES SHOW THE RESULTS OF THREE DIFFERENT SCAN STRATEGIES/HATCH (Y HATCH, ALTERNATING X/Y HATCH, AND 67° ROTATION HATCH) AT TWO DIFFERENT ENERGY DENSITIES.	123
TABLE 15 TEST MATRIX FOR INVESTIGATING PROCESSING OF THIN-WALLED CYLINDERS ON GLASS SUBSTRATES.	128
TABLE 16 PROCESS PARAMETERS FOR INVESTIGATING THE FEASIBILITY OF PROCESSING SODA LIME SILICA BEADS (GTS-2) AT VARYING LASER POWER AND SCAN SPEED.....	152
TABLE 17 PROCESS PARAMETERS FOR FEASIBILITY INVESTIGATION OF BOROSILICATE (GTS-4) AND FUSED SILICA (GTS-5) GLASS COMPOSITIONS.	152
TABLE 18 AVERAGE POWDER FEED RATE OF GTS-6 AT 2 RPM AND 4 RPM POWDER WHEEL SPEEDS.....	174
TABLE 19 RESULTS OF THE INVESTIGATION INTO THE EFFECT OF LASER FOCAL POSITION ON GLASS DEPOSITION.	177

Abbreviations

AM	Additive Manufacturing
ASTM	American Society for Testing and Materials International
BAG	Biologically Active Glass
BFE	Basic Flowability Energy
CAD	Computer Aided Design
CBD	Conditioned Bulk Density
CFR	Continuous Flow Reactor
CNC	Computer Numerical Control
CW	Continuous Wave
DED	Directed Energy Deposition
DIW	Direct Ink Writing
DLP	Digital Light Processing
DMD	Direct Metal Deposition
DoE	Design of Experiments
DTA	Differential Thermal Analysis
Dv10	10% of the powder is below that specified size value
Dv50	50% of the powder is below that specified size value
Dv90	90% of the powder is below that specified size value
ED	Energy Density
EDX	Energy Dispersive X-Ray
FDM	Fused Deposition Modelling
FRI	Flow Rate Index
FT4	Powder Rheometer System
FTIR	Fourier Transform Infrared Spectroscopy
GCFR	Glass Continuous Flow Reactor
LPBF	Laser powder Bed Fusion

NIR	Near Infrared
PBF	Powder Bed Fusion
PSD	Particle Size Distribution
RPM	Rotations Per Minute
SE	Specific Energy
SEM	Scanning Electron Microscopy
SLA	Stereolithography
SLM	Selective Laser Melting
SSS	Solid State Sintering
Tg	Glass Transition Temperature
TPP	Two Photon Polymerisation
UV	Ultraviolet
UV-Vis	UV Visible Spectroscopy
XCT	X-Ray Computed Tomography
XRD	X-Ray Diffraction
XRF	X-Ray Fluorescence

Chapter 1

Introduction

1.1 Glass

Glass has been exploited by society for many millennia thanks to its unique and interesting properties. Over the centuries, glass manufacturing has been adapted and innovated, and has become a ubiquitous material, used for many different applications. Industries such as aerospace, automotive, medical implants, electronics, and optics have all found commercial value in glass processing. To understand the appeal of glass materials in industry, it is important to first understand the material properties that it offers.

Atomically, glass materials have no long-range order, and behave as solids frozen in a liquid state. They are formally defined as x-ray amorphous materials which exhibit a glass transition¹. Generally, glass materials are characterised by thermal and chemical resistance, durability, and transparency, as well as aesthetic appeal. These properties can be tailored to particular requirements simply by modifying their chemical composition^{2,3}. Common soda lime silica glass offers a wide working temperature range, making it easy to manipulate and form. Borosilicates, phosphate glasses, and compositions modified by dopants are good examples of the tunability of glass properties. Borosilicate glass boasts a low thermal expansion coefficient, giving it high resistance to thermal shock and chemical attack, and phosphate glasses are biologically active, promoting bone regeneration⁴. Doping of glass compositions can lead to simple colour changes, or even impart properties such as luminescence, or enhancement of biocompatibility (e.g., Iron Oxide dopants in phosphate glasses)⁵. Another desirable trait for industry is the potential unlimited recyclability of glass⁶.

The versatility of glass materials explains the market demand for glass production. In 2019, the global flat glass market was worth \$115.8 billion USD, and growth is expected to continue for the foreseeable future⁷. Currently, global industry produces more than 209 million tonnes of glass annually, almost quadrupling in the space of a decade^{6,8}. A large proportion of this is produced in the form of float glass, sheet glass, and rolled glass, for architectural and automotive applications. There is also significant demand for glass production to satisfy specialised glass applications. There are many different methods for glass forming, from hand

working decorative glass products, to press and blow forming of glass containers, to industrial scale float glass production³ (Figure 1). The float glass process (or Pilkington process) produces flat glass in sheet form, by floating a ribbon of molten glass on a bath of molten tin⁹. Glass can be cast in moulds to create more complex shapes¹⁰, but customisation comes at a high cost, and geometrical freedom is still limited. Innovation in glass processing is still thriving, with interest in development of glass processing by Additive Manufacturing increasing within the research and industry community.



Figure 1 Glass manufacturing processes in industry. Left: Glass blowing. Image source: Corning Museum of Glass¹¹. Right: The float glass process. Image source: Pilkington¹².

From decorative glass forming, to sheet glass manufacturing, glass processing has come a long way. For certain applications, e.g., specialist and scientific glass, the experience and knowledge of a skilled glassblower is still required. For a reliable and repeatable method of forming complex glass objects, Additive Manufacturing (AM) offers a solution. With greater geometric freedom than many other manufacturing techniques, AM has the potential to fabricate high value, bespoke glass parts that are cost effective for small production volumes^{13,14}.

1.2 Additive Manufacturing

Additive Manufacturing (AM) is the term used to describe a group of manufacturing techniques that share the same key principles – creating 3D parts, defined by 3D model data, usually through layer-wise addition of material^{15,16}. This is distinct from subtractive techniques that create parts by removal of material (e.g., machining), and formative techniques (such as injection moulding).

The late 1960s saw the first AM innovation at the Battelle Memorial Institute, where a dual laser beam was used to solidify a DuPont photopolymer resin¹⁷. In the 80s, Hideo Kodama developed this technology further to use a single-beam laser to cure photopolymer material in a layer-wise manner to fabricate 3D objects, demonstrating Vat Photopolymerisation (stereolithography) for the first time¹⁸. Stereolithography was later commercialised by 3D Systems in 1987, alongside the introduction of the STL file format (Standard tessellation language, stereolithography file format describing a surface using a triangular mesh). The development of Additive Manufacturing coincided with advances in other technologies, such as 3D graphics and Computer Aided Design software (CAD), laser technology, and printing technology. Integration of these features, and exploitation of the ever-improving computing power, brought about development of sophisticated, automated AM systems. In 1990, Beaman and Deckard developed and patented Selective Laser Sintering (powder bed fusion AM)¹⁹, and in 1991, Stratasys commercialised Fused Deposition Modelling (FDM) (Material Extrusion AM), and Helisys commercialised Laminated Object Manufacturing (LOM) (Sheet Lamination).

The 1990's saw the development of metal Additive Manufacturing processes, with direct metal laser sintering introduced by EOS in 1994, and Laser Engineered Net Shaping (LENS) commercialised by Optomec in 1998, allowing the rapid production of metal tools. Selective Laser Melting (SLM) was first patented in 1995 at the Fraunhofer Institute for Laser Technology²⁰, with Dr Schwarze and Dr Fockele of F&S Stereolithographietechnik GmbH later collaborating with the ILT researchers to develop the technology, before being commercialised in the early 2000s.

Industrial adoption of these technologies started with rapid manufacturing of prototype objects and was commonly referred to as Rapid Prototyping (RP). As the technology became more advanced, a wider range of applications were identified, including fabrication of end use parts, and thus the term Additive Manufacturing was defined by ASTM¹⁶. There are seven categories of AM processes as defined by ASTM standards, which differ in the form of starting

material and method of consolidation (Table 1). Each process has its merits and limitations for processing certain materials, and are discussed in detail in Chapter 2.

Table 1 Seven AM process categories as defined by ASTM, with example technologies and typical materials^{16,21}.

Process Types	Brief Description	Example Technology	Typical Materials
Powder Bed Fusion	Thermal energy selectively fuses regions of a powder bed	Electron beam melting (EBM), laser sintering (LS), selective laser melting (SLM), direct metal laser sintering (DMLS)	Metals, Polymers
Directed Energy Deposition	Focused thermal energy is used to fuse materials by melting as the material is being deposited	Laser metal deposition (LMD)	Metals
Material Extrusion	Material is selectively dispensed through a nozzle or orifice	Fused deposition modelling (FDM), Direct Ink Writing (DIW)	Polymers, Ceramics
Vat Photo polymerization	Liquid photopolymer in a vat is selectively cured by light-activated polymerization	Stereolithography (SLA), digital light processing (DLP)	Photopolymers, Ceramics
Binder Jetting	A liquid bonding agent is selectively deposited to join powder materials	Powder bed and inkjet head (PBIH), plaster-based 3D printing (PP)	Polymers, Foundry sand, Metals
Material Jetting	Droplets of build material are selectively deposited	Multi-jet modelling (MJM)	Polymers Waxes
Sheet Lamination	Sheets of material are bonded to form an object	Laminated object manufacturing (LOM), ultrasonic consolidation (UC)	Paper, Metals

There is a wealth of knowledge available for AM of metals and polymers, and it has become a key manufacturing technique for many industries that have found commercial value for the utilisation of AM technology, such as GE Aviation, and Airbus. For many years AM was used for rapid prototyping, however, there are now many examples of AM being used to fabricate functional, end use components²². Confidence in AM parts has steadily grown, with some AM parts out-performing machined components, and custom AM parts even being used on the Mars Curiosity and Perseverance rovers²³.

There are multiple ways in which AM can offer benefits over traditional manufacturing methods, including^(1,24-25):

- Capability of a level of geometric complexity that is unachievable with conventional manufacturing methods.
- Customisation per part is achievable without the need for custom tooling or moulds, so bespoke items are cost effective.
- Reduced waste – only the material necessary for each build is used, with potential for complete recyclability of materials for certain AM technologies.
- Reduced transit and storage of goods – On-site and on-demand manufacturing saves cost of goods storage and transport.

One of the main factors limiting the widespread adoption of AM in industry is the limited number of suitable materials, where parts can achieve comparable performance to conventionally manufactured components²⁷. Part cost is also a significant consideration for AM in industry. For low production volumes (e.g., 1-100 parts), AM avoids costs associated with tooling, however, raw materials can be expensive. While AM offers customisation at no added cost, it is unlikely to be cost-effective for mass manufacture when compared to traditional template-based manufacturing processes. Additionally, particularly for powder-based AM, the surface finish of parts can be unsatisfactory, with many AM processes requiring further steps to reach a desired part quality. Post processing often incurs additional time and cost that must be considered. Other practical limitations of AM include dimensional restrictions and production time, often dictated by hardware. The use of AM is therefore most popular for applications requiring high geometrical complexity and customisation, particularly for low production volumes.

To further advance the field of AM, and fully discover the potential it holds, more work is necessary to expand and improve the catalogue of AM suitable materials. For glass materials, research has already started to explore the potential of AM processing. There are various applications for complex glass structures that would benefit from the geometric freedom associated with AM processing, and the interesting properties of glass. For example, the transparency of some glass compositions has inspired research into AM processing by Material Extrusion methods to produce lenses and decorative objects. Other work has started to explore the potential to create geometrically complex glass structures by Vat Photopolymerisation and Powder Bed Fusion AM methods. Other interesting applications for glass AM includes the fabrication of biologically active glass scaffolds for medical implants,

and fabrication of bespoke glass microfluidic devices with complex geometries²⁸. The state of the art in glass AM is further described and evaluated in Chapter 2.

This thesis describes research carried out exploring two specific AM methods for glass processing: Selective Laser Melting (SLM) and Directed Energy Deposition (DED). The motivation behind this work is to prove the feasibility of glass processing by these methods, optimise and make recommendations for processing parameters and set-ups, and demonstrate potential applications. The challenges and benefits of processing glass materials by SLM and DED are explored in this work, ultimately contributing further understanding to the field of glass AM processing.

Chapter 2

Background and Literature

2.1 Background Information: Glass Materials

As defined in Section 1.1, glasses are x-ray amorphous materials which exhibit a glass transition (T_g). Different compositions of glass offer different properties and characteristics. In this research, several compositions of glass are used, with a particular focus on soda lime silica, 13-93 biologically active glass, and Borosilicate. This section introduces these materials in terms of chemical composition and structure, properties, and manufacture.

Silicon dioxide (SiO_2) is the most common component for glass materials. It can form an amorphous quartz glass itself (vitreous silica), as well as a crystalline quartz with a regular repetition of SiO_4 tetrahedral units²⁹. As different oxides are added to the system, the properties and characteristics are altered^{3,30}. The chemical structure of these multicomponent silicate glasses is based on the tetrahedral SiO_4 unit – a central silicon bonded to four oxygen atoms, making up a three-dimensional network via covalent bonding. Oxygen bridges of varying bond lengths and bridging angles connect the tetrahedral units (Figure 2 A). Rings of a varying number of Si-O-Si (up to about 6-7 Si members) are formed, with smaller rings suffering more strain. These glass structures therefore exhibit short-range order but no long-range order thanks to the random orientation about Si-O bonds, creating a random network^{29,31}. The addition of different oxides, for example sodium oxide (Na_2O), breaks up the bridging oxygen bonds, creating space in which the larger cations occupy¹. The Si-O-Si bridging bonds are partially replaced with non-bridging bonds - $\text{SiO}^- \text{Na}^+$. Figure 2 shows schematic diagrams for the chemical structure of a crystalline SiO_2 (quartz), an amorphous SiO_2 glass with a random network (quartz glass/vitreous silica), and a sodium silicate glass $\text{Na}_2\text{O} \cdot \text{SiO}_2$, displaying the modified random network with large Na^+ cations.

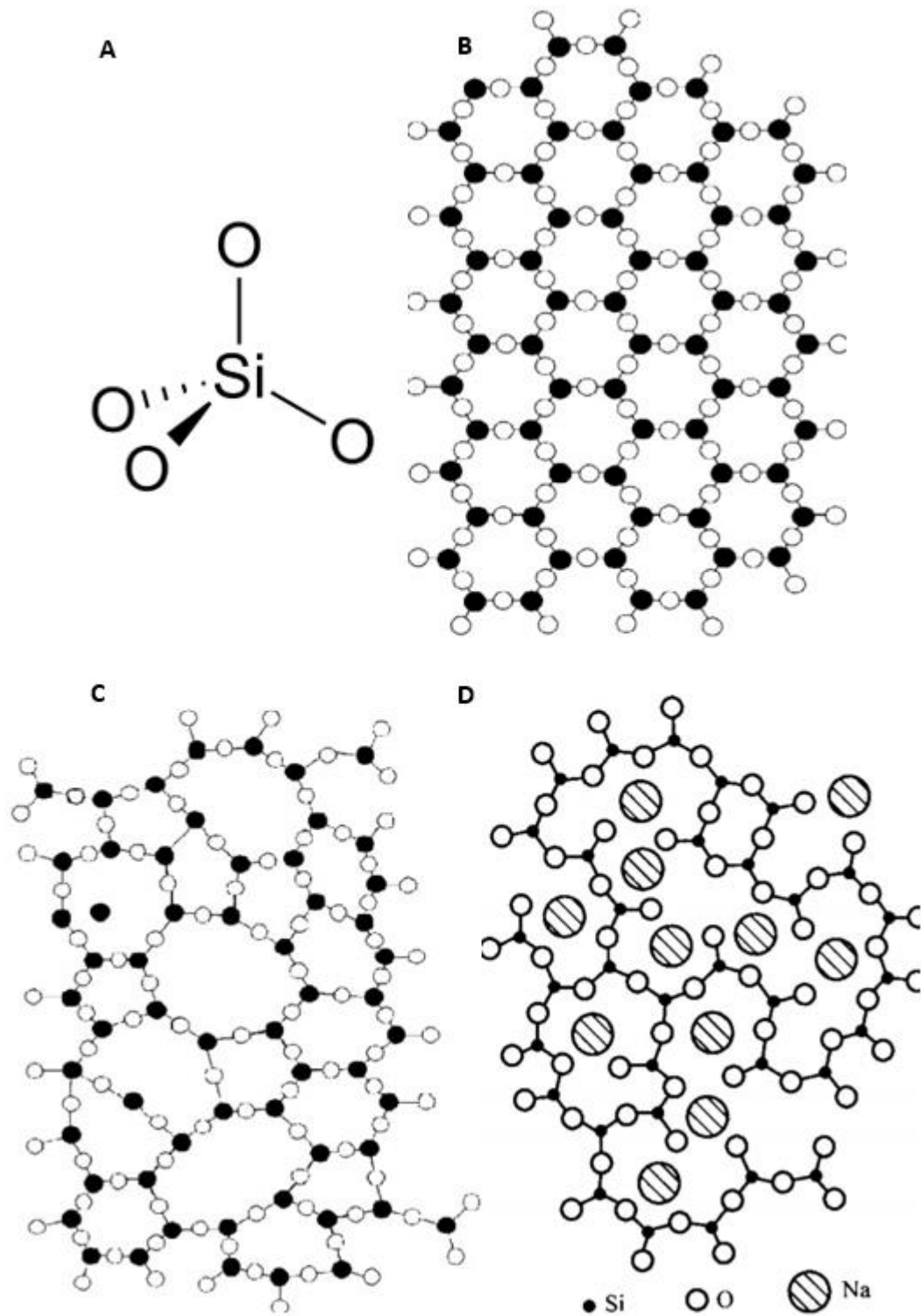


Figure 2 A: SiO_4 tetrahedral unit. B: Schematic of the structure of a quartz crystal, showing a regular repeating pattern of SiO_4 tetrahedra. C: Schematic of the amorphous quartz glass, showing a random network of SiO_4 tetrahedra. D: Schematic of the random arrangement of atoms in a sodium silicate glass, where Na^+ cations break up bridging Si-O-Si bonds and occupy the available space.

To form an amorphous glass, the temperature of the glass components is raised high enough to melt (i.e., above its liquidus – the temperature at which the material is completely liquid), and then cooled rapidly to a supercooled liquid state. The fast quenching allows the chemical structure to “freeze in” as a liquid, as crystallisation (atoms/ions/molecules becoming ordered) is avoided. Providing the cooling rate is fast enough to prevent crystallisation, as the material is further cooled and solidifies (below T_g), it can be referred to as a glass. This process is visualised in a volume/temperature diagram in Figure 3^{2,32}. The crystallisation curve shows a marked increase in density at T_m as the material crystallises on cooling. Under these conditions, cooling is not rapid enough to prevent atomic ordering, and a crystalline solid is formed. For glass formation, cooling is fast enough to transform the material into a supercooled liquid as volume decreases. This is due to decreasing amplitude of atomic vibrations and the melt becoming more compact, and the viscosity of the melt increases. The change in slope indicates the glass transformation range, or glass transition temperature, where a supercooled melt transforms into an amorphous solid (glass) on further cooling, with a further increase in viscosity. For glass working, the material can be heated up and shaped in the supercooled liquid phase, before being cooled to a glass once more.

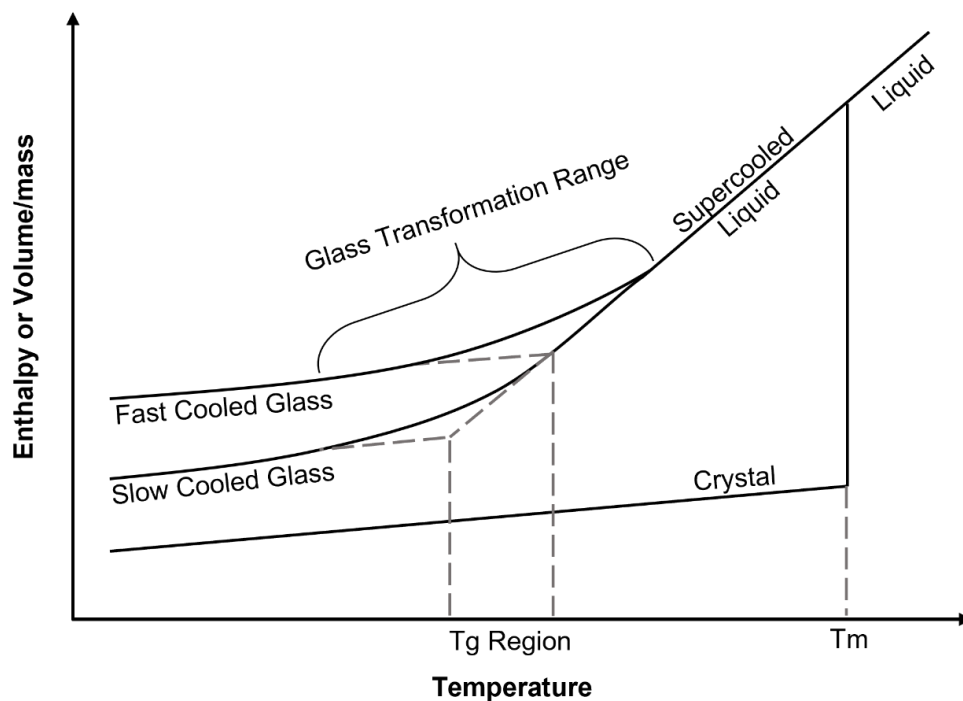


Figure 3 Volume/temperature diagram for crystallisation and glass formation. The curve shows the transformation of a liquid to a crystal at T_m during crystallisation. The liquid may also transform into a supercooled melt under rapid cooling, with a gradual decrease in volume to the glass transformation range. The intersection between the supercooled liquid and glass state curve indicated the glass transition temperature (T_g). The material solidifies to a glass below the T_g on further cooling.

Traditional glass manufacturing depends on the viscosity of the glass, which varies considerably with temperature. Glass technicians may refer to the working range of a glass, where the melt (supercooled liquid) flows sufficiently to shape and form the glass, but not so much that control of form is lost. The T_g of a glass is taken to be the temperature at which the supercooled liquid exhibits a viscosity of 10^{12} - $10^{12.5}$ Pa s, where the glass melt is thick but exhibits flow properties. A viscosity of 10^3 Pa s is used to indicate a working temperature, $10^{6.6}$ Pa s represents the softening temperature, and 10^{12} is used as an annealing point^{33,34}. Glasses that have a narrow working range are known as short glasses, where the viscosity changes significantly with a change in temperature, in contrast, long glasses have wider working temperature ranges, and can be shaped more easily. This is an important distinction for glass manufacturing methods, such as glass blowing, pressing, drawing, or rolling, that are impacted by the working ranges of different glass compositions³.

For hand working methods, glass technicians shape a gob of molten glass using a blow pipe. The glass object is formed by turning the pipe, blowing in the pipe to cool the glass, and reheating as needed. When finished, glass parts are annealed in a lehr. The annealing process is used to gradually cool glass parts so that residual internal stresses can be relieved^{35,36}. Glass parts are usually held at an annealing temperature (usually $T_g - 10$ - 20°C) for a sufficient time to obtain a uniform temperature, before being slowly cooled to room temperature ($\sim 5^\circ\text{C}$ per hour for 10 g melts), reducing permanent strain within parts. For efficient large-scale production of glass containers, an Individual Section machine (I.S. Machine) is used for automated manufacture. Gobs of glass are automatically fed from a furnace to the I.S. machine. The gobs are shaped into an initial container form by pressing or blowing in a blank mould, and then the final shape is formed in a finishing mould by blowing. This industrial process can produce up to 700 containers per minute. Other glass manufacturing processes include the production of flat glass, in the form of sheet, cast, plate, and float glass, and fibres can be drawn manually from a glass melt, or on an industrial scale using a fibre drawing tower.

A benefit of manufacturing products out of glass, with soda lime silica glass making up a large proportion of glass packaging, is that it is exceptionally recyclable. Glass products can be easily crushed and turned into glass cullet, which can then be remelted and formed into new glass products (at reduced energy cost – 2-3% energy reduction for every 10% cullet in the feedstock), or used in different applications, e.g., as an aggregate or filler in concrete³⁷. The recyclability of glass has made it an important material through history, with evidence of glass recycling during the Roman and Byzantine Empires^{38,39}. The benefits of glass reuse and

recycling are still important today, particularly in the packaging industry, as consumers demand a reduction in single use plastic packaging and the waste of raw materials⁴⁰. In 2020, the UK recycled (and recovered) 1800 tonnes of glass packaging, with a recycling rate of 75.8%, while in comparison, the recycling rate of plastic packaging was much lower, at 47.4%⁴¹. The combination of recyclability, chemical and thermal durability, transparency, and appealing aesthetic make glass an important material for the packaging industry, as well as many others.

In general, glasses are well known for their transparency. Glasses are often characterised as being highly transmissive in the visible (350-750 nm) and near-IR region (750 nm- 2 μm), with absorption increasing in the UV (200-350 nm) and long wave IR region (8-15 μm) (Figure 4)⁴². This is an important characteristic to consider when processing glass materials by laser radiation, as the absorption of the laser wavelength used may be limited by the transmissivity of the glass in that region. The transmission of laser wavelengths is impacted by the composition of glass, with the presence of certain ions known to increase absorption, whether they are impurities, or components deliberately added to the glass batch. For example, the addition of transition metal ions, such as Ti^{3+} , V^{3+} , Fe^{2+} , Co^{2+} , Cu^{2+} , Mo^{3+} etc, are known to impart colour in glasses, even in small quantities (e.g., <0.1% of CoO can be added to give a pale blue colour to a glass)^{43,44}. The addition of Co to a soda lime silica base glass composition (71.4% SiO_2 , 18.4% NaO , 10.2% CaO) was reported to increase absorption in the near IR region (between 1-2 μm) (Figure 5)⁴⁴. The transmissivity of glasses at 1.06 μm has historically hindered the processing of transparent glass materials by Nd:YAG lasers, however, there are examples of these lasers being used to machine glasses by subsurface engraving, cutting, and drilling⁴².

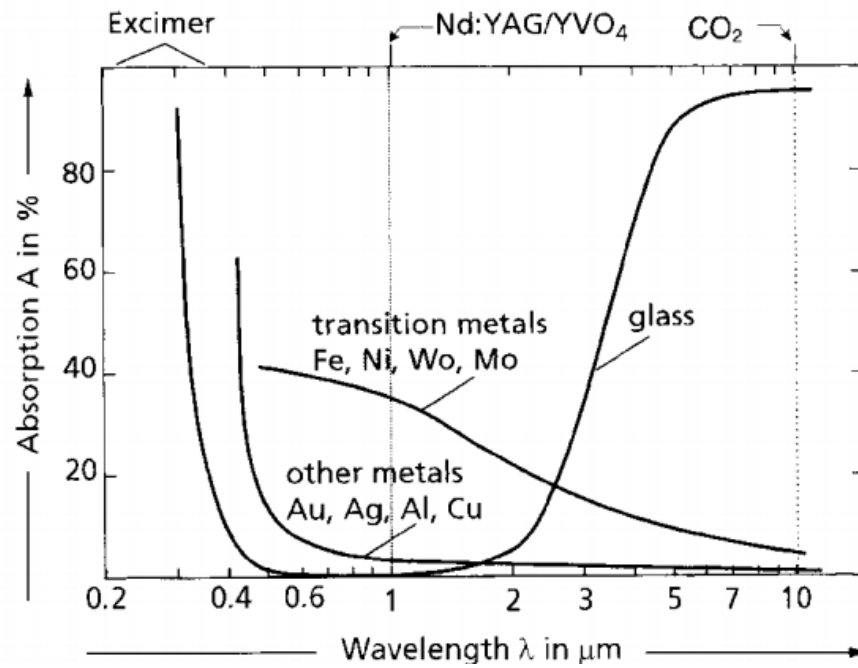


Figure 4 Absorption of different materials as a function of the wavelength. Glass shows greater absorption in the ultraviolet and long wave IR regions, with low absorption at near IR wavelengths⁴².

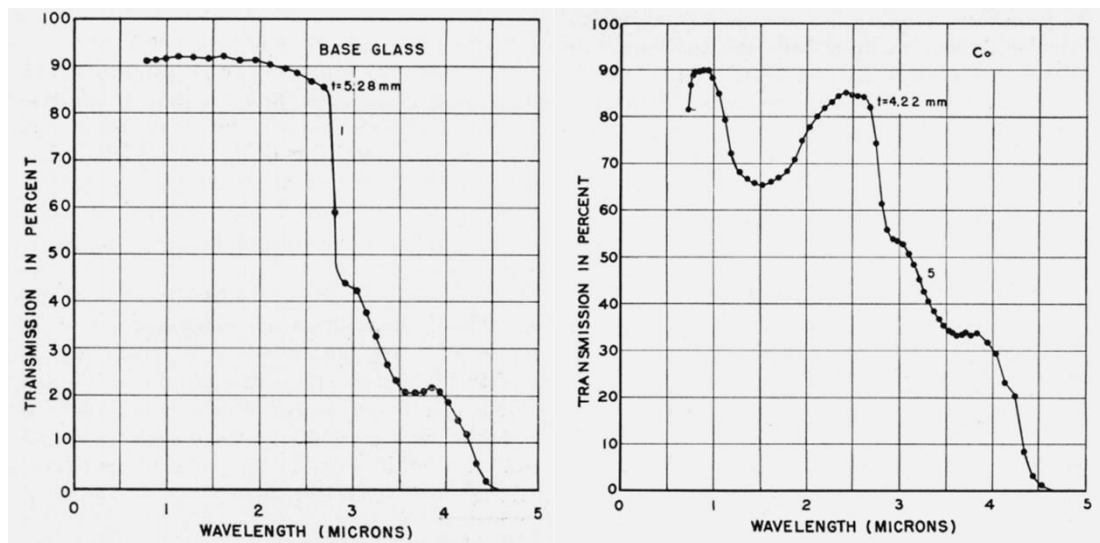


Figure 5 Percentage transmission in the 0-5 μm wavelength region of Left: base glass (soda lime silica), and Right: the base glass doped with cobalt. An absorption peak is seen between 1-2 μm wavelength in the Co doped glass⁴⁴.

2.1.1 Glass Compositions

Soda lime silica is a popular commercial glass composition, generally used for everyday applications such as windows, and glass packaging and containers. The components of this glass system typically include 70% SiO_2 , 15% Na_2O , 10% CaO and MgO , and 5% other oxides⁴⁵. Soda (Na_2O) is added to the system as a flux, reducing the temperature at which softening occurs, by replacing some of the strong covalent bonds between tetrahedra via bridging

oxygens, with non-bridging oxygens (connected to only one Si atom). This addition of bridging oxygens reduces the glass transition as the network is weakened^{34,46}. In comparison to vitreous silica, which has a softening temperature of $\sim 1600^{\circ}\text{C}$, soda lime silica glass softens around $675\text{-}725^{\circ}\text{C}$, allowing working of the glass at lower temperatures during manufacture^{3,30}. The addition of soda reduces the strength of the glass at high temperatures, and also makes the glass soluble in water. To counter this, lime is added as a stabiliser, increasing the chemical durability of the glass. The linear coefficient of thermal expansion (CTE) of vitreous silica is very low at $\sim 0.5 \times 10^{-6}/^{\circ}\text{C}$, indicating the strong chemical bonding in the glass structure. In comparison, soda lime silica glass has a much higher CTE at $\sim 9.2 \times 10^{-6}/^{\circ}\text{C}$ due to the weaker bonding within the chemical structure.

Borosilicate is another common glass composition with the typical chemical composition of 70-80 wt% SiO_2 , 7-13 wt% B_2O_3 , 4-8 wt% Na_2O or K_2O and 2-8 wt% Al_2O_3 ³². Pyrex is a well-known commercial borosilicate glass, particularly used for high temperature cookware, but has also been identified as a suitable glass for optical applications. Borosilicate is popular for applications requiring chemical durability, e.g., pharmaceutical packaging, and high thermal resistance e.g., labware and cookware, due to its low coefficient of thermal expansion ($3.3\text{-}5.0 \times 10^{-6}/^{\circ}\text{C}$)³³. The softening point of borosilicate is higher than that of soda lime silica, but lower than vitreous silica, at $\sim 820^{\circ}\text{C}$.

Some glass compositions can be considered to be biologically active. These glasses typically have phosphates in their composition and work by attaching to soft and hard tissues, stimulating bone growth, and degrading over time⁴⁷. Bioactive glasses are a popular material for research into implantable devices, with significant advantages over metal implants which require follow up surgeries for removal, allo- (same species) and xenografts (different species) which can be rejected by an immune response, and autografts (same body) which require multiple surgeries. There exists a wide range of biologically active glass materials, with varying properties in terms of biological activity, thermal profiles, and mechanical strength.

13-93 bioactive glass is composed of 53 wt% SiO_2 , 6 wt% Na_2O , 12 wt% K_2O , 5 wt% MgO , 20 wt% CaO , and 4 wt% P_2O_5 . It has a wide working range ($\sim 600\text{-}700^{\circ}\text{C}$)⁴⁸ compared to other bioactive glass compositions and was designed to not devitrify (crystallise) at high temperatures^{49,50}. Manufacturing of 13-93 bioactive glass fibres and cylinders has been demonstrated thanks to the wide working range of this composition, and recent literature demonstrates the fabrication of 13-93 bioactive glass bone scaffolds by AM methods (further

discussed in this chapter)^{49,51,52}. The glass transition temperature (T_g) of this glass composition is reported around 600°C, with a liquidus of 1150-1250°C⁵³. Studies suggest that 13-93 bioactive glass has enhanced viscous flow compared to 45S5 bioglass, and can promote osteogenesis by the formation of hydroxyapatite (HA) on scaffold surfaces⁵⁴⁻⁵⁶. This glass composition is a promising candidate for bone scaffold implants, particularly when combined with the geometrical capabilities of AM techniques for fabricating customised, patient-specific devices. A comparison of properties for vitreous silica, soda lime silica, borosilicate, and 13-93 bioactive glasses can be found in Table 2.

Table 2 Compiled data for the properties of vitreous silica, soda lime silica, borosilicate (pyrex) and 13-93 bioactive glass compositions, including characteristic temperatures for softening, annealing, and strain point, coefficient of thermal expansion, and mechanical properties^{30,57}.

Property	Vitreous Silica	Soda Lime Silica	Borosilicate (Pyrex)	13-93 Bioactive
Strain Point (°C)	1000°C	470°C	520°C	533°C
Annealing Point (°C)	1100°C	510°C	565°C	572°C
Softening Point (°C)	1600°C	700°C	820°C	729°C
Coefficient of Thermal Expansion (x 10 ⁻⁶ /°C)	0.55	9.2	3.2	10.9
Young's Modulus (10 ⁻¹⁰ Y/N m ⁻²)	7.4	7.4	6.1	-
Rigidity Modulus (10 ⁻¹⁰ G/N m ⁻²)	3.2	3.1	2.5	-
Poisson's Ratio (ν)	0.16	0.21	0.22	-
Vickers Hardness Number	710	540	580	-

2.2 Current State of the Art in Glass Additive Manufacturing

Whilst there is a large amount of research into metals, polymers, and certain ceramics for AM, the exploration of glass AM has only skimmed the surface. As the field of glass AM is still emerging, some of the methods described in Chapter 1 have not yet been explored for glass processing. This is likely because some techniques have been identified as more promising for glass material processing than others, and therefore have been the focus in research. The review of literature in this chapter describes the most popular AM methods investigated for glass processing, including Material Extrusion (Section 2.3), Vat Photopolymerisation (Section 2.4), Powder Bed Fusion (Section 2.5), and Directed Energy Deposition (Section 2.6).

2.3 Material Extrusion

Material Extrusion typically fabricates parts additively by the selective deposition of material through a nozzle. This process is typically used for polymer materials in filament form, which is heated to allow consistent flow and bonding of melted material in subsequent layers. For the application of achieving optically transparent glass, Klein described the creation and optimisation of a bespoke material extrusion setup for processing molten glass^{58,59}. In this work, a custom set-up was required to withstand the high temperatures necessary to melt soda lime glass, with custom-made chambers and nozzles from alumina-silica material (Figure 6). Molten glass was extruded at 1040-1165°C, and deposited layer wise onto a ceramic kiln shelf in a chamber maintained at 480-515°C (above the glass transition temperature (T_g) of feedstock glass) to form various geometries such as cylinders and objects with varying concave and convex forms. The ceramic kiln shelf allowed sufficient adhesion during processing, and easy removal at annealing temperature. Thermal post processing was carried out to anneal the soda lime glass parts, using an annealing cycle of 1 hour dwell at 480°C, cooling at 25°C/h to 400°C, cooling at 50°C/h to 150°C and 80°C, and cooling at 120°C/h to 20°C, reducing stress concentrations. Defects and rough surfaces were ground and polished to present a smooth aesthetic. The resulting parts of both colourless and coloured glass showed optical transparency, with a proposed application for decorative art pieces (Figure 7).

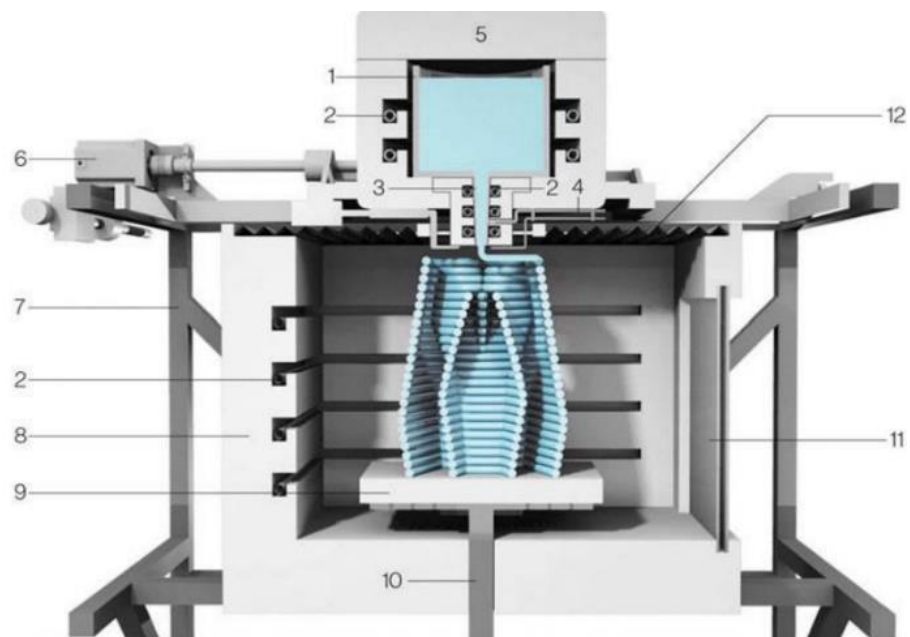


Figure 6 Bespoke FDM set-up for extrusion of molten soda lime silica glass. 1: crucible, 2: heating elements, 3: nozzle, 4: thermocouple, 5: feed access lid, 6: stepper motors, 7: printer frame, 8: print annealer, 9: ceramic print plate, 10: z-drive train, 11: ceramic viewing window, 12: insulating skirt.^{58,59}



Figure 7 Glass objects presented by Klein et al.⁵⁸ Left: A coloured glass object fabricated by material extrusion, with visibly discernible layers. Right: a clear glass fabricated part demonstrating optical transparency.

The custom extrusion system was costly and presented certain functional limitations, such as molten glass solidifying and obstructing the nozzle orifice disrupting part processing and resulting in uneven glass distribution, and the lack of automatic control of combined systems during operation. The produced glass parts were attractive and transparent, however, layers were visibly discernible, reducing the optical quality. Nozzle diameter was fixed at 10 mm, resulting in a large layer thickness. As a consequence, resolution and geometrical accuracy of parts was low (layer height was 4.5 mm, and layer width varied by structure, with an average layer width of 7.95 mm \pm 0.19 mm measured by CT reconstruction of a cylinder geometry). Due to the nature of the gravity fed system employed, the nozzle diameter could not be altered to improve resolution or dimensions of parts. These issues could be solved by further machine adaptation but the limitations of Material Extrusion processing would likely remain.

The work did not demonstrate processing structures with substantial overhangs, which would not be achievable without the use of sacrificial support structures. Additionally, support structures make it difficult to fabricate parts with complex internal geometry by this method compared to other AM techniques (particular those that do not require support structures e.g., powder bed fusion). Additionally, the geometries demonstrated could arguably be achievable using traditional glass processing, through the use of moulds. This work described the processing of a glass composition with relatively low working temperatures (soda lime glass - System 96® Studio Nuggets™: softening point 682°C, anneal point: 515°C). In order to process compositions with higher transition and melting temperatures, a much higher temperature would be needed, requiring costly rebuild of the machine set up, and increased operating costs.

Zaki et al. reported Fused Deposition Modelling (FDM) of a phosphate glass composition (42.5 P₂O₅, 25 Na₂O, 25 K₂O, 7.5 Al₂O₃, -PNKA7), with a T_g of 317°C⁶⁰. A commercial FDM set up was modified to increase the temperature of the extrusion nozzle to 470 – 510°C, and the substrate temperature to 320 – 350°C. Phosphate glass filaments of 1.9 mm diameter were selectively melted by FDM, and processed layer-wise to form simple shapes. Europium doped phosphate glass (PNKA7:Eu, PNKA7 modified with 42 P₂O₅ and 0.5 mol% Eu₂O₃. T_g = 333°C) was also processed to demonstrate the retention of luminescent properties in printed glass. Similar to the work by Klein et al., using material extrusion has limitations to achievable geometric complexity in terms of overhangs and internal features. Zaki et al. only demonstrated rudimentary structures of glass processed by FDM.

Baudet et al. processed arsenic sulphide chalcogenide glass by material extrusion, exploiting the low glass transition temperature of this composition (As₄₀S₆₀, T_g= 188°C)⁶¹. This allowed extrusion of the glass filament feedstock at ~330°C through a modified commercial material extrusion set-up. A 0.4 mm diameter nozzle was used, and a preheated substrate (80°C) of the same As₄₀S₆₀ glass composition was used to ensure adhesion was achieved (by matching the coefficient of thermal expansion of deposited and substrate glass). Care was taken to avoid exposure to toxic vapour created during processing due to the high vapour pressure of the chalcogenide glass at high temperatures. Parts were coloured yellow due to this sulphide vapour deposit (Figure 8). The processed glass parts had discernible layers, and cracking was unavoidable when post process polishing was attempted. The geometries processed were not very complex, and dimensional accuracy was not reported. Further assessment of the geometrical accuracy would help to assess the quality of parts. This work demonstrated the potential for material extrusion of glass compositions with lower working temperatures, requiring simple modification of commercially available material extrusion hardware. Further work may optimise the process to produce accurate and complex glass structures using this method and glass composition.

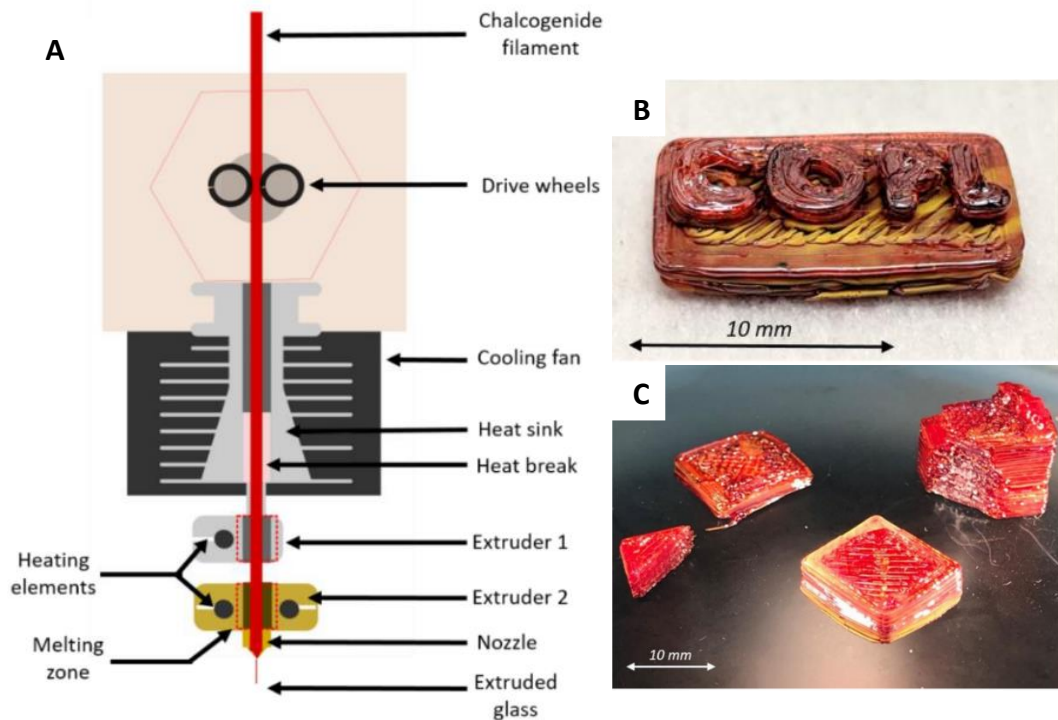


Figure 8 A: Material extrusion set-up used to process $As_{40}S_{60}$ chalcogenide glass filaments, B-C: Processed chalcogenide glass structures with visibly discernible layers, and a yellow colour from sulphide vapour⁶¹.

Direct Ink Writing (DIW) is another extrusion-based AM method that has been used to explore glass processing. In comparison to extruding molten glass, requiring very high temperatures to melt feedstocks ($>1000^{\circ}\text{C}$) and a suitable set-up that can resist such high temperatures, this method allows extrusion at lower temperatures. Processing at lower temperatures (e.g., room temperature) reduces thermal gradients and thus helps to prevent part failure due to thermal shock and build-up of residual stresses during processing. DIW works by selectively extruding composite inks, and building the desired geometries layer by layer, to form a green part. Thermal post processing dries and consolidates the green part. This method has been used to investigate glass processing, and examples of fabricating transparent glass structures and glass optics with gradient refractive index have been shown^{62–65}.

During DIW of hydrophilic fumed silica nanoparticle inks, Nguyen et al. reported anisotropic shrinkage during the densification stage (heating at 1500°C) and observed volumetric changes that were dependent on the silica content of the ink feedstock. At 20 wt% silica content, volumetric shrinkage was reported as 90% of the original volume. Parts fabricated from a higher silica content ink (23 wt% silica) shrank from 250 μm diameter to 140 μm diameter. Increased silica content of the ink resulted in higher viscosity, better retention of

shapes, but increased the visibility of print tracks in monolithic structures. One application demonstrated was hollow channels for glass microfluidic devices. These had a level of transparency, and were leak tight, however print tracks were visible (Figure 9)⁶². DIW of gradient refractive index lenses was demonstrated in rudimentary structures, however fabrication of complex, three-dimensional structures was not reported⁶³. Sol gels of Silica (SiO_2) and Silica-titania ($\text{SiO}_2\text{-TiO}_2$) glass compositions were used for DIW, and investigation into processing other glass compositions by this method has not yet been reported. One of the drawbacks of DIW is the need for post-process heat treatments to densify parts and remove organic content. This post processing incurs additional costs, and more significantly can lead to anisotropic shrinkage, reducing dimensional accuracy, and compromising part resolution.

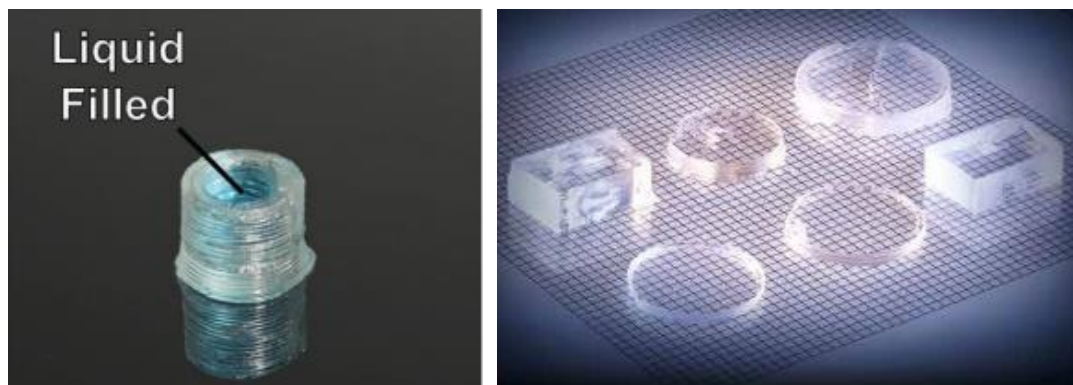


Figure 9 Examples of glass parts produced by Direct Ink Writing. Left: Hollow glass cylinder of 20wt% silica ink filled with liquid⁶² Right: example of silica-titania glass optics with gradient refractive index⁶³.

Material extrusion has also been used alongside direct laser melting to process a fused silica paste (silica powder, deionized water, + others) in an integrated system⁶⁶. The silica paste was extruded to form layers and then selectively irradiated by a CO_2 laser to melt and consolidate silica material. Transparent fused silica parts were fabricated without the use of post process heat treatments, but further investigation is needed to characterise built parts for complete evaluation. The state of the art in glass processing by material extrusion has demonstrated promising results for retaining transparency in parts but has mostly presented rudimentary geometries with discernible layers. The processing set-ups described have often been bespoke or adapted to process glass materials, with further work necessary to standardise the hardware for glass processing.

2.4 Vat Photopolymerisation

Stereolithography (SLA) is an example of the Vat Photopolymerisation AM technique and has been used to demonstrate its potential for processing glass parts for various applications. The technology involves polymerisation of photo-curable resins using UV light, selectively solidifying material layer by layer to create a “green” part. Post processing of green parts is required to completely remove any remaining non-glass material and to achieve a fully dense part. Digital Light Processing (DLP) is another lithography method that uses digital light instead of UV to cure photosensitive material. The two techniques share similar principles and have both been utilised for glass processing research.

Literature has described processing of biologically active glass material by SLA to fabricate cellular tissue scaffolds^{67–71}. These biologically active glass compositions are of interest for tissue scaffold fabrication due to the material stimulating bone regeneration when interacting with bone tissue⁶⁷. SLA (and AM in general) allows parts to be highly customised, making it ideal for fabricating bespoke medical implants. Tesavibul et al. selectively polymerised a photosensitive slurry of 45S5 bioglass, acrylate monomer, organic solvent, light absorber, and photoinitiator by DLP, and sintered the parts post process⁶⁸. Customised bone implant structures were demonstrated, however, compressive strength was lower than desired for this application, and parts was partially crystallised – reducing the biological activity of the glass material (Figure 10). Glass ceramics, such as wollastonite diopside ($\text{CaSiO}_3\text{-CaMgSi}_2\text{O}_6$), have been presented as an alternative biologically active glass material that could be processed by SLA to produce customised bone scaffolds^{70,71}.

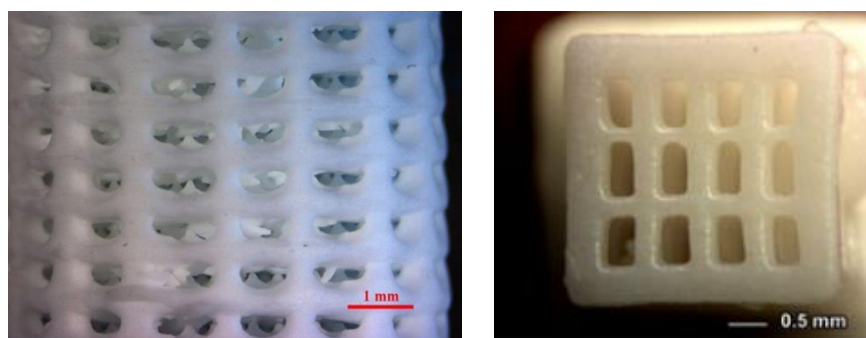


Figure 10 Examples of structures fabricated by stereolithography Left: 45S5 Bioactive Glass fabricated in a scaffold geometry⁶⁸. Right: WDE glass ceramic scaffold fabricated by DLP and heat treated at 90°C⁷⁰.

Promising progress in SLA of glass materials has been made by Kotz et al., demonstrating the fabrication of highly transparent, complex geometries for various applications, including

microfluidic reactors and micro-optical lenses (Figure 11)^{72,73}. This work processed photocurable silica nanocomposite material by SLA to form a green part, before sintering at 1300°C to achieve full densification and remove non-glass content. Shrinkage due to the necessity of post process sintering occurred, and a method of predicting this shrinkage was proposed. Coloured glass parts were also achieved through the addition of metallic salts. Kotz et al. explored glass processing beyond SLA, as one of the identified limitations to this method was the challenge of removing partially cured material from hollow structures. Sacrificial template replication was presented as an alternative method to producing transparent, freeform three-dimensional, hollow glass microstructures⁷⁴.

Further, Two-photon polymerisation (TPP, aka Direct Laser Writing) of silica nanocomposite material (altered to improve optical transparency) has been reported in several publications^{75,76}. The nanocomposite was selectively polymerised by near-IR light (two-photon) to form the green part, heat treated at ~600°C for debinding, and then sintered at ~1300°C to leave transparent, fused silica parts with tens of micrometer resolution.

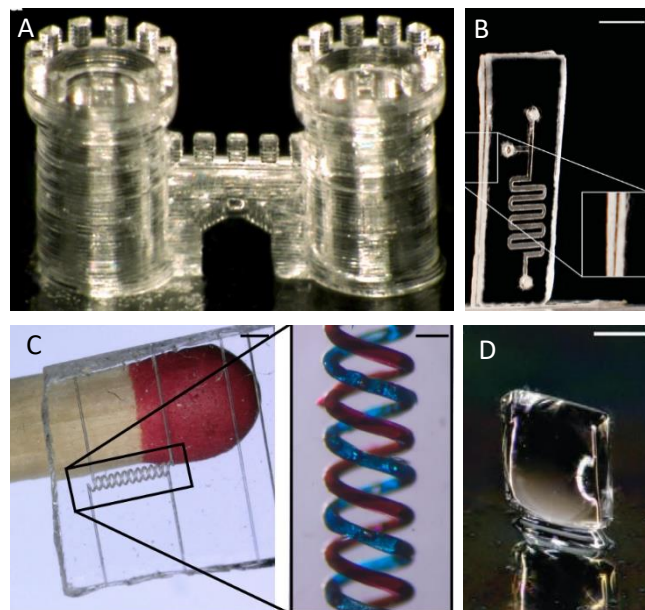


Figure 11 Investigation of glass processing by Kotz et al A: Fused silica glass part fabricated by SLA⁷³. B: Fused silica glass microfluidic chip fabricated by "LiqGlass" lithography.⁵ C: Fused silica glass microfluidic spiral channels fabricated by sacrificial template replication⁷⁴. D: Fused silica glass lens fabricated by Two-Photon Polymerisation⁷⁵.

Variations of the SLA process have been used to demonstrate glass AM. Cooperstein et al. used DLP to process a sol ink consisting of a silica compound and photoinitiators (and other components)⁷⁷. The material was selectively polymerised by UV light, forming desired geometries layer wise. The parts were dried and heat treated to remove solvents and organic

residues, and to achieve dense, transparent, silica parts. Farrell et al used a similar approach to produce complex geometries, such as ordered mesoporous silica structures⁷⁸. Other work has explored processing of silica glass doped with various rare-earth ions by SLA, forming multicoloured luminescent, transparent silica glass parts⁷⁹, and DLP of multicomponent glasses⁸⁰.

Processing of fused silica glass by SLA has shown much promise, producing transparent glass parts with high resolution and exceptionally smooth surface texture. Currently the investigation of glass material is limited to very few compositions, and the potential of processing other glass compositions by SLA has yet to be explored. Silica glass has been shown to achieve amorphous, transparent glass structures, however, so far literature describing SLA of other glass compositions have produced opaque or crystallised glass parts. Generally, SLA requires lengthy post processing times to completely densify built parts, or remove non-glass content (Kotz reported a fabrication process time of 61 h, with post processing accounting for 52 h⁷²). Support structures are also required for certain structures, and removal of uncured material from designed voids/hollow areas can be challenging, e.g. microfluidic devices. Additionally, many of these investigations demonstrate processing of parts in the micro-scale, particularly with DLP processing, due to being limited in size by the projector or LCD screen used.

2.5 Powder Bed Fusion

Powder bed fusion describes a group of AM techniques that utilise a heat source, e.g., laser or electron beam, to fuse material in a powder bed to fabricate objects. Selective Laser Melting (SLM) and Laser Sintering are examples of Laser Powder Bed Fusion (LPBF) that have been investigated for processing glass materials. These techniques process powder through layer-wise consolidation by laser irradiation of predefined CAD geometries. Laser sintering typically utilises a CO₂ laser (wavelengths of 10.2-10.8 μm) and is used primarily for polymer processing as they have acceptable absorption at CO₂ laser wavelength. For metals, or materials with higher melting temperatures, SLM is often selected over laser sintering, and typically uses higher powered lasers (e.g. fibre lasers) to achieve material fusion⁸¹. A distinction is sometimes made between laser sintering and SLM by the different mechanisms of fusion, where generally materials consolidate by solid state sintering (SSS) in laser sintering, and by full melting in SLM^{15,82}. Generally, in laser sintering, feedstocks and process chambers are heated to a few degrees below the material melting point, using laser energy to tip the material beyond the melting point, consolidating powder at low energy laser irradiation. Typically, feedstock materials are completely melted by laser irradiation in SLM processing. For glass materials, the consolidation mechanism for powder bed fusion has not yet been characterised.

2.5.1 Laser Sintering

Laser sintering can be further classified as “Direct” or “Indirect”, describing the feedstock and method of consolidation. Indirect laser sintering refers to feedstocks that are not homogenous in nature, and processing relies on the presence of a binder, where binding particles have a lower melting temperature than other particles present in the feedstock. Binding material is sintered by the laser, forming a composite green part that requires post processing for removal of binder and densification – normally resulting in significant shrinkage. Direct laser sintering refers to the consolidation of powder particles with a homogenous chemical composition, eliminating the need for post processing⁸³. Both direct and indirect laser sintering have been used to explore processing of glass materials, however, there is little literature available on direct laser sintering of high temperature materials due to machine limitations, as processing these materials requires high energy to sinter⁸⁴. Models have been made to describe the physical process of sintering glass, and “necking” of glass

particles during sintering was shown by Prado et al.^{85,86}. Laser sintering has been of particular interest for processing biologically active glass powders for the purpose of customisable medical implants⁸⁷⁻⁹¹.

Kolan et al. described additive manufacturing of 13-93 bioactive glass (53% SiO₂, 4% P₂O₅, 20% CaO, 5% MgO, 6% Na₂O and 12% K₂O) by laser sintering, fabricating porous scaffold structures for bone repair applications (Figure 12)^{87,88}. In this research, polymeric binder (stearic acid) was mixed between 12-22 wt% with 13-93 bioactive glass to form the feedstock. The feedstock was processed by laser sintering, holding the powder bed at temperatures just below the melting point of the binder, then using the laser to tip over the melting point, thereby allowing consolidation at low laser powers, and reducing temperature gradients in the powder bed. Heat treatments at 550°C for de-binding, and 700°C for densification was carried out post process. Anisotropic shrinkage was reported, with greater shrinkage related to increased binder content. Dimensional accuracy and resolution was lacking, and surface finish was rough due to fusion of unwanted powder particles adjacent to the built structures. 13-93B3 glass was also investigated and used to demonstrate complex lattice structures for biomedical implants⁹². Kolan et al. recommended consideration of pore size reduction from sintering of excess glass powder inside pore structures during the CAD creation stage. Volumetric porosity was reduced by up to 25% depending on designed geometry. Lin et al. summarised that poor dimensional accuracy (loss of feature sharpness and increased dimensions leading to geometry distortion) and rough surface finish was commonly reported for laser sintering of scaffold structures due to unwanted fusion of adjacent powder from conduction and diffusion of laser energy⁹³. While high porosity and surface roughness could be desirable for certain applications (e.g., bone scaffolds), it would be considered a disadvantage for others, along with low dimensional accuracy, part shrinkage (volumetric shrinkage caused by debinding stages during indirect laser sintering), and low mechanical properties.

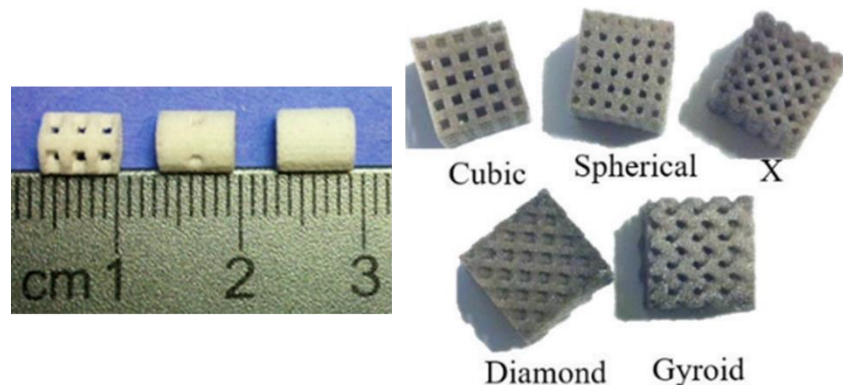


Figure 12 Left: Fabricated "green part" scaffolds of 13-93 bioactive glass with various geometries⁸⁷. Right: Scaffold architectures of 13-93B3 bioactive glass⁹².

Direct laser sintering provides an opportunity for glass processing without shrinkage associated with post process heat treatments. The feasibility of processing borosilicate glass powder by Laser Sintering was investigated through direct laser sintering, and indirect laser sintering by the addition of carbon black⁹⁴. For direct laser sintering, single layer processing was carried out to identify suitable process parameters for consolidation of borosilicate glass powder. Optimal parameters were judged by layer thickness, which was found to increase with increasing energy density (the measure of energy imparted to the powder due to the laser power, scan velocity, or scan vector overlap). Multi-layer cubes were processed to assess surface roughness and density. These parts exhibited cracking due to thermal stresses introduced during processing as a consequence of rapid temperature changes, despite borosilicate's reputation for thermal resistance and durability – low coefficient of thermal expansion ($3 - 6 \times 10^{-6} \text{ K}^{-1}$)(See Section 2.1)⁹⁵ (Figure 13). One of the limitations stated was the narrow window for balancing optimal parameters, with surface roughness and part density competing for optimal scan speed. The dimensional accuracy of sintered parts was affected by heat transfer from irradiated areas to the surrounding powder bed. As processed, parts showed density of less than 50% of theoretical density. Post process heat treatments were used to densify the parts, however this resulted in anisotropic shrinkage, and loss of the desired geometry. A small quantity of carbon black (0.05 wt%) was added to the borosilicate feedstock with the aim of increasing energy absorption. This approach resulted in a small increase in the density of the built part. The processing window did not change significantly and the increase in part density was too small to justify the additional steps necessary to remove the additive.

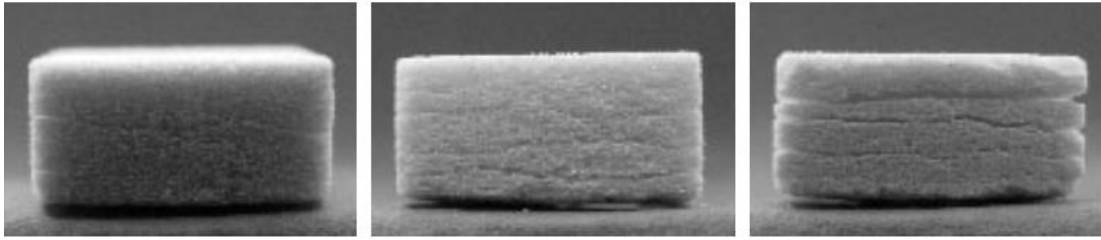


Figure 13 Laser sintering of borosilicate glass by Klocke et al. with laser power increasing from left to right, with visible cracks and rough surface⁹⁴.

While some progress has been made to prove the feasibility of glass processing by laser sintering, the literature reports common limitations⁹³. For example, dimensional accuracy is often limited due to surrounding powder influenced by a heat affected zone, expanding the built part. Delamination and cracking of parts was frequently observed due to large thermal gradients during processing, and crystallisation of glass was reported in some cases, particularly with biologically active glass compositions, and linked with a slow sintering rate (nano-58S Bioactive glass (58% SiO₂, 33% CaO, and 9% P₂O₅⁹¹, 13-93 53% SiO₂, 4% P₂O₅, 20% CaO, 5% MgO, 6% Na₂O and 12% K₂O⁸⁷). This may be related to the presence of P₂O₅ in the silicate glass compositions that can cause phase separation and crystallisation⁹⁶. Heating of powder beds to just below the melting temperature of feedstock materials is recommended practice for laser sintering processes. As many glass materials are characterised by high glass transition temperatures, e.g., soda lime silica T_g = ~550-600°C (see Section 2.1), direct laser sintering of glasses proves challenging as processing temperatures must be high enough to accommodate these thermal demands. Using an indirect method to reduce the required temperature of the powder bed results in anisotropic shrinkage of parts and a further reduction in geometrical accuracy as a consequence of post process de-binding and densification. Finally, glass powder feedstocks demonstrated a “balling” effect at high energy density processing due to the surface tension of the material and the porosity inherent in powder beds, this is a common phenomenon also reported with metal laser powder bed fusion AM⁹⁷. Optimising laser sintering parameters to account for this effect, as well as surface roughness, density, and dimensional accuracy of glass parts has proven challenging, offering narrow processing windows for certain glass compositions (Klocke et al. reported a narrow processing window of 5-9 W laser power, 300-550 mm/s scan velocity, and 0.12-0.18 mm hatch spacing for laser sintering of borosilicate glass⁹⁴).

Zocca et al. investigated laser sintering of lithium aluminosilicate glass ceramic (LAS: Li₂O-Al₂O₃-SiO₂) tapes at a range of parameters⁹⁸. The tapes were prepared by mixing with water

and an organic binder (polyethylene glycol) to create a slurry, and so differs to the traditional laser sintering method of irradiating a powder bed. The authors described the process as “selective laser treatment” and utilised a YAG-fibre laser (1064 nm wavelength, often used in SLM) as opposed to a CO₂ laser (10.6 µm wavelength, often used in Laser Sintering). The slurry was spread onto a ceramic tile and dried. The deposited tape was scanned in 10 x 10 mm square areas, using 15-39 W laser power and 20-80 mm/s scan velocities (hatch spacing = 0.1 mm). Porosity was observed in the samples by SEM imaging and was understood to be caused by the decomposition of the organic binder within the tape generating gas bubbles. This could not be avoided however, as the organic binder was found essential for densification by laser irradiation (LAS tape without the binder did not densify by laser irradiation, even at high energy). This was attributed to the low absorption of LAS feedstock at YAG-fibre laser wavelength. Similar characteristics were found for parameter combinations of similar calculated energy, with a processing window for defect free samples defined as 0.32 – 0.8 W s/mm. This work demonstrated the relationship between laser sintering process parameters and the quality of LAS glass ceramic parts, however only single layers were processed, with further work necessary to investigate the effect of processing parameters on multi-layer structures.

In summary, processing glass materials by laser sintering still seems promising for biomedical applications, with biologically active glass feedstocks of most interest to the research community. The thermal profiles of biologically active glasses tend to be more moderate, with lower melting temperatures than other glass compositions, allowing melting and laser processing at lower temperatures. Various biologically active glass compositions have so far been investigated for fabrication of custom, porous bone scaffold structures, with several studies successfully defining laser sintering process parameters for these glasses, and evaluating them for their biological activity in in vivo testing⁹⁹. There is still much to gain from research into laser sintering of glass materials, particularly in exploration of optimal process parameters for laser sintering of different compositions of glass.

2.5.2 Selective Laser Melting

Selective Laser Melting (SLM) is another laser powder bed fusion (LPBF) method of additive manufacturing. In general, a single layer of powder is spread across the build platform (by a blade or roller). Laser irradiation selectively fuses the material based on predefined CAD data. The build platform is lowered by a layer, and the process repeated until a full part is

fabricated. Figure 14 shows a schematic of the SLM process and a SLM set-up using a double bladed wiper unit for powder spreading¹⁰⁰.

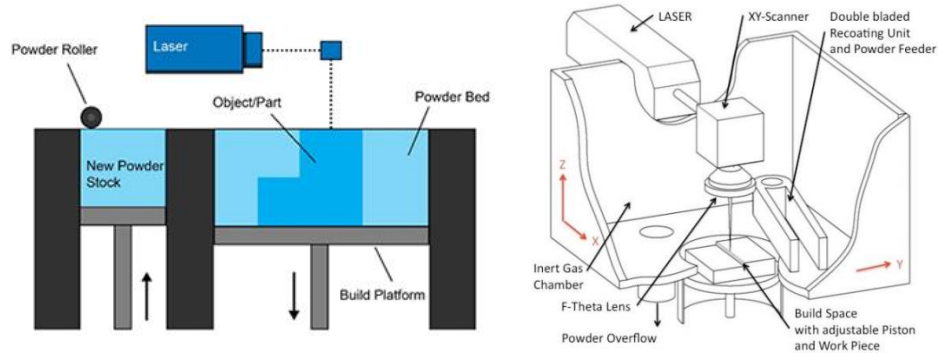


Figure 14 Schematic of a typical SLM/LPBF process¹⁰¹ and typical build chamber¹⁰⁰. A roller or wiper may be used to spread powder across a build platform.

The SLM process is commonly used to process various metals and alloys, with limited literature available on processing ceramics and glasses. Industry has identified multiple applications for SLM processing, particularly for light weight structures through exploitation of the geometrical freedom offered by SLM, and for medical and dental applications⁸¹. SLM is characterised by certain advantages over alternative AM methods for certain materials. The lasers typically utilised in SLM are often more suited for melting high temperature materials than, for example, material extrusion. Fabricated parts may have higher density than in sintering processes, and may require fewer support structures than other techniques (such as Material Extrusion and SLA), as powder beds offer integrated support¹⁰². SLM also offers significantly increased geometrical complexity, outperforming some AM methods, like material extrusion, and many conventional manufacturing techniques, such as machining.

2.5.2.1 Parameters for SLM

For SLM processing, there are many variables that can impact success of processing and resulting part quality (e.g., microstructure and mechanical properties). Important parameters to consider include laser power, laser wavelength, spot size, scanning speed, hatch spacing, layer delay, and layer thickness, as these can all impact the melting behaviour of powder materials in SLM¹⁰³. Energy density is sometimes used to relate SLM processing parameters to describe energy absorption and is discussed in Section 2.5. Powder feedstock characteristics are equally important to consider in SLM.

Hatch spacing refers to the distance between adjacent laser scans in any SLM part. A small hatch spacing defines scan tracks as closer together, with a greater number of scans per given area (than compared with a large hatch spacing). Scanning strategy refers to the programmed travel of the laser during processing, and has been shown to have an effect on part properties, including part density, geometrical accuracy, and cracking in SLM of metals^{104–106}. There are multiple options for scan strategy in commercial SLM systems, from simple line scans, to checkerboards, to complex fractal scans, as well as utilising multiple scans per layer for remelting, all of which have an impact on melt pool orientation (Figure 15)¹⁰⁷. Scanning strategy has been found to have a significant effect on residual stress in SLM, with short scan tracks inducing less residual stress than longer ones¹⁰⁸. Island scan strategy is recommended for reducing residual stress due to the short scan tracks utilised in this pattern¹⁰⁹. A rotation of 67° between layers maximises the number of layers between repeated scanning of the same direction and orientation on the build (360 layers). This is thought to reduce build up of stresses from repeated laser scanning in adjacent layers. Scan rotation has been reported to have no effect on part density, but may impact mechanical characteristics^{105,110}. More complex fractal scan strategies utilising short length scan tracks produced superior bulk density of parts to the island scan strategy. Directionality has also been found to effect part characteristics, with unidirectional scanning resulting in isotropic stress fields¹¹¹.

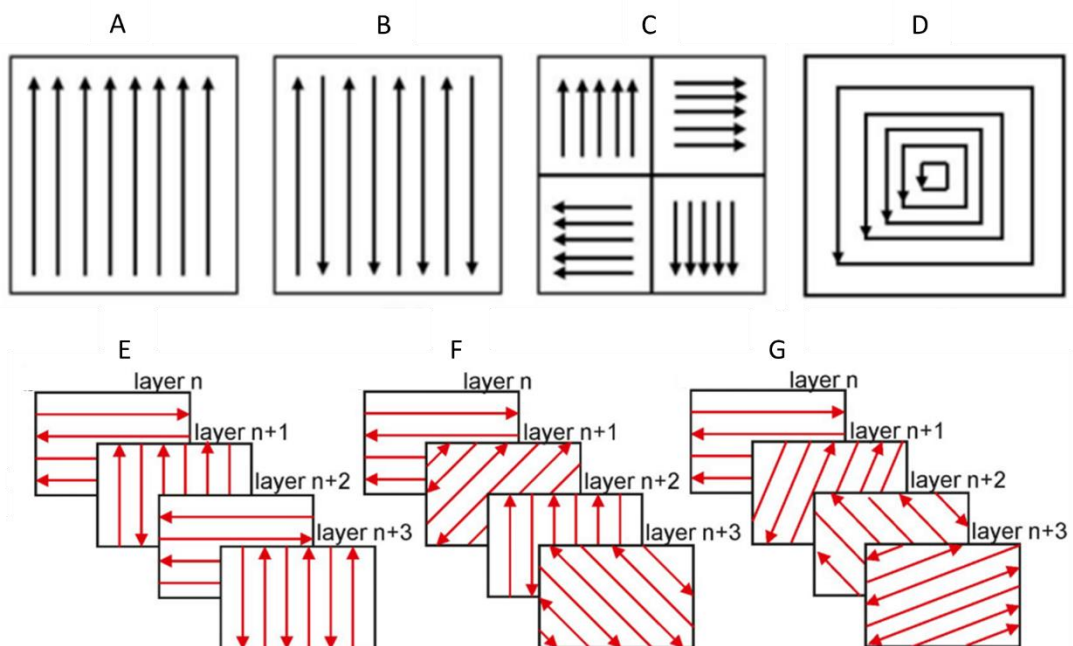


Figure 15 Examples of SLM scan strategies (A: Unidirectional scan, B: Bi-directional scan, C: Island scan, D: Helix scan)¹⁰⁷ and hatch rotations (E: 90° rotation, F: 45° rotation, G: 67° rotation)¹⁰⁵.

In SLM, a powder must have sufficient flowability to form a homogenous powder bed, with consistent layer thickness determined partially by particle size, to allow successful processing¹¹². Particle size and size distribution impacts the flowability of a material as well as packing density within powder beds, and has been reported to impact SLM part properties as a consequence¹¹³. In SLM, particle size dictates the minimum layer thickness, and therefore surface finish and resolution of parts¹⁵. Powder beds consisting of large particles or agglomerates result in poor packing density and can lead to porosity within built parts¹¹². Recommendations have been made for suitable particle size distributions (PSD) of powder materials for SLM processing; 15 – 45 μm particle size distribution is often used for laser powder bed fusion AM, and is expected to provide a well packed powder bed, where fine particles fill the voids around larger particles¹¹⁴. Finer particles are recommended in small proportions to fulfil this function without causing a significant reduction in flowability due to increased inter-particulate forces¹¹⁵.

The presence of fine particles within a powder feedstock increases the pick-up of moisture, increasing cohesion (and therefore reducing flow characteristics)¹¹⁴, with Muniz-Lerma et al. reporting a reduction in moisture sorption when a narrow particle size distribution and large spherical particles ($>48 \mu\text{m}$) are used. Moisture containing powders have also been linked with the formation of agglomerates during spreading, impacting the uniformity of powder beds, and a reduction in relative density of powder layers¹¹⁶.

Another powder characteristic that has a large impact on the formation of powder beds is particle morphology. Compared to angular or irregularly shaped particles within a feedstock, spherical particles have lower surface friction and are less impacted by mechanical interlocking^{114,117,118}. Spherical powders are recommended^{114,117,118} in order to achieve a sufficient flowability for powder spreading, and a high packing density¹¹⁸. A high packing density (ratio of the solid volume to the total volume in the powder bed) is beneficial in SLM as it increases the absorptivity of the powder bed, and the thermal conductivity via increased particle contact, with Tran et al. suggesting a packing density above 50% as suitable for SLM¹¹⁹⁻¹²². Liu et al. compared a wide PSD (0-45 μm) with a narrow PSD (15-45 μm) for SLM processing and reported that a wide PSD can result in high density parts with smooth surface finish thanks to a high packing density, however, powder flowability may be superior for powders with a narrow PSD¹²³. Additionally, Sofia et al. reported particle size and modality significantly affected energy density required for SLM of glass beads¹²⁴. For these reasons, powder characteristics such as PSD, morphology, and flowability (including cohesion, moisture

content etc) should be considered when optimising glass powder processing by SLM. For example, ideal glass feedstocks should have a largely spherical morphology, have an appropriate PSD for SLM processing (<100 µm), a flowability that allows a suitable packing density (above 50%) and formation of uniform powder layers, and be dried of moisture before processing.

The time between laser scanning and spreading of a subsequent powder bed layer, referred to as “layer delay” within this work, (also known as inter layer time, and dwell time, among others) has also been shown to impact LPBF. The time taken between laser scanning and spreading of the next powder layer alters temperature gradients during processing, impacting the energy density required for processing. Depending on the material, a short delay may result in accumulation of energy focussed around the scanned area, resulting in excess heat transferring to new layers of virgin powder, distorting geometries as excess powder is melted by conduction¹²⁵. A longer delay may be considered in order to allow dissipation of heat from scanned areas, however this must be balanced to avoid the higher temperature gradients from cooling and possible delamination or curling of parts¹²⁶. Mohr investigated “inter layer times” (ILT) of 18 s, 65 s, and 116 s when processing 316L stainless steel by LPBF, reporting that a short ILT (18 s) resulted in significant heat accumulation over the build height, an increase in the melt pool depth of up to 20%, increased porosity, and a reduction in hardness by 20% when compared to intermediate ILT (65 s)¹²⁶. Other studies investigating the impact of layer delay for other AM techniques generally agree, such as Laser Engineered Net Shaping (LENS) of 316L stainless steel, and Ti-6AL-4V^{127,128}. Yadollahi et al. reported that a short ILT (10 s) resulted in a coarser microstructure of LENS fabricated 316L stainless steel parts, lower compressive strength, tensile strength, and hardness when compared to specimens fabricated with a long ILT (100 s), due to the decreased cooling rate¹²⁷. The size or number of parts on a build platform influences the delay between laser scanning and powder spreading, and has been shown to have an effect on mechanical properties for some materials¹²⁹. This can be exploited to control the layer delay in systems that do not offer direct control over this variable.

2.5.2.2 State of the Art in Glass SLM

For glass processing, SLM presents certain challenges to overcome. Particularly, large thermal gradients required for processing high temperature materials (such as glass) by laser power subjects parts to thermal stresses, creating residual stresses within parts, and risking formation of cracks and fracture from thermal shock. The thermal gradients for glass processing by SLM are dictated by the temperature of the substrate/chamber (e.g., room temperature for no heating, 250°C for some SLM machines), and the temperature of the laser irradiated glass (dependent on the composition, e.g., T_g of soda lime silica is ~550-600°C (see Section 2.1), and the laser processing parameters). To counter these high thermal gradients, utilising a high temperature chamber and powder bed could allow processing at lower energy density, protecting parts from thermal shock. Similarly, gradual cooling over a long period of time post process will protect parts from the thermal stresses related to part cooling.

Processing glass by SLM has been of interest in recent years, with a few publications demonstrating the potential of glass AM by this technique. Fateri et al. demonstrated the feasibility of processing soda lime glass by SLM, using a Yb:YAG fibre laser at 1070 nm wavelength to fabricate multilayer parts and reported suitable processing parameters¹³⁰. The work confirmed that melting of soda lime silica could be achieved using laser irradiation in the NIR wavelength region. Low surface roughness (R_a0.88 µm), and high part density (99%) were reported for selected geometries and processing parameters. Geometrical accuracy was influenced by laser processing parameters, with the potential for 100% dimensional accuracy suggested to be achievable with optimal parameters. Cylinders of 20 mm total diameter, 18 mm inner diameter and 10 mm height were fabricated using parameters of 60 W laser power, 67 mm/s scan speed, 50 µm hatch spacing (referred to as offset value), and a layer thickness of 150 µm. 99% part density and 100% accuracy was reported for this geometry. A heat affected zone was observed for non-optimal process parameters, distorting the desired geometry, and rapid cooling of parts led to parts cracking from thermal shock. Structures were fabricated to demonstrate achievable geometries such as dental prototypes, thin pin specimens, and objects for jewellery applications¹³¹. In further work, Fateri et al. investigated the effect of scan strategy on glass SLM, presenting significant differences in part appearance as a consequence of scan patterns (Figure 16)¹³².

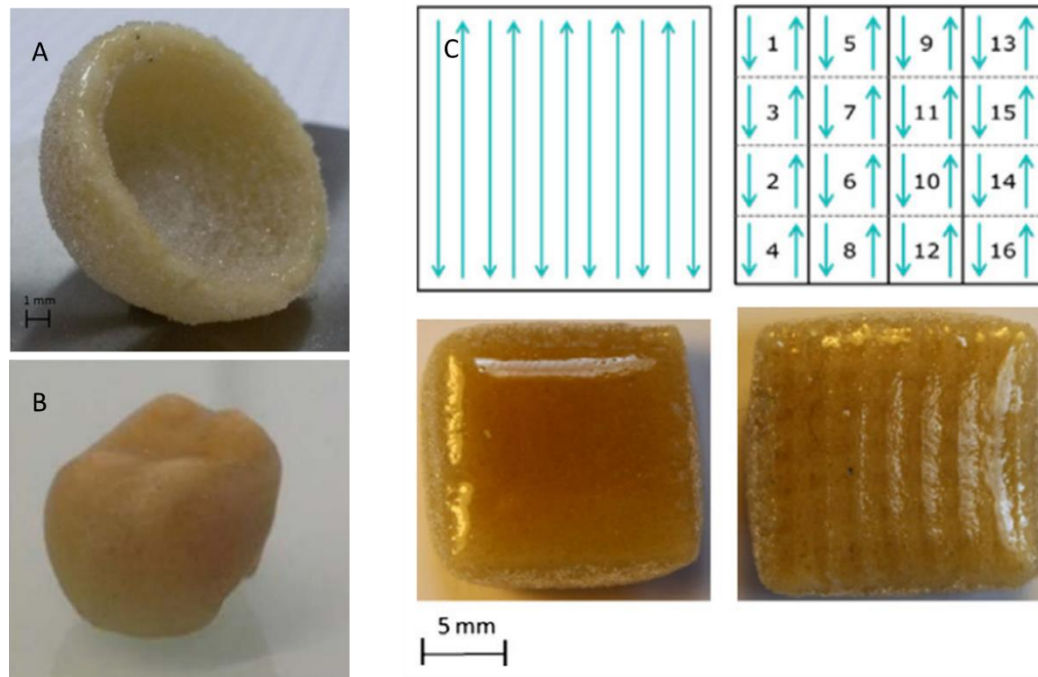


Figure 16 Investigations into SLM of soda lime glass by Fateri et al.^{130,132} A: A dome geometry, B: Tooth prototype, C: The effect of scan strategy on glass part appearance, Left: “line”, Right: “checker-board”.

Khmyrov et al. explored the feasibility of processing fused silica on substrates of fused silica by SLM^{133,134}. A CO₂ laser was operated out of focus to melt the silica powder bed at various parameters. Silica beads melted and adhered to the substrates which did not crack during single layer SLM processing. The avoidance of cracking is likely due to the thickness of the fused silica substrates (5 mm), and the durability of the composition (fused silica glass has the lowest specific thermal expansion and highest resistance to temperature changes). A small particle size (<20 μm) and small layer thickness was found to improve porosity of parts and adhesion of melted feedstock to substrates. Further, a model was presented for estimating the thermal conductivity of the fused silica feedstock, predicting improved consolidation with reduced feedstock particle size and layer thickness¹³⁵. The method of creating a powder layer in this study was through water suspension and deposition of the material on substrates. While this accommodated the fine particle size, it was not representative of the powder bed formation methods in commercial SLM systems, where powder flowability would be essential for formation of a homogenous powder bed. This method of powder bed formation would be unsuitable for preparing glass compositions that show water solubility. Additionally, for some glass compositions (e.g., soda lime silica), the presence of moisture may cause bubbles to form within the glass melt during laser irradiation as the water evaporates¹³⁶. Preheating of feedstock was suggested to increase the temperature of the powder bed prior to laser scanning to accelerate consolidation, as well

as reduce residual stresses. The work presented by Khmyrov et al. demonstrated the feasibility of melting fused silica glass by laser irradiation, and described challenges such as narrow processing windows. The reported processing window was 21-24 W laser power, 0.9 mm/s scan speed, and 150-200 μm layer thickness. Geometries were limited to fused beads, single tracks, and monolayers. Parameter investigations did not consider hatch spacing and scan strategies for multi-layer processing, and material composition was limited to fused silica, a glass known for its durability (exceptionally low thermal expansion coefficient, $\text{CTE} = 0.5 \times 10^{-6}/^{\circ}\text{C}$)³. While cracking of substrates was avoided, it is possible, though the authors of the study did not comment on this, that this is due to the glass composition of feedstocks, the thickness and composition of substrates, and the geometries processed.

Due to the use of a powder feedstock, SLM parts are often characterised by high surface roughness, and poor dimensional accuracy. Surface roughness can be attributed to partially fused powder particles adhered to melted structures, reducing the smoothness of parts. Surface roughness depends on many factors, such as material, particle size distribution, layer thickness, processing parameters (laser power, scan speed, hatch spacing etc), scan strategy and post processing of parts^{113,137}.

Surface roughness of glass LPBF parts were reported by Fateri and Gebhardt, and Klocke et al, reporting R_a (average roughness of a surface) or R_z (maximum height of the profile, based on the average of the five tallest peaks and five biggest troughs in the profile) to represent surface roughness. Laser sintering of borosilicate using optimal parameters (9 W laser power, 225 mm/s scan velocity, 0.15 mm hatch spacing, and 100 μm layer thickness) resulted in a R_z value of 152 μm ⁹⁴. Laser sintering of other materials is known to produce varying surface roughness values depending on build orientation, and post processing treatments are often used to improve surface quality, e.g., lacquering¹³⁸. Laser sintering of polyamide 11 with a 100 μm layer thickness has been reported to have R_z values of 75-100 μm depending on orientation and process parameters¹³⁹, much lower than the R_z value reported for laser sintering of borosilicate by Klocke et al. In Fateri et al's study, surface roughness and part density of SLM fabricated soda lime silica glass cubes of 15 x 15 x 7 mm were measured and reported. Optimal process parameters of 100 W laser power, 50 mm/s scan speed, 100 μm hatch distance, and 500 μm layer thickness were used. The average surface roughness of the top surface was reported as $R_a = 1.70 \mu\text{m}$ and $R_z = 7.81 \mu\text{m}$ ¹³². To improve surface roughness and appearance of glass parts, post processing steps may be required (as suggested by Fateri et al.), such as polishing or remelting of surfaces through heat treatments. Fateri reported an

improvement of SLM borosilicate glass surface roughness from $R_a = 2 \mu\text{m}$ to $R_a = 0.9 \mu\text{m}$ after CO_2 laser polishing¹⁴⁰

Gan et al. investigated SLM processing of spodumene glass ceramic powder (wt%: 65.7 SiO_2 , 25.4 Al_2O_3 , 7.1 Li_2O 1.8 others)¹⁴¹. A SLM system equipped with a Yb fibre laser was used to process 45 x 4 x 3 mm spodumene samples using different layer thickness (50, 100, 150 μm), and different post process heat treatment cycles (as printed, 850°C or 950°C for four hours with a heating/cooling rate of 5°C/min). Characterisation of parts was carried out to assess porosity by micro computed tomography (XCT), flexural strength by three-point bend testing, and crystallinity by X-Ray Diffraction (XRD). It was found that porosity was inversely proportional to the layer thickness. Thinner layer thickness was more sensitive to vaporisation caused by excessive heating during processing, leading to bubble formation, and therefore increased the internal porosity of parts. Flexural strength was found to improve with post processing at higher temperatures and XRD revealed crystallinity within parts. The dimensional accuracy of parts was not reported, and images showed variation in the appearance of the top surface of parts (Figure 17).

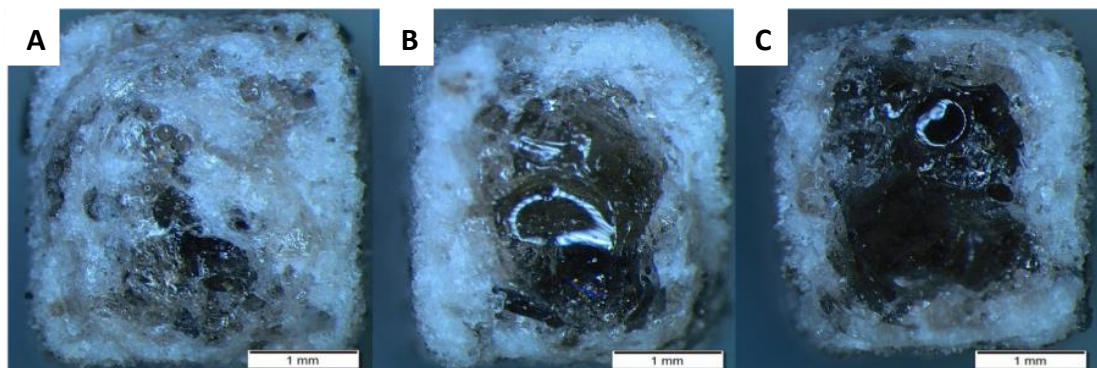


Figure 17 SLM processing of spodumene glass ceramic using A: 50 μm layer thickness, B: 100 μm layer thickness, and C: 150 μm layer thickness. The appearance of the top surface of parts shows variation in transparency/appearance¹⁴¹.

Bulk metallic glasses (metallic amorphous alloys, made by rapid quenching of metallic liquids) have also been of interest for SLM processing in literature, due to the potential for good mechanical properties (low Young's moduli, high yield strength, good fatigue resistance), and biocompatibility^{142–144}. Deng et al. investigated SLM of a biocompatible bulk metallic glass: 47% Ti, 38% Cu, 7.5% Zr, 2.5% Fe, 2% Sm, 1% Si, 2% Ag, for the application of biomedical implants¹⁴⁵. Laser processing parameters were 60 W laser power, 2000 mm/s scan speed, 140 μm hatch distance, and 40 μm layer thickness, with a 90° scan rotation. High density was

reported for fabricated parts (>98%), with evidence of 10-30 μm diameter pores present in cross sections, and larger defects present on the sample edges. The authors reported that SLM samples fractured at lower stress than as-cast samples of the same material (SLM:~ 1690 MPa, As-cast: 2000 MPa), and attributed this to defects introduced during SLM processing. Complex geometries were fabricated and reported to be fully glassy with a relatively smooth surface (Figure 18). Further optimisation and investigation into mechanical properties of parts would be required to assess the suitability of this material and processing technique for the suggested application.

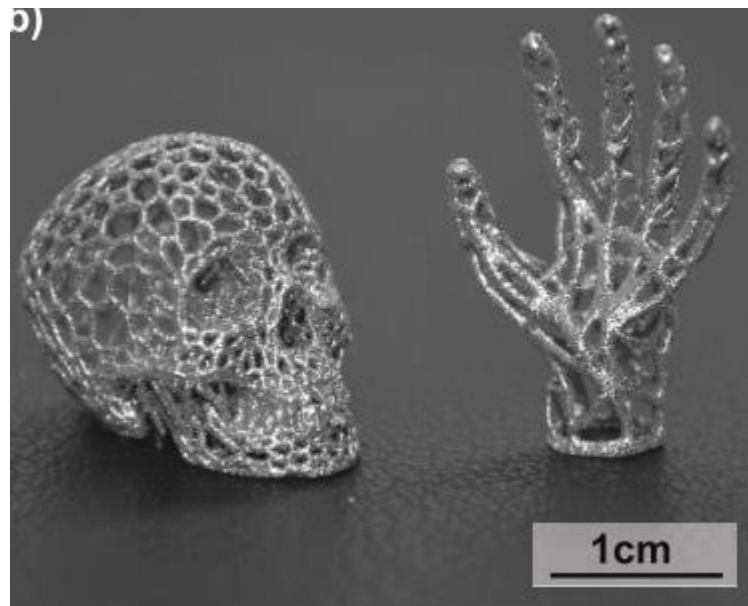


Figure 18 Examples of complex geometries fabricated by SLM of a Ti-based bulk metallic glass. Parts were reported to be fully glassy and relatively smooth.

Poor dimensional accuracy of LPBF of glass parts is often reported and attributed to conduction of energy through the powder bed to adjacent particles, resulting in unintentional fusion of additional material to processed surfaces^{94,130}. This could potentially be accounted for in the CAD creation stage, or resolved through optimisation of processing set-up and parameters (e.g. optimisation of energy density and scan strategy)¹²⁴.

2.6 Directed Energy Deposition

Directed Energy Deposition (DED) is an AM technique that utilises a high powered energy source to simultaneously melt wire or powder feedstock as it is delivered to a substrate. The method is also known as Laser Engineered Net Shaping (LENS), Direct Metal Deposition (DMD), Laser Cladding, Electron Beam Additive Manufacturing, and Directed Light Fabrication. This AM technique is well established for processing metal feedstocks, yet little literature is available on DED processing of glass and ceramic materials^{15,146–148}.

A typical DED machine setup comprises three parts: a focused energy source (e.g. a laser, electron beam, or plasma arc), a nozzle for feedstock delivery (usually made of copper, stainless, or hardened steel) be it powder, wire, or fibre form, and a build platform (Figure 19). Due to the potential for mounting nozzles on a 4 or 5 axis arm, this method is often used for repairing defects on existing parts, or fusing additional material to built components, however, it can also be used to fabricate whole parts from start to finish. While many setups mount the material delivery nozzles on a multi-axis arm which travels around a fixed object or substrate during processing, it is also possible to utilise a fixed nozzle with a moveable build platform via a translational or rotational stage. With multi-axis DED, material flow rate does not change with movement of the feed head, however, a system utilising fixed, vertical deposition may be affected by this¹⁵. Like many AM methods, the DED process can be controlled by 3D CAD data, translating 3D models into multiple slices for layer processing.

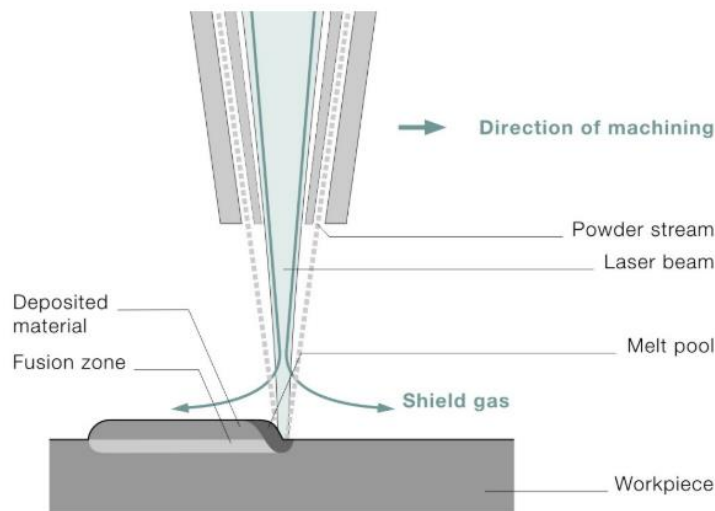


Figure 19 Schematic of the DED process (for powder feedstock)¹⁴⁶.

Post processing is usually required for DED fabricated parts. Heat treatments reduce the residual stresses in parts and improve mechanical properties, and often subtractive techniques (e.g., machining) are used to achieve the final desired part or improve surface finish. For some parts, removal from substrates may be required. Hybrid processes are being developed to integrate DED processing and post processing tools for efficient, one-step manufacturing¹⁴⁹.

In DED, feature size (the smallest scale at which a feature can be fabricated) and layer thickness (the thickness of a deposited layers) are limited by the size of the feedstock (powder particle size or wire diameter), and by the diameter of the heat source (laser spot size). Higher resolution (small layer thickness, small feature size) and dimensional accuracy is generally achieved with powder-fed DED compared to wire processing, but presents higher surface roughness¹⁵⁰. Theoretically, 100 % feedstock capture is possible when using a filament fed process, and capture rate is lower with powder delivery, however, as a result, powder-fed DED can offer greater geometric flexibility, allowing overlap of scan lines without losing dimensional accuracy¹⁵. DED processing of wires and filaments often suffer from visible layers within parts, requiring further optimisation or post processing to improve appearance.

In powder-fed DED, flowability impacts the way a powder behaves when fed through nozzle systems, effecting powder delivery and deposition rates. Powder can be delivered to substrates via different nozzle systems (Figure 20). An off-axis configuration, where a single nozzle delivers powder to the substrate laterally to the laser beam, and a coaxial nozzle that delivers a toroid powder flow to the laser are common in DED. Lateral nozzles are most suited to 2D applications due to the effect of processing direction on scan tracks¹⁵¹. Off-axis nozzles are easy to use, but have been reported to result in varying deposit height dependent on scan direction with relation to direction of powder delivery¹⁵². Coaxial nozzles do not suffer from this limitation and provide higher powder capture rates. DED processing using powder feedstocks is sensitive to many factors, including process parameters, material properties, and machine set-up¹⁵³. Processing glass feedstocks by powder-fed DED requires consideration of material characteristics, such as particle size distribution, morphology, and flowability, and their behaviour through automatic powder feed systems. Optimisation of feed parameters is also necessary to achieve accurate and consistent delivery of material to the substrate. This may include consideration of the nozzle position in relation to the laser beam, and the rate of material delivery, for example, the speed of metering discs (i.e., rotation speed, RPM), and the pressure of carrier gas^{150,154}.

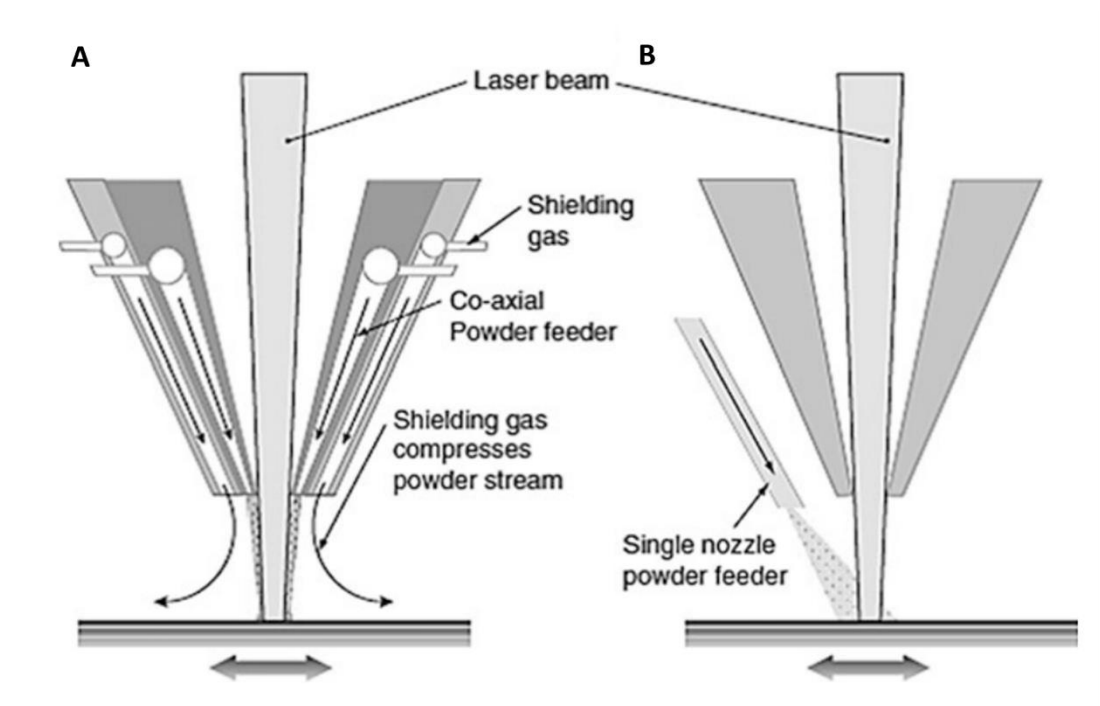


Figure 20 Schematic of two powder delivery nozzles for DED processing. A: Coaxial nozzle, indicating the stream of powder delivered through an annular orifice, compressed by shielding gas. B: Single nozzle for powder delivery laterally to the laser beam. Taken from Gibson, Rosen and Stucker¹⁵.

2.6.1 State of the Art in Glass DED

Glass filaments have been used to demonstrate the feasibility of glass processing by DED methods. Rudimentary geometries of single tracks/walls were fabricated through deposition of soda lime silica glass filaments (“1 mm soda lime glass stringer, Bullseye Glass Co”) onto glass microscope slide substrates (of the same composition), and simultaneous irradiation by a CO₂ laser (Figure 21)^{155,156}. The initial parameters used to process the soda lime glass filaments were 25 W laser power and 1 mm/s scan speed. Stage heaters were employed to reduce thermal gradients during processing by heating to around the glass annealing temperature of the feedstock and substrates (~530°C), and parts were allowed to cool gradually, thus reducing the chance of cracks forming within parts. Filament quality impacted optical properties and transparency of fabricated parts. Geometrical complexity wasn’t explored beyond simple structures, and post process polishing was used to improve the appearance and transparency of fabricated parts. In further experiments, a scan speed of 0.5 mm/s and laser powers between 10-50 W were investigated for processing the same soda lime glass filaments, and the contact angles (θ , angle of a liquid-solid interface) of the cross sections of deposited soda lime tracks were recorded. The lowest energy density tested (10

W, 0.5 mm/s) was insufficient for melting the filament. For laser powers above 35 W (at 0.5 mm/s scan speed), full melting was achieved as indicated by a contact angle below 90° . The effect of last processing parameters on the temperature of the melt pool was estimated. A model was used to estimate the temperature of the melt pool at different combinations of laser power and scan speed. The melt pool temperature at 10 W laser power and 0.5 mm/s scan speed was estimated as 1233°C , corresponding to a viscosity of 1000 Pa s for the soda lime silica glass.

Luo et al. investigated DED of borosilicate glass filaments (Schott Duran 3.3: $\sim 80 \text{ SiO}_2$, $12 \text{ B}_2\text{O}_3$, $4 \text{ Na}_2\text{O}$, $2 \text{ Al}_2\text{O}_3$ – Tg 525°C , softening point: 825°C , annealing point: 560°C), using a CO_2 laser to melt 2 mm diameter filaments¹⁵⁷. Bubble entrapment from filament defects, and bubble formation from reboil (the sudden reappearance of bubbles during remelting of glass or increases in melt temperature³⁴) reduced the optical quality of processed glass structures. The temperature of melt pools increased with laser power, as did bubble concentration. Luo used a spectrometer to monitor temperatures within melt pools for filament-fed DED of borosilicate glass¹⁵⁸. Temperatures between $\sim 700^\circ\text{C}$ to $>1900^\circ\text{C}$ were measured depending on laser power and scan speed, with the highest melt pool temperature measured for 0.1 mm/s scan speed and 60 W laser power. The contact angles of the deposited glass filaments (cross sections) were inspected for processing parameters of 0.5 mm/s scan speed and 25-60 W laser power. $\theta > 90^\circ$ was used to define instances where the deposited glass was not fully melted. Processing parameters that resulted in a contact angle of $<90^\circ$ were 0.5 mm/s scan speed at laser powers of 50 - 60 W, with lower energy densities resulting in $\theta > 90^\circ$. Contact angle measurements suggested that the viscosity of the borosilicate filaments was sufficient when melt pool temperatures were between $1500\text{-}1800^\circ\text{C}$. In this study, substrate temperatures were maintained at 450°C to prevent cracking of glass parts during processing from thermal shock. A correlation between temperature of the melt pool and bubble formation within melted glass structures was also found, with the chance of reboil in borosilicate melt pools during DED increasing as the temperature approached 1600°C . A model for calculating average melt pool temperatures was also proposed. Annealing and polishing of parts was used to reduce residual stresses and improve optical appearance.

Fused silica (quartz) has also been used to demonstrate the potential of filament fed DED processing of glass materials^{159,160}. Initial studies investigated the welding of two quartz glass plates of 2.6 mm thickness by a CO_2 laser of varying spot size diameter (5, 8, 10, 12 mm), using a scan speed of 0.5 mm/s and laser powers between 40-130 W¹⁵⁹. The required temperature to achieve a suitable viscosity ($10^4 - 10^{7.5}$ Pa s) of the quartz glass used in the

experiment was reported to be 1800 – 2230°C. The surface temperature of the glass plates was monitored by IR pyrometer, with higher surface temperatures recorded for smaller spot sizes, suggesting larger spot sizes (>5 mm) related to a wider processing window. For example, with a constant scan speed of 0.5 mm/s, a narrow processing window was seen for the 5 mm diameter spot size, with temperatures of ~2200°C being reached at laser powers below 200 W, whereas a larger spot size diameter of 12 mm showed a wider processing window with laser powers up to 600 W not reaching 2200°C. Pohl et al., also reported the benefits of a polymer coating on quartz glass fibres to allow fibre delivery without breaking the feedstock¹⁵⁹. The coating was reported to evaporate during processing, leaving a trace amount of carbon on the glass surface after combustion by laser irradiation.

Developing the investigations further, von Witzendorff et al. demonstrated the melting of the 0.5 mm diameter polymer coated quartz glass filaments using a CO₂ laser to create rudimentary structures on glass substrates¹⁶⁰. The parameters investigated were 90 and 120 W laser power, at scan speeds between 20-400 mm/min. Suitable parameters for continuous processing of a multi-layer cylinder were 120 W laser power and 250 mm/min with fibre feed and axis movement in the same direction. The processed glass was transparent but had discernible layers, with resolution limited by the wire feedstock diameter (0.5 mm). Quartz fibre feedstock required a 50 µm thick polymer coating to avoid breaking during feeding. The possibility of shrinkage due to polymer content evaporation during processing was considered, however no detrimental effect was reported. Discontinuous processing was possible when laser processing parameters resulted in very high fibre temperatures, leading to a low viscosity, and regular deposition of glass droplets onto the substrate surface.

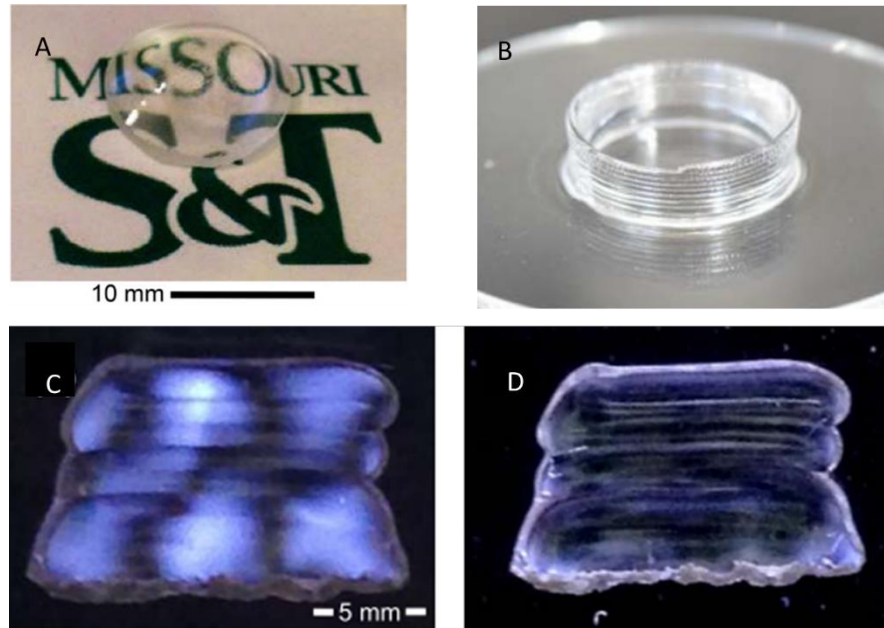


Figure 21 Glass processing by filament-fed DED A: Convex soda lime glass part¹⁵⁶. B: 20 mm diameter hollow cylinder of quartz glass¹⁶⁰. C: Glass wall before post-process heat treatment and D: Glass wall after post process heat treatment showing reduction in residual stresses¹⁵⁷.

CO ($\lambda = 5.3 \mu\text{m}$) and CO₂ ($\lambda = 10.6 \mu\text{m}$) lasers were used to melt quartz filaments of 0.5 and 1 mm diameter¹⁶¹. The volumetric deposition rate was measured for 0.5 and 1 mm filaments processed by CO and CO₂ laser irradiation. A slow deposition rate was required for filament-fed glass processing by CO₂ laser irradiation due to necessary conduction of sufficient heat through filament surfaces to the substrate interface. For 0.5 and 1 mm fibres, less than 2 mm³/s was measured as the maximum volumetric deposition rate by CO₂ laser irradiation. Faster deposition rate and lower vaporization was reported for CO laser processing as this allowed volumetric heating of glass feedstocks. The maximum volumetric deposition rate for 0.5 and 1 mm fibres was measured as above 12 mm³/s by CO laser irradiation. The vaporization of glass was reported as a normalised cross-sectional area as a function of scan speed for each laser and filament diameter tested. For example, greater vaporization by CO₂ laser irradiation on 0.5 mm fibres was indicated by a normalised cross sectional area of ~ 0.4 at scan speeds of 0.5 mm/s, compared to a value above 0.6 recorded for CO laser irradiation under the same conditions. A correlation between contact angle and temperature was suggested, concluding that increasing laser power (temperature) altered the morphology of printed tracks, affecting the contact angle of molten glass filament on substrates. A contact angle of $<90^\circ$ was achieved at lower energy for CO laser irradiation compared to CO₂ laser irradiation. For example, at 0.5 mm scan speed, the CO₂ laser required ~ 10 W higher laser power than the CO laser to deposit 0.5 mm fibres with a 90° contact angle. A model was made to analyse the effects of volumetric heating (CO laser radiation) of glass fibres on

contact angle and therefore print quality. Filament-fed glass processing by DED has also been used to demonstrate fabrication of fused silica micro lenses for optics on printed waveguides¹⁶².

Literature scratches the surface of processing oxide glass compositions by DED methods, with particular focus on wire/filament fed processing^{160,161,163}. The feasibility of wire-fed DED processing of a few glass compositions has been proven, achieving rudimentary geometries with a degree of optical transparency. Layers are often discernible, and post processing to improve appearance or reduce residual stresses has been recommended. While there are some publications demonstrating the potential of glass filament melting by DED, there appears to be no reports on the feasibility of powder-fed glass DED, which promises greater geometric complexity and part resolution¹⁵.

2.7 Considerations for Glass Powder Processing by AM

Energy density (ED) has been used in literature to quantify laser energy absorption by powder feedstocks, assigning a single value to different combinations of parameters. This is used to estimate the total energy input to a powder feedstock, under the assumption that a certain energy must be absorbed by powder feedstocks to achieve melting, and that too much energy input would cause unwanted vaporization, helping to define suitable parameters or “processing windows” for different materials¹⁶⁴. For example, volumetric energy density has been shown to effect density, microstructure and mechanical properties of AM parts of various materials^{165–167}. There are different methods of calculating an ED value, and the preferred equations used to describe energy absorption for DED and SLM of glass during this research are defined below.

$$ED = \frac{P}{v \times t} \quad \text{(Equation 1)}$$

$$ED = \frac{P}{v \times h \times t} \quad \text{(Equation 2)}$$

The equations are used to calculate values for “2D” processing (Equation 1) with units of J/mm², and “3D” processing (Equation 2) with units of J/mm³. In these calculations, P: laser power (W), v: scan speed (mm/s), h: hatch spacing (mm), and t: layer thickness (mm). For DED processing, Equation 1 is used with the assumption of t = 1 mm.

Energy density calculations are used to estimate the energy required to melt glass materials in these investigations. Data available in literature of glass processing parameters for SLM and DED of different glass compositions are compiled in Table 3. Unfortunately, ED calculations fail to recognise the effect of every variable within each laser processing system, such as temperature, time, laser spot size, and properties of feedstock materials (such as particle size and specific heat capacity)^{168,169}. With various factors playing a role in glass melting, ED considers just a few of the most significant variables. The use of ED allows population of process maps based on the variables accounted for in the equations, but the limitations of this method should be acknowledged when evaluating the results. Process

maps are not always reported in literature for glass AM processing, and so examples have not been included in this review.

Table 3 Process parameters reported in literature for SLM and DED of different glass compositions. Energy density calculations have been made based on reported parameters and the energy density equations (1) and (2).

Reference	Fateri and Gebhardt (2015) ¹³²	Fateri et al. (2014) ¹³⁰	Luo et al. (2017) ¹⁵⁶	Luo (2017) ¹⁶³	Von Witzendorff (2018) ¹⁶⁰
Material	Soda Lime Silica		Soda Lime Silica	Borosilicate	Quartz Glass
Material Form	Powder		Fibre		
AM Method	SLM		DED		
Fabricated Geometry	15 x 15 x 7 mm Cube	20 mm \varnothing Cylindrical Tube	Wall	Wall	Wall
Laser Power	80 W	60 W	20 W	29 W	120 W
Scan Speed	50 mm/s	67 mm/s	0.25 mm/s	0.1 mm/s	4.2 mm/s
Layer Thickness	0.5 mm	0.15 mm	0.5 mm	1 mm	0.5 mm (fibre \varnothing)
Hatch Distance	0.1 mm	0.05 mm	-	-	-
Energy Density	32 J/mm ³	119 J/mm ³	160 J/mm ²	290 J/mm ²	57 J/mm ²

For SLM, and powder-fed DED, powder characteristics have an impact on processing performance as well as fabricated part quality. Characterisation of feedstock materials is useful for predicting and understanding powder behaviour during AM processing, whether in forming a powder bed, or delivering powder through nozzle systems. Characterisation of morphology, particle size distribution (PSD), chemical composition, transmittance of certain wavelengths, and flowability are some of the main material properties to consider for powder processing by SLM and DED.

The flow characteristics of powders are influenced by the morphology and size distribution of the particles, as well as extrinsic factors such as moisture, and the interactions between moisture and the glass powder. Cohesion of particles within a powder feedstock, caused by electrostatic interactions between particles (particularly between fine particles), also reduces the flowability of a material¹⁷⁰. Cohesive powders can agglomerate due to the strong interactive forces between fine particles, reducing flowability. Moisture content is also worth consideration when dealing with fine powders, as fine particles intensify the pick-up of moisture, increasing cohesion, and reducing flowability^{114,171}. To counter this, drying of

feedstock materials prior to processing to reduce moisture content is recommended. Particle morphology is known to impact flow characteristics of powders, and consequently the success of processing powders by AM¹¹⁴. A Hall Flowmeter gives a simple measurement of powder flowability, however, this data is not always given in literature, and is limited in its ability to quantitatively measure the flowability of a powder (many powders will not flow and are given a value of 0). Characterisation of flow properties using powder rheology can provide more sophisticated measurement of a materials resistance to flow, cohesivity, and packing behaviour^{172,173}.

A flow Rheometer (FT4, Freeman Technology, UK) can obtain quantitative measurements for the flowability of a powder feedstock by rotation of a geometrically complex blade (impeller) (Figure 22). As the blade moves, particles interact and flow relative to one another, the resistance experienced by the blade is measured and used to characterise the bulk flow properties of the material. Multiple material parameters can be measured by this method to indicate flowability, such as Basic Flowability Energy (BFE), Specific Energy (SE), Conditioned Bulk Density (CBD), and Flow Rate Index (FRI).

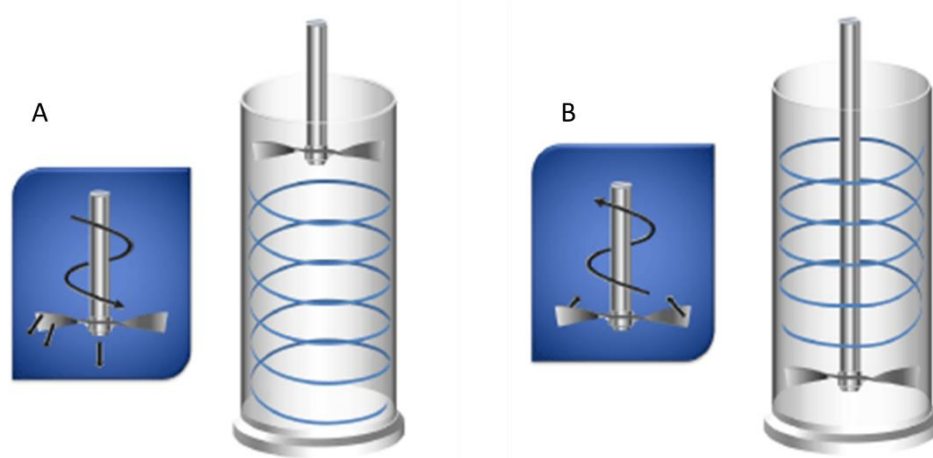


Figure 22 A: Downward motion of FT4 blade to measure BFE. B: Upward motion of blade to measure SE.

Well flowing powders are often characterised by spherical morphology, whereas irregular or angular particles are known to impede flow in various ways¹⁷⁴. Spherical particles reduce friction between particles and suffer less mechanical interlocking than angular particles. It has also been suggested that spherical powders have superior thermal conductivity in powder beds compared to irregular particle feedstocks, increasing the density of laser processed parts¹⁷⁵. As glass powder samples are often prepared through ball milling, resulting powder feedstock is most likely to have angular and irregular morphology (Figure 23)¹⁷⁶.

While flowability of non-spherical powder samples can be improved by adding flow agents, for glass materials morphology can be altered by spheroidising methods. Flame spheroidisation and plasma spheroidisation are the two main methods by which spherical glass materials can be produced (Figure 24).

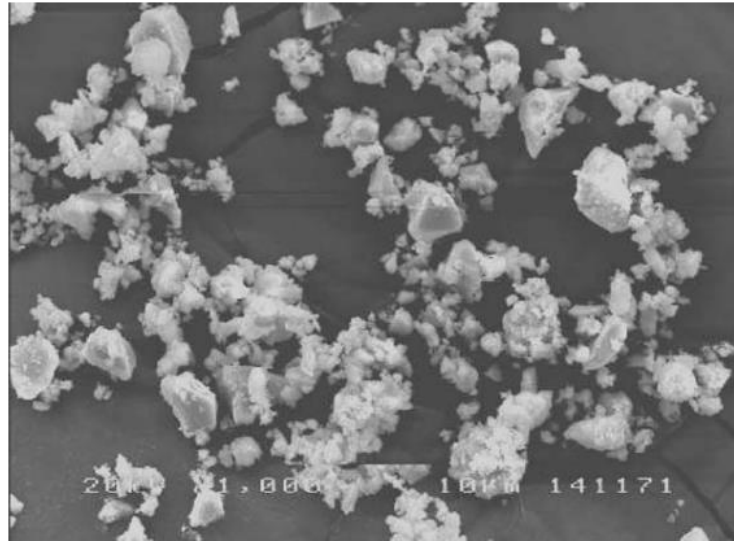


Figure 23 SEM image of a typical angular/irregular morphology of a ball milled phosphate glass powder¹⁷⁶.

Plasma spheroidisation and flame spheroidisation modify particle shape using the same basic principles. Irregular shaped particles are introduced to a hot flame, or high energy plasma, and are melted by the high temperatures. Due to the high surface tension of powder materials, angular or irregular shaped particles become spherical.

Flame spheroidisation has been reported to alter the morphology of different glass compositions, such as phosphate based biologically active glasses (e.g., $45\text{P}_2\text{O}_5$, 16CaO , 24MgO , $11\text{Na}_2\text{O}$, $4\text{Fe}_2\text{O}_3$)¹⁷⁶⁻¹⁷⁹. One of the reported drawbacks to this method is the loss of fine particles during processing, reducing the yield of the spheroidisation process. Flame spheroidised particles are collected in a series of trays set at different distances from the flame, and sphericity varies depending on particles residence time in the flame. In a study by Gupta et al., flame spheroidisation of the previously mentioned phosphate glasses was affected by particle size, with particles $<45\ \mu\text{m}$ undergoing a compositional change, and particles $>200\ \mu\text{m}$ resulting in a large proportion of angular particles and aggregates¹⁷⁸. Additionally, porosity due to gas entrapment was reported. The compositional change was proposed to be caused by more volatile oxides (such as Na_2O and P_2O_5) vaporising more

readily from smaller particle due to their larger surface area to bulk ratio compared to larger particles.

Plasma spheroidisation of glass materials has been shown to produce powders of spherical or near-spherical morphologies¹⁸⁰. Optimisation of plasma process parameters is necessary as the degree of spheroidisation is dependent on plasma power and particle dwell time, as well as feedstock composition¹⁸¹. This method can be used for industrial scale processing using commercial systems with high feed rates, but yield may be low due to vaporisation of particles or material wasted through collection of particles in process chambers¹⁸². Contamination of material is also a risk, and the resulting particle size distribution may be significantly altered^{183,184}.

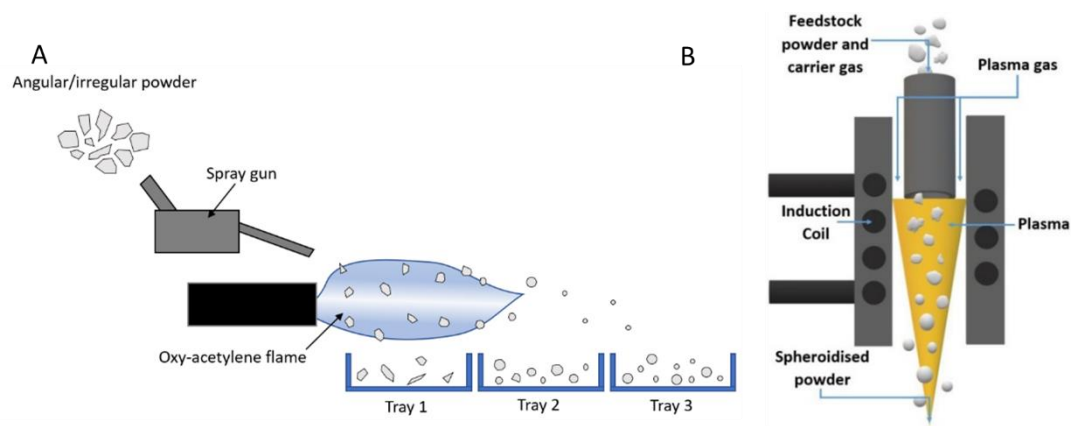


Figure 24 A: Schematic of the flame spheroidisation process. B: Schematic of the plasma spheroidisation process¹⁸⁵.

Another method currently in development for spheroidising powder materials is electron beam irradiation. This process uses a pulsed electron beam to agitate powders whilst remelting their surfaces, modifying morphology, and improving flow characteristics¹⁸⁶. So far this method has only processed small quantities of powder (<10 g per process). With further optimisation, this method could potentially be used to spheroidise glass materials on a larger scale than so far demonstrated.

Finally, the affinity of a material for laser absorption should also be considered when processing powders by laser power. Transparent glass materials are highly transmissive in the near-IR region, meaning that laser absorption could be limited for clear glass. Characterisation by UV-Visible-NIR spectroscopy helps to identify how well a particular material will absorb laser energy at the measured wavelengths. Addition of dopants to glass compositions is thought to improve laser absorption at certain wavelengths. For example, an

Iron Oxide dopant results in a blue-green coloured glass (depending on iron content), with Fe^{2+} and Fe^{3+} existing in equilibrium, increasing the absorbance of soda lime silica at 1050 nm wavelength.^{187–189} Improving the laser absorption of glass compositions could allow laser-based AM processing at lower energy densities, reducing thermal gradients and thus protecting glass parts from thermal shock. Transparent glass substrates should also be taken into account, as transmittance of laser energy at substrate surfaces could impact absorptivity of glass powders.

Glass processing by different laser wavelengths has been reported in literature, such as CO (5.3 μm), CO₂ (10.6 μm), and Nd:YAG (1064 nm) lasers^{98,159–161}. Shi et al., reported that glass materials absorb radiation of $\sim 10 \mu\text{m}$ wavelength (CO₂ laser) at the material surface, and $\sim 5 \mu\text{m}$ (CO laser) is absorbed in the bulk of the material¹⁹⁰. Transmittance was reported as 10.24% at a wavelength of 5.65 μm , and 0% at CO₂ laser wavelengths (Figure 25). Despite the slight increase in transmittance at the CO laser wavelength, the authors suggested that CO laser radiation didn't rely on conduction of heat through the glass surface, as heat was deposited directly into the bulk of the glass ($\sim 300\text{--}400 \mu\text{m}$ penetration). In contrast, CO₂ laser radiation relied on diffusion of heat from the surface, as heat only penetrated $\sim 10\text{--}50 \mu\text{m}$ deep on irradiation. In contrast to CO and CO₂ laser radiation, Nd:YAG/fibre lasers may provide a higher energy density laser spot, capable of fully melting glass materials, compared to laser sintering, however, these lasers may be more expensive^{82,97}.

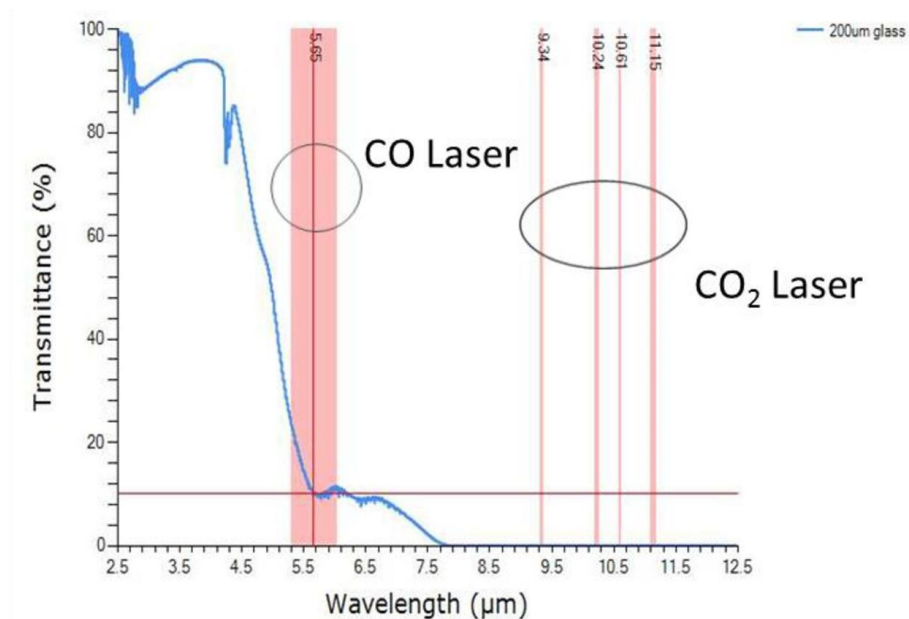


Figure 25 Transmittance spectrum for 200 μm glass, highlighted at CO laser and CO₂ laser wavelengths. An increase in transmittance is seen at CO laser wavelength (5.65 μm), compared to CO₂ laser wavelengths (9.34–11.15 μm)¹⁹⁰.

Soda lime silica, a popular glass for many applications thanks to its low cost, transparency, and wide working temperature range, shows generally high transmissivity at fibre laser wavelengths (Near IR ~700 nm - 2.2 μ m region). Figure 26 A shows a transmission spectrum for a typical soda lime silica glass composition (~73% SiO₂, 15% Na₂O, 7% CaO, 5% others)¹⁹¹. While absorption peaks are more significant beyond 2500 nm, going towards the mid-long wave IR region, there is an absorption peak around 1000 nm, suggesting a soda lime silica glass composition may absorb somewhat at Nd:YAG laser wavelength (1064 nm). For borosilicate glass, transmissivity is also high at 1064 nm, with Figure 26 B showing a transmission spectrum for a commercially available borosilicate glass, Schott Borofloat 33 - Multi-Functional Float Glass, at different glass thickness - 0.7, 2, 5, 9, and 19 mm. The measured absorption also depends on the quality of the glass, and thickness of the glass sample measured, with high purity raw materials leading to higher transmissivity, and increased thickness relating to increased absorption^{192,193}. Figure 26 C shows transmission spectra for a bioactive phosphate glass (45S5 clean and Cu doped), showing similarly high transmission at 1064 nm (Nd:YAG laser wavelength) for the un-doped composition¹⁹⁴. These spectra also demonstrate the increase in absorption in the near-IR region associated with the addition of Cu dopant.

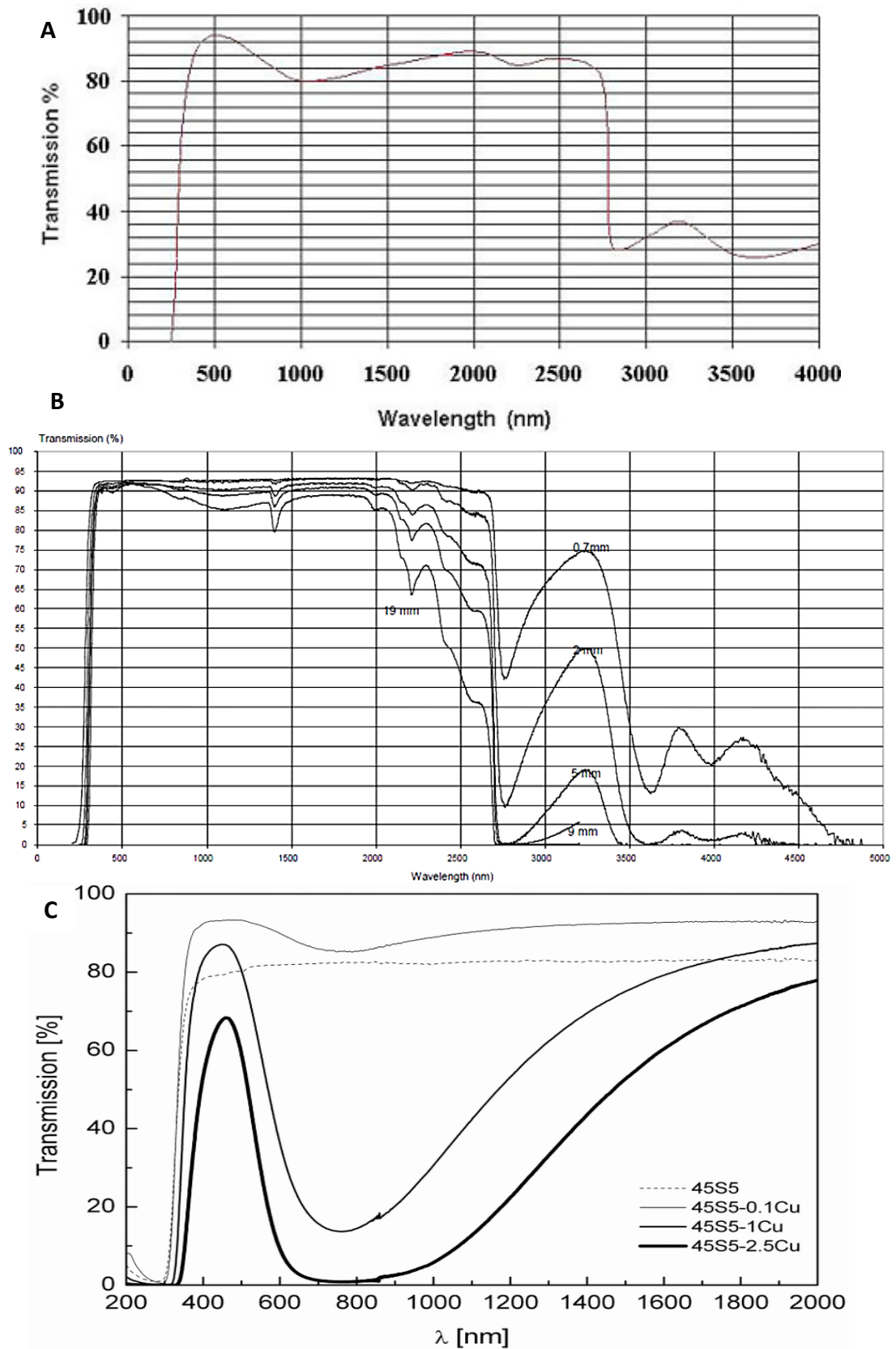


Figure 26 Transmission spectra for A: A typical soda lime silica composition¹⁹¹, B: A commercially available Schott Borofloat® 33 composition at different glass thicknesses¹⁹², and C: A clean and doped bioactive glass (45S5) composition¹⁹⁴.

2.8 Summary

The feasibility of processing glass materials by various Additive Manufacturing methods has been demonstrated in the literature. Each method has presented certain benefits and limitations for glass processing. Some of the key findings from the literature discussed in Chapter 2 are summarised in Table 4. The AM techniques discussed in chapter two, the glass compositions investigated, proposed applications and some key points ascertained from literature are compiled, with some key references stated.

Table 4 Summary of key points from glass AM literature including technique, glass compositions, applications, and strengths and weaknesses.

Technique	Materials	Applications	Key Points	Key References
Material Extrusion	Soda Lime Silica Phosphate Glass (PNKA7) Chalcogenide glass (As ₄₀ S ₆₀) Silica Titania Inks	Tableware Gradient Refractive Index Optics	<ul style="list-style-type: none"> • Low cost • Transparency demonstrated • Complexity and resolution limited 	[58] [60] [61] [62] [63]
Vat Photo-polymerisation	Bioactive Glass (45S5) Glass Ceramics (WDE) Fused Silica	Medical Implants Microfluidics Micro-lenses	<ul style="list-style-type: none"> • Transparency demonstrated • Post processing necessary • Shrinkage common 	[68] [73,75]
Laser Sintering	Bioactive Glass (13-93) Borosilicate Glass Ceramics (LAS)	Medical Implants	<ul style="list-style-type: none"> • High achievable complexity • Post processing often necessary • Shrinkage common • High surface roughness and porosity 	[92] [94] [98]
Selective Laser Melting	Soda Lime Silica Fused Silica Glass Ceramic (Spodumene) Bulk Metallic Glass	Jewellery Prototypes Medical Implants	<ul style="list-style-type: none"> • High achievable complexity • High density parts • Opacity • High surface roughness 	[130–132] [133,134] [141] [145]
Directed Energy Deposition	Soda Lime Silica Borosilicate Fused Silica	Optics	<ul style="list-style-type: none"> • Versatile feedstock (filament/powder) • Glass powder processing not reported • Resolution and complexity limited 	[156,157] [160] [161]

Fabrication of transparent glass parts by AM has been achieved using Material Extrusion, filament-fed DED, and Stereolithography AM techniques. The resolution and geometrical complexity of structures fabricated by extrusion of molten glass was limited and required expensive customised set-ups to accommodate the high temperatures for processing and annealing. DIW and SLA showed promise for processing glass at lower temperatures, using composite inks, and resins as binding mechanisms. The benefit of this is avoidance of large thermal gradients, reducing residual stresses and therefore protecting glass materials from thermal cracking. Anisotropic shrinkage was characteristic for these glass parts due to the necessary removal of non-glass content from the green part via post-process heat treatments. Increased processing time and costs are incurred as a result, and dimensional accuracy of parts was compromised.

Laser powder bed fusion has been explored for a few glass compositions, with and without the use of binding agents, as described in this section^{94,130,196}. Direct laser sintering and SLM does not necessitate the removal of binding agents and offers direct fusion or melting of glass powders in a single step. While direct laser sintering of glass would require high chamber temperatures to allow consolidation by laser irradiation, SLM allows direct melting of glass powders using high power laser energy. Powder bed fusion methods have shown limitations to achievable transparency and have so far produced opaque glass structures of simple geometries (e.g., cubes). Other challenges include thermal stresses associated with high temperature gradients during laser processing, distortion of part geometry due to the nature of powder bed fusion, and feedstock-substrate adhesion. With further optimisation, and consideration of these challenges, SLM has the potential to reliably fabricate geometrically complex glass parts.

DED has been used to melt glass wire/filament feedstocks to form transparent parts. So far in the literature, rudimentary geometries have been presented and resolution was limited due to the nature of processing filament feedstocks. Powder-fed DED of glass materials has not been reported in literature and offers a novel approach to glass processing. While certain challenges would need to be overcome, such as achieving consistent delivery of powder feedstock to substrates, powder-fed processing may have certain advantages over wire fed-DED, such as higher achievable resolution, and higher geometric complexity.

It has been shown that the success of glass processing by AM is influenced by multiple factors, including process parameters, powder characteristics, and processing conditions. The successes and limitations reported in the literature have helped to inform this investigation

into glass processing by AM. Two laser-based AM techniques were identified for further experimentation: SLM and DED.

Chapter 3

Aim & Objectives, and Research Methodology

3.1 Introduction

The versatility of glass lends itself to a variety of applications and industries. The compositions described in Section 2.1 were selected for investigations based on their various properties and characteristics. Soda lime silica was used predominantly throughout experimental investigations due to its low T_g , wide working range, low cost, and availability to the project. As soda lime silica is a common glass composition for glass packaging, this material was chosen for exploring the application of imparting customised décor onto glass packaging for brand differentiation and premiumisation. Borosilicate was another glass of interest due to its low coefficient of thermal expansion and therefore its high thermal resistance, and its chemical durability. This glass was of interest for fabricating customised geometries for glass continuous flow reactors by AM techniques for these reasons. Lastly, 13-93 Bioactive Glass was of interest for investigation into fabrication of customised bone scaffolds. There are other glass materials that have been reported in literature to demonstrate the potential of AM processing, such as metallic glasses and other glass ceramic materials^{145,197,198}. However, in this work the focus was on oxide glasses, as they were chosen based on their chemical properties and the suitability of these glasses for the chosen applications (e.g., soda lime silica for glass bottle décor). These oxide glasses were used throughout experimental research in this work.

From extensive review of the current state of the art in Additive Manufacturing of glass, Selective Laser Melting and Directed Energy Deposition were identified as promising techniques for glass processing. While other techniques have shown promising results for glass processing, many of them required post-process heat treatments to fully consolidate parts and remove non-glass content, often resulting in volumetric shrinkage (e.g., Vat

Photopolymerisation and Indirect Laser Sintering). In contrast, the consolidation of glass materials by SLM and DED has the potential to fabricate glass parts without the need for modification of feedstocks (e.g., formation of a photocurable resin) or thermal post processing, allowing single step fabrication of glass parts. In addition, the industrial sponsor for this project requested the development of techniques for two specific applications – continuous flow reactors (e.g., Figure 27 A-B) and glass bottle décor (e.g., Figure 27 C-D). The geometric complexity achievable by SLM makes it a good candidate for fabricating complex, customised, continuous flow reactor (CFR) geometries. This advantage has been shown for metal reactors^{199,200}, but manufacturing flow reactors from glass would have additional benefits such as transparency (for photochemistry), thermal durability, and chemical inertness. Current methods (e.g., acid etching) for fabricating customised glass continuous flow reactors are time consuming and incur high costs²⁰¹. In contrast, SLM allows cost-effective fabrication of customised, complex CFR geometries, particularly for high value, small production volumes. DED was selected for the application of glass bottle décor, as this technique is suited for processing on large substrates of varying shape and dimensions. It is also a versatile technique able to process different feedstock forms (filaments/powders). Despite the high cost associated with high energy lasers used in these techniques, SLM and DED are capable of directly consolidating high temperature materials, and are likely to achieve superior mechanical properties compared to other AM techniques¹⁵.

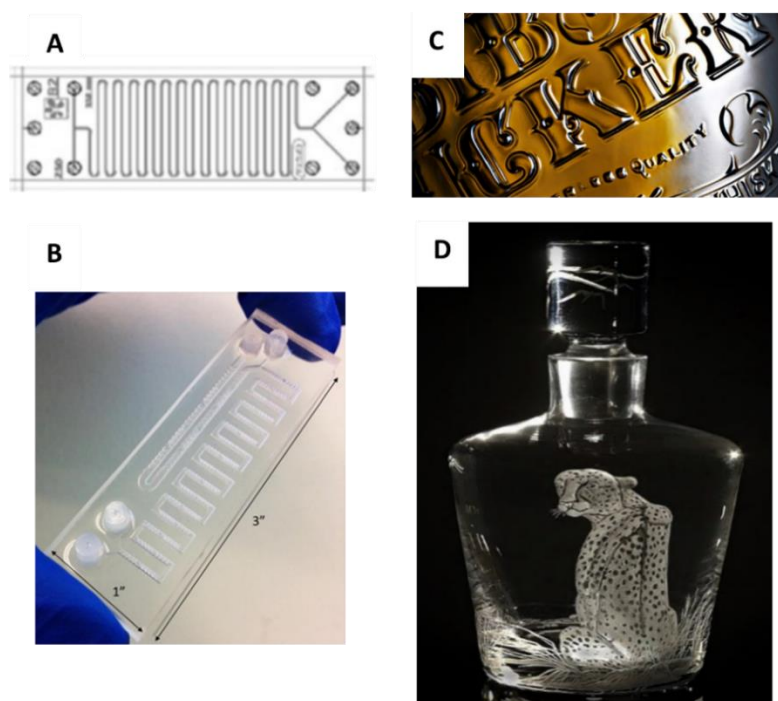


Figure 27 A-B Example microfluidic reactor design.²⁰² Examples of glass décor by C: embossing and D: Engraving.

Chapter three describes the identified research opportunity for developing SLM and DED processing of glass materials (3.2). The aim and objectives of this research are defined in 3.3, and the overall research methodology is presented in 3.4.

3.2 Gap in the Research

Selective Laser Melting is a promising AM method for fabricating geometrically complex glass structures, however, literature has so far only reported simple shapes. Soda lime silica was selected for processing by SLM for this work as it is inexpensive, was available in bulk in spherical form, has a low glass transition temperature (T_g : 550-600°C), and a moderate thermal profile (as described in Section 2.1). Borosilicate was considered for SLM investigations as it is a popular glass material for applications demanding thermal and chemical durability (e.g., microfluidic reactors) thanks to its low thermal expansion coefficient ($\sim 3-5.0 \times 10^{-6} / ^\circ\text{C}$) compared to soda lime silica ($\sim 9.2 \times 10^{-6} / ^\circ\text{C}$)³⁰, however, it was anticipated that higher energy densities would be required to melt and consolidate the feedstock by SLM and may prove more challenging to process. Soda lime silica was supplied in spherical form as commercial ballotini soda lime silica beads, and was expected to show superior flowability to the other angular feedstocks (borosilicate and 13-93 Bioactive Glass) due to the impact of morphology and particle size distribution on flowability and packing density^{114,117,118}.

Several challenges with glass processing by SLM were highlighted in Chapter 2, such as conduction of heat through powder beds causing distortion of geometries, and thermal stresses from high temperature gradients causing structures to crack. There is therefore a need to fully understand the effect of laser processing parameters on laser powder bed fusion (LPBF) of glass, and optimise SLM processing to allow fabrication of complex geometries whilst avoiding thermal shock. Understanding the effects of laser power, scan speed, hatch spacing and scan strategy, as well as material composition, on glass SLM, would help to achieve this, and ultimately define suitable SLM processing parameters for the chosen glass compositions. Installation of substrate heaters may offer a solution to the high thermal gradients inherent to laser processing of high temperature materials and has been utilised in literature for this purpose¹⁵⁵. Understanding glass-substrate interfaces may be gained through investigation of glass SLM processing on different substrate materials. SLM of glass parts on glass substrates is likely to show greater adhesion than other materials due to matching thermal expansion coefficients. Conversely, processing on ceramic substrates could allow easy removal of built parts from substrates post process. In general, a difference in thermal expansion coefficients of less than $2 \times 10^{-7} / ^\circ\text{C}^{-1}$ is recommended for glass sealing and avoidance of fracture at the interface⁴⁵. The greater the difference in CTE, the greater the chance of thermal fracture/seal failure. Optimisation of process parameters for glass-on-

glass SLM has not yet been reported, and could inspire new applications for one-step glass AM processing.

A potential application for SLM of glass on glass substrates is fabrication of bespoke glass continuous flow reactors (CFRs). AM processing offers a high degree of geometrical freedom, allowing the fabrication of complex geometries, with customisation incurring no added cost. Fabrication of CFR geometries by AM techniques offers precise control over geometries (and therefore functionality) with the potential to incorporate advanced mixing features such as baffles, faster manufacturing times, and reduced manufacturing costs compared to existing methods of microreactor fabrication²⁰³. Additive manufacture of CFRs has been demonstrated using polymer and metal feedstocks using material extrusion technology, vat photopolymerisation, and LPBF (Figure 28)^{200,203–207}. The reported polymers lack the chemical and thermal resistance that glass compositions can offer, limiting their application, and fabricated parts were often opaque or semi-transparent^{204–206}. SLM has been used to manufacture opaque, metal CFR geometries, presenting challenges such as hollow structures blocked by unwanted melting of powder via conduction, and difficulties evacuating unmelted powder from hollow structures^{203,200}. These challenges were anticipated going forward. As glass materials have good thermal stability, as well as high chemical durability and inertness, with only hydrofluoric acid, strong alkaline solutions, and concentrated phosphoric acid causing adverse effects, glass CFRs can facilitate a wide range of chemical reactions. Additionally, the potential for transparency, allowing easy monitoring and analysis of reactions, make glass the perfect candidate for glass CFR fabrication^{208,209}. An opportunity to investigate customisable CFR fabrication by SLM of glass powder was identified. As soda lime silica was used preferentially for parameter optimisation, and borosilicate was anticipated to require higher energy densities than soda lime silica for melting and consolidation by SLM, CFR geometries were explored using soda lime silica feedstocks in SLM processing despite its higher thermal expansion coefficient and lower thermal shock resistance.

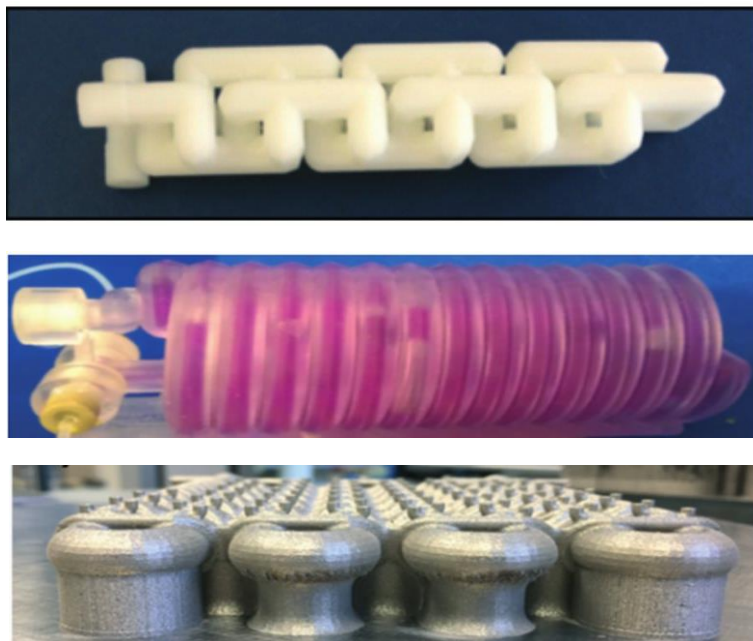


Figure 28 Additively manufactured CFR structures. A: Fused Deposition Modelling (FDM, Material Extrusion) split-and-recombine mixer²⁰³, B: SLA split-and-recombine mixer²⁰³, and C: LPBF stainless steel reactor²⁰⁰.

Directed Energy Deposition is a promising AM method for producing transparent glass structures from glass filament feedstocks. Powder-fed DED has not yet been reported in literature, and offers greater resolution and geometrical freedom compared to wire-fed DED processing. Proving the feasibility of processing glass powder feedstocks by DED, and presenting initial process parameter optimisations would be the first steps towards evaluating powder fed DED as a method for AM of glass.

A potential application for DED of glass powders onto glass substrates is in high value, customised glass packaging, adding value to the glass packaging industry through brand differentiation by customised décor. Soda lime silica glass is a common composition for glass packaging, and therefore soda lime silica powder feedstocks were selected preferentially for DED investigations, to match the composition and CTE of bottle substrates. Glass powder properties were an important consideration for delivery of glass feedstocks, with spherical glass powder expected to provide superior flow rates for consistent powder delivery, compared to angular/irregular feedstock morphologies^{114,117}. Current techniques for imparting design on glass products include embossing, etching, and engraving. Embossing imparts decoration by pressing a mould onto the heated glass object. Customisation of design requires costly fabrication of new moulds, increasing the production cost for bespoke glass packaging. Etching and engraving are subtractive techniques. Etching removes material using hydrofluoric acid or plasma, and engraving removes material by laser or mechanical

means (abrasive wheels and drills, or diamond tipped burrs)^{210,211}. These methods are known to introduce flaws in the surfaces of glass, risking the integrity of glass packaging decorated by these means²¹².

Using DED to impart decoration onto glass surfaces could avoid the high customisation costs and introduction of defects associated with subtractive techniques. As DED is also used to repair objects regardless of their form, curved packaging could be accommodated in certain set-ups.

3.3 Aim and Objectives

The overall aim of this research was to investigate Additive Manufacturing of glass using two direct laser processing techniques: powder-fed DED and SLM. Development of glass processing by AM would improve the catalogue of materials for AM, and encourage adoption of glass processing by AM in industry, inspiring innovation in the field.

This aim was achieved by the following objectives:

- Prove the feasibility of processing soda lime silica glass on a substrate of the same composition by SLM and powder-fed DED
- Adapt experimental set-ups and make recommendations for optimised processing of glass powder materials onto glass substrates by these methods.
- Characterise glass feedstocks for flowability, and assess suitability for processing by SLM and DED.

SLM specific objectives:

- Investigate the effects of processing parameters on glass SLM and populate process maps for processing soda lime silica glass powder on glass substrates.
- Investigate adhesion of glass SLM parts on glass substrates.
- Investigate the effect of temperature on SLM processing through installation of a high temperature substrate heater.
- Define a suitable processing window for glass-on-glass processing by SLM.
- Demonstrate fabrication of complex glass geometries on glass substrates by SLM.

DED specific objectives:

- Investigate the effects of processing parameters on powder-fed DED and populate process maps for processing soda lime silica glass powder on glass substrates.
- Investigate the effect of temperature on powder-fed DED of glass by mildly heating glass substrates during processing.
- Define a suitable processing window for powder-fed DED of glass materials.
- Demonstrate the application of glass décor onto different glass substrates by DED for customisable glass packaging.

3.4 Research Methodology

A framework for fulfilling the outlined research objectives was proposed and applied to both AM methods for glass processing (Figure 29).

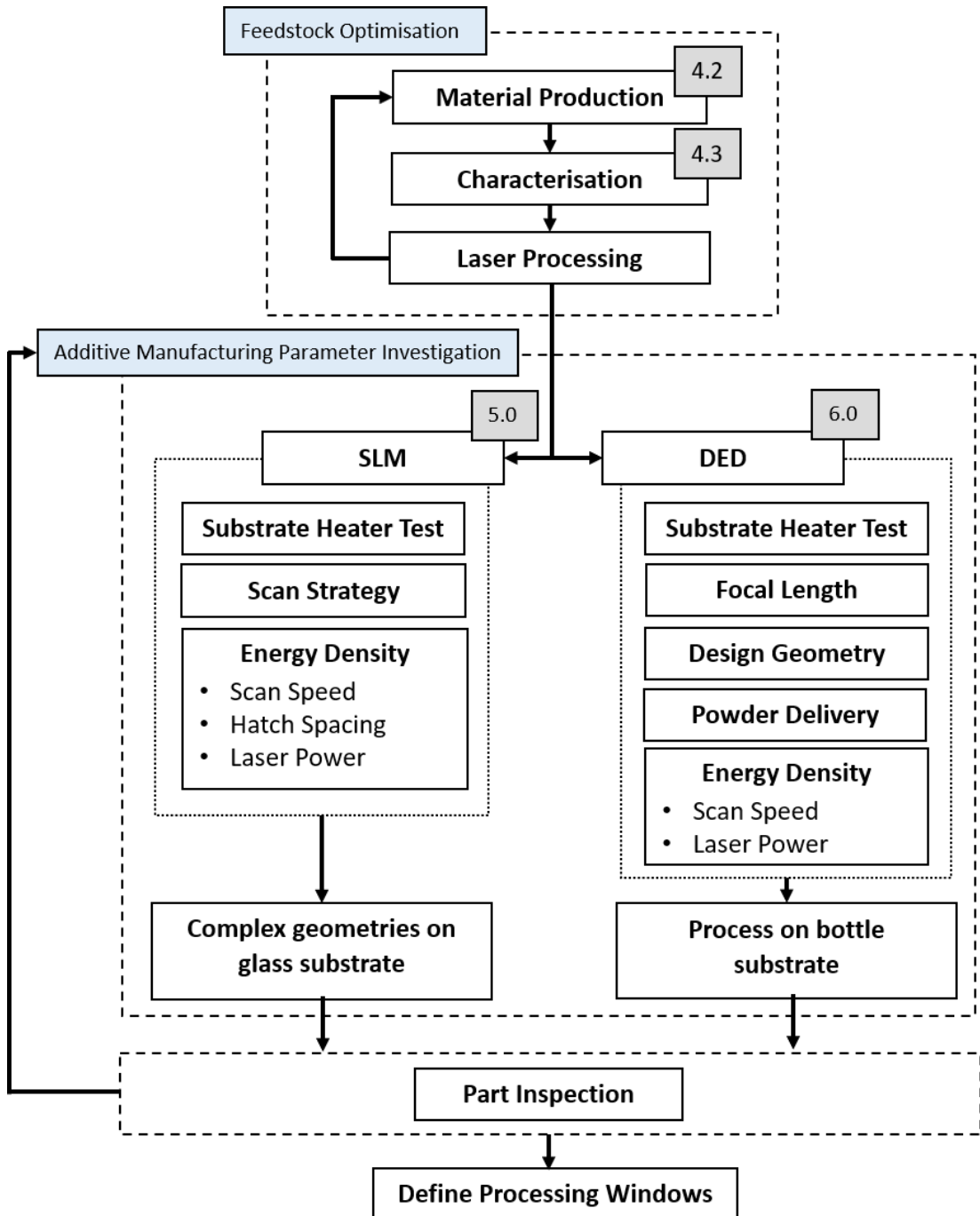


Figure 29 Research framework for investigating the effect of AM process parameters on glass materials, and ultimately defining processing windows for DED and SLM of glass.

As the characteristics of glass powder feedstocks play a large role in AM processing, process optimisation feeds back to the material phase for each new composition of glass. Investigations into process parameters follow a similar route for DED and SLM processing, with the effect of different variables examined systematically or through research led investigations. Experimental investigations are described and reported in Chapter 5 for SLM, and Chapter 6 for DED. For SLM, parameter investigation involved observations of the effect of energy density (including laser power, scan speed, and hatch spacing) and scan strategy on processing of glass feedstocks on glass substrates (Section 5.3). For DED processing, energy density (including laser power and scan speed), laser focal length, design geometry, and powder delivery parameters were investigated for their effect on glass processing (Section 6.4). Additionally, the effect of substrate heating on glass AM processing and thermal shock was investigated.

After optimisation of processing set-ups and parameters, complex geometries were fabricated on glass substrates to demonstrate the potential applications of glass processing by DED and SLM. Inspection of glass parts was typically carried out visually or through microscopy. The crystallinity of glass parts was evaluated post-process by X-ray Diffraction (XRD) to ensure glass material remained amorphous.

Parts were inspected and parameter investigations were used to populate process maps for each AM technique, specific to the glass compositions used. These investigations were used to define suitable processing windows and make recommendations for SLM and DED set-ups for glass processing.

Chapter 4

Experimental Materials and Procedures

4.1 Introduction

This chapter introduces the glass materials used for SLM and DED investigations. The production of feedstock materials is described in 4.2, and the results of feedstock characterisation are presented in 4.3. Two case studies are also included in this chapter: a case study on the flowability of soda lime silica in different ratios of sphericity is described in 4.4, and a case study on the modification of powder morphology by different spheroidising methods is presented in 4.5.

Glass materials of different composition and form were used during investigations of glass processing by Additive Manufacturing. The glass materials used throughout were either supplied by Glass Technology Services Ltd. (GTS), or created using GTS facilities and resources. The chosen glasses were selected based on material properties, and promise shown in the literature described in Chapter 2. Table 5 presents the materials used in this work, highlighting the investigations each material was used for.

Table 5 List of glass materials supplied or produced for this research, indicating the materials used for characterisation only, case studies, and DED or SLM experimental investigations.

Name	Composition	Form	Source	Investigation
GTS-1	Soda lime silica	Spherical Powder	Supplied	SLM / DED
GTS-2	Soda lime silica	Spherical Powder	Supplied	SLM / DED
GTS-3	Fe doped 13-93 BAG	Irregular/Angular Powder	Supplied	SLM / Case Study
GTS-4	Borosilicate	Irregular/Angular Powder	Supplied	DED / Case Study
GTS-5	Fused Silica	Irregular/Angular Powder	Supplied	DED
GTS-6	Soda lime silica	Spherical Powder	Supplied	SLM / DED
GTS-7	Soda lime silica	Large beads	Supplied	Case Study
SLSG	Soda lime silica	Milled powder	Produced	Characterisation
SLSG-Fe	Fe doped soda lime silica	Milled powder	Produced	Case Study
13-93 BAG	13-93 Biologically active glass	Milled powder	Produced	Characterisation
BAG –Fe	Fe doped 13-93 BAG	Milled powder	Produced	Characterisation
BSG	Borosilicate	Milled powder	Produced	Case Study
BSG-Fe	Fe doped borosilicate	Milled powder	Produced	Case Study
SLSG-Fibre	Soda lime silica	Fibre	Produced	DED

Soda lime silica was preferentially used in the experimental investigations throughout this research. It is inexpensive, and widely used, making up 90% of glass manufacture. Soda lime silica glass spheres; GTS-1, GTS-2, and GTS-6, were supplied as “ballotini soda lime silica glass beads internal commercial stock” from industrial sponsor (GTS). GTS-7 consisted of large soda lime silica beads, created using a bead furnace. In traditional glass forming, this material is easy to work with, with a wide working temperature range, and good recyclability. A relatively low glass transition temperature (~550-600°C) made this glass a good candidate for laser processing by SLM and DED. Several soda lime silica feedstocks were supplied or produced for this work.

Several other compositions of glass were of interest for AM investigations. AM of 13-93 biologically active glass showed scope for medical applications, e.g., customised, biologically active tissue scaffolds. Clean (un-doped) and iron doped 13-93 glass compositions were created with SLM in mind, to explore the effect of Iron dopant on SLM parameters for 13-93 bioactive glass. Borosilicate and fused silica were also of interest for AM investigation due to their durability and thermal resistance (as described in Section 2.1). Many of the glass compositions were found to be incompatible with the AM processing systems used in this work (due to restrictive material characteristics e.g., low flowability, as explored in Section 4.3) and were characterised and used for feasibility studies and case studies only.

4.1.1 Materials for SLM

SLM investigations were focussed on soda lime silica glass compositions (Table 6). Soda lime silica glass with two different particle size ranges (as measured in Section 4.3) were used – GTS-2 (84-124 µm), and GTS-6 (29-65 µm). An iron doped 13-93 biologically active glass was investigated for the feasibility of processing by SLM. Other glass compositions of interest for SLM (borosilicate and fused silica) were not investigated in depth due to machine limitations, with recommendations for future investigations into SLM of these materials discussed in Chapter 8.

Table 6 Glass materials used in SLM investigations.

Name	Composition	Form	Features	Source	Investigation
GTS-2	Soda lime silica	Spherical Powder	PSD: 84-124 µm	Supplied	Feasibility
GTS-3	Fe doped 13-93 BAG	Irregular/Angular Powder		Supplied	Feasibility
GTS-6	Soda lime silica	Spherical Powder	PSD: 29-65 µm	Supplied	DoE/Optimisations

4.1.2 Materials for DED

For AM of glass materials by DED, soda lime silica feedstocks were selected due to the popularity of this material in industry for bottles and drinkware (see section 2.1). Soda lime silica substrates were chosen to ensure compatibility of feedstocks and substrates for adhesion by matching the coefficient of thermal expansion. Three soda lime silica glass feedstocks of varying particle size distribution were used in DED investigations – GTS-1 (178-375 μm), GTS-2 (84-124 μm), and GTS-6 (29-65 μm). These feedstocks were supplied in the stated particle size ranges, which were confirmed by Laser Diffraction (Section 4.3.3). These feedstocks were provided in a large quantity (~ 1 Kg) and their spherical morphology was expected to be desirable for flowability (Section 4.3.2), and hence were preferentially used in investigations. Due to the high potential laser power of the DED system (IPG, 2 kW), borosilicate (GTS-4) and fused quartz (GTS-5) powders were explored in DED feasibility studies (Chapter 6.2). Borosilicate and fused quartz glass compositions were anticipated to require high laser powers to melt and consolidate due to their high processing temperatures (Section 2.1). Additionally, a soda lime silica fibre feedstock (SLSG-Fibre) was prepared for a feasibility study into fibre-fed DED. The materials used in DED investigations are summarised in Table 7.

Table 7 Glass materials used for DED investigations.

Name	Composition	Form	Features	Source	Investigation
GTS-1	Soda lime silica	Spherical Powder		Supplied	Feasibility
GTS-2	Soda lime silica	Spherical Powder	Coarse powder	Supplied	Feasibility
SLSG-Fibre	Soda lime silica	Fibre		Produced	Feasibility
GTS-4	Borosilicate	Irregular/Angular Powder	Low flowability	Supplied	Feasibility
GTS-5	Fused Silica	Irregular/Angular Powder	Low flowability	Supplied	Feasibility
GTS-6	Soda lime silica	Spherical Powder	Fine powder	Supplied	DoE/Optimisations

4.2 Feedstock Production

4.2.1 Glass Fibres

Soda lime silica glass was prepared using Soda Ash, Potash, Magnesium carbonate, limestone and sand precursors. The batch was melted at 1400°C and cooled to a supercooled melt at 1200 °C in a platinum crucible. The melt was removed intermittently from the furnace and a recrystallised alumina rod was dipped into the centre of the melt and drawn to a maximum height before being broken off to produce a solid glass fibre. Fibres were cut to size and measured by digital calliper at varying diameters between 0.3 to 1 mm, and viewed by optical microscopy (Nikon Eclipse, Lv100ND, NIS Elements) (Figure 30). The fibres, SLSG-Fibre, were used in a feasibility study for DED processing (Section 6.2.2)

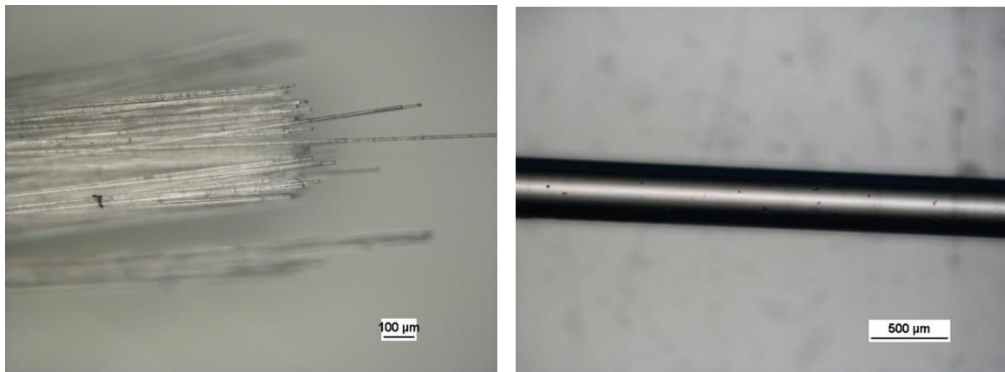


Figure 30 Optical microscopy of drawn glass fibres (SLSG-Fibre). A bundle of fibre ends (left) and a single fibre at 5x magnification (right).

4.2.2 Glass Powder Preparation

Different compositions of glass powder were batched and melted using the same procedure outlined above. Soda lime silica was prepared using sand, soda ash, and limestone as precursors. The batch was mechanically mixed (Turbula shaker) for 20 minutes to ensure an even distribution and homogeneous mixture. The batched soda lime silica was melted in a silica crucible at 1350°C for 60 minutes (SLSG). A batch of Fe doped soda lime silica was batched in the same way, with iron oxide added to the batch making up 0.5wt% of the composition (SLSG-Fe).

A biologically active glass (BAG) was prepared using sand, soda ash, potash, magnesium carbonate, limestone and diammonium hydrogen orthophosphate precursors and thoroughly mixed. 13-93 bioactive glass was melted in a silica crucible at 1250°C for 60

minutes. A doped 13-93 bioactive glass was prepared using 1wt% iron oxide (BAG-Fe). This was melted under the same conditions as the clean 13-93 BAG. Borosilicate glass powder was batched using sand, soda ash, boric acid, and alumina. The borosilicate batch (BSG) and Fe-doped borosilicate (BSG-Fe) were melted at 1500°C for 360 minutes in a platinum crucible.

Molten glasses were poured onto a stainless-steel plate and allowed to cool. When at room temperature, the bulk glasses were crushed, before being ground by a planetary mill, using a quartz mill and balls, at 250 rpm for 15 minutes. Powders were sieved to below 106 μm in size (Figure 31).

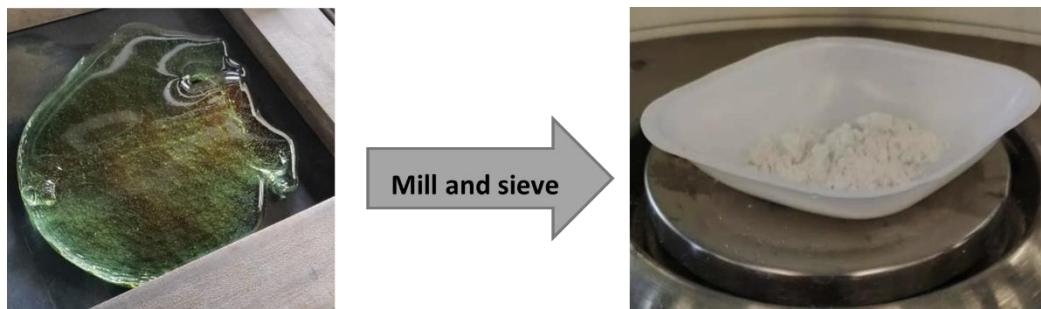


Figure 31 Image of poured bulk glass (left) and milled and sieved powder (right).

4.3 Material Characterisation

Material characteristics play an important role in Additive Manufacturing, and understanding material properties can provide valuable insight into the behaviour of a powder during these processes. The way glass powders behave in formation of powder beds for SLM, and through nozzle delivery in DED, has so far not been described in detail in the literature^{140,163}. The glass compositions of interest were characterised to gain understanding of powder feedstock behaviours in SLM and DED.

4.3.1 Composition Analysis

The compositions of supplied powders were confirmed by Energy Dispersive X-ray Spectroscopy (EDX; FEI XL30 SEM equipped with an electron beam detector) using secondary electron detection at 15kV and analysing oxide percentage. The compositions of powders produced in-house were confirmed by X-Ray Fluorescence (XRF; Wavelength Disperse XRF S4 Pioneer, Bruker AXS GmbH, US). XRF measurements were used to compare the dopant percentage of three Fe-doped 13-93 biologically active glasses (GTS-3, and 0.4% Fe and 1% Fe). The samples were prepared by mixing 2 g of binder with 8 g of glass powder, and hydraulically pressed into a disc for measurement by XRF. The compositions were recorded as oxide weight percentage (Table 8).

Table 8 Glass compositions as measured by EDX as oxide weight percentage.

Name	Form	SiO ₂	Na ₂ O	CaO	MgO	K ₂ O	Al ₂ O ₃	B ₂ O ₃	P ₂ O ₅	Fe ₂ O ₃
GTS-1	Spherical	72.8	13.4	9.2	3.8	0.3	0.4			
GTS-2	Spherical	72.6	13.6	9.6	3.2	0.2	0.6			
GTS-3	Angular	50.55	5.93	22.17	4.94	9.46	--	--	4.16	2.78
GTS-4	Angular	83.1	5.23	--	--	--	2.4	9.2	--	--
GTS-5	Angular	100	--	--	--	--	--	--	--	--
GTS-6	Spherical	72.1	13.7	10.2	2.5	0.5	1.1	--	--	--
13-93 BAG	Angular	53	6	20	5	12	--	--	4	--
BAG-Fe	Angular	51.45	5.83	19.42	4.85	11.65	--	--	3.88	3
SLSG-Fe	Angular	73.75	16.45	9.3	--	--	--	--	--	0.5

In order to analyse the composition of the originally supplied biologically active glass, (GTS-3 13-93), and to assess the difference between the two measurement methods, EDX and XRF analysis of this powder was compared. 13-93 glass samples were batched according to the

following quantities (wt%): Na₂O (6%), MgO (5%), SiO₂ (53%), P₂O₅ (4%), K₂O (12%), CaO (20%), and adjusted respectively to add Fe₂O₃ in quantities of 1 wt% and 0.4 wt%.

Similar results were seen with XRF and EDX of the same glass sample (GTS-3) (Table 9). Variations in composition measurement could be attributed to the presence of impurities, or the uneven distribution of compounds in different samples of the same glass. It could be argued that XRF showed a higher sensitivity than EDX, with XRF measuring close to 100% oxide concentration, and over 1% oxide percentage unaccounted for in EDX measurement.

Table 9 Comparison of measured oxide concentration of GTS-3 and two Fe doped 13-93 glass compositions by EDX and XRF.

Glass Sample	GTS-3		0.4% Fe	1% Fe
Method	EDX	XRF	XRF	XRF
Compound Formula	Concentration (%)			
SiO ₂	50.55	50.29	51.55	51.37
CaO	22.17	22.06	22.03	22.38
K ₂ O	9.46	11.48	11.82	11.98
Na ₂ O	5.93	5.47	5.68	5.36
MgO	3.8	4.43	4.52	4.37
P ₂ O ₅	4.16	3.86	3.94	3.93
Fe ₂ O ₃	2.78	2.1	0.17	0.35
Al ₂ O ₃	NA	0.2	0.09	0.09
SrO	NA	0.01	0.01	0.01
Total	98.85	99.9	99.81	99.84

Both EDX and XRF verified the composition of these glass samples as 13-93 biologically active glass (and its doped counterpart), with oxide percentage matching closely to the composition intended by the batch. While XRF is argued to be a more accurate measurement of composition, EDX is the faster method, and does not require the formation of a pressed powder disc for measurement, saving time and resources.

4.3.2 Morphology

Scanning Electron Microscopy (SEM) was used to visualise glass materials under high magnification. This allowed observation of particle morphology and a general understanding of particle size distribution. GTS-1-5 powders were mounted on aluminium stubs using carbon tabs and were sputter coated with 8-12 nm of gold to reduce charge accumulation. These powders were visualised at high magnification (FEI XL30 SEM), by detection of secondary electrons, at 15kV. Resulting images revealed the spherical morphology of soda

lime silica beads (GTS-1, GTS-2, Figure 32: A, B) and the angular morphology of borosilicate, fused quartz and doped 13-93 BAG (GTS-3 – GTS-5, Figure 32: C, D, E) supplied powders. Also evident from this investigation, was the large particle size distribution of GTS-3 and GTS-4, with evidence of large quantities of very fine particles. SEM of GTS-6 (TM 3030, Hitachi, JP) showed general sphericity, but showed evidence of irregularly shaped particles, as well as fine particles and a large particle size distribution (Figure 32: F, G).

GTS-1, GTS-2, and GTS-6 were supplied by industrial sponsor (GTS) as “ballotini soda lime silica glass beads internal commercial stock”. These glass feedstocks are likely to have been made using an industrial bead furnace, resulting in a highly spherical powder. GTS-3 and GTS-4 were also supplied by industrial sponsor (GTS), and were prepared by melting a glass batch, quenching, crushing, and milling to a powder, before sieving. These powders therefore showed irregular morphologies, with the presence of fine particles.

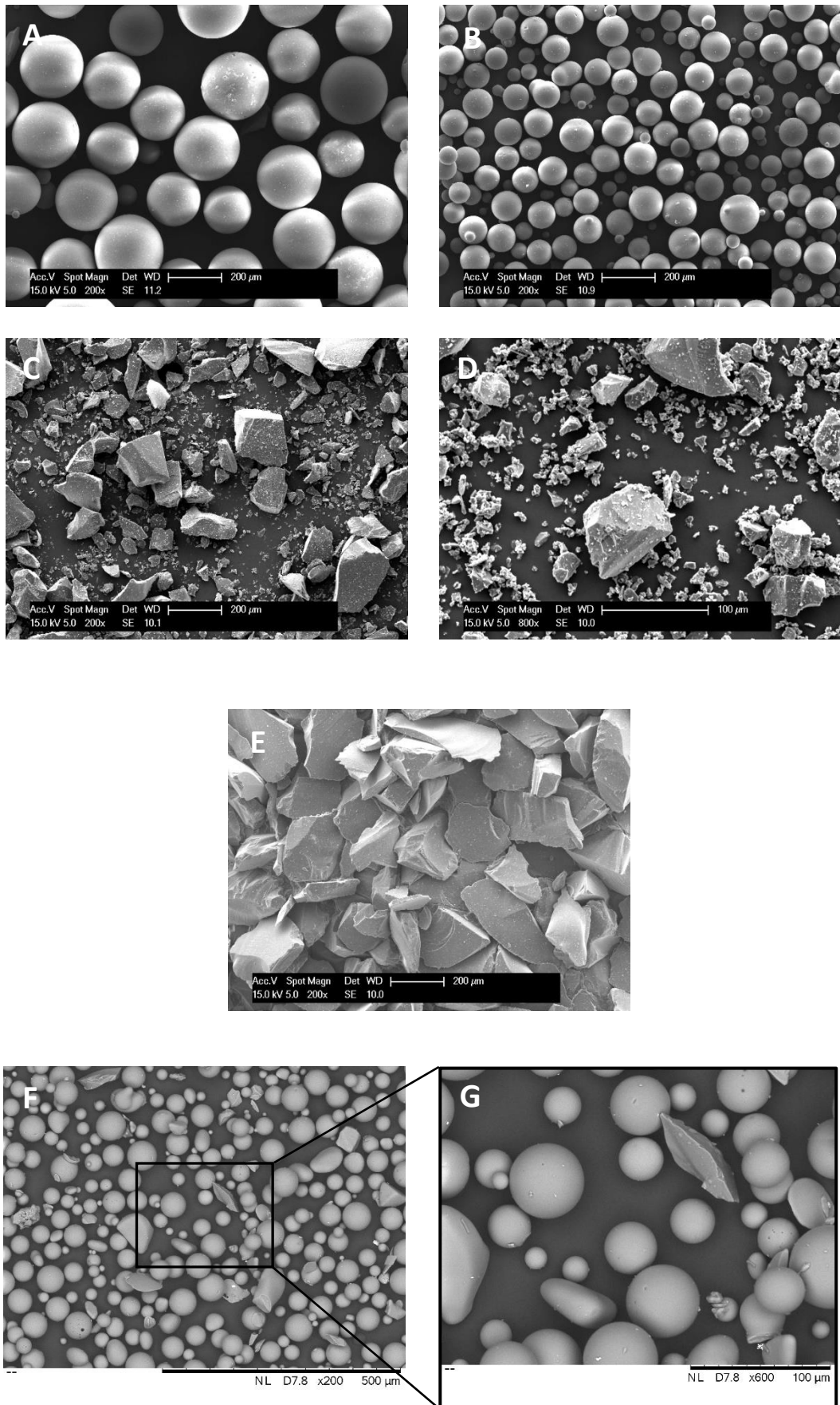


Figure 32 SEM images of several glass powder samples. A-F = GTS-1 - GTS-6 respectively. G: Higher magnification of GTS-6 to show angular particles and irregularities.

4.3.3 Particle Size Analysis

Particle size analysis was carried out using laser diffraction (Mastersizer 3000, Malvern, UK). Measurements were taken under the following conditions: particle refractive index 1.5, particle absorption index 1.0, and general calculation model for irregular particles. Regular spherical particles were easily measured by this method, however, the variation of morphology in angular samples has been known to result in inaccurate measurement.

Supplied spherical soda lime silica powders (GTS-1, GTS-2, and GTS-6) all showed a gaussian, monomodal particle size distribution. GTS-1 was the coarsest sample, with the largest average particle size of 258 μm , and a wide particle size distribution between 178-375 μm . The average particle size of GTS-2 was measured at 102 μm , with a sharp peak and therefore small particle size distribution (84-124 μm), particularly when compared to GTS-1 and GTS-6. The finest spherical powder was GTS-6, with an average particle size of 44 μm . GTS-6 showed a particle size range of 29-65 μm (Figure 33).

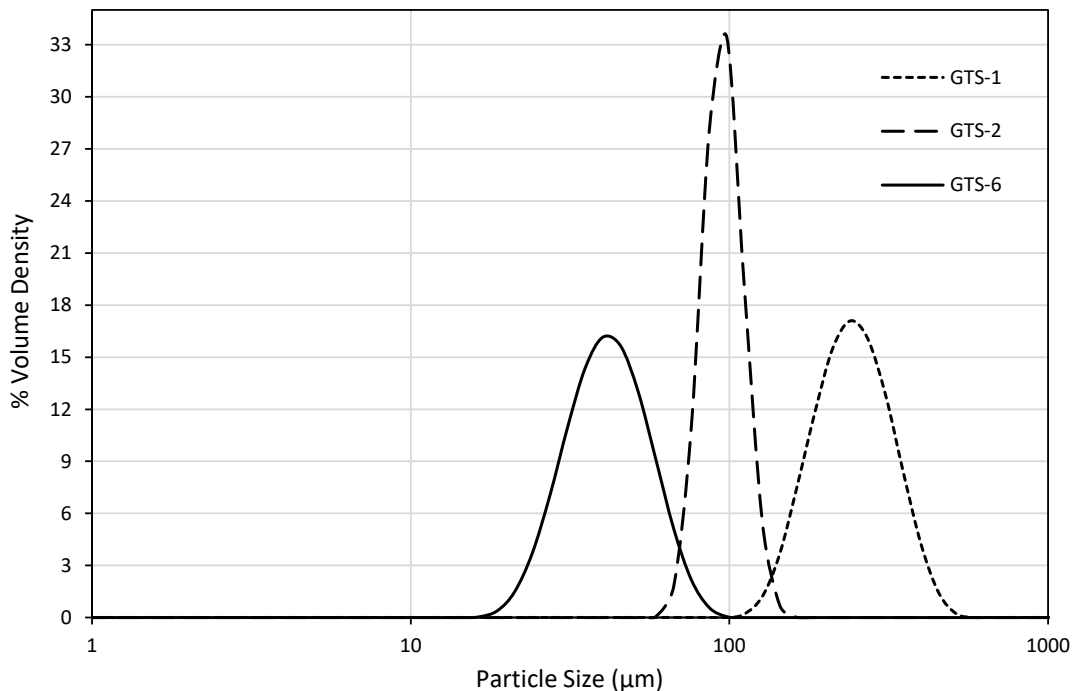


Figure 33 Particle size analysis of spherical soda lime silica glass powders - GTS-1, GTS-2, and GTS-6.

Figure 34 shows the overall investigation of particle size distribution on many of the glass samples used throughout experimental studies, including the three spherical soda lime silica described in Figure 33. Angular samples, in particular GTS-3 (supplied Fe doped 13-93), GTS-4 (supplied borosilicate) and SLSG-Fe (custom made Fe doped soda lime silica), all displayed very wide particle size distributions. GTS-3 also showed evidence of bi-modality, with a soft peak at 11 μm and a more significant peak at 40 μm . GTS-7 was a soda lime silica bead, produced by an industrial bead furnace (VitriTech Ltd, UK). Angular soda lime silica glass was introduced to the top of a vertical bead furnace, forming spherical particles as their surfaces melted during travel through the furnace. The resulting glass beads were very large, with an average particle size of 926 μm – too large to consider for AM processing during this investigation. Table 10 shows the particle size distribution of the glass samples discussed.

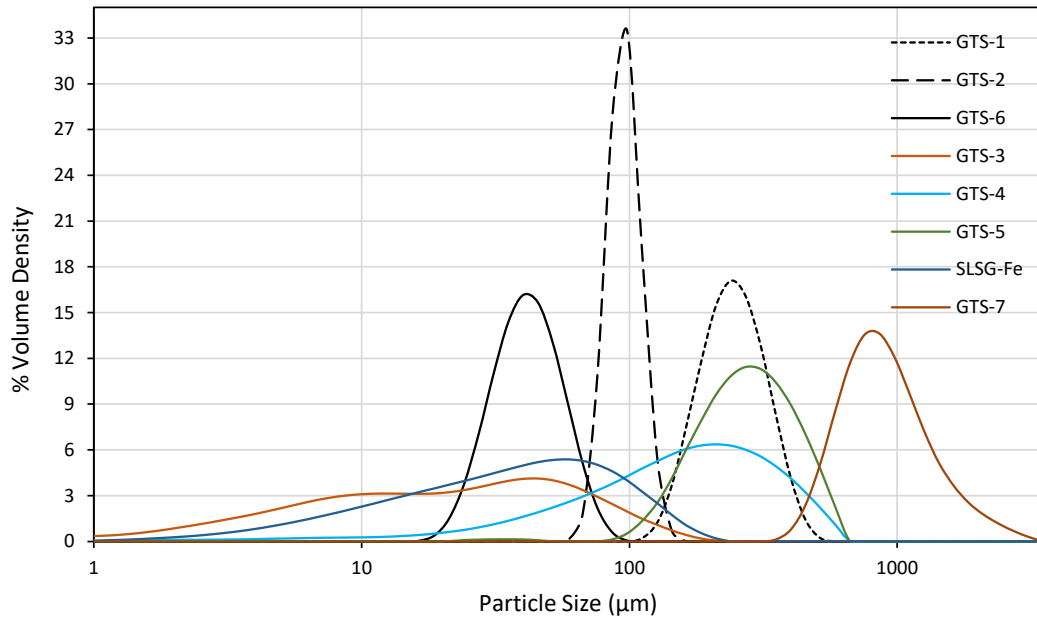


Figure 34 Particle size analysis of original glass samples (GTS-1 - GTS-6), an angular, doped soda lime silica (SLSG-Fe), and soda lime silica beads created in a bead furnace (GTS-7).

Table 10 Particle size analysis of glass samples showing percentage volume distribution. “SLSG” indicates soda lime silica composition. “(s)” indicates spherical morphology.

	GTS-1	GTS-2	GTS-3	GTS-4	GTS-5	GTS-6	GTS-7	SLSG-Fe
Material	SLSG (s)	SLSG (s)	13-93 Fe	Borosilicate	Fused Silica	SLSG (s)	SLSG (bead)	SLSG Fe
Dv ₁₀ (μm)	178	84	2	42	166	29	601	8
Dv ₅₀ (μm)	258	102	20	171	292	44	926	39
Dv ₉₀ (μm)	375	124	80	408	489	65	1630	109

4.3.4 Powder Flowability

Powder flowability can generally be described as a material's resistance to flow. Powder properties such as particle size and size distribution, morphology, and inter-particle forces all impact a material's flowability. These flow characteristics have a large impact on additive manufacturing processes, as they have a significant impact on interactions between powders, and interactions between powders and experimental equipment (e.g., nozzles). For powder bed fusion, powder must have sufficient flow to form a homogeneous powder bed layer of a particular thickness. In Selective Laser Melting, powders are spread across a build platform using a blade or a roller. For this investigation, rubber wiper blades were used to form powder beds of glass powder feedstocks. Similarly, AM techniques that require powder delivered through a pressurised system, such as Directed Energy Deposition, require sufficient powder flowability to ensure a consistent delivery of feedstock through nozzles.

Two methods were used to measure the flowability of powders, Hall Flow Testing (ASTM B213) and Powder Flow Rheometry (ASTM-D7891). These methods were used to better understand the flowability of powders and their behaviour in the AM techniques used.

4.3.4.1 Hall Flow Testing

A simple method of observing powder flow characteristics is to measure the hall flow rate. An AS-300 Hall Flowmeter (carefully calibrated funnel with a 2.54 mm diameter orifice) was used to measure the time it took for 50 g of glass powder to completely flow through. The resulting flow rate (g/s) can be used to compare flowability, however can also return a no-result, i.e. the powder does not flow through the funnel at all. This method was used to compare three spherical glass powder samples: GTS-1, GTS-2 and GTS-6, and one angular powder – GTS-3.

GTS-1, a spherical soda lime silica powder with a particle size distribution of 178-375 μm was recorded as 0.81g/s flow rate. In comparison, GTS-2, a spherical soda lime silica powder with a particle size distribution of 84-124 μm , was measured at 1.0 g/s hall flow rate. GTS-6, spherical soda lime silica powder of particle size 30-65 μm and GTS-3, an angular glass powder (13-93 bioactive glass with Fe dopant), did not flow (0 g/s), indicating poor flowability. The results suggested that generally spherical powders have a superior flowability than angular powders, as reported in the literature^{117,174}. However, spherical powders with very fine particle size (GTS-6), showed reduced flowability, likely due to

increased inter-particle forces between fine particles, potentially due to increased pick-up of moisture and agglomeration of fine powders (see section 2.7). GTS-2 showed better flowability over its coarser counterpart (GTS-1) (Figure 35). While the hall flow testing method is relatively quick and gives a general idea of a material's flow, it did not provide as in-depth understanding of flowability as powder rheometry.

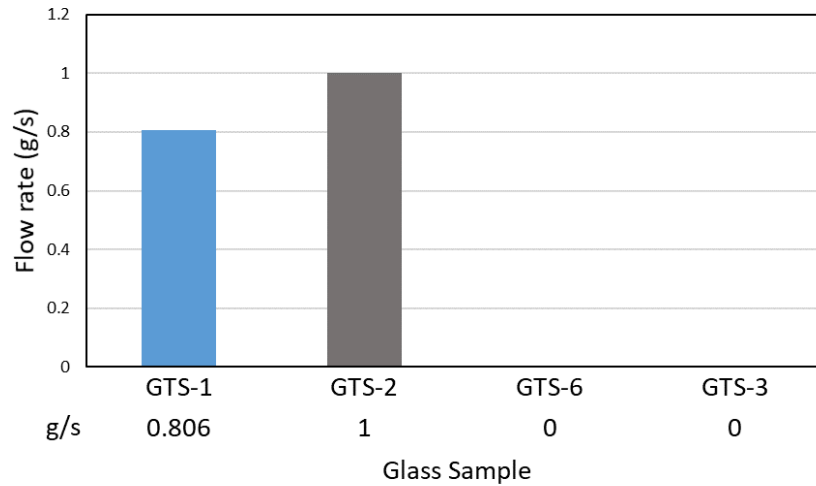


Figure 35 Flowability by hall flow meter testing of four glass samples. A 0 measurement indicates material did not flow through the hall flow meter nozzle.

4.3.4.2 Powder Rheology

The FT4 rheometer (Freeman Technology, UK) was used to characterise the flowability of glass powders of interest for additive manufacturing. Investigations included measurement of five samples, with particular interest in the comparison of three spherical soda lime silica powders (GTS-1, GTS-2, and GTS-6), and two angular powders, borosilicate (GTS-4), and soda lime silica powder (SLSG). The measured parameters of interest for SLM and DED processing were Basic Flowability Energy (BFE), Specific Energy (SE), Conditioned Bulk Density (CBD), and Flow Rate Index (FRI).

BFE is a measurement of forced (confined) flow, using the bottom of the vessel to confine the powder. This is representative of the conditions used when spreading powder material in a powder bed (e.g., SLM). BFE is considered as a measurement of total energy, and a low BFE is generally considered to correspond to a material that flows freely²¹³. SE is the measurement of low stress (unconfined) flow, measured on upward travel of the blade. This may represent powder flow through nozzles, such as in DED processing. CBD is used to represent packing behaviour, and FRI measures a powder's sensitivity to flow rate, indicating cohesion.

CBD was calculated during a conditioning cycle before test cycles started. Tests 1-8 were used to calculate the BFE, with confined blade motion, tests 6 and 7 were used to calculate the SE under low stress conditions, and tests 9-11 were used to calculate the FRI (Figure 36).

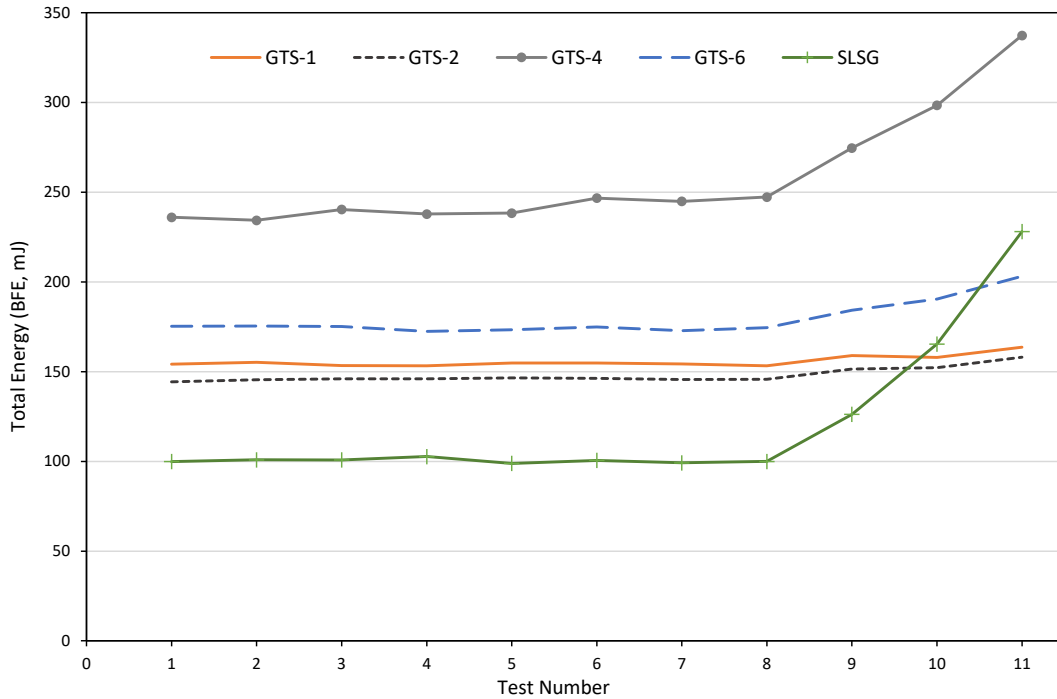


Figure 36 Basic flowability energy of five glass sample. Spherical soda lime silica of varying particle size (GTS-1, GTS-2, GTS-6), and angular borosilicate (GTS-4), as well as angular soda lime silica (SLSG).

At a glance, the results show spherical soda lime silica powders, GTS-1, GTS-2, and GTS-6 to have similar rheological profiles as measured by FT4 powder rheometry. Interpreting BFE alone can fail to give a complete picture of flowability, as it is often assumed that a low BFE value corresponds to a well flowing powder, and a high BFE a poorly flowing powder^{172,213}. While this is generally correct, the opposite can often be true where powders with a good flowability under gravity result in a high BFE, and cohesive powders show a low BFE^{213,214}. Due to this, it is valuable to consider the various flowability measurements of materials together when assessing a bulk powders flowability.

When considering only the spherical soda lime silica powders, the sample with the smallest average particle size (GTS-6 – $Dv_{50}=44 \mu\text{m}$) has the highest BFE at 173 mJ. GTS-1 ($Dv_{50}=258 \mu\text{m}$) and GTS-2 ($Dv_{50}=102 \mu\text{m}$) record BFE measurements of 154 mJ and 145 mJ respectively. These values suggest that of the three spherical samples, GTS-2 has the best flowability, and GTS-6, has the worst. A higher BFE value for GTS-6 is likely due to the large proportion of fine particles causing cohesion due to inter-particular forces. A possible explanation for GTS-1 measuring a higher BFE value than GTS-2 (thus inferior flowability), is the wider particle size distribution of GTS-1, impeding flow.

Considering angular particles, GTS-4 and SLSG, the BFE values differ significantly, taking other measurements into account help to explain this. A more accurate picture of flowability can be gained by using other measurements from rheology, including values for sensitivity to

flow rate (FRI), and flowability in low stress conditions (SE), as well as conditioned bulk density to suggest packing behaviour. A summary of these values can be seen in Table 11.

Table 11 Flowability data for glass samples, as measured by FT4 powder rheometry.

Material	BFE (mJ)	SI	FRI	SE (mJ/g)	CBD (g/ml)
GTS-1	154.24	1.00	1.07	1.45	1.51
GTS-2	145.65	1.01	1.08	1.68	1.48
GTS-4	244.89	1.04	1.36	4.44	1.09
GTS-6	172.82	0.99	1.16	2.22	1.53
SLSG	99.2	0.99	2.28	5.94	0.75

Using this data, the difference in behaviour of the two angular glass samples, SLSG and GTS-4 (borosilicate), compared to spherical samples can easily be seen. SLSG shows a low BFE, which suggests good flowability in confined conditions, however, a high FRI (2.28) suggests a significant amount of cohesion caused by fine particles within the powder sample. A high FRI value (and reduced flowability) can also be caused by mechanical interlocking, as irregular particles experience greater friction at low flow rates²¹³. SLSG also has a significantly lower CBD than the other samples, suggesting poor packing efficiency due to air trapped within the bulk powder. The FT4 impeller blade therefore travels easily through the powder during downward travel, compressing the powder and travelling through air pockets, explaining the low BFE value measured. On upward travel, flowability is low (SE=5.94 mJ/g), as the previously mentioned properties are no longer countered by confinement.

BFE of GTS-4 suggests low flowability in confined conditions. A high FRI value suggests there are more cohesive forces acting on GTS-4 compared to spherical soda lime silica. The difference in FRI between GTS-4 and SLSG is likely due to GTS-4 having a larger average particle size than SLSG, and therefore fewer cohesive forces acting between particles. CBD of GTS-4 is low compared to spherical powders, but not as low as angular SLSG. This likely provides better packing compared to SLSG, and therefore a better flowability in unconfined flow (SE=4.44 mJ).

Figure 37 shows the BFE and FRI values for the glass samples tested. This selection of data is useful in material selection for SLM processing, as these measurements are most relevant to the environment of a powder bed. Of the three spherical soda lime silica samples, GTS-1 and GTS-2, there is little difference in terms of flowability. GTS-6 shows highest flowability in confined conditions, however the large FRI suggests significant cohesion within the bulk

sample, and the impact of this on processing by SLM should be considered. The performance of angular particles in SLM processing is difficult to predict using FT4 rheometry only.

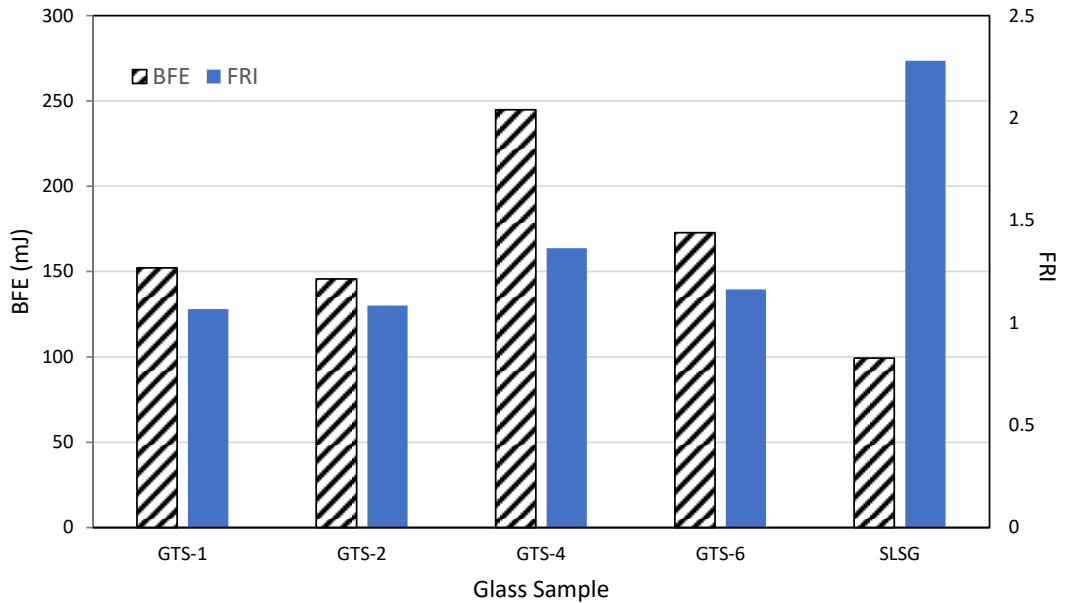


Figure 37 BFE and FRI values measured for different glass samples.

For DED processing, the measurements of most interest are SE and FRI. These measurements are shown in Figure 38. In unconfined flow, reminiscent of flowability through powder feed nozzles used in DED, the results suggest GTS-1, the coarsest, spherical soda lime silica, shows the best flowability under these conditions.

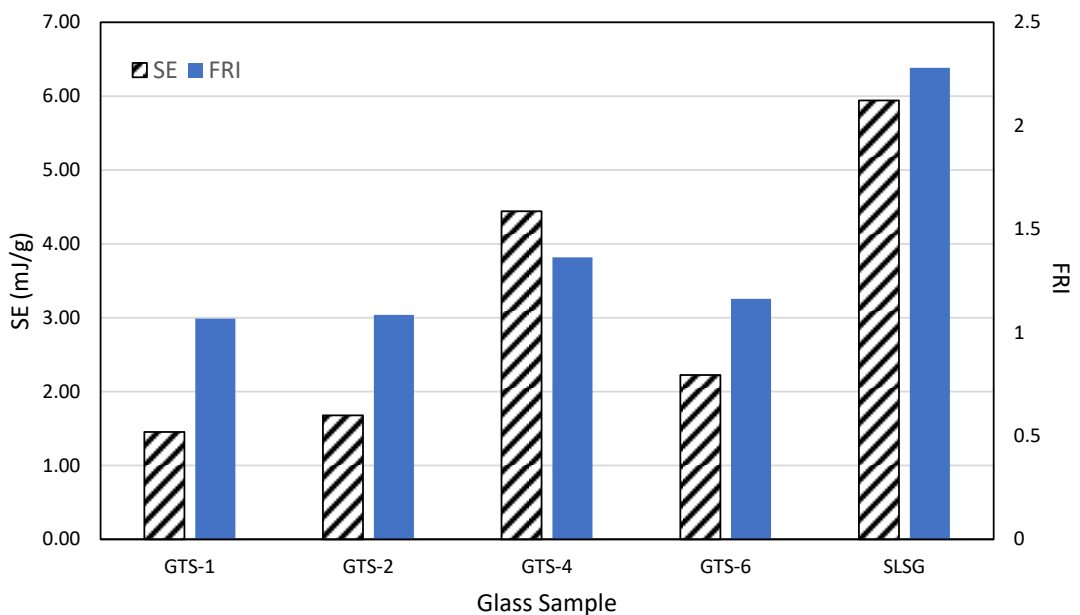


Figure 38 SE and FRI values measured for different glass samples.

4.3.5 Other Characterisation Methods

Other methods of material characterisation were carried out on glass samples, including Differential Thermal Analysis (DTA), UV Visible Spectroscopy (UV -Vis), and X-ray Diffraction (XRD). Soda lime silica (GTS-6) was measured by these three techniques, as this material was primarily used for experimental investigations, due to the availability of this feedstock to the project, its sufficient flowability, and the lower particle size range (compared to other available soda lime silica) anticipated to provide higher resolution parts.

4.3.5.1 Differential Thermal Analysis (DTA)

Differential Thermal Analysis (DTA) was carried out to assess the thermal profile of two glass samples. Understanding the thermal characteristics of a material can help to instruct process conditions for additive manufacturing. The two materials investigated by DTA were GTS-2, a spherical soda lime silica glass powder, and GTS-3, a Fe-doped 13-93 biologically active glass. SDT Q600 (TA Instruments, DE) was used to measure DTA of each sample, using a Nitrogen atmosphere. Alumina pans (90 μ L) were used for reference and sample material. Baseline measurements were taken by the same procedure as sample measurement and subtracted from resulting data.

23 mg of GTS-2 was weighed into an alumina cup on one balance, with an empty reference cup on the other. Temperature was ramped at 15°C per minute to 1500°C and held isothermally for 5 minutes. For measurement of GTS-3, 14 mg of sample was prepared in the same way. Heating procedure was ramped at 20°C per minute to 1500°C, and held isothermally for 5 minutes. Measurements of heat flow (mW) and weight (mg) were recorded over time in reference to temperature change. Results are shown in Figure 39, notation shows an endothermic transition around 550-600°C, relating to the glass transition temperature (T_g). T_g onset, inflection, and end are calculated for a selected endothermic transition (the first endothermic transition after dehydration). Calculating the inflection of T_g as the portion of curve between the first and third tangents with the steepest slope. T_g transitions were measured around 570-600°C for GTS-2, and 575-625°C for GTS-3. These measurements indicate the energy required to begin softening these glass compositions.

Exothermic transitions can be seen for both glass samples during the heating cycle, with more significant exothermic peaks seen in GTS-3 (~750, ~920) than GTS-2, suggesting that GTS-2 is

more thermally stable in comparison. These exotherms can represent crystallisation occurring within the glass samples during melting (above T_g as a supercooled liquid). The extent of these crystallisation events are dependent on kinetic factors and the heating rate during the DTA cycle. As the temperature further increases, these crystals melt, characterised by endothermic transitions, until the glass has reached the liquidus (temperature at which the material is a thermodynamically stable liquid).

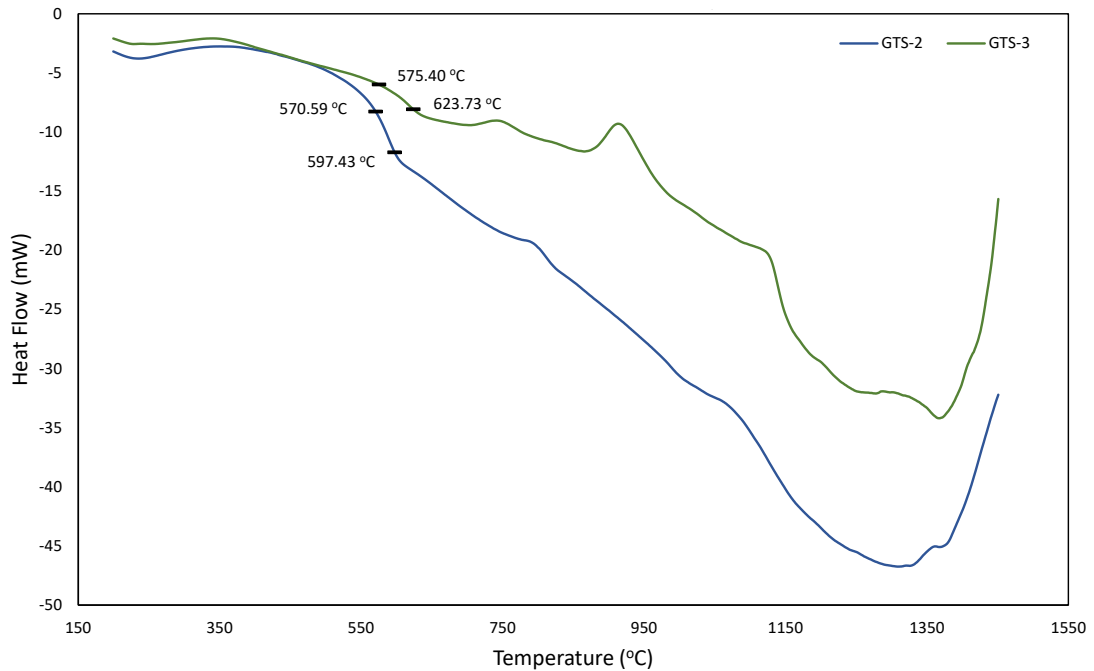


Figure 39 DTA curves of GTS-2 and GTS-3 glass samples showing temperature vs heat flow.

4.3.5.2 UV Visible Spectroscopy (UV Vis)

This characterisation technique was used to measure the absorption of light at the UV and near IR wavelengths. Of particular interest was the light absorption of glass materials in the region of 1064 – 1070 nm, as these are the wavelengths of the lasers utilised in SLM and DED processing. For glass powders, particularly spherical and transparent glass beads, absorption of laser energy can be low due to the transmission of light through particles. For doped glass compositions, measurement of UV Vis spectroscopy can indicate any improvement or reduction in light absorption at the wavelength of interest.

UV Vis (UV-3600 Series, Shimadzu GmbH, JP) was used to understand the absorption of light at the UV and near IR wavelengths of GTS-6. For GTS-6 an absorbance peak was identified at 300 nm ($A = 10.2 \text{ cm}^{-1}$), with much lower absorbance measured at 1064 - 1070 nm ($A = 0.4$

cm^{-1}) (Figure 40). The measured absorbance was in agreement with the transmission spectra shown in Figure 26 (Section 2.7), where soda lime silica was highly transmissive at 500 nm – 2 μm wavelengths.

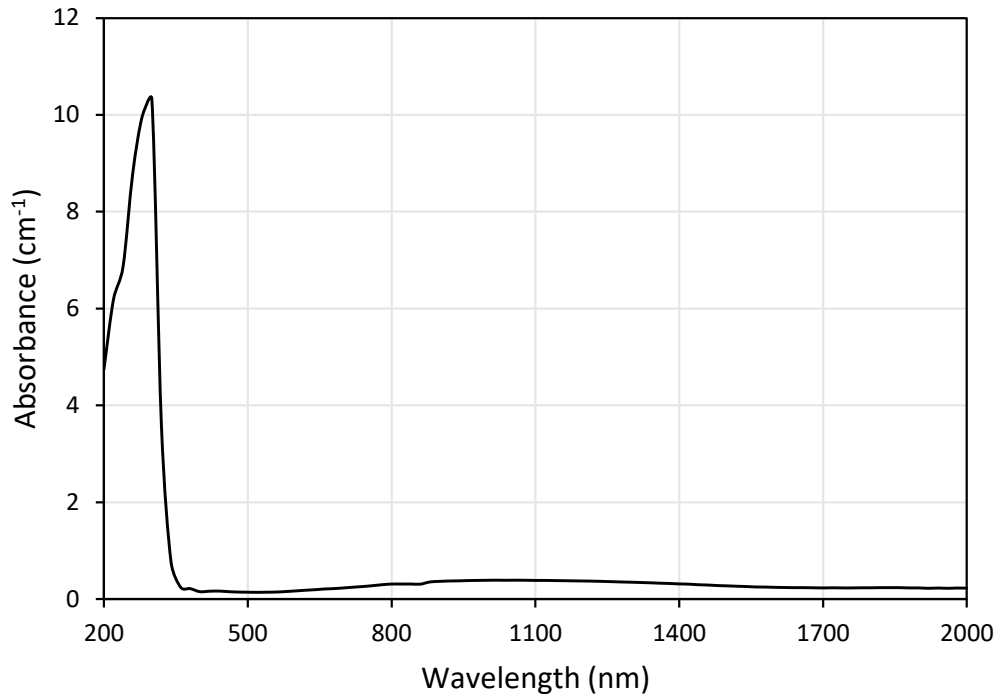


Figure 40 UV Vis absorption spectra of GTS-6 soda lime silica glass.

UV Vis was also used to measure the absorbance of two bulk glass samples of Fe doped soda lime silica (SLSG-Fe, and SLSG-FeC). The data was normalised by sample thickness. Compared to virgin soda lime silica (a colourless/clear glass), SLSG-Fe manifested a grey/blue colour, and SLSG-FeC had a darker grey hue. SLSG-Fe had a similar measured absorbance to virgin soda lime silica at 1064-1070 nm ($A = 0.4 \text{ cm}^{-1}$), whereas SLSG-FeC showed a much higher absorbance in comparison ($A = 2.5 \text{ cm}^{-1}$) (Figure 41). The addition of small quantities of Iron and Carbon to the soda lime silica composition resulted in a significantly increased absorbance of 1064-1070 nm wavelengths, suggesting processing by laser irradiation may be more successful with these doped glass compositions.

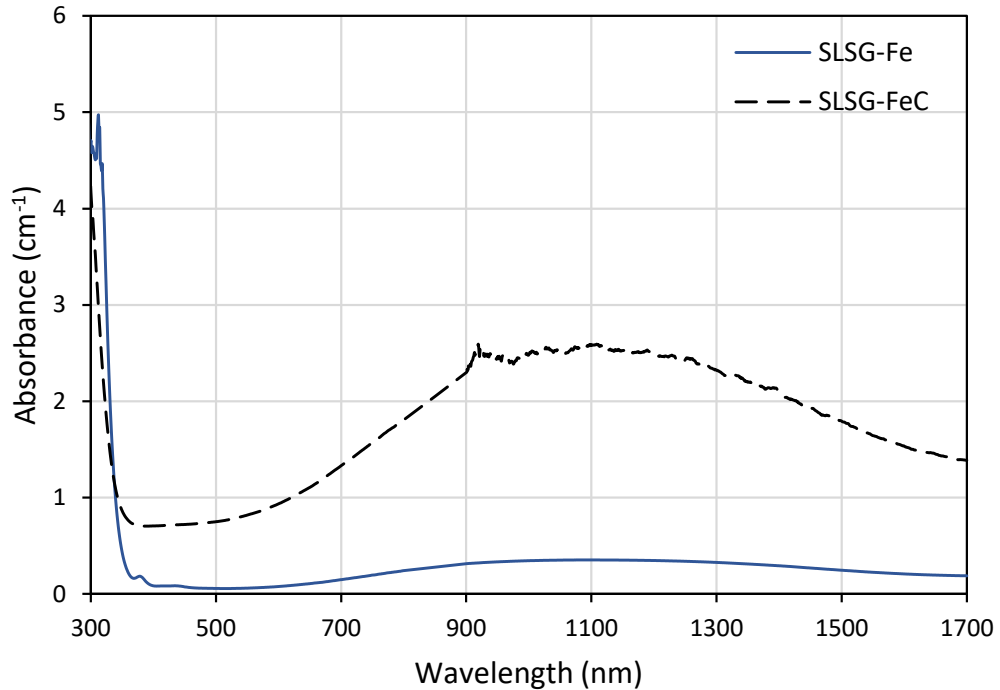


Figure 41 UV Vis absorption spectra for two iron doped soda lime silica compositions (SLSG-Fe and SLSG-FeC).

4.3.5.3 X-Ray Diffraction (XRD)

A glass is characterised as an amorphous material, showing no long-range atomic order, but exhibiting short range order, a solid frozen in liquid state. Crystallinity influences many properties of materials, such as transparency, and for a material to be considered glass it must remain amorphous. When adding dopants to glass compositions, one concern is crystallisation during melting. To confirm lack of crystallisation in doped glass compositions, XRD was carried out.

Two compositions of soda lime silica were investigated by XRD (D8 Advance with DaVinci, Bruker, GmbH, US): SLSG-Fe, a soda lime silica with 0.5wt% Fe dopants, and SLSG-FeC, a soda lime silica with 0.5wt% Fe and 1wt% Carbon (Figure 42). Melted SLSG-Fe was transparent with a grey/blue colouring, and SLSG-FeC was darker in colour and less transparent.

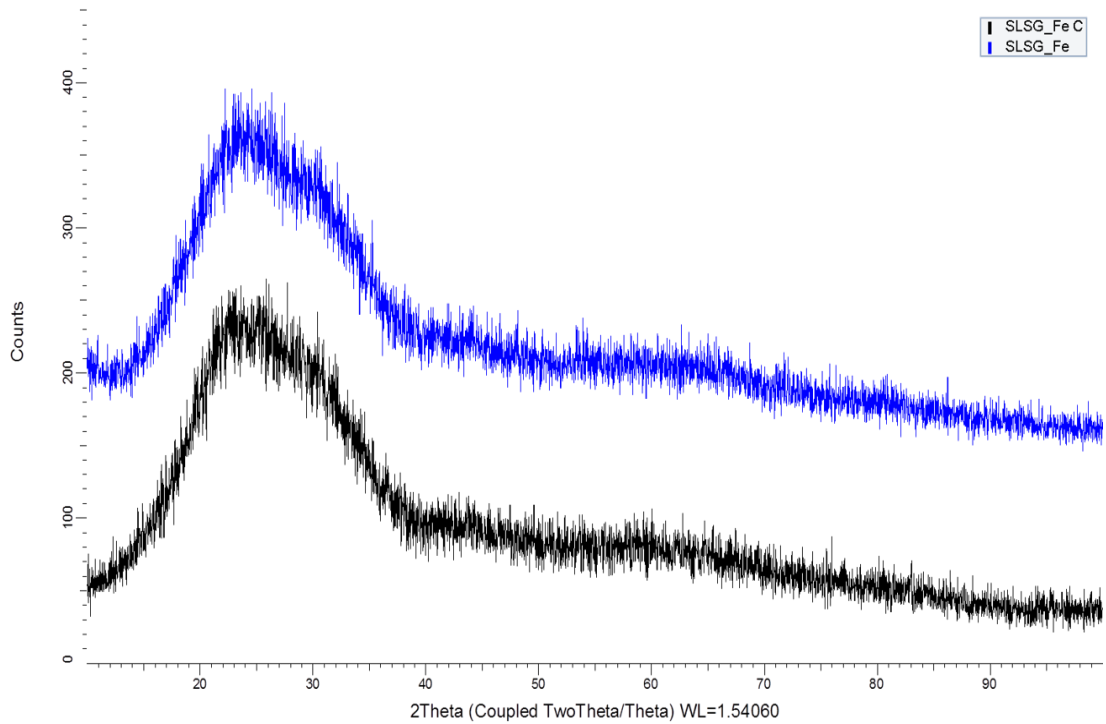


Figure 42 XRD measurement of two Fe doped soda lime silica glasses, SLSG-Fe and SLSG-FeC. Both glass composition are amorphous.

Concerns of crystallinity within the samples were countered by XRD investigation, confirming the samples remained amorphous, due to a presence of a single curve and no periodicity that would indicate crystallinity (multiple distinct peaks). Virgin soda lime silica glass powder (GTS-6) was investigated by XRD, to confirm amorphous nature (Figure 43).

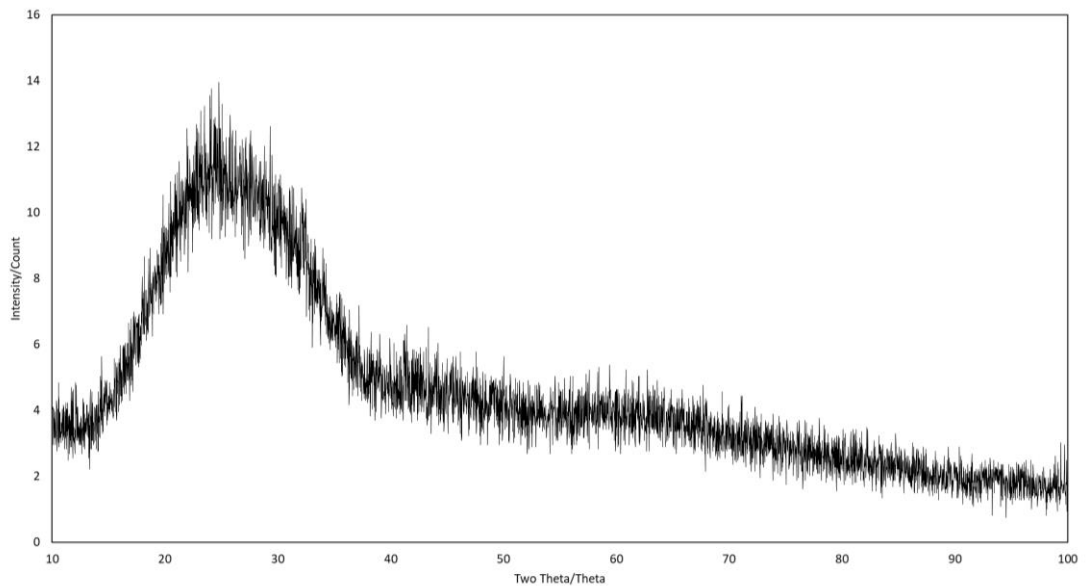


Figure 43 XRD measurement of virgin soda lime silica glass (GTS-6) showing no crystallinity.

4.3.5.4 Micro X-Ray Computed Tomography (XCT)

Micro X-Ray Computed Tomography (XCT) was used to inspect the microstructure and internal porosity of AM processed parts. Parts were imaged using Nikon MCT 225 (Nikon, JP) or XRADIA Versa XRM-500 (ZEISS, Germany). This non-destructive technique transmits X-rays through a sample, generating 2D cross-sectional data as a projected image as the sample is rotated. The data is reconstructed into a 3D digital representation of the sample including internal detail. The resolution of CT slices was 4 μm through cubic samples, which were further analysed to quantify porosity through image processing (ImageJ) (see appendix).

4.4 Case Study: Glass Flowability

FT4 rheology was used to measure the flowability of soda lime silica glass powder of different ratios of spherical and angular morphology, in order to observe the impact of morphology ratio on flowability. This particular investigation was also used to inform flow characteristics for the purpose of dosing glass powder through a mechanical powder doser (Lambda doser 0.2 L, Lambda Instruments, CZ).

Three samples were measured; a sample of spherical soda lime silica (GTS-6 “100% Beads”), a sample of angular soda lime silica (SLSG “Angular”) and a mixture of 50% beads (GTS-6) and angular (SLSG) by weight percentage (50% Beads) (Figure 44). Ratios between these were tested through the doser but not characterised by FT4. Measurement by FT4 was used to quantify the impact of the ratio of spherical beads to angular particles (by weight percent) on powder flowability.

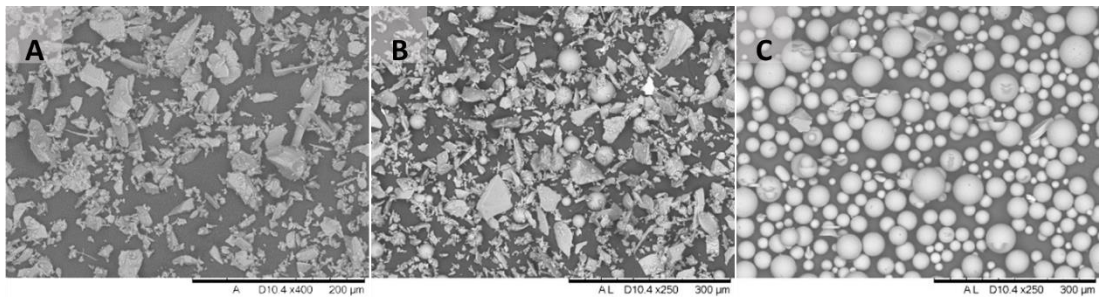


Figure 44 SEM images visualising the different morphology mixtures of soda lime silica A: Angular, B: 50% Beads, C: 100% Beads.

4.4.1 Powder Rheology

CBD was calculated during a conditioning cycle before test cycles started. Tests 1-8 were used to calculate the BFE, with confined blade motion, tests 6 and 7 were used to calculate the SE under low stress conditions, and tests 9-11 were used to calculate the FRI (Figure 45).

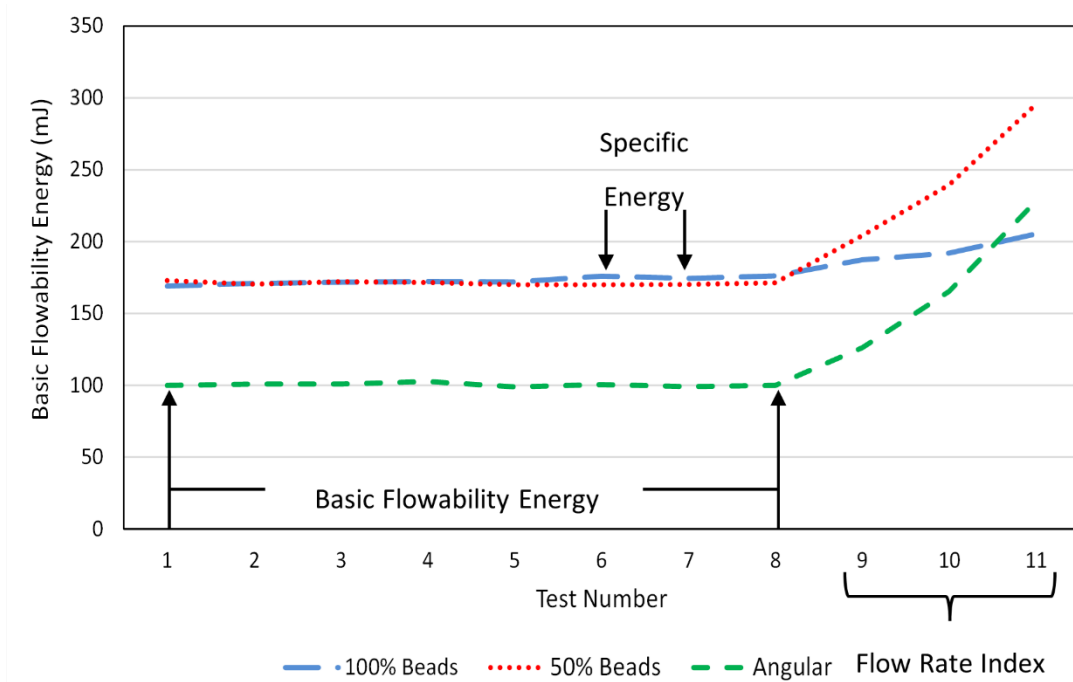


Figure 45 Flowability of soda lime silica with varying percent sphericity. GTS-6 “100 % Beads”, SLSG “Angular” and a mix of both at 50 wt% “50% Beads”. Graph indicates test cycles used for each measurement.

FRI measurements showed that with increasing angularity ratio, the powders became more sensitive to flow rate (Figure 46). This was indicated by FRI measurement of sensitivity to flow rate, with 100% beads measuring close to 1, indicating a non-cohesive powder. The FRI of 50% Bead and Angular samples increased by the same factor, with an increase of 0.56 between 100% Bead to 50% Bead and between 50% Bead and Angular samples, indicating an increase in cohesion correlating with percentage angularity. This increase in cohesion correlates with decreasing flowability.

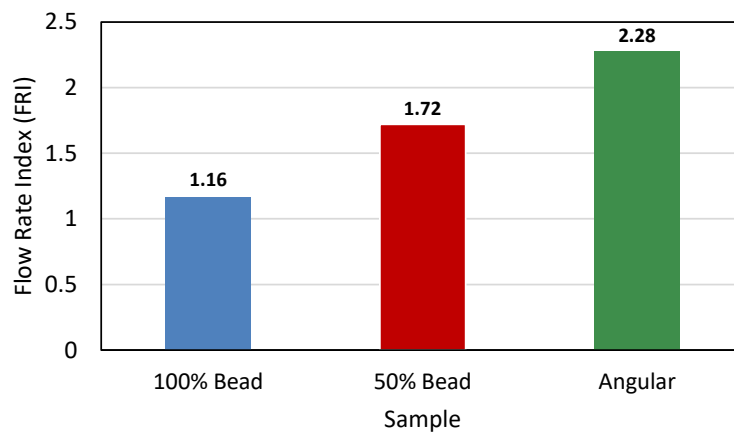


Figure 46 Flow Rate Index (FRI) of glass samples by sphericity. A flow rate index close to unity represents a low sensitivity to flow rate.

The Basic Flowability Energy and Specific Energy were measured for each sample, with BFE representing flow under confined conditions, and SE representing flow under non-confined or low stress conditions. The correlation between percentage angularity and flowability was seen for both confined and unconfined flow, with the sample of 100% bead showing the highest flowability, and the Angular sample showing the lowest flowability, as expected (Figure 47).

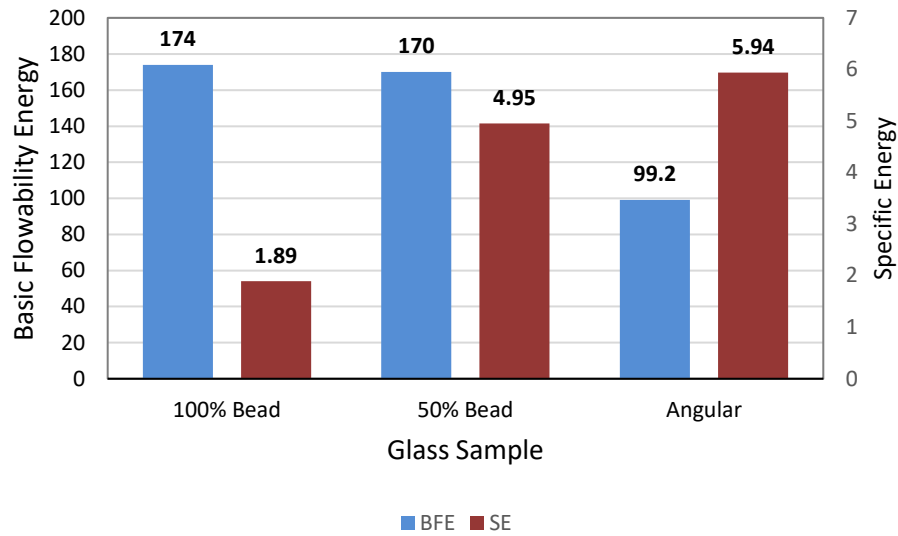


Figure 47 Flowability (BFE and SE) of soda lime silica glass samples: 100 % bead, 50% bead, and Angular.

4.4.2 Observation of Sample Spreading for Powder Bed Formation

A single layer of 100% bead, 50% bead and Angular samples of glass were spread in the Realizer SLM-50 (Realizer GmbH, DE), to assess the impact of flowability on homogenisation of powder bed during powder spreading, and evaluate correlations with rheology assessments of flowability (Figure 48).

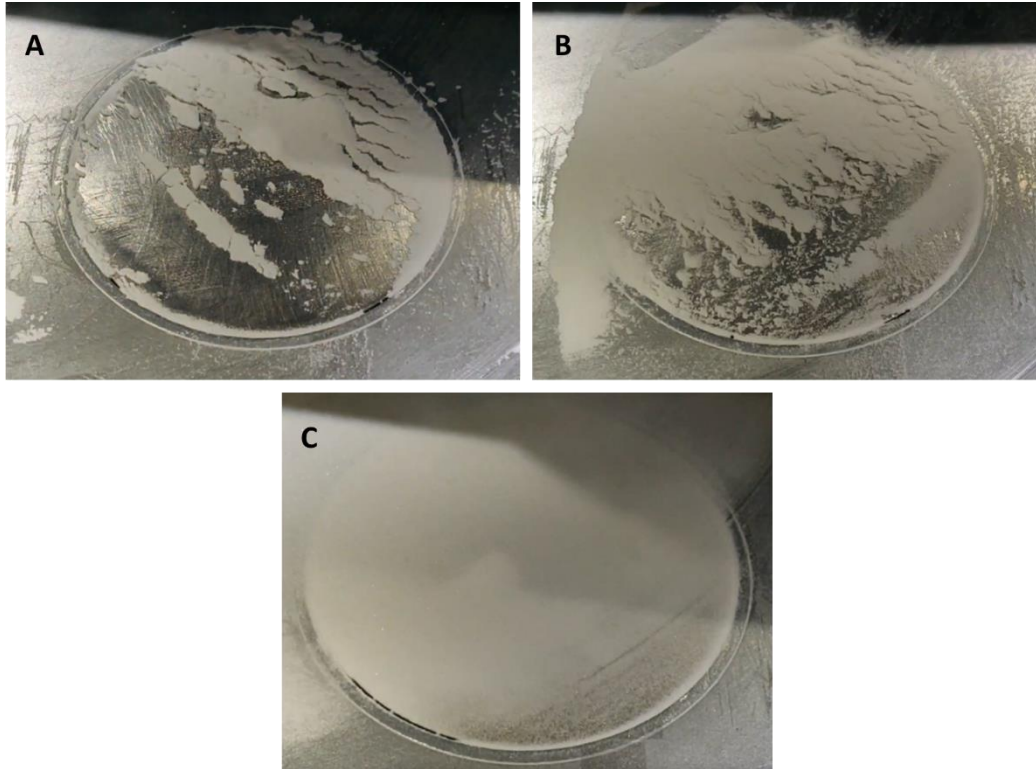


Figure 48 Glass powder samples as spread on an SLM base plate to form a single layer powder bed. A: Angular, B: 50% bead, C: 100% bead.

Angular particles were unable to form a homogenous, even layer of powder across the base plate, showing cohesive behaviour with the wiper blade dragging powder to one side of the base plate (A). 50% bead sample displayed improved flow behaviour compared to angular glass. The addition of spherical particles acted as a flow agent, reducing cohesion and allowing better coverage of the SLM base plate (B). 100% spherical glass sample showed the greatest flowability, forming a homogenous single layer of glass on the SLM powder bed. By visual assessment, flowability significantly improved based on percentage sphericity, confirming the flowability measurements carried out by powder rheology. This was also common to literature, where angularity was related to flowability in powder bed formation¹⁷⁴. Muñiz-Lerma et al, reported enhanced powder spreading when spherical

particles larger than 48 μm with a narrow particle size range were present in a powder feedstock, due to reduced moisture sorption, cohesion, and surface energy¹¹⁴.

To combat the low flowability of angular glass particles, alteration of powder morphology and particle size distribution was considered. One method considered for improving the flow characteristics of glass powders was to reduce the particle size distribution to a limited range. This is because powder samples with angular morphology and a large particle size distribution tend to suffer from mechanical interlocking, as well as high inter-particulate forces between fine particles causing powder cohesion. Attempts were made to reduce the particle size range through manually sieving powder samples to a desired range, until a flowability was improved. The time consumption and material waste resulted in this method being inefficient for our research purposes.

4.5 Case Study: Powder Spheroidisation

An important powder characteristic to consider for Additive Manufacturing of glass was morphology, as particle shape is known to have a strong effect on bulk powder flow. Observed during flowability characterisation, angular powders generally suffered from particle cohesion, mechanical interlocking, and low flowability (as observed by Hall Flow Meter testing, and SE and BFE measurements). For experimental glass powders created for the application of AM, processes of morphology alteration were considered in order to improve the flowability of these milled, angular particles. The three morphology altering methods trialled were flame spheroidisation, plasma spheroidisation, and electron beam irradiation. Another benefit of pre-processing glass powders by spheroidisation, particularly GTS-3 which showed a bimodal particle size distribution, is the potential to transform to a better flowing, monomodal distribution.

4.5.1 Flame Spheroidisation

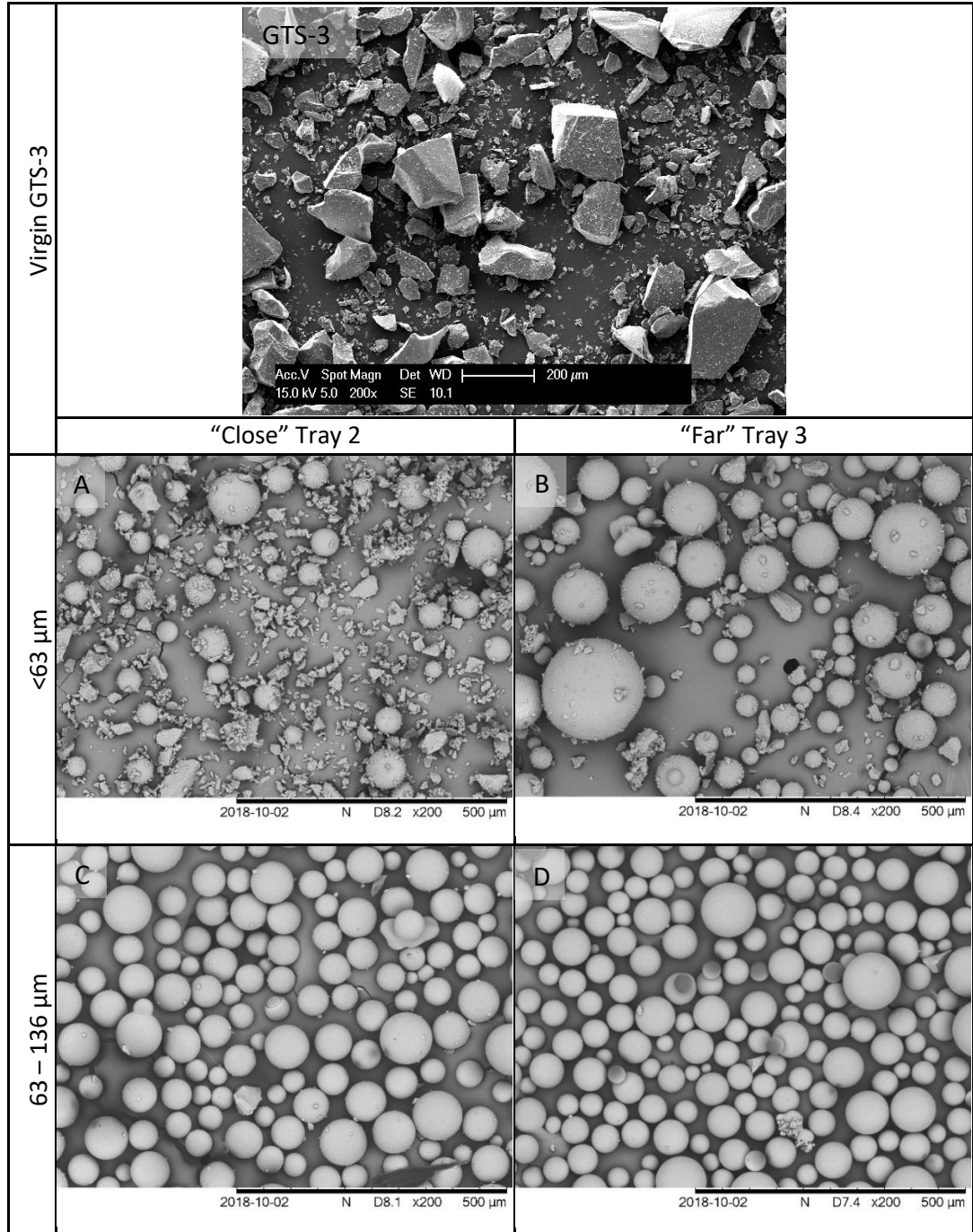
The flame spheroidisation process works by delivering irregular particles into a hot flame to melt the particle surface and mould them into spheres due to the high surface tension of glass particles (See Section 2.5). This concept was applied to angular glass particles intended for additive manufacturing by selective laser melting, in particular an Fe doped 13-93 biologically active glass (GTS-3).

Due to the lack of flowability of GTS-3, with the large particle size range of 8-136 μm , the powder was unable to be processed by flame spheroidisation. The large proportion of fine particles caused powder to agglomerate in the thermal spray nozzle. In order to process by flame spheroidisation, angular particles of GTS-3 were prepared into two particle size ranges using a 63 μm sieve. One fraction contained angular particles of <63 μm , and the other fraction contained particle sizes between 63-136 μm . Particles were introduced to an oxy-acetylene flame (ratio of 3:3) of a thermal spray gun (Metallisation Ltd, UK). Processed particles were collected in two cooling trays, one at a close distance to the spray gun (Tray 2 "close"), and one further away (Tray 3, "far"). Particles that did not travel far enough for spheroidisation were collected for repeat processing.

Particle morphology of flame spheroidised glass was investigated by SEM (Table 12). GTS-3 particle morphology was significantly altered by flame spheroidisation. A significant difference was found between processing particles of <63 μm and particles of 63-136 μm .

Angular particles between 63-136 μm that were processed by flame spheroidisation resulted in a majority uniform and spherical particles. For particles $<63 \mu\text{m}$, a distinct spheroidisation of the larger particles was observed, however fine particles did not significantly alter morphology. Particles that spent a longer time travelling in the flame (collected in the far tray) were more likely to have a spherical morphology after processing than those collected in the closer tray.

Table 12 GTS-3 powder processed by flame spheroidisation. A: Fine particles collected in Tray 2, B: Fine particles collected in Tray 3, C: 63-136 μm particles collected in Tray 2, D: 63-136 μm particles collected in Tray 3.



Processing angular glass particles by this method resulted in a definite spheroidising effect, however, a wide particle size range lacked the flowability required to be processed efficiently by this method. The required sieving increased the flowability by reducing the particle size range, perhaps making the purpose of spheroidising obsolete. Finer particles were also difficult to spheroidise by flame with efficiency, with many fine particles being lost in the process via air extraction. Whilst effective for spheroidising glass materials, this method was inefficient for the quantities of glass needed for additive manufacturing, and a larger scale method was investigated – plasma spheroidisation.

4.5.2 Plasma Spheroidisation

Funding for plasma spheroidisation of experimental glass powders was granted by the Henry Royce Equipment Share Scheme, and work was carried out at the Royce Translational Centre, Sheffield, with support from Dr Vahid Nekouie.

Plasma spheroidisation operates similarly to flame spheroidisation described in 4.5.1. The method spheroidises material by passing angular particles through high energy plasma gas. The particles melt and mould into spheres due to surface tension. Plasma spheroidisation is argued to produce highly spherical feedstocks with few satellites, reduced porosity, and with little to no contamination, with surface vaporisation of high temperature materials limited thanks to the generation of a homogenous temperature profile²¹⁵.

Iron-doped soda lime silica glass powder (SLSG-Fe), and borosilicate (BSG) was plasma spheroidised using a Teksphero-15 (Tekna, CA). Due to the angularity of powders and the wide particle size distribution of each (Dv_{10} - Dv_{90} SLSG-Fe: 8-109 μm , BSG: 4-108 μm), the familiar issue of low flowability was encountered. Sieving was required to remove fine particles and increase the flowability to allow delivery of material through the machine. SLSG-Fe powder was sieved to 66-103 μm PSD, and BSG was sieved to 43-113 μm PSD.

The process involved initial feed rate calibration, verifying the need for sieving to allow sufficient feed of angular glass particles. A design of experiments was used to develop four different process cycles with various processing parameters. SLSG-Fe was fed at a rate of 5 g/min and processed at 12 kW plasma power. BSG was fed at a rate of 6.6 g/min and processed at 11 kW plasma power. Argon gas was used for sheath gas (40 standard litre per minute, SPLM), central gas (10 SLPM), and carrier gas (4 SLPM). Powders were processed in 50 g quantities for each cycle for parameter optimisation. The percentage yield during optimisation was 25%.

Processed powders were investigated by SEM to visualise morphology alteration. Borosilicate powder showed a significant alteration of particle morphology, with spheroidisation resulting in a high volume of spherical particles compared to the virgin powder. SLSG-Fe showed similar results from plasma spheroidisation (Figure 49). Post processing was necessary to remove moisture in SLSG-Fe powder by drying in a vacuum oven, and to remove satellite particles from BSG samples by ultrasonic bath. Moisture was present in the powders as a consequence of powder retrieval method (water was used to collect

spheroidised material). Final PSD of plasma spheroidised BSG was 53-116 μm and for SLSG was 66-110 μm . With further optimisation of process parameters, and an increase in % yield, plasma spheroidisation shows promise for bespoke glass powder spheroidisation.

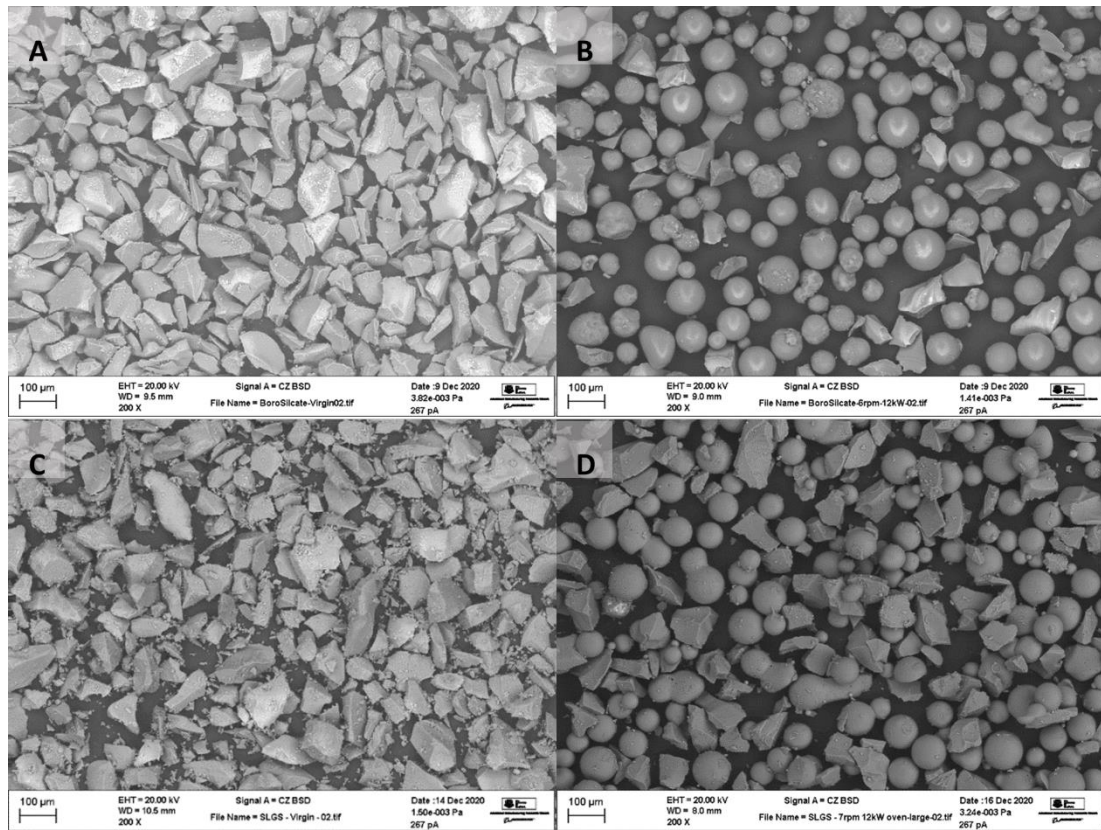
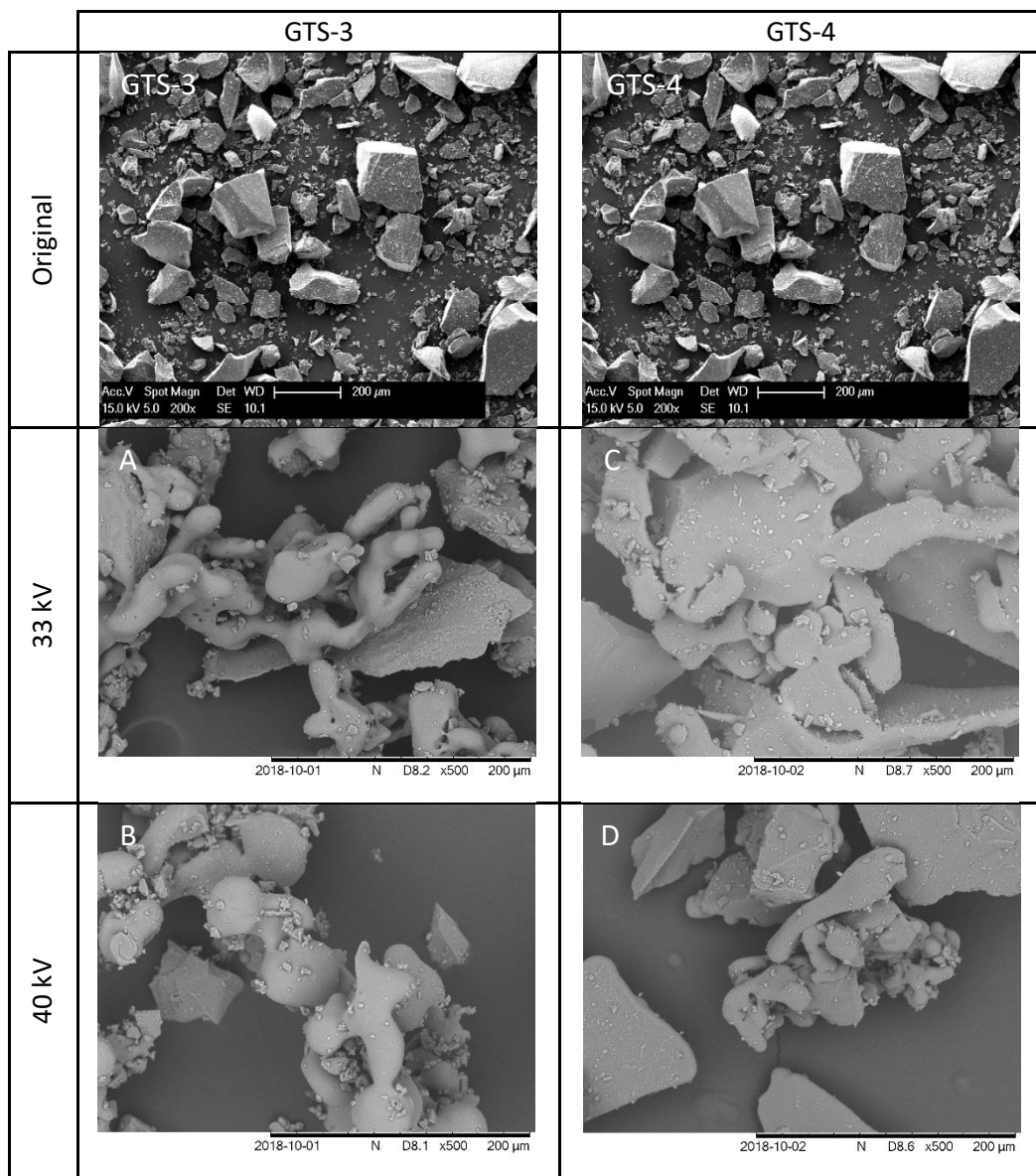


Figure 49 SEM images of A: Virgin borosilicate (BSG), B: Plasma spheroidised BSG, C: Virgin doped soda lime silica (SLSG-Fe), and D: Plasma spheroidised SLSG-Fe.

4.5.3 Electron Beam Irradiation

Another method of altering particle morphology was proposed by Murray et al¹⁸⁶. This method was developed as a new powder spheroidisation process through pulsed electron beam irradiation of particles. This method was used to investigate the potential for altering the particle morphology of two glass materials, GTS-3 (Fe-doped 13-93) and GTS-4 (Borosilicate glass). A small sample of each glass was processed to test the feasibility. Glass particles were irradiated at 33kV and 40kV, using 50 pulses (Table 13).

Table 13 SEM micrographs of glass feedstocks before and after electron beam irradiation.



Generally, pulsed electron beam irradiation altered the morphology of angular particles. For GTS-3 powder, electron beam irradiation at 33kV showed the merging of fine particles, and softening of angular edges. At 40kV, particles started to show more sphericity than the angular precursor. In comparison, GTS-4, a borosilicate glass with a much higher melting point, showed a less distinct effect from electron beam irradiation. At 33kV and 40kV the agglomeration of fine particles can be seen, with a softening of angular edges, however, only minor changes were seen across the whole sample studied, and little sphericity was observed. This method showed an overall, minor alteration to particle morphology, with promise of further optimisation for spheroidising angular particles. This method currently processes material on a very small scale. The limited quantity of altered particles produced by this method inhibited further characterisation and experimentation. Significant scale-up would be required to confirm any changes in flowability to electron beam irradiated glass powders.

4.6 Conclusions

Glass materials were characterised and assessed based on material properties relevant to AM processing conditions. Some of the conclusions made during characterisation of materials and case studies described in Chapter 4 were:

- In confirmation with the literature^{114,174,184}, a spherical morphology was deemed superior to angular or irregular powder feedstocks to allow efficient delivery of powder or powder bed formation in AM processing.
- Custom powder compositions created for AM purposes required alteration to morphology or particle size range to improve flowability.
- Flame spheroidisation was successful in spheroidising glass powders, but lacked a sufficient yield and scale for AM processing purposes.
- Plasma spheroidisation resulted in a significant alteration of particle morphology, but had a low yield and requires further optimisation for bespoke glass compositions.
- Electron beam irradiation caused promising, subtle morphology changes in glass materials but would require further optimisation for improved results, as well as scaling up to allow processing of larger quantities of feedstock for processing.
- Addition of spherical glass particles to angular glass powder acted as a flow agent, improving the measured flowability by FT4 analysis.

Soda lime silica glass thermal profiles, as measured by DTA and as consistently recorded in literature⁴⁵, have a lower T_g and working temperature ranges than compositions such as Borosilicate and Fused Silica (see section 2.1). This suggests soda lime silica compositions require less energy to melt, and therefore less energy density required during AM processing. With the potential benefit of processing and melting glass powder at lower energy density

(i.e. lower laser power or faster scan speed), glass structures and substrates would be subjected to reduced thermal stress and therefore be at a lower risk of fracture.

GTS-6, spherical soda lime silica with the smallest average particle size, was preferentially used during experimental procedures. This material was available in the largest quantity, and with a smaller average particle size range, and spherical morphology, it offered the potential for higher resolution during SLM (largest particle size relates to the smallest layer height useable).

Chapter 5

Selective Laser Melting of Glass

5.1 Introduction

Selective Laser Melting (SLM) was identified as a promising Additive Manufacturing technique for processing glass material, with research opportunities including processing novel glass compositions, and achieving successful glass-on-glass manufacture. The state of the art in SLM of glass materials was thoroughly explored in Chapter 2, highlighting some of the known challenges associated with glass manufacturing by laser powder bed fusion AM methods:

- High thermal gradients inherent to laser processing of high temperature materials can lead to thermal shock of parts and substrates.
- Glass materials, particularly transparent soda lime silica, may suffer lack of laser absorption due to high transmittance in the near-IR and visible wavelength range.
- Glass powder feedstocks have shown particular sensitivity to energy density.

Investigation into SLM of glass powders was split into three parts. The first was an initial investigation into the feasibility of processing glass compositions onto ceramic and glass substrates. This was used to narrow down processing parameters to achieve melting of glass powders, and to understand the interaction of glass powders with substrates (Section 5.2). The second was to optimise parameters of the chosen glass composition, to fully understand the effect of processing parameters on glass SLM. This includes investigation into the effect of laser power, scan speed, hatch spacing, and scan strategy on melting and consolidation of glass (Section 5.3-5.4). For on-glass processing the effect of parameters on thermal shock, and adhesion of processed structures to substrates was investigated. Finally, a case study was carried out to investigate glass SLM at high substrate temperatures, with the aim of assessing the effect of high temperature substrate heating on glass SLM (Section 5.5). The research incentive towards investigating SLM of glass materials includes the potential applications in research and industry, e.g., for fabrication of customised glass continuous flow reactors.

5.1.1 Experimental Set-Up

For these experimental investigations, a Realizer SLM-50 (Realizer GmbH, DE) was used for laser powder bed fusion of glass powders (Figure 50). The Realizer system is equipped with a 1064 nm fibre laser capable of laser power up to 100 W and scan speed up to 200 mm/s. A laser focal position of 9.6 mm was used throughout this investigation to form a spot size of 20 μm diameter. The build platform has a diameter of 70 mm, with a substrate heater capable of temperatures up to 250 °C. An inert Argon atmosphere is used during processing to prevent oxidation of reactive/sensitive powders, and for powder spreading, a dual wiper blade is employed. The small build volume allows efficient investigation into experimental materials, and is therefore useful for feasibility studies.



Figure 50 The Realizer SLM-50 machine.

5.1.2 Substrates

Two substrates were of interest, high purity (99.8%) alumina discs (Almath), and soda lime silica glass microscope slides (Biosigma). Ceramic and glass substrates were selected to closely match the CTE of the soda lime silica powder, with the aim of achieving sufficient adhesion of processed glass powder onto substrates (and to prevent delamination during processing), and to accommodate thermal expansion (Alumina CTE: $\sim 7.2 \times 10^{-6} \text{ }^\circ\text{C}^{-1}$ (40-400°C), Soda lime silica CTE: of $\sim 9 \times 10^{-6} \text{ }^\circ\text{C}^{-1}$ (100-300°C))⁴⁵. Alumina substrates were expected to allow sufficient adhesion of glass parts during processing, and easy removal post-process.

Processing on glass substrates was done with the aim of achieving permanent adhesion of glass parts to substrates. To accommodate alumina discs of 2.5 mm thickness, a stainless-steel base plate (69 mm diameter) was modified to incorporate a recess of 2.5 mm with a diameter of 50.5 mm, and two small holes were drilled in the base to allow easy removal of substrates after use. Carbon tape was used to secure the alumina substrate to the stainless-steel base plate.

For processing on glass substrates, the white alumina substrate was darkened with graphite before affixing the glass substrates on top. As the base plate was 70 mm diameter, 75 mm microscope slides were cut by diamond pen to a suitable size to fit the available base plate/alumina surface. Carbon tape was used to secure the glass slides, and processing was only carried out on the area of glass substrate directly above the graphite darkened alumina substrate. 1 mm thick glass slides were expected to be more susceptible to thermal shock and fracture than 2.5 mm alumina substrates. Process parameters were investigated for processing on each type of substrate.

For trials involving a high temperature coil heater, a stainless-steel base plate was designed to accommodate the geometry of the substrate heater and ceramic insulation, as well as an alumina disc substrate. The recess was 54 mm diameter and 20 mm deep. A 5 mm diameter hole was cut by waterjet in an Alumina substrate to allow positioning of a KType thermocouple close to the coil heater. Installation of the substrate heater is described in Section 5.5.

5.1.3 Glass Powder Feedstocks

For SLM investigations, a range of glass powder feedstocks were considered. Through thorough material characterisation (Chapter 4), glass powders with spherical morphology were prioritised for experimental investigation by SLM. This included GTS-1, GTS-2, and GTS-6 soda lime silica glass beads of varying particle size distribution: $D_{v50} = 258 \mu\text{m}$, $102 \mu\text{m}$ and $44 \mu\text{m}$ respectively. GTS-6 was used most frequently due to the smaller average particle size, which related to a smaller powder bed layer, and therefore a higher achievable part resolution.

GTS-3, a Fe doped 13-93 biologically active glass, was also used experimentally despite its poor flowability measured in Chapter 4. This material was used in a feasibility study to observe the effect of glass composition on SLM processing parameters. The poor flowability

of this material inhibited SLM processing and prompted the investigations into spheroidising methods described in Section 4.5.

5.1.4 Evaluation of Processing Parameters

SLM processing parameters that were investigated in this research include laser power (W), scan speed (mm/s) and hatch spacing (mm). Scanning strategy and layer delay were also investigated for their effect on glass processing (described in Section 2.3).

A series of experiments were planned to evaluate the effects of processing parameters on SLM processing of soda lime silica glass. The results were used to populate process maps, evaluating the effect of laser power, scan speed, and hatch spacing on glass melting and consolidation. To do this, energy density was used to relate laser parameters (as described in Section 2.7). For on-glass processing, cracking of glass substrates and adhesion of parts to substrates was taken into account when evaluating process parameters.

5.2 Process Parameter Investigation

Experiments were carried out to observe the effects of laser power and scan speed on processing soda lime silica by SLM. This was done to define a suitable processing window, whereby successful processing of glass powder on glass substrates would be most likely. Hatch spacing was also included in parameter investigation, as this parameter also impacts energy density and therefore glass processing. Scanning strategy was also investigated, including the effect of incorporating a delay between layer processing.

5.2.1 Energy Density

To define a suitable processing window for SLM of soda lime silica glass feedstock (GTS-6), experiments were carried out systematically to evaluate the effect of laser power (W), scan speed (mm/s), and hatch spacing (mm) on glass processing. Energy density was used to assign a single value to each combination of parameters (as described in Section 2.5).

Experiments for an initial process map were carried out for glass processing on a ceramic substrate (99.8% purity Alumina) (Section 5.3). Combinations of parameters were tested sequentially, assessing the effect of energy density on glass processing. These parts were assessed based on level of glass melting and consolidation observed at different energy densities. Later, a process map was generated for processing on glass substrates (soda lime silica microscope slides), to determine the effect of laser processing parameters on glass-on-glass processing (Section 5.4). Assessment of these parts included the presence or absence of substrate cracking, and adhesion of processed glass structures to substrates.

For glass-on-ceramic processing, thin walls (7 x 3 mm) and cube structures (5 x 5 x 5 mm) were used to investigate process parameters. Combinations of laser powers between 20-100 W, and scan speeds between 5-60 mm/s were used to populate the thin wall process map. For cube processing, energy densities between 15-30 J/mm² and hatch spacings between 0.1 – 0.5 mm were used. For glass-on-glass processing, cuboid structures (1 x 3 x 6 mm) were processed on a soda lime silica microscope slide (above a blackened base) and assessed at energy densities between 60-94 J/mm³. Layer height and hatch spacing were kept constant at $t=0.07$ mm, and $h=0.369$ mm. Process maps were generated and used to suggest suitable processing windows for each experimental set-up and their defined conditions.

5.2.2 Hatch Spacing

The sensitivity of glass powder processing to hatch spacing was highlighted in early experimental trials, particularly with processing on glass substrates. A small hatch spacing would lead to an expanded heat affected zone, and occasionally resulted in glass substrate fracture due to severe thermal stresses. Hatch spacing showed an impact on energy density, requiring it to be balanced with scan speed and laser power (Section 2.5, Equation 2), and was considered alongside scanning strategy.

Hatch spacing was investigated to determine a suitable distance between adjacent laser scans for glass powder SLM processing. For processing on ceramic substrates, hatch spacings of between 0.11 and 0.45 mm were used during parameter investigations. For on-glass processing, hatch spacing was investigated using 1 x 3 x 6 mm built structures, using an alternating y-hatch, at a fixed scan speed of 37 mm/s, and at varying laser power between 65 - 80 W. Two hatch spacings were used: 0.33 mm (9 scan tracks per 3 mm structure), and 0.355 mm (8 scan tracks per 3 mm structure).

The effect of hatch spacing was also tested using a more complex geometry (“3DGLaSS” logo), with hatch spacing of 0.369 mm and a reduced hatch spacing of 0.245 mm, using an alternating x/y hatch. Other parameters were kept constant (100 W, 47 mm/s, ED= 30.4 J/mm²). The overall energy density of these combinations of parameters are calculated as 82 J/mm³ and 124 J/mm³ respectively. The logo design was also processed using an x hatch and a y hatch at the same parameters (100 W, 47 mm/s, ED= 30.4 J/mm², h= 0.369) to show the effect of scan direction on SLM of glass.

5.2.3 Scanning Strategy

For initial investigation of the effect of scanning strategy on SLM processing of glass, 1 x 3 x 6 mm structures were built. An alternating y hatch, alternating x-y hatch, and 67° rotation hatch (Figure 51) were tested at various parameters on a glass substrate, and the resulting structures inspected by SEM. Parameters of 65-80 W, 37 mm/s scan speed, and 0.369 mm hatch spacing were used. These scan strategies were also explored through fabrication of the text design “3DGLaSS”.

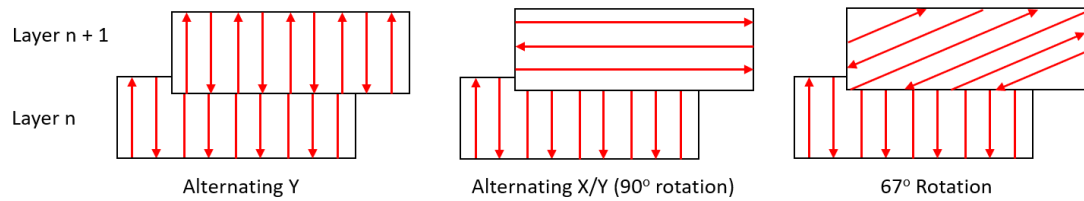


Figure 51 Schematic for SLM scan strategy investigations (alternating = bi-directional).

5.2.4 Layer Delay

Another important aspect of glass processing by SLM was the time between laser scanning and spreading of subsequent powder layers (as described in Section 2.3). For example, a short layer delay could lead to conduction of heat from previously scanned layers to the virgin powder, altering the energy required to melt by laser irradiation. Implementation of a laser “dead time” was used to alter the time between laser scanning and powder spreading. This was achieved by preparing additional artifacts during build set-up, and defining their laser power as 0 W. Arrangement of these parts on the build platform allowed definition of a length of time during which laser processing was paused. For glass processing this was suspected to be beneficial to allow excess heat to dissipate from the built parts.

5.2.5 Design Geometry

Different geometrical structures were created by 3D CAD software (Solidworks, Dassault Systemes, FR) and edited for use in the Realizer SLM-50 (Magics, Materialise, BE). 1 x 2 x 1 mm elements were processed for the first on-glass SLM trials, to prove feasibility. These rudimentary elements were visualised by SEM, and an estimation of geometrical accuracy was obtained for two samples using edge detection (Sobel Operator) and binary conversion (MATLAB, MathWorks, US). The calculated values were compared to a reference of the intended dimensions to represent the expansion or shrinkage of dimensions during processing at the given process parameters (78.5 J/mm³).

Simple 1 x 3 x 6 mm cuboids were used for parameter investigations. Other geometries such as hollow cylinders, rods, channels, “3DGLaSS” text logo, and lattices were also created for investigation. Lattice structures, such as gyroid matrices and diamond lattices of varying

internal dimensions were made using FlattPack (University of Nottingham). Structures were built on ceramic or glass substrates, and parameters were directed by process parameter investigations.

1 x 2 mm elements were arranged to make up joined structures on glass substrates. An example arrangement was to form two continuous walls, parallel to each other, creating a channel. Utilising these elements to make up continuous structures allowed finer control over scan patterns, ensuring that no two adjacent 1 x 2 mm elements were processed consecutively.

5.3 Processing Glass onto Alumina Substrates

The following section describes processing of glass powder onto ceramic substrates. The majority of this work was carried out by, in collaboration with, or under the supervision of, K. Datsiou. The findings from this work helped to guide the experimental investigations into SLM of glass onto glass substrates.

This initial investigation into glass processing by SLM has been published in two journal papers: “Additive manufacturing of glass with laser powder bed fusion”²¹⁶, and “Laser powder bed fusion of soda lime silica glass: Optimisation of processing parameters and evaluation of part properties”²¹⁷. For this investigation, soda lime silica glass structures were built on Alumina discs, with and without sacrificial support structures. Investigation into optimal parameters, processing of complex geometries, and characterisation of built parts was described.

5.3.1 Process Maps

Thin walls (single tracks) and 5 x 5 x 5 mm glass cubes were processed at a range of parameters and mapped to define a suitable processing window for GTS-6 soda lime silica glass feedstock on alumina substrates (Figure 52). Processing between 80-110 J/mm³ was recommended for this glass feedstock based on the observed consolidation of powder at different parameter combinations. The optimal parameters defined for processing glass structures on ceramic substrates was assumed to effect on-glass processing.

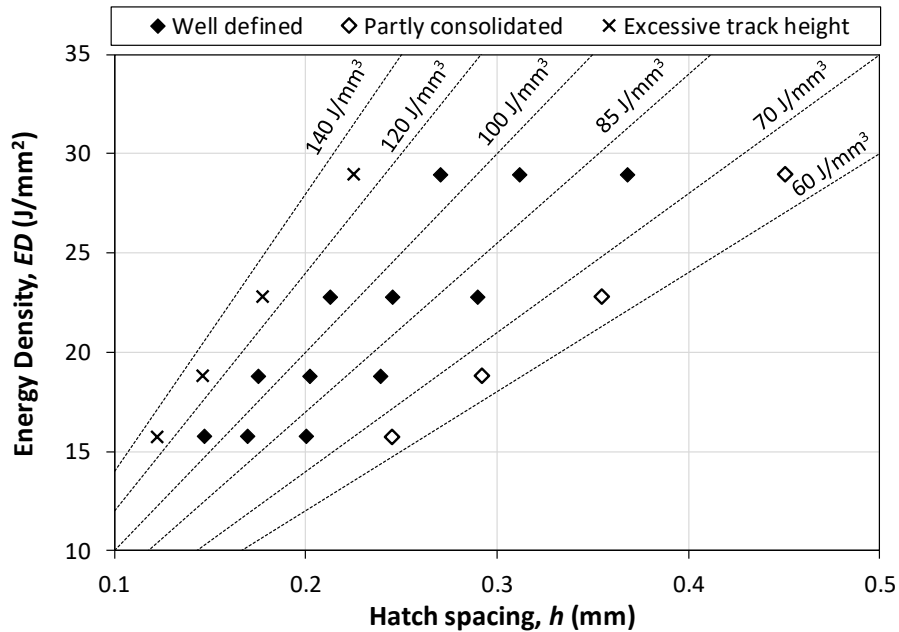


Figure 52 Process map for 5 x 5 x 5 mm soda lime silica (GTS-6) cubes fabricated on ceramic substrates.

Porosity of cubes was measured using micro-CT (XCT), and analysis of cross-sectional data via ImageJ. Internal porosity decreased marginally as energy density increased ($78.5 \text{ J/mm}^3 = 12.1\%$ porosity, $107.1 \text{ J/mm}^3 = 11.3\%$ porosity). Porosity was identified as pores, cracks, and areas of un-sintered powder particles. These defects are thought to be the cause of opacity of SLM glass structures (as well as satellite powder attached to structure surfaces). This level of porosity is expected in glass structures processed at similar parameters on glass substrates.

5.3.2 Catalysts

Rectangular grids of various dimension were processed from GTS-2 and GTS-6. Visualisation by SEM revealed higher part resolution for the feedstock with the smaller particle size distribution (GTS-6)(Figure 53). These structures were utilised as supports for cuboid parts, and also developed as structured catalysts for chemical engineering applications (e.g. monolithic reactors)²¹⁸. The presence of unfused powder on the surfaces of these structures arguably increases the available surface area, and thus increases the efficiency of catalysis²¹⁹.

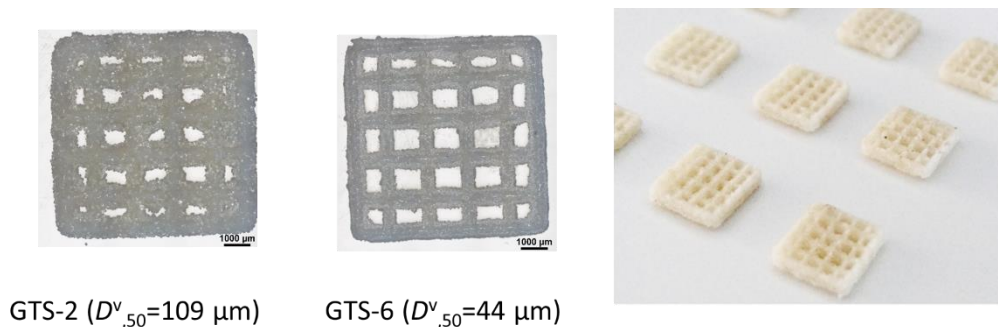


Figure 53 Rectangular grid structures for catalysis and support structures. Left: SEM micrographs of GTS-2 and GTS-6 grids. Right: Structured catalysts.

5.3.3 Glass Continuous Flow Reactor Channels

Various geometries were designed for the application of glass continuous flow reactors. Different build orientations were investigated for successful fabrication of hollow, tubular structures on ceramic substrates. Internal diameters ranged from 2 to 5 mm, and both cylindrical and angular geometries were used (Figure 54). The build orientation had a large effect on success of printing. For certain build orientations, such as straight channels built vertically in the z direction, warping sometimes occurred. Additionally, unfused powder within channel cavities limited the dimensional accuracy. Support structures were required internally for square shaped channels to support overhangs. These support structures were difficult to remove post process, and prevented the evacuation of powder from channels. Discolouration of parts sometimes occurred. This may have been caused by impurities or contamination present during processing.

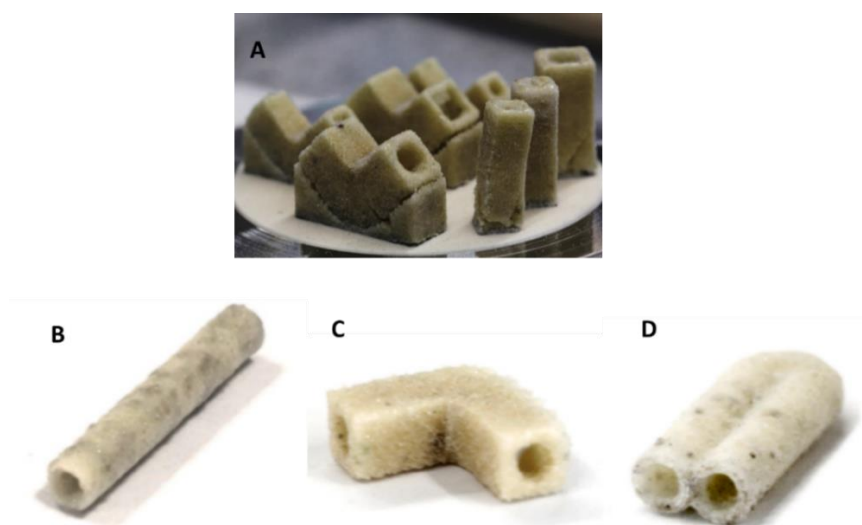


Figure 54 Examples of channel structures fabricated by SLM A: Channels on ceramic substrate with support structures, B: 2 mm diameter linear channel, C: 3 mm diameter angles channel, D: 2 mm diameter u-shaped channel.

Hollow cylinders were processed at parameters of 75 W laser power, 37 mm/s scan speed, and hatch spacing of 0.3 mm ($ED= 96.5 \text{ J/mm}^3$). For bend sections, the hatch spacing was increased to 0.369 mm, reducing the energy density (78.5 J/mm^3), and x hatch, y hatch, and alternating x-y hatch (90° rotation) was investigated. The results showed more cracking associated with x and y hatch scan strategies than with alternating scan strategy (Figure 55 A-D). Additionally, x hatch scan strategy resulted in a distortion of geometry. For this reason, an alternating x-y scan strategy was selected for the bend portion of the channel structures. More complex channel structures were built using separate parameters for straight sections and bend sections. Sacrificial structures were used for supports - these were fabricated using the same material as the built parts and resembled the grid structures in Figure 53 . Parts were easily removed from the built structures post process thanks to the brittle nature of the supports. Bend sections were positioned to connect straight channels, at the top and bottom of the build. Demonstration parts showed some cracking, but the geometry was generally preserved (Figure 55 E).

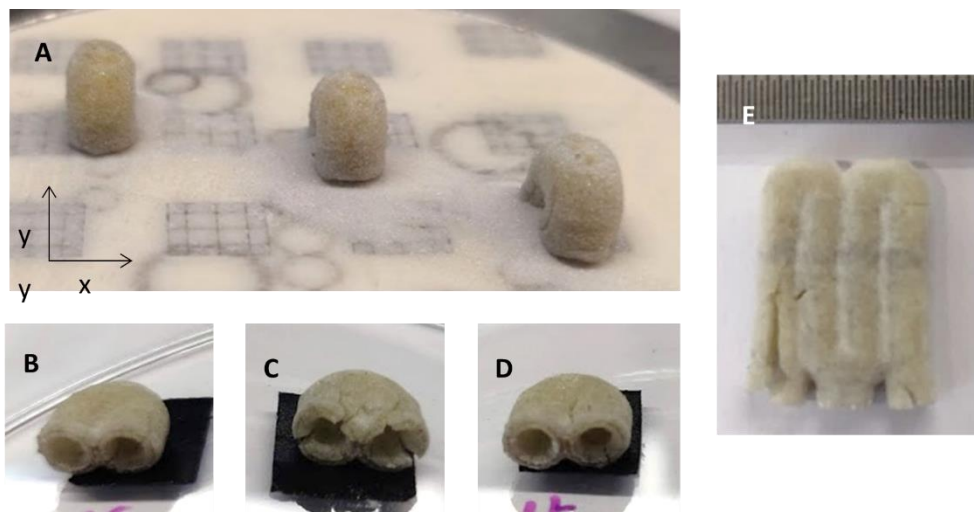


Figure 55 A: Bend portions of channel structures. B: x hatch, C: y hatch, D: alternating x/y hatch, E: Demonstration of channel structure with multiple bends.

5.3.4 Discussion

In this work, the feasibility of processing soda lime silica glass by SLM was demonstrated, using a commercially available SLM system (Realizer GmbH SLM-50). This expanded on the work described by Fateri and Gebhardt (2015)¹³², demonstrating fabrication of parts with greater geometric complexity than previously presented, and providing further insight into the effect of SLM processing parameters for soda lime silica glass.

The feedstock was characterised and processed at various parameters to define a suitable processing window for the material. Thin walls and cubes were built on high purity alumina discs to populate process maps, observing the appearance of fused glass, and assessing parameters based on consolidation of glass powder and dimensional accuracy. A processing window was identified for fabricating well defined, consolidated glass structures. The processing window identified in this work was 70-120 J/mm³ for GTS-6 soda lime silica, and 65-110 J/mm³ for GTS-2 soda lime silica. In literature, suitable processing parameters for SLM of soda lime silica glass were reported as 100 W, 0.05 m/s, 500 µm layer thickness, and 50-100 µm hatch spacing, relating to 40-80 J/mm³. In comparison, these recommended processing parameters show some agreement. Fabricated structures were opaque due to internal porosity and excess powder particles fused to structure surfaces, similar to glass structures presented in literature on powder bed fusion AM of glass compositions (soda lime silica, quartz, and borosilicate)^{94,131,132,220}. This effect is often reported with powder bed fusion additive manufacturing, due to the conduction of laser energy to powder adjacent to laser scanned areas. Thermal post processing (at 650°C for 5 hours, with the aim of improving translucency by remelting the structure surface) reduced opacity of parts somewhat, but also resulted in volumetric shrinkage due to further consolidation of material and therefore reduced geometrical accuracy. Further work into optimising thermal post processing cycles for SLM glass structures is recommended to fully assess the effect on glass porosity, appearance, and geometrical accuracy.

Complex geometries were achieved by SLM, including lattices and hollow channels (Figure 56). Further optimisation of parameters was required for variation in geometry, as process maps related only to the geometries used. Sacrificial support structures were used for certain builds, with the purpose of aiding removal of parts from ceramic substrates. Parts appeared opaque with high surface roughness, and certain processed geometries were brittle. Hollow channels were designed for the application of glass continuous flow reactors in this work, however, the opacity and high porosity of as-built parts is unlikely to achieve leak proof flow of liquids. In order to achieve leak-tight transport of fluids (for microfluidic reactors), reduction of porosity would be essential. SLM processing at higher temperatures than permitted by the SLM system (just below the glass transition temperature of the glass composition, ~500°C for soda lime silica) was anticipated to improve melting and consolidation of glass powders, whilst retaining geometrical features (unlike surface remelting mentioned above). This was explored in Section 5.5, with the aim of achieving fully

melted glass SLM parts, with reduced porosity, and reduced thermal stress as a result of the reduced temperature gradients.

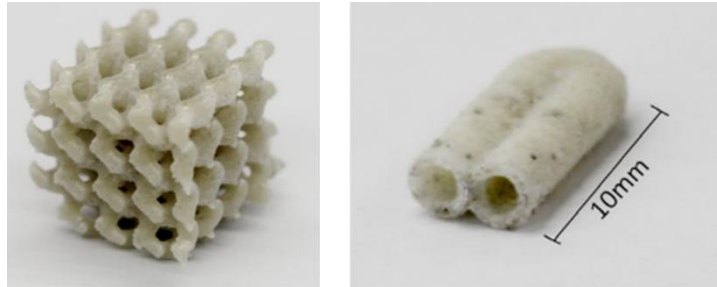


Figure 56 Demonstrated geometries for SLM of soda lime silica glass. Left: Lattice geometry. Right: Hollow channel structure.

The work also assessed SLM glass parts in terms of porosity and flexural strength, and defined geometrical limits based on optimal processing parameters. Porosity was assessed through micro-computed tomography (XCT) cross sections of cubic SLM glass parts, and the average porosity was calculated for processing at different energy densities. 11 – 12 % porosity was measured for the samples, and was marginally lower for glass cubes processed at higher energy density. Porosity was only investigated for a small sample size – using two samples of different energy density. Three point bending tests (see appendix) were used to measure 1 x 2 x 8 mm built parts, using the test protocol presented by Focatiis and Buckley²²¹. The tests revealed a flexural strength between 6 – 7 MPa – far inferior to glass processed by the float glass method, as expected²²².

In these investigations, machine limitations meant that SLM processing was carried out at substrate temperatures of up to 250°C. Maintaining a substrate or chamber temperature around the glass transition temperature of the feedstock is suspected to reduce internal porosity and the effect of thermal stress from high temperature gradients. It is also speculated that higher temperature processing would allow glass material to fully melt whilst retaining geometrical accuracy, and therefore transparency of structures may be improved.

High purity alumina discs were used to complement the coefficient of thermal expansion of soda lime glass. This provided good adhesion during processing to prevent delamination, and parts were removed from the substrate post process. Support structures were also utilised to allow easy removal of parts without jeopardising part structure, however cracking was often seen. Processing on glass substrates would likely introduce further challenges for glass

SLM, such as avoiding thermal shock in substrates and achieving sufficient adhesion of structures to substrates.

5.4 Experimental Results

5.4.1 Energy Density

Process mapping of glass-on-glass SLM parameters revealed the effect of scan speed and laser power on processing. Resulting SLM structures of GTS-6 at parameters between 37-57 mm/s and 65-75 W showed variation in appearance and level of glass consolidation (Figure 57). The visibility of scan tracks increased with increasing scan speed (reduced energy density). Scan tracks were also comparatively more visible at 41 mm/s scan speed than at 37 mm/s, however this was visibly more subtle, but clearly seen under SEM (Figure 58). Processing at slower scan speeds, e.g., 37 mm/s, resulted in greater consolidation of glass material, due to the higher energy density. Geometrical accuracy appeared to be compromised with decreasing energy density, with these structures appearing incomplete, suggesting an insufficient energy for glass consolidation. In general, with increasing energy density, scan tracks became less visible, and structures appeared to be more consolidated, with improved geometrical accuracy.

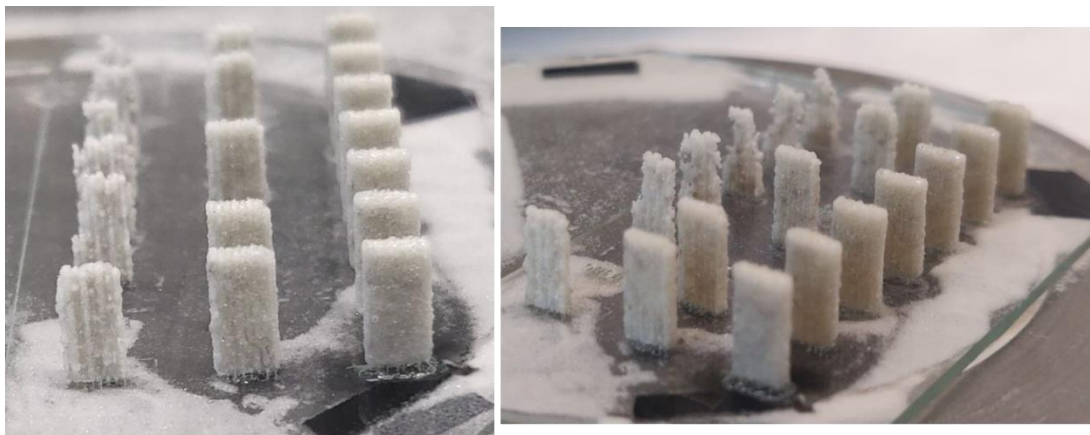


Figure 57 SLM of GTS-6 on glass substrate. Energy density decreasing front to back, and scan speed increasing left to right.

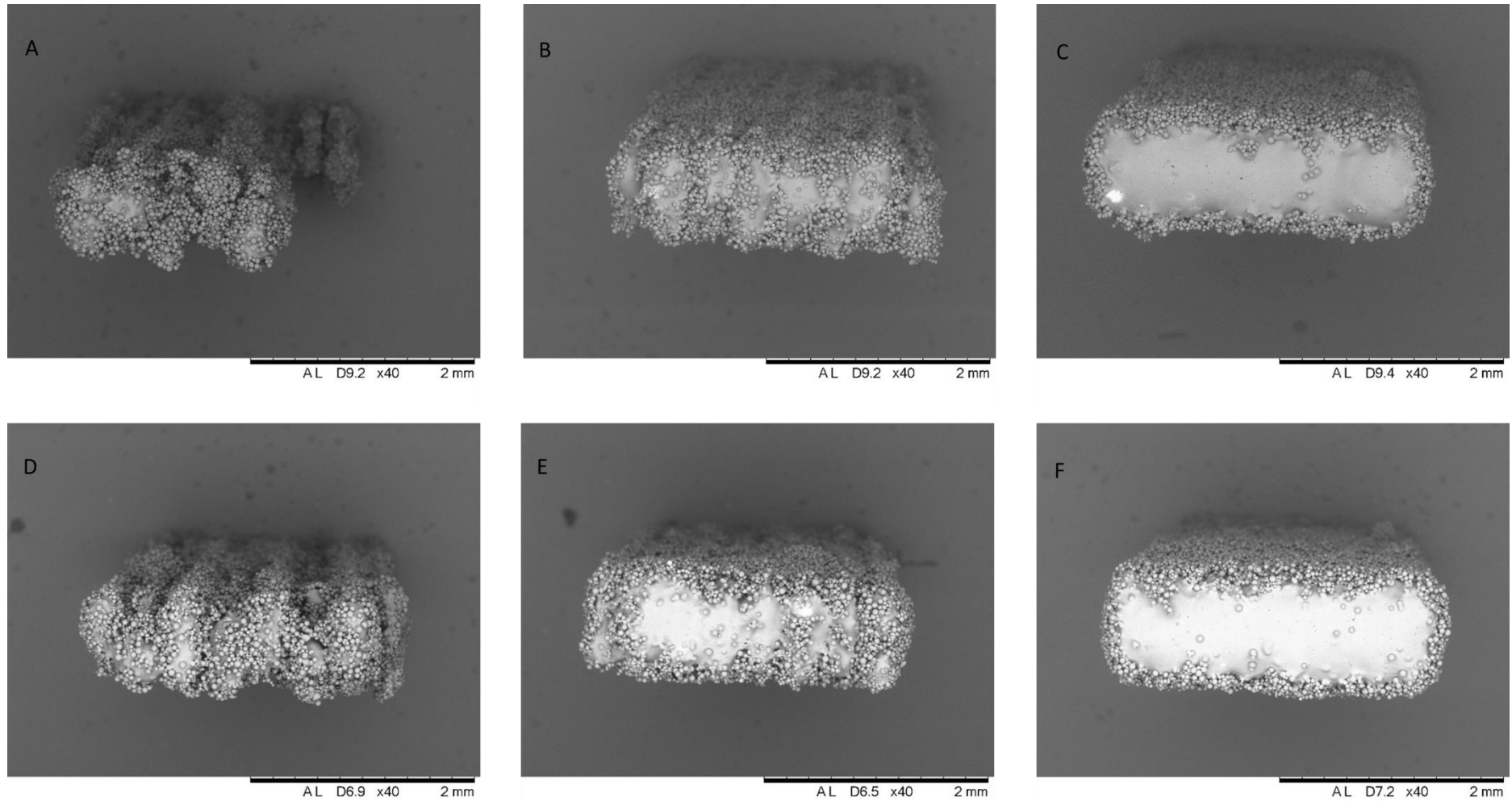


Figure 58 SEM micrographs (x40 magnification) of SLM GTS-6 on glass substrate. A: 67.5 W, 57 mm/s, B: 67.5 W, 47 mm/s, C: 67.5 W 37 mm/s, D: 75 W, 57 mm/s, E: 75 W, 47 mm/s, F: 75 W, 37 mm/s.

The populated process map defined each set of parameter combinations based on consolidation (Figure 59). “Full Consolidation” was seen at higher energy densities, and denoted structures that were complete and where scan tracks were not visible. “Visible Scan Tracks” refers to structures where partial consolidation was seen. Geometrical accuracy was high, but the visibility of scan tracks suggested insufficient energy density for complete consolidation of glass feedstock. “Incomplete Consolidation” referred to structures that lacked geometrical accuracy, resulting in incomplete built structures.

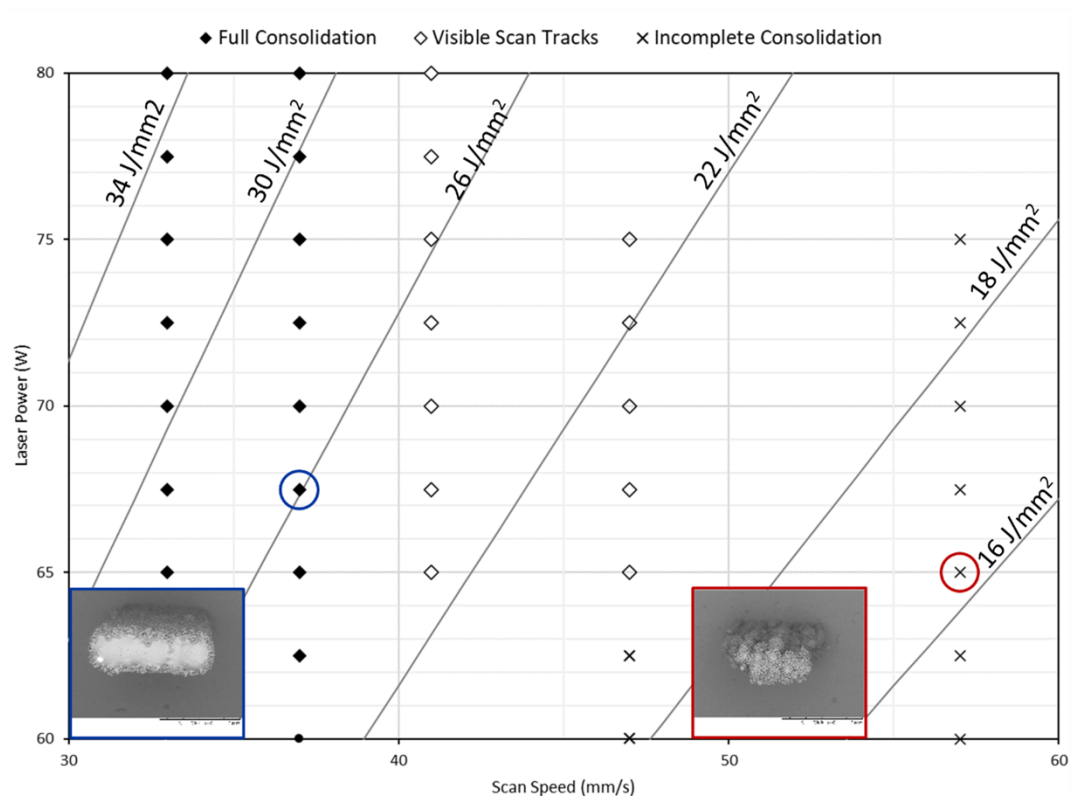


Figure 59 Process map showing SLM of glass (GTS-6) at different parameter combinations. Examples of “Full Consolidation” and “Incomplete Consolidation” highlighted.

A relationship is shown between energy density and success of processing. In general, processing below 18 J/mm^2 resulted in incomplete consolidation of glass feedstock, suggesting insufficient energy for glass melting. In contrast, above 28 J/mm^2 every tested combination of parameters resulted in complete consolidation of feedstock and high geometric accuracy. However, some tested combinations had a similar calculated energy density, yet showed different effects on processing due to laser power and scan speed differing for each combination. For example, glass processed at 67.5 W and 37 mm/s ($\text{ED} = 26.06 \text{ J/mm}^2$) was classified as “Full Consolidation”, yet glass processed at 65 W and 41 mm/s

(ED= 26.13 J/mm²) presented as “Visible Scan Tracks” due to the appearance of the structure. The process map indicates the effect of energy density, but this value shows less of an impact on processing than variation in scan speed or laser power independently. Variation in build success was larger with varying scan speed than with laser power within the parameters tested.

To compare the resulting on-glass processing window with processing parameters for glass-on-ceramic SLM (Section 5.3), and with the previously reported literature, the processing window is defined using a hatch spacing of 0.369 mm for the parameter combinations reported above. With this in mind, on-glass processing of GTS-6 is recommended between 49-76 J/mm³. The processing window was in good agreement with literature (40-80 J/mm³)¹³², but narrower than recommended for the same composition on ceramic substrates found in this work at 70-120 J/mm³. This difference is likely due to the additional requirement in glass-on-glass processing to adhere to glass substrates and avoid substrate cracking.

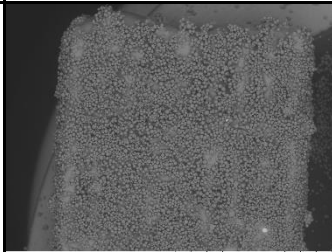
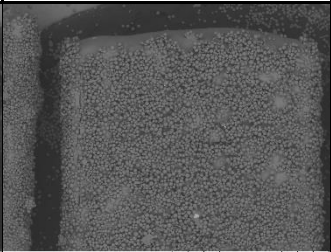
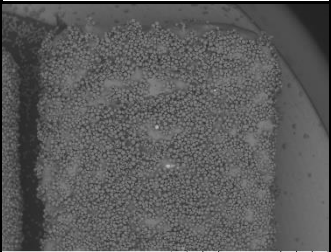
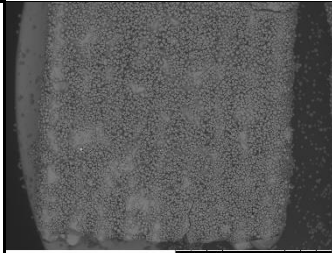
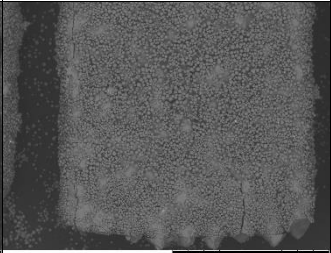
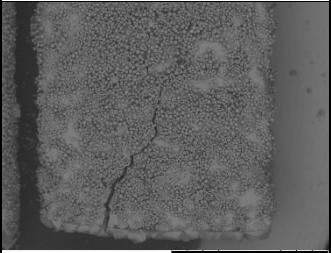
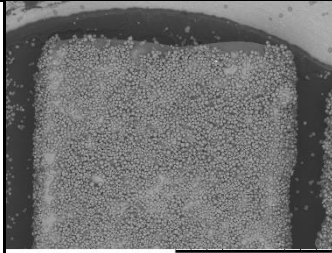
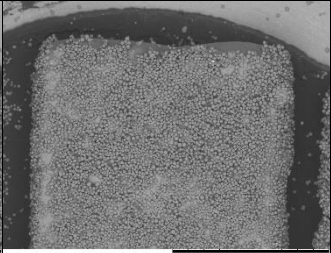
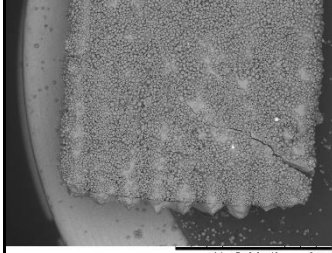
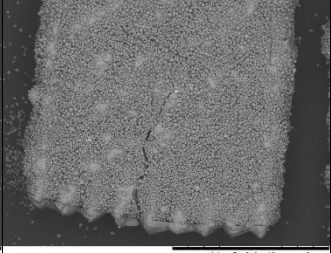
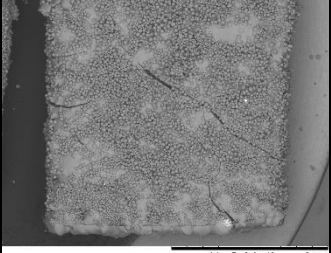
Of the parameters displayed in the process map, no substrate cracking occurred. This is due in part to the small process area of each part, and therefore a limited area of the substrate was affected by laser radiation. Additionally, structures were built in a semi-randomised manner, whereby no two adjacent structures were processed immediately after the other. Another important experimental condition that ensured substrates and structures resisted cracking from thermal shock was the time defined between each processed layer. A delay of 6 seconds between layer processing was used to allow excess energy to dissipate after a structure was processed, meaning that the subsequent powder layer would not melt prematurely to laser processing. This helped to prevent distortion of part geometry.

5.4.2 Hatch Spacing and Scanning Strategy

5.4.2.1 The Effect of Scanning Strategy on Small Elements

Small elements showed no significant difference between 0.355 mm and 0.33 mm hatch spacing. 1 x 3 x 5 mm structures that were processed using a y hatch, alternating x/y hatch, and 67° rotation hatch were viewed under SEM to investigate visual differences (Table 14).

Table 14 SEM images of 1 x 3 x 6 mm structures after removal from glass substrates. Images show the results of three different scan strategies/hatch (Y hatch, alternating X/Y hatch, and 67° rotation hatch) at two different energy densities.

		Y	Alternating X/Y	67° rotation
70 W, 37 mm/s	Top			
	Bottom			
75 W, 37 mm/s	Top			
	Bottom			

For y hatch, scan tracks were visible. For alternating x/y hatch, scan tracks were less visible and structures appeared more defined. Similarly, for 67° rotation hatch, structures did not show distinct scan tracks. For each sample, cracking of structures was seen, particularly in lower layers of the parts. Cracking was more severe in 67° rotation samples than in y or alternating x/y hatch samples. Another similarity between samples was the appearance of the top surface of parts. When viewed by SEM, each top surface was not uniform, showing less glass fusion on the middle section of structures.

5.4.2.2 The Effect of Hatch Spacing and Scan Strategy on Text Design

The “3DGLaSS” logo was built using different hatch spacing or scan strategies, and the effect on processing was observed (Figure 60). For hatch spacing, a distinct difference can be seen between $h = 0.245$ mm (A) and $h = 0.369$ mm (D). The smaller hatch distance resulted in a clear loss of geometric accuracy, due to the increased energy density, and therefore expanded heat affected zone. The surrounding feedstock in the powder bed was affected by the excess energy, fusing, and therefore compromising the definition of part features.

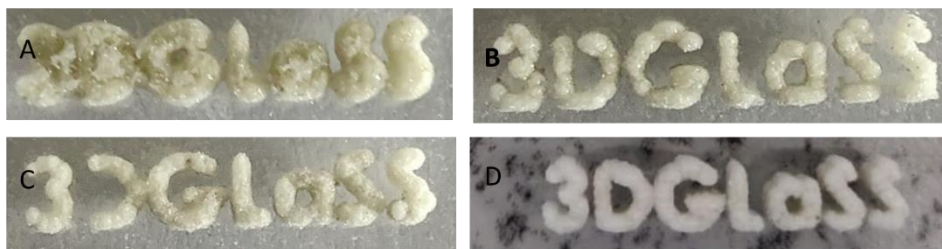


Figure 60 “3DGLaSS” logo processed onto glass substrates by different scan strategy or hatch spacing. A: reduced hatch spacing, B: X hatch, C: Y hatch, D: alternating x/y hatch.

For x hatch (B) and y hatch (C) scanning strategies, definition of features was compromised when compared to alternating x/y hatch (D). Due to the small size of the parts processed, using a single axis scanning strategy resulted in a loss of geometrical accuracy. Using a moderate hatch spacing (0.369 mm) and an alternating x/y scan strategy resulted in the most successfully processed structure within this investigation.

To assess the effect of scan strategy on more complex designs, the “3DGLaSS” logo was processed using 90° rotation hatch and 67° rotation hatch. Sections of the processed glass structures were compared by SEM, and geometrical accuracy was assessed by eye (Figure 61). The complex geometry of “3DGLaSS” logo, compared to simple cuboid structures, emphasises the effect of hatch rotation on glass SLM. Geometrical accuracy was observed to be altered with 67° hatch rotation compared to 90° hatch rotation. On 90° hatch rotation, some geometrical accuracy appears lacking, with edges appearing to be less defined compared to 67° hatch rotation. Glass fusion appears to be more concentrated in locations where laser radiation would start/finish (e.g. as seen in , A and C) for 90° hatch rotation. Glass fusion appears to be more prevalent in 67° rotation hatch, as this potentially allows glass feedstock to absorb energy over a greater area. Geometrical accuracy is potentially reduced in the opposite manner to 90° rotation hatch, as the heat affected zone is expanded, affecting a greater volume of glass feedstock. This could be further explored using ImageJ analysis to measure the % geometrical accuracy.

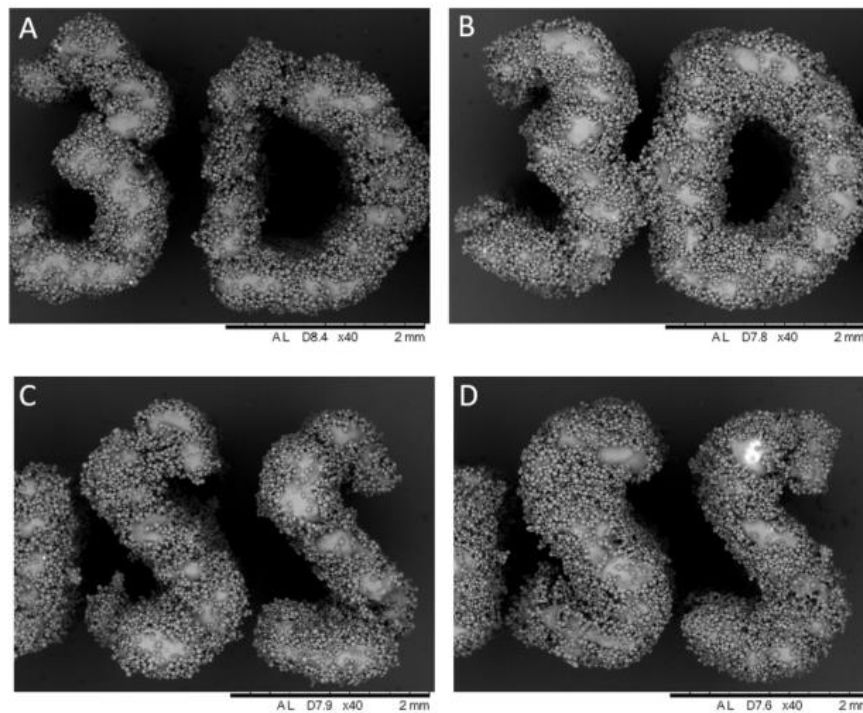


Figure 61 SLM micrographs comparing features of built parts. A,C: 90° rotation hatch, B,D: 67° rotation hatch.

5.4.3 Design Geometry

5.4.3.1 Cuboids and Cylinders

Elementary structures of 1 x 2 x 1 mm and 1 x 3 x 5 mm cuboids, and cylinders (3 mm external diameter, 2 mm internal diameter, $z = 3.57$ mm) were built on glass substrates to explore the effect of geometry on glass SLM processing (Figure 62). Cuboid structures were built in an array of 4 x 3, and cylinders were built in 5 x 3. The effect of scan strategy was again observed by comparing cylinders processed by Y hatch and alternating x - y hatch. Process parameters, guided by the results of process mapping, were set as 75 W and 37 mm/s, with hatch spacing of 0.369 mm ($ED = 78.5$ J/mm³).

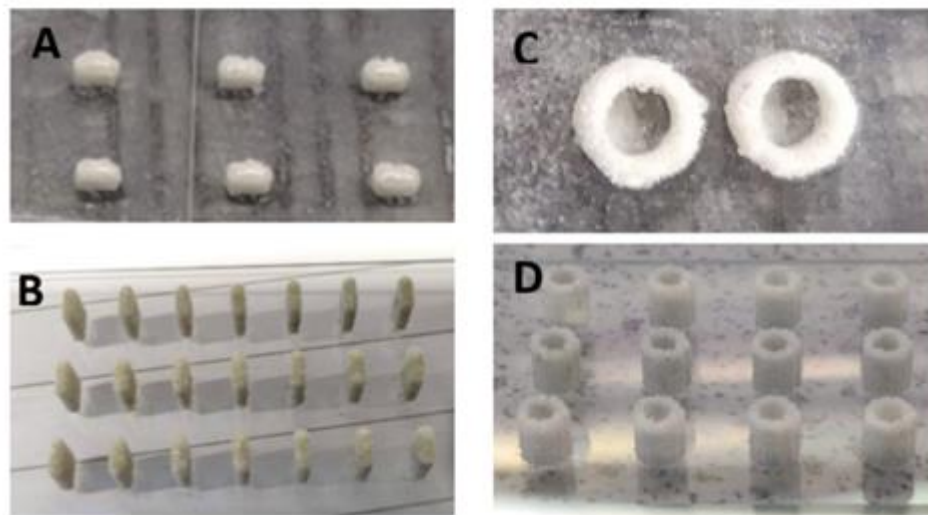


Figure 62 Cuboid and cylinder structures on glass substrates, A: 1 x 2 x 1 mm cuboids, B: 1 x 2 x 5 mm cuboids, C: Cylinders (3 mm \varnothing , 2 mm \varnothing internal - alternating x-y hatch), D: Cylinders alternating x hatch (3 mm \varnothing , 2 mm \varnothing internal).

Organising the build volume in arrays allowed randomised scanning of each element, and increased the time between layer processing, thus reducing the build-up of thermal stresses. The benefit of this strategy was observed, with the expansion of heat affected zone being limited (process area would glow brightly when energy density too high, affecting surrounding powder, and distorting geometry). Under SEM, processed structures revealed a glassy surface, with unfused powder adhered to the sides of parts (Figure 63). Geometrical accuracy was estimated for two 1 x 2 x 1 mm samples built using the same process parameters, with an average of 64%. This percentage was calculated based on the maximum deviation from part geometry in the x-y plane, as processed parts expanded in relation to the intended dimension, reducing the geometrical accuracy (see appendix).

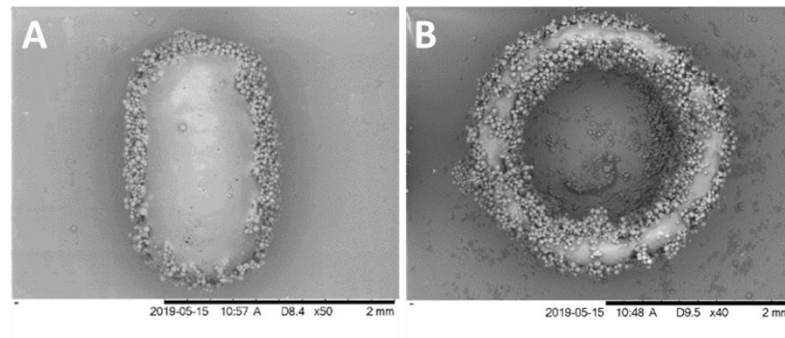


Figure 63 SEM micrographs of A: 1 x 2 x 1 mm cuboid elements, and B: 3 mm \varnothing cylinder (2 mm \varnothing internal) alternating x/y hatch (90° rotation).

Elements arranged on the build platform to create continuous walls showed distinct boundaries between elements, despite a defined offset of 0 mm being used (Figure 64). For most samples, dimensional variation due to scanning strategy was not obvious to the naked eye. When visualised by SEM, differences in geometry were observed across the four scanning strategies used (Figure 65). Elements built using 90° hatch rotation appear to have more irregular edges compared to 67° hatch rotation elements, however the indentation formed between elements appears to be more defined in 67° than 90° hatch rotation. Elements built with a y hatch show the most defined boundaries between adjacent elements, with x hatch showing the least defined edges. The hatch direction shows the largest impact on element edges joining. This is due in part to the hatch spacing used for these test pieces. During y hatch scanning, scan tracks were oriented in the same plane as the joins between elements, causing hatch spacing to be exaggerated between elements. During x hatch scanning, the scan tracks were perpendicular to the element joins, meaning scanning of adjacent elements was continuous, leading to a less defined join. This helps to explain why alternating x-y hatch showed an intermediate effect.

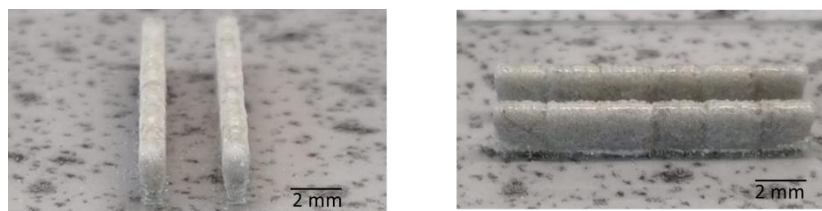


Figure 64 Channel structures built with 1 x 2 mm elements on glass substrates.

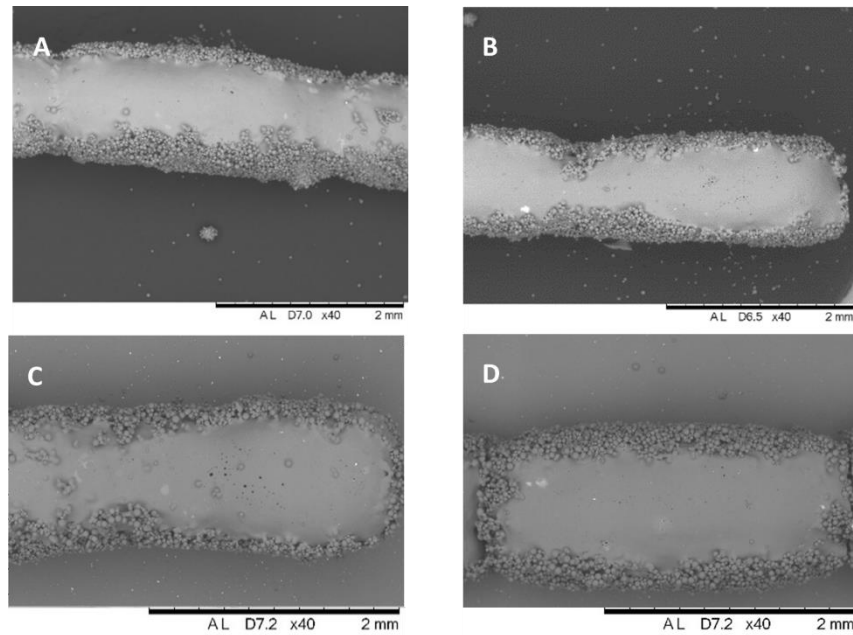


Figure 65 40x magnification SEM micrographs of channel elements based on scanning strategy/hatch spacing A: 90° hatch rotation, B: 67° hatch rotation, C: alternating x hatch, D: alternating y hatch.

Arrays of 30 hollow cylinders were processed on glass substrates to investigate processing of thin-walled structures. Fifteen cylinders of varying diameter and wall thickness were processed with varying energy density (dictated by hatch spacing). For thin-walled structures, a smaller hatch spacing (than used for other structures) was necessary ($h = 0.1\text{--}0.12$ mm). Process parameters were adapted iteratively based on observations (Table 14).

Table 15 Test matrix for investigating processing of thin-walled cylinders on glass substrates.

	Cylinder Trial			
	1	2	3	4
Inner \varnothing (mm)	0.9-2.1	0.9-2.1	0.9-2.1	0.9-2.1
Wall Thickness (mm)	0.15/0.2/0.35	0.15/0.2/0.35	0.15/0.2/0.35	0.15/0.2/0.35
Hatch (mm)	0.1/0.11/0.12	0.1/0.11/0.12	0.1/0.11/0.12	0.1/0.15/0.2
Laser Power (W)	75	75	70	72.5
Scan Speed (mm/s)	37	37	37	37
Scan Strategy	X-Y	X-Y	X-Y	X-Y/67° Rotation
Layer Delay (s)	0	21	21	21
ED (J/mm^3)	241-290	241-290	225-270	140-280
# Combinations	15			30
Repeats	2			1

Trial one resulted in substrate cracking due to a build-up of thermal stresses from processing adjacent structures consecutively at high energy density. To counter this, a layer delay of 21 s was implemented. This was accomplished by placing 30 additional cylinder structures on the built plate, with a defined laser power of 0 W. This effectively delayed powder spreading and helped to prevent adjacent structures from being processed consecutively, reducing the thermal shock experienced by the glass substrate.

Trial two successfully processed every thin-walled cylinder structure, and parts were assessed visually (Figure 66 A). Cylinders with the largest wall thickness (0.35 mm) that were processed at higher energy densities did not preserve a hollow inner diameter, with unfused powder adhered to the wall surfaces inside the cavity. Hollow cylinders were achieved for structures with wall thickness of 0.15 mm, and for the largest diameter cylinder of 0.25 mm wall thickness (2.1 mm \varnothing inner). Energy density was reduced to improve the evacuation of unfused powder from fused glass cylinder structures for trial three. For trial three, hollow cylinders were achieved for a wider range of cylinder dimensions/wall thicknesses (Figure 66 B). Only the largest energy density samples suffered from unfused particles unable to be removed from the inside of cylinder structures. Another issue observed with these process parameters was the increase in instance of delamination of structures from the glass substrate.

For trial four (Figure 66 C), energy was altered by increasing the range of hatch spacing, and by using a moderate laser power of 72.5 W. Another alteration was the use of both alternating x-y hatch (90° rotation) and 67° rotation hatch scan strategies. None of these parameter combinations resulted in delamination, with adhesion to the glass substrate satisfactory for each sample. For the majority of samples, little difference was observed between scan strategy of 90° rotation and 67° rotation hatch, however, for the cylinders of the smallest dimension (0.9 mm inner \varnothing , 0.15 mm wall thickness, h= 0.1 mm), a hollow cavity was only achieved using 67° rotation hatch.

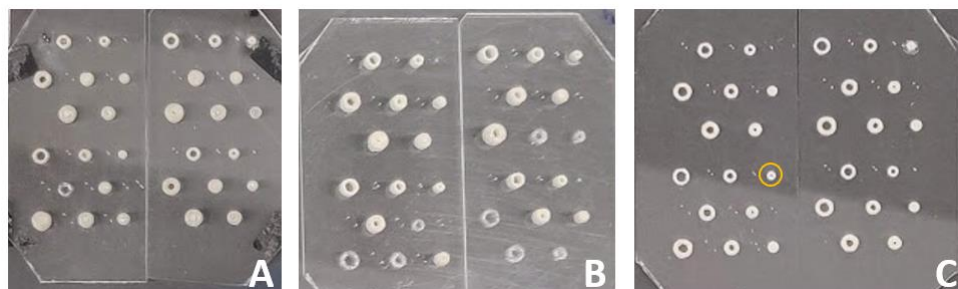


Figure 66 Thin-walled cylinders processed on glass substrates. A: Trial 2, B: Trial 3, C: Trial 4. Highlighted structures shows hollow cylinder processed using 67° rotation hatch

5.4.3.2 Lattices and Text

Attempts were made to process lattice structures on glass substrates, without causing thermal shock. Two challenges were identified: the adhesion of glass to glass, and the tailoring of energy density for on-glass processing.

The optimal parameters for processing glass lattice structures on ceramic substrates utilised an energy density too high for processing on glass substrates ($\sim 124 \text{ J/mm}^3$), and frequently resulted in glass substrate fracture, despite utilising the previously described layer delays to reduce the accumulation of latent heat in each part. Tailoring the energy density for on-glass processing was difficult, as a reduction in energy density (78.5 J/mm^3) to compensate for this resulted in brittle structures that had little structural integrity. Successful parameters for processing glass lattice structures without fracturing glass substrates were found at 75 W, 37 mm/s, 0.33 mm hatch spacing (87.75 J/mm^3), and a layer delay of 21 s

Adhesion of structures to glass substrates was limited due to the small area of processed glass in contact with glass substrate, particularly for structures less than 10 x 10 x 10 mm in size. Of all the lattice structures trialled on glass substrates, only one showed adequate adhesion to a glass substrate: the 10 x 10 x 10 mm diamond lattice, processed at 87.75 J/mm^3 (Figure 67).

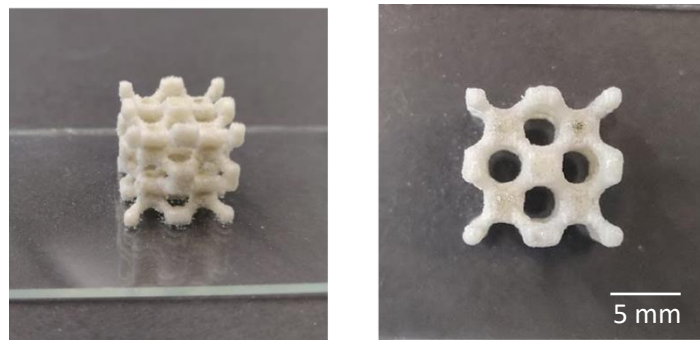


Figure 67 Glass diamond lattice processed on a glass substrate at 87.75 J/mm^3 energy density.

Text design was optimised for on-glass processing, up to a build height of 5 mm. Multiple text designs could be processed on the same glass substrate without cracking or fracture occurring (Figure 68). The text feature was small in size, with an approximate size of 3 x 15 mm for the “3DGLaSS” logo. Through observations of the effect of hatch spacing, scan strategy, and energy density, the recommended parameters were: 75 W laser power, 37 mm/s scan speed, 0.369 mm hatch spacing, 24 s layer delay, and a scan rotation of 67° or 90° for feature definition, adhesion to substrates, and avoidance of cracking.

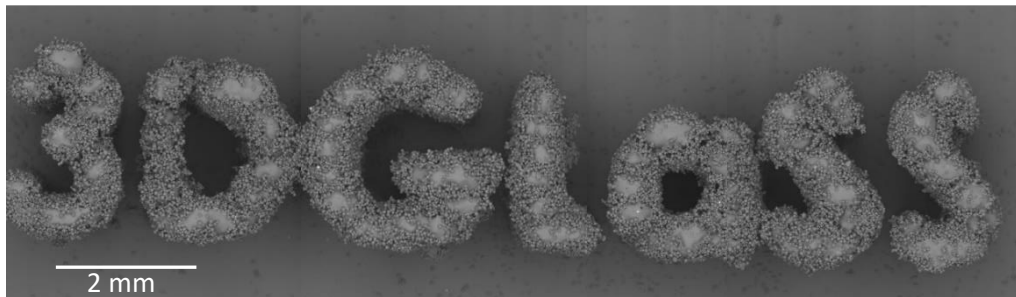


Figure 68 SEM image of "3DGLaSS" logo built on a glass substrate using x-y alternating hatch (90° rotation).

5.4.4 Substrate-Glass Interface

It was observed during many of the glass-on-glass processing trials that an “etching” effect was occurring on the surface of the glass microscope slide. In order to investigate this further, parts were observed by SEM (TM 3030, Hitachi, JP). 1 x 3 x 5 mm samples described in Section 5.4.2 were removed from the glass substrate and viewed in multiple planes. The corresponding glass substrate was also visualised to show the effect on the substrate surface.

Samples removed from the substrate surface showed small sections of substrate glass adhered to the bottom edge of processed glass. Under SEM, the interface showed that these areas corresponded with the process scan tracks. A sample processed at 80 W, 37 mm/s and hatch spacing of $h=33$ showed a regular pattern of adhered substrate glass on the bottom surface of processed glass (Figure 69 A-B). The pattern of adhered substrate glass to the bottom of processed structures agreed with the indentations seen in the substrate. These indentations were visible through the bottom surface of glass substrates, appearing as etched patterns or micro-cracks (Figure 69 C).

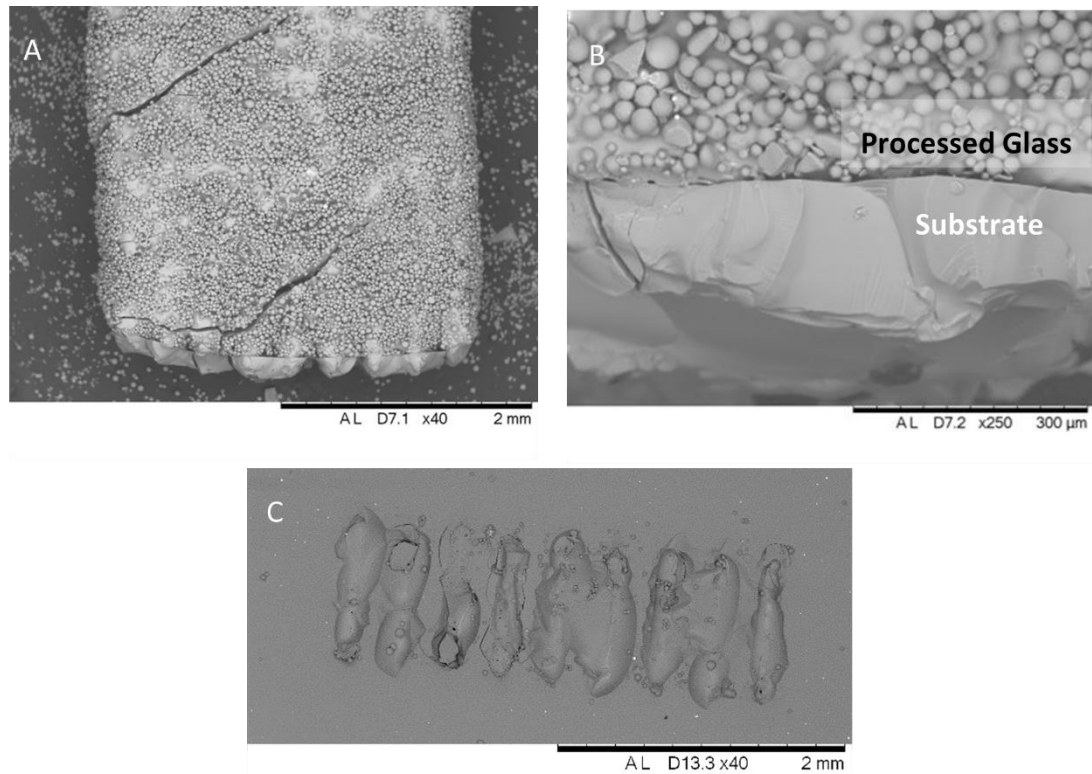


Figure 69 A, B: 1 x 3 x 5 mm glass structure (processed at 80 W, 37 mm/s, $h = 0.33$ mm) removed from glass substrate. C: Glass substrate after part removal.

Samples of processed glass powder feedstock on glass substrates at parameters of 80 W, 37 mm/s and hatch spacing of $h = 0.33$ mm were visualised by SEM to investigate micro-cracking (Figure 70). Single layer processing revealed initial melting of glass powder. Processed powder was severely limited, as the initial powder layer showed a balling effect, whereby powder particles showed initial agglomeration in some areas. Micro-cracks formed surrounding the process track, appearing to initiate from the ends of scan tracks, propagating away from the scan track, and in some cases merging with already present cracks. On visualisation of two layers of processed glass, melting was more apparent, with longer, fused glass structures beginning to form. Unconsolidated glass can be seen surrounding melted glass structures.

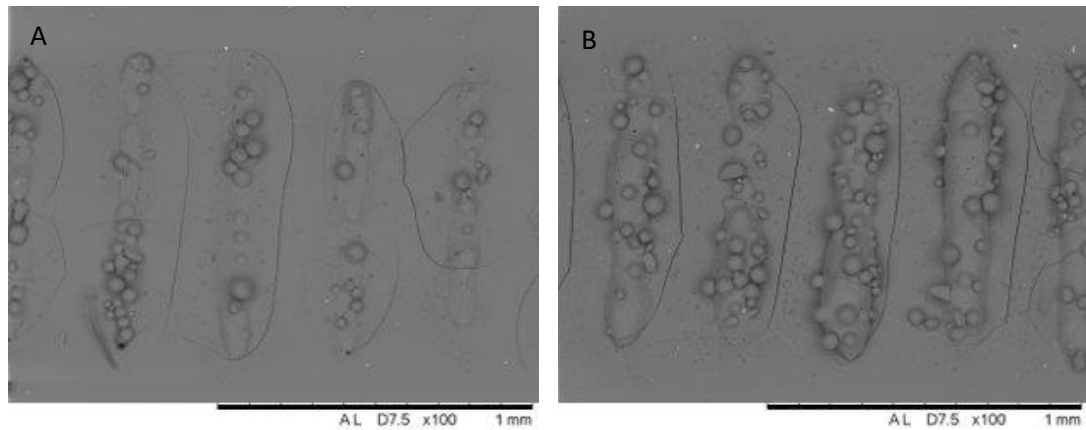


Figure 70 SEM micrographs of glass powder processing by SLM A: Single layer, B: Two layers.

Glass substrate was also processed in the absence of soda lime silica powder feedstock (Figure 71). The same patterns of micro cracks were seen in these instances as when glass processing occurred. The thickness of a single layer of GTS-6 feedstock was 70 μm , as this accounted for the largest particle size in the feedstock distribution (as measured by laser diffraction, Section 4.3). A similar effect on the glass substrate is seen when processed with no glass feedstock layer, and a single glass feedstock layer. This suggests that the glass substrate experienced significant thermal shock in both instances to cause formation of micro-cracks. Transmission of excess laser radiation through glass feedstock, and absorption of this energy at the substrate surface is the likely cause of substrate cracks forming during processing.

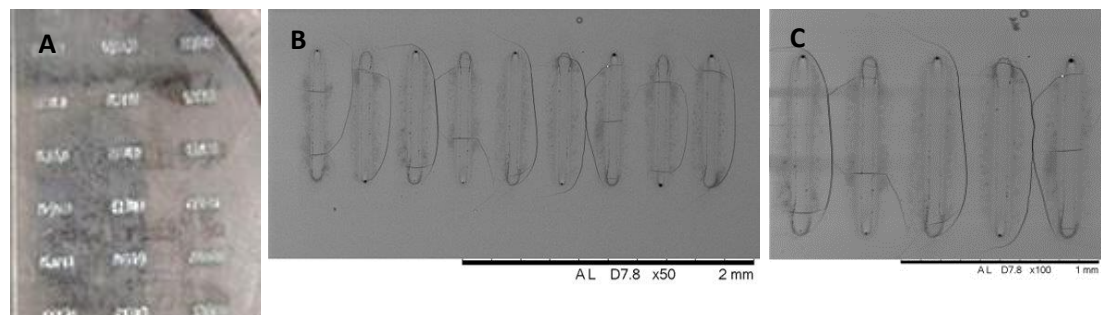


Figure 71 Laser processing of glass substrate in the absence of feedstock layer A: Processed glass substrate as seen B:50x magnification SEM, C: 100x magnification SEM.

These two observations lead to the conclusion that glass feedstock adheres strongly to substrate glass along process tracks. It is suspected that the surface of the microscope slide is softened by the laser energy as it absorbs energy, allowing feedstock and substrate to melt together, forming a seal. The micro-cracks that form around process tracks as a result of thermal shock weakens the substrate, and thus structures are easily broken off of the substrate. In order to strengthen the processed glass-substrate interface, further optimisation of process parameters to reduce thermal gradients should be undertaken.

Optimising energy density to allow sufficient processing at the lowest possible energy density is one option for reducing the thermal shock on glass substrates during SLM. While theoretically this is true, during process mapping for this SLM set-up and glass composition, it was found that lower energy density processing resulted in reduced geometrical accuracy and had a limited effect on thermal shock experienced by substrates. One possible way to reduce thermal gradients during processing is increasing the temperature chamber and substrate temperature, ideally close to the transition temperature of the glass substrate and feedstock. The feasibility of this was explored through implementation of a high temperature substrate heater (Section 5.5). Another consideration that is worth making is the composition of glass feedstock used based on its thermal profile. A glass composition with lower processing temperatures, e.g., a lower T_g and working temperature, may allow processing at lower energy densities, requiring less energy input to melt. Dopants added to glass compositions are expected to lower melting temperatures, and therefore reduce the energy density requirements for SLM processing. Another consideration is the addition of dopants to glass compositions to improve laser absorbance at the SLM wavelength. Additives often impart colour to glasses, with iron dopants in glass causing a yellow colour from Fe^{3+} ions and a blue colour from Fe^{2+} ion content. Iron exists in equilibrium between Fe^{3+} and Fe^{2+} in glass with Fe^{2+} showing an increased absorbance at 1050 nm, close to the laser wavelength used in this work^{189,223}. An iron doped soda lime silica glass (GTS-3) was therefore of interest for investigations into the effect of iron dopant on SLM process parameters for glass, to observe any effects on thermal shock. A feasibility study was carried out using this material, but low flowability prevented in-depth investigation. Further work is planned to investigate SLM processing of plasma spheroidised SLSG-Fe, a bespoke iron doped soda lime silica glass described in Section 4.5.2.

5.5 Case Study: SLM Machine Modification – Microheater

5.5.1 Introduction

A micro heater (MHI, USA) was purchased for installation in the Realizer SLM-50, with the aim of investigating processing with substrate and chamber temperatures around the glass transition temperature of the glass feedstock material (Figure 72). The installation of the micro-heater presented significant challenges.

The Tg of soda lime silica glass is known to be between 550-600°C³. It was also measured by DTA analysis (4.3.5) at around 570-590°C. The MHI spiral heater, capable of a maximum temperature of 1400°C, was expected to supply temperatures close to the Tg of soda lime silica glass feedstocks. The original substrate heater built-in to the Realizer SLM-50 was capable of achieving temperatures up to 250°C. Thermocouples measured the direct temperature of the substrate heater, however actual powder bed temperature was not recorded and relied on conduction of the heat through any substrates.

Materials within the build chamber had to be considered when installing a high temperature heater, including wiper blades, substrates, and thermocouples. The heater was supplied with ceramic insulating discs and high temperature, fibre glass insulated wires to connect the micro-heater to the transformer. High temperature fire cement was primarily used to surround the microheater and prevent damage to the Realizer.



Figure 72 MHI Micro heater as supplied with ceramic insulating discs.

5.5.2 Bench Testing

The MHI-GAXP Spiral Microheater, equipped with ceramic base and end connectors, was tested and modified for compatibility with the Realizer SLM-50. The MHI coil heater was bench tested to assess its thermal capability in free radiating conditions. Temperatures up to 550°C were set and monitored. During operation, the microheater glowed bright orange at high temperatures, with a higher temperature radiating from the centre of the coil compared to the outside of the coil (Figure 73). The highest temperature was measured at the inside of the coil at 503°C, while the lowest temperature was measured at the outside of the coil at 375°C. The time taken for coil temperatures to reach 500°C from ambient temperature was approximately 30 minutes.

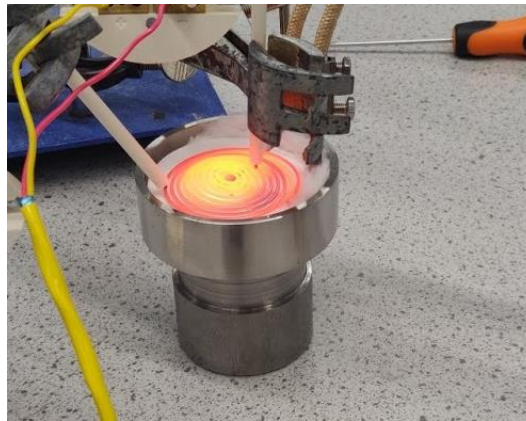


Figure 73 Bench testing of the substrate heater (Up to 550°C as programmed into the heater controller). The coil glows brightly, suggesting the actual temperature of the coil is higher than recorded by thermocouple.

To assess the capability of the microheater to maintain a thermostatic temperature, a target of 90°C was programmed and monitored. The coil temperature fluctuated between 69-93°C over a ten minute period. In another test, the microheater was programmed to ramp up to 900°C to assess its high temperature capability. The microheater reached 503°C after approximately 30 minutes, reaching a maximum temperature of 533°C after 60 minutes (recorded by K-type thermocouple positioned very close to the microheater coil, <1 mm away).

5.5.3 Installation

In order to install the coil heater within the constraints of the Realizer base plate, the heating elements were bent upwards 90°, and shortened. The coil heater and ceramic insulation were positioned in the stainless-steel base plate and adjusted to ensure substrates would be flat and flush with the base plate edges. Fire cement was used as insulation, and to secure the micro-heater in place. In the Realizer chamber, the assembly was positioned so that heating elements were on the far edge of the base in relation to the wiper blades (Figure 74 A). A ceramic substrate (Alumina) with a 5 mm diameter hole was placed on top of the microheater, creating a flush surface for powder bed spreading.

K Type Thermocouples with ceramic coating were positioned as recommended by the manufacturer; one at the substrate surface, i.e., the powder bed, and the other through the ceramic surface close to the micro heater (Figure 74 B). Thermocouples were positioned perpendicularly to the substrate, and located on the front edge of the build platform, to allow 1: the base plate to move vertically, and 2: powder spreading to not be impeded by thermocouple position.

When operated, the glow of the micro-heater was visible through the ceramic substrate (Figure 74 C). Temperatures were recorded by thermocouples at the substrate surface, and at the heater coil. The alumina substrate insulated the microheater, reducing the temperature transmitted to the substrate surface. At a programmed temperature of 600°C, the coil temperature measured 590°C and substrate was temperature measured as 478°C.

The Realizer SLM-50 wiper blade was programmed to suit the new set up. The new commands instructed the wiper to maintain the back wiper in an upright position, and move the blade unit no further than the position of the thermocouples. This was done to allow the front wiper to spread powder over the substrate in a single pass, before returning to its home position.

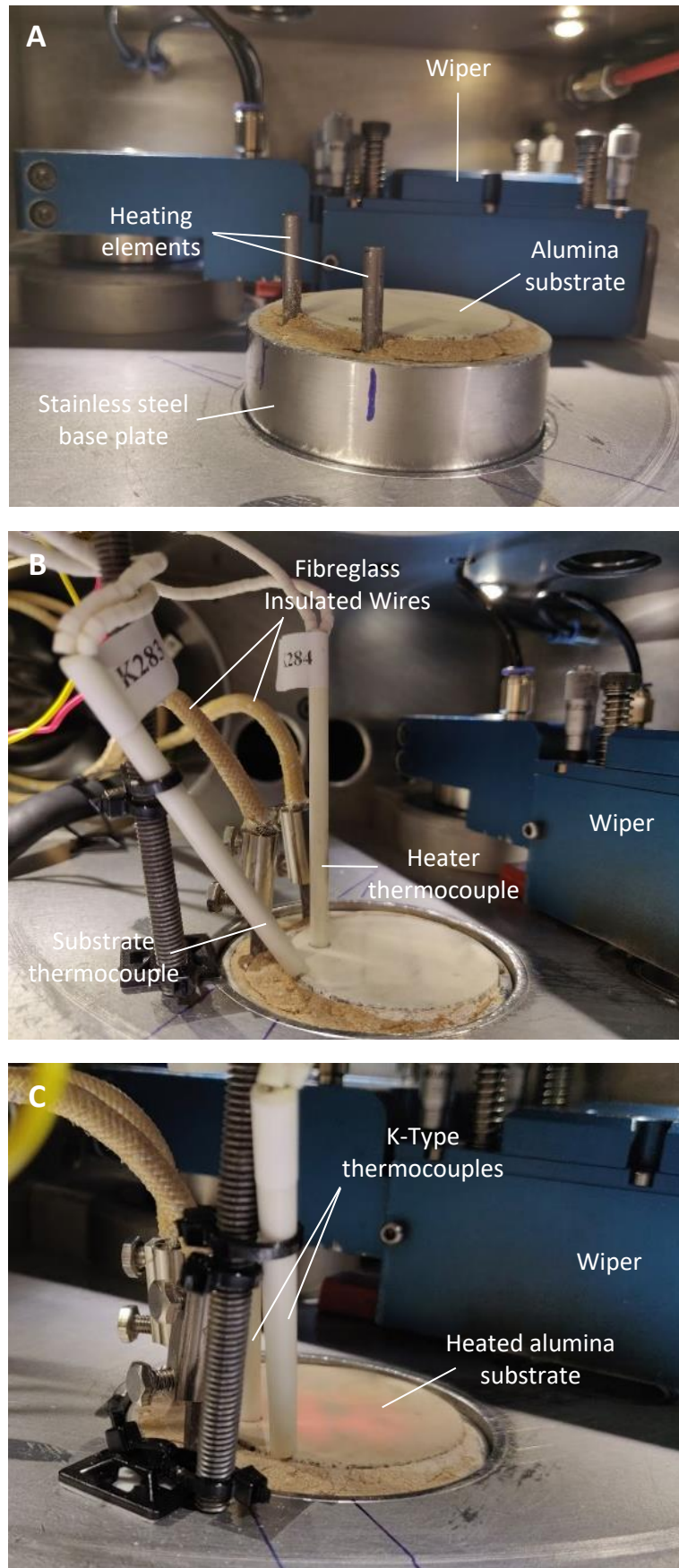


Figure 74 Set-up of microheater in the Realizer SLM-50. A: positioning of heating elements, B: set up showing thermocouple placement C: Set-up during operation of micro-heater.

5.5.4 Experimental Description and Results

The Realizer SLM-50 was set up with a high temperature coil heater installed in a custom-made base plate. A ceramic substrate (50 mm \varnothing) was placed on top of the substrate heater, and the base plate was lowered by a single layer. A small reservoir of GTS-6 soda lime silica glass powder was deposited between the substrate and wiper unit. The front wiper blade was used to spread a single layer of glass powder onto the substrate surface. The substrate heater was programmed to ramp up to 600°C, to account for the heat insulation through ceramic substrates, with the aim of reaching \sim 500°C at the substrate surface.

Just before laser processing, a final spread of the wiper blade is recommended to ensure there is sufficient powder packing, and a homogenous surface. At 500°C the powder bed reduced in flowability as glass powder reached T_g. As wiper blade material would melt at this temperature, a stainless steel blade was manually used to do a final spread of powder. Variations in powder bed height occurred as a result of the increased cohesion of the glass powder, and the manual spreading of the material across the base plate.

All wiring was contained within the build chamber, and seals were formed to ensure a concealed chamber. Argon gas was used to create an inert atmosphere within the machine. The temperature was monitored at the substrate surface, and at the coil heater. When temperatures of 500°C were recorded, laser processing was started.

Single layer processing of 5 x 5 mm cubes was carried out at the following parameters: 75 W laser power, 47 mm/s scan speed, 0.213, 0.245, or 0.29 mm hatch spacing, and x hatch scan strategy. 9 samples were processed in a 3 x 3 array on the same substrate at these parameters. The glass powder melted, producing single layer cubes with a range of transparency (Figure 75).

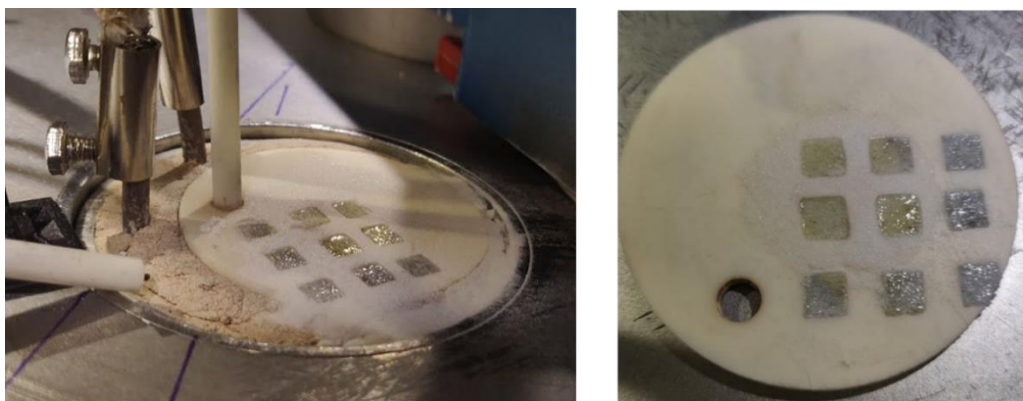


Figure 75 Single layer soda lime silica glass cubes processed by SLM on alumina substrate during high temperature substrate heater trials.

The glass powder showed signs of sintering as a result of the increased substrate temperature. Under SEM, powder that was not irradiated by the laser during processing showed “necking” where particles softened and began to merge (Figure 76-A). This suggests that the powder bed temperature reached the softening point of the glass powder feedstock, causing particles to begin consolidating. While fragile, these areas of the powder bed formed a solid layer. This occurred in areas of larger powder bed thickness (caused by manual powder spreading). The processed glass structures in the areas of larger powder bed thickness showed a gradient of melting between laser processed and unprocessed glass (Figure 76-B).

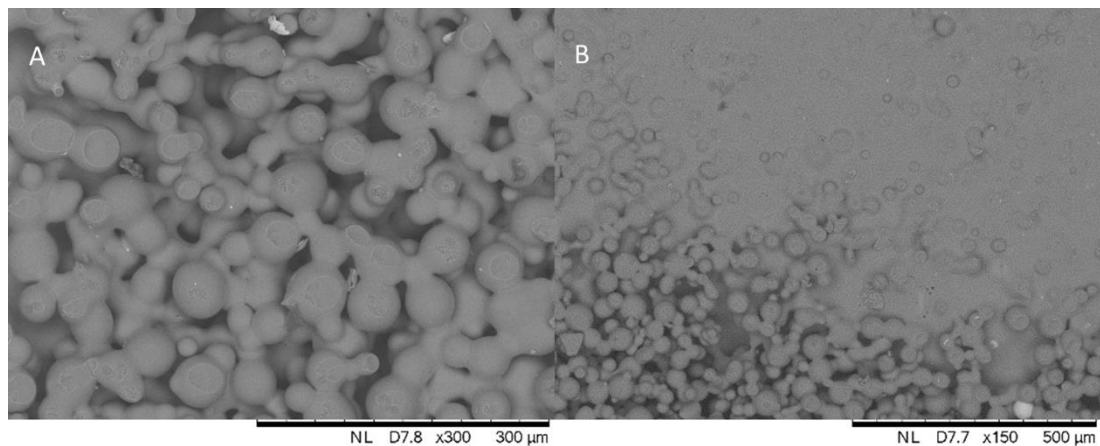


Figure 76 SEM micrographs showing A: sintering of glass powder bed and B: interface between laser processed and unprocessed glass powder during high temperature processing.

In areas of moderate powder bed thickness, the edges of processed glass structures were more distinct, with little unfused glass powder seen adhered to edges (Figure 77). This presented a clear difference between processing at 250°C substrate temperature and at ~500°C substrate temperature, as processing at 250°C frequently suffered from adhesion of unfused powder to edges of built parts. Under optical microscopy structures appeared transparent. Scan tracks were visible on processed glass parts, manifesting as a variation in height. For multi-layer processing, visibility of scan tracks is likely to depend on the scan strategy used.

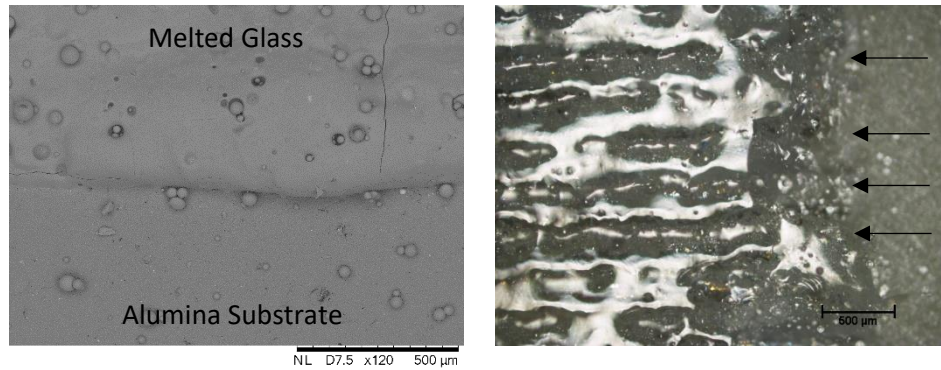


Figure 77 Glassy SLM structures. Left: SLM micrograph of SLM processed glass on ceramic substrate. Right: Optical microscopy of SLM glass structure on ceramic substrate. Arrows indicate visible scan tracks.

5.5.5 Discussion

Compared to processing at 250°C at the same process parameters, processing with a micro-heater produced melted structures that appeared glassy and transparent, suggesting the glass material had fully melted during processing. Glass processing, without the high temperature substrate heater (at previously defined optimal parameters), consistently resulted in opaque structures, with high porosity, and a rough surface texture from unfused powder particles. In these conditions, when energy density was increased to achieve visible effects of glass melting, the high surface tension of glass (128-167 dynes per cm, dependent on composition and temperature²²⁴) frequently led to a balling affect where the melted glass contracted. This is reported throughout literature on laser powder bed fusion of different materials. Balling is attributed to excessive energy input, and is often counteracted by parameter optimisation^{97,169}. As preheating of LPBF substrates has been reported to reduce the laser power (energy) requirements for processing, optimisation of processing temperature may also be effective for counteracting this effect²²⁵.

The difference in behaviour of glass powder and the resulting transparency of parts in these two separate conditions (substrate heating at 250°C and heating at ~500°C), suggests that the implementation of a substrate heater significantly reduced the thermal gradients during SLM processing. The reduction of these thermal gradients allowed glass powder feedstock to soften before laser irradiation, reducing the energy required to achieve full melting and consolidation, whilst maintaining an optimal energy density. Processing at the same energy density as non-heated processing, with reduced thermal gradients, avoided the contraction of glass powder, thus preserving the desired geometry, without causing glass powder to shrink or ball. Another possible benefit of substrate preheating is the generation of a

homogenous temperature profile in glass powder layers. This was predicted by Protasov et al. whose model suggested that preheating of fused silica powder beds for SLM would have a large effect on material consolidation rate, allowing lower laser powers to provide sufficient heat for complete melting¹³⁵.

Installation of the high temperature coil heater into the Realizer-SLM50 was difficult, with multiple challenges to overcome. Accommodation of all microheater parts and wiring was challenging within the confines of the Realizer build chamber. Forming a sealed environment for SLM processing was challenging, as wires partially obstructed the view of the build platform and positioning was dependent on available exits for these wires. The build volume was greatly reduced due to the larger dimensions of the custom base plate designed to accommodate the micro heater and insulating discs. The maximum achievable build height was reduced from 44 mm to 21.5 mm with the heater installed.

The melting temperature of the supplied wiper blade material was around 300°C, meaning that powder spreading at temperatures beyond this would not be possible using these blades. The purpose of the original dual wiper blade was to deliver feedstock to the substrate with the back blade in the first movement, and then create a homogenous powder bed layer with the front blade during a second movement. Due to the positioning of thermocouples and heating elements perpendicular to the substrate, this method of powder spreading couldn't be utilised.

Powder spreading was achieved manually at high substrate temperatures by using a stainless-steel blade. This was only sufficient for a single layer trial. As reported in literature, preheating of powders can reduce the flowability of material as particles start to bind within the powder bed, resulting in challenges with powder spreading²²⁵. This was observed during glass processing as glass powder particles started to sinter together before laser processing began. A homogenous powder layer was difficult to achieve with high temperature substrate heating. Additionally, due to the space constraints, manual spreading during processing whilst in an inert atmosphere was not ideal, and would have required opening of the build chamber. Therefore, multi-layer processing at high substrate temperature was not investigated.

The temperature of the heater and the substrate surface was monitored using K-Type thermocouples. K-Type thermocouples are inexpensive and have a wide temperature sensing range (~200-1300°C), however, may suffer from inaccuracy²²⁶. A high temperature pyrometer is recommended as an alternative, but for this set-up, the sealed build chamber

prevented access for pyrometer readings. The micro heater coil was also inaccessible for pyrometer readings, due to it being secured in the base plate.

The micro-heater was designed to quickly reach temperatures up to 1400°C, however during bench testing and processing, temperatures above 600°C were not recorded. A rapid increase in temperature was seen up to 300°C, but slowed significantly when increasing beyond these temperatures. For this application, the desired substrate temperature was near 500°C. This temperature was achieved, however the efficiency of the micro-heater reaching this temperature was low. As the monitoring of coil and substrate temperature was potentially inaccurate due to the use of KType thermocouples, it is possible the temperatures reached by the micro heater were much higher than recorded. This is evidenced by the brightly glowing coil seen in Figure 73.

The temperature of the micro heater and the powder bed were monitored as temperature was ramped up to 600°C. Conduction of heat was impeded by the ceramic substrate (as expected), with coil temperatures measuring ~125°C higher than the recorded temperature of the powder bed during bench testing. For future testing of high temperature SLM of glass powder feedstocks, an integrated chamber heater would likely provide more consistent powder bed heating than the substrate heater testing during this research.

5.6 SLM Discussion and Conclusions

The challenges faced during investigation of powder bed fusion of glass materials included the impact of feedstock flowability on powder bed formation, the effect of substrate properties on laser absorption, and the sensitivity of glass feedstocks to process parameters. Many of these are known challenges when optimising processing of powder materials^{117–119,227}. For glass materials, there are limited reports of optimal processing conditions for different glass compositions. In literature, some parameters have been reported for SLM of a few glass compositions, such as soda lime silica glass by Fateri et al., and fused silica by Khmyrov et al^{130–134}.

During early investigations several initial observations helped to guide conditions towards improved processing of glass feedstocks. Firstly, spherical glass feedstocks proved superior to irregular or non-spherical powders when it came to forming a homogenous, single layer powder bed. This was predicted by reports in literature and the measurement of flowability by powder rheology¹¹⁵. The reduced friction and mechanical interlocking of spherical particles likely contributed to the superior flowability over angular feedstocks^{174,228}. The low flowability of many of the glass powder feedstocks impeded the spreading of a powder bed, making it difficult to process effectively or accurately. For investigations into SLM of bespoke glass compositions, spheroidisation is recommended to improve flowability of milled feedstocks. For on-glass processing, a dark surface beneath glass substrates was found beneficial for improving laser absorption.

Processing on ceramic substrates allowed the use of sacrificial support structures, designed to be removed post process. This was particularly useful for processing structures such as simple 5 x 5 x 5 mm cubes. For processing on glass substrates, with the intention of achieving good adhesion of glass parts to the substrate, support structures were not used. Processed structures showed adhesion to the glass substrates, however these structures were easily broken from the substrates. This is because substrates were affected by laser processing, forming micro-cracks after the first layer was processed. These micro-cracks weakened the substrate, allowing structures to more easily be removed, showing a distinct pattern of adhesion and cracking by SEM, that corresponded with scan tracks.

In order to improve glass-on-glass SLM, further work to reduce the thermal stresses introduced by laser processing should be carried out. One possible solution is to optimise the chamber and substrate temperature, to reduce the thermal gradients in processing, and increase the powder absorptivity¹⁶⁴. Micro heater trials highlighted some of the limitations

to this, with glass spreading becoming more challenging at higher temperatures as glass feedstocks heat towards softening point. A similar effect was reported by Liu et al²²⁵. Further investigation into the thermal conditions during SLM processing would require a suitable set-up with high temperature capabilities.

Alteration of glass composition to lower the required energy density for processing is another possible method of reducing thermal stress in glass-on-glass SLM. Tailoring the glass composition to have a lower melting point through the addition of particular dopants to the glass batch could allow melting to be achieved at lower energy density, reducing the thermal stresses acquired, and protecting parts and substrates from failure. During the course of this PhD, an Fe doped 13-93 biologically active glass (GTS-3) was used in a feasibility study to investigate SLM processing at lower energy densities. Unfortunately, low flowability prevented thorough exploration of SLM of this glass. Further work is underway to investigate SLM processing of Fe-doped glass compositions with superior flowability, thanks to spheroidisation of bespoke glass feedstocks.

Efforts were made to define suitable processing parameters for SLM processing of glass. While a processing window can be suggested for achieving general glass melting by SLM, build geometry has a large impact on success of processing. Process maps are relevant for the conditions and glass feedstock stated, as well as the geometry tested. This suggests that optimisation of process parameters is required for each desired geometry, including part dimensions, hatch spacing, scan strategy, and energy density. Once suitable parameters are tailored for a specific geometry, small structures with high resolution can be achieved using this method. The processing window for SLM of soda lime silica glass (GTS-6) was identified as 70-120 J/mm³ for processing on ceramic substrates, and 49-76 J/mm³ for on-glass processing. The lower energy density of the latter processing window is essential to prevent cracking of glass substrates and is in line with the processing parameters reported by Fateri and Gebhardt¹³².

The overall conclusions for the investigations into glass processing by SLM are:

- The feasibility of processing soda lime silica onto substrates of the same composition was proven, with various geometries demonstrated.
- A delay between layer processing was observed to be beneficial for glass processing, helping to preserve geometrical accuracy by allowing residual heat to dissipate between layers. Further work is necessary to define optimal layer delays for glass processing.

- 67° rotation hatch was observed to be beneficial for geometrical accuracy of glass parts of complex geometry. For simple structures, alternating x-y hatch (90° rotation) performed better than mono-axis scanning.
- The effect of SLM laser processing on glass substrates was inspected for the first time, showing the formation of micro-cracks along scan tracks, worsening as energy density increased due to the effects of thermal stress.
- Glass parts were opaque, with unfused glass powder coating exposed edges. Only some areas looked glassy and fully melted through SEM investigation.
- Process maps were populated for soda lime silica glass processing on ceramic and glass substrates.
- A processing window was defined for glass processing on ceramic substrates between 70-120 J/mm³, and 49-76 J/mm³ on glass substrates.
- Scan speed and laser power displayed independent effects on glass processing. However, all energy densities below 28 J/mm² were insufficient for successful processing for GTS-6 on soda lime silica substrates.
- A high temperature substrate heater had a positive effect on forming transparent, glassy parts with preserved geometrical accuracy in initial trials.

Chapter 6

Directed Energy Deposition of Glass

6.1 Introduction

One of the two methods selected for processing glass materials in this research was Directed Energy Deposition (DED). After reviewing the literature on AM of glass by laser processing, a research gap was identified for DED processing using a powder-fed method. The following research questions were considered:

- Is it feasible to process glass powder materials by powder-fed DED?
- What effect do process parameters such as laser power, scan speed, powder delivery method, and substrate properties, have on glass processing?
- Is it possible to produce customisable décor for high value glass packaging using this AM method for glass powder processing?

The exploration of glass powder processing by powder fed DED was expected to encounter similar challenges to processing glass by other AM methods. High transmissivity in the visible and near-IR wavelengths of transparent glass feedstocks mean that sufficient laser absorption for glass melting could be difficult to achieve. Another concern was the likelihood of cracking and fracture of substrates and processed parts due to thermal stresses imparted during laser processing. The aims and objectives for this study included proof of feasibility of glass powder processing by DED, investigation of process parameters, and demonstration of processing glass powder onto glass substrates, to prove concept of customisable décor for high value glass packaging using this method.

This chapter describes the DED process used in this investigation, experimental procedures, and results. 6.2 describes the feasibility studies, and their results, that were used to inform later investigations described in 6.3-6.5. The results relating to these investigations are presented in 6.5.

6.2 DED Processing System

The DED system utilised in this investigation was modular in nature, with multiple systems employed to allow processing. A 2 kW CW Yb fibre laser (IPG photonics, USA,) was mounted to an arm in the z direction. Capable of movement vertically in the z, this allowed multi-layer processing, by raising the laser to a position determined by layer thickness. The laser operates at 1070 nm at focus, and uses a converging lens to form a focused laser beam. The different fibres compatible with the system were: 200, 400, and 600 μm fibres, to form spot sizes of approximately 300, 600 and 900 μm respectively. The 600 μm fibre (0.9-1 mm spot size, as measured in 2008²²⁹) was used primarily during these investigations. A schematic of the laser processing set up is shown in Figure 78.

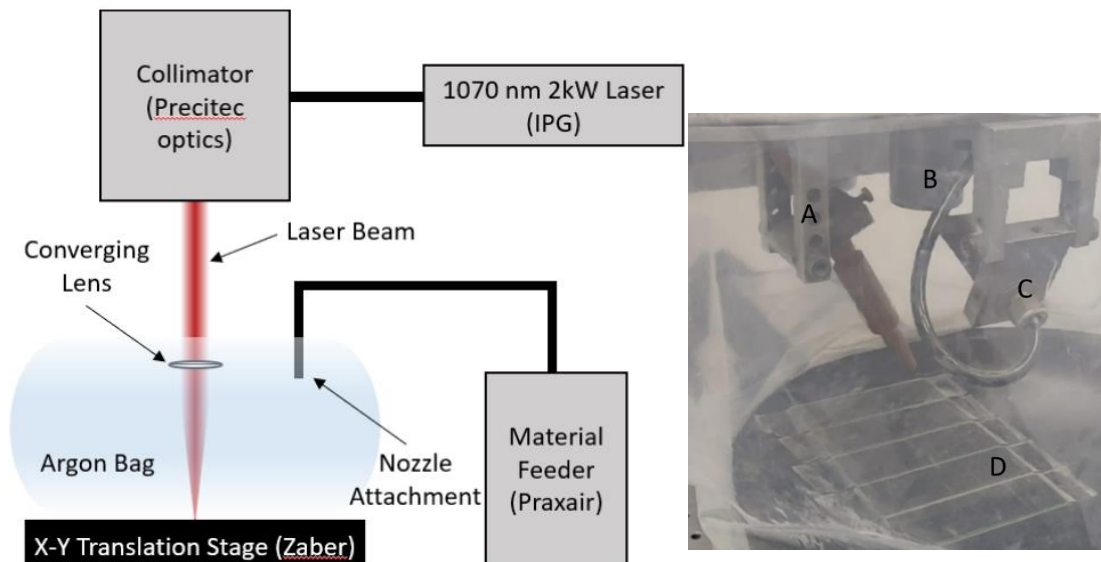


Figure 78 Left: DED Schematic for experimental set-up. Right: Example of experimental set-up A: Lateral powder nozzle, B: Laser C: Argon Nozzle, D: Glass substrates affixed to base plate.

For material delivery, various attachments were available to suit different forms of feedstock. A 1 mm nozzle with an automatic spool feeder was utilised for wire feedstocks. For powder feedstocks, an automatic powder feeder (Praxair 1264, Miller Thermal Inc) was used in conjunction with a coaxial nozzle, and a lateral nozzle for side fed powder delivery. For lateral powder feed, a 2 mm copper nozzle was positioned at 27.5° to the laser beam, with a 2 mm Teflon tube used to deliver the material through the nozzle. The coaxial nozzle attachment, with a 1 mm annular orifice, was attached to the laser head in the z axis for coaxial delivery. Powder was supplied to nozzles automatically by a volumetric feed principle whereby

powder was rotated and collected in small slots and then metered into a Teflon powder hose and delivered to the nozzle. The rate of powder supply was controlled in terms of carrier gas pressure (L/min) and powder wheel speed (rpm). The two powder nozzles are shown in Figure 79. The processing area was contained within a plastic “bag”, and Argon gas was delivered to the laser for shielding.

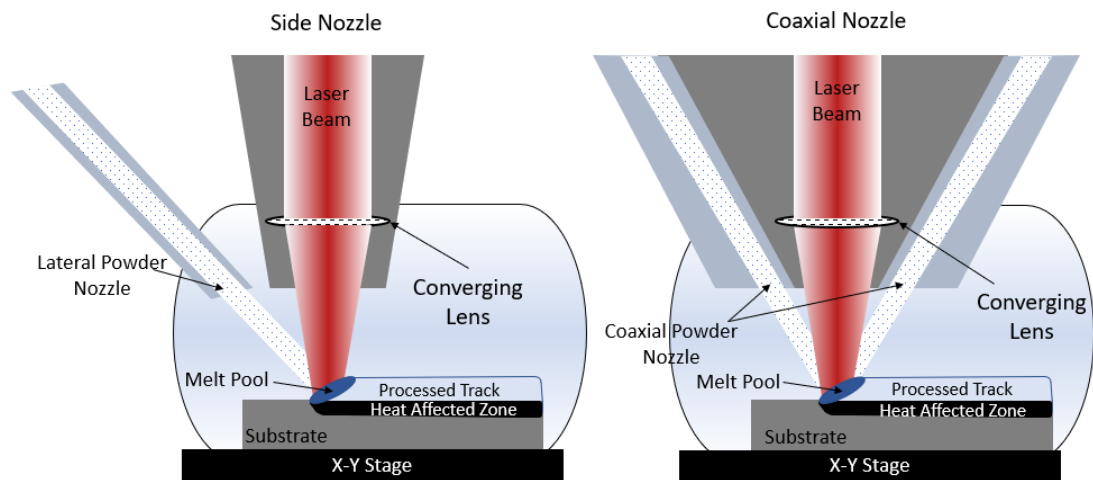


Figure 79 Powder-fed DED set-ups Left: Lateral nozzle, Right: Coaxial nozzle.

An x-y coordinate CNC stage was used to mount substrates, and was later used to mount an x-y translation stage (Zaber) with greater automation. The Zaber stage had a movement range of 600 mm, and a speed range of 0.000119 mm/s to 100 mm/s, and used software that translated simplified GCode into streamed commands before operation. GCode was written to instruct the Zaber stage for simple movements, such as single tracks, but for more complex structures, designs were created using 3D CAD software, and edited for translation to GCode.

6.3 Investigating the Feasibility of Glass Processing by DED

6.3.1 Introduction

A series of feasibility studies were carried out as part of the initial investigations into glass processing by DED. The aim of the feasibility studies was to inform future experiments for ideal feedstock form, and experimental set-up, and to achieve melting of glass feedstocks by DED. Glass materials considered for the feasibility studies included two different particle size distributions of soda lime silica beads (GTS-1, and GTS-2), borosilicate (GTS-4), and fused silica (GTS-5) glass powders. The two soda lime silica powders were chosen to make initial observations on the effect of particle size (and flowability) on powder-fed DED. Borosilicate and fused quartz composition were considered to indicate the effect of glass composition and their different thermal profiles on DED processing. Soda lime silica glass fibre (SLSG-Fibre) was also used for a fibre feasibility study, to assess the compatibility of glass fibre processing with the DED set-up. The studies looked at the potential for consistent delivery of glass materials via the wire and powder feeder attachments. The experimental set-up was adapted to accommodate potential substrates to allow processing. Machine adaptations were made iteratively to improve processing.

6.3.2 Methods

Three feasibility studies were designed for the initial investigations into DED of glass powders, and a fourth to investigate wire-fed glass DED. Three baseplates were designed for these investigations (Figure 80). 3D CAD models of the baseplates were created using a CAD package (Solidworks, Dassault) and machined out of 16 mm thick aluminium.

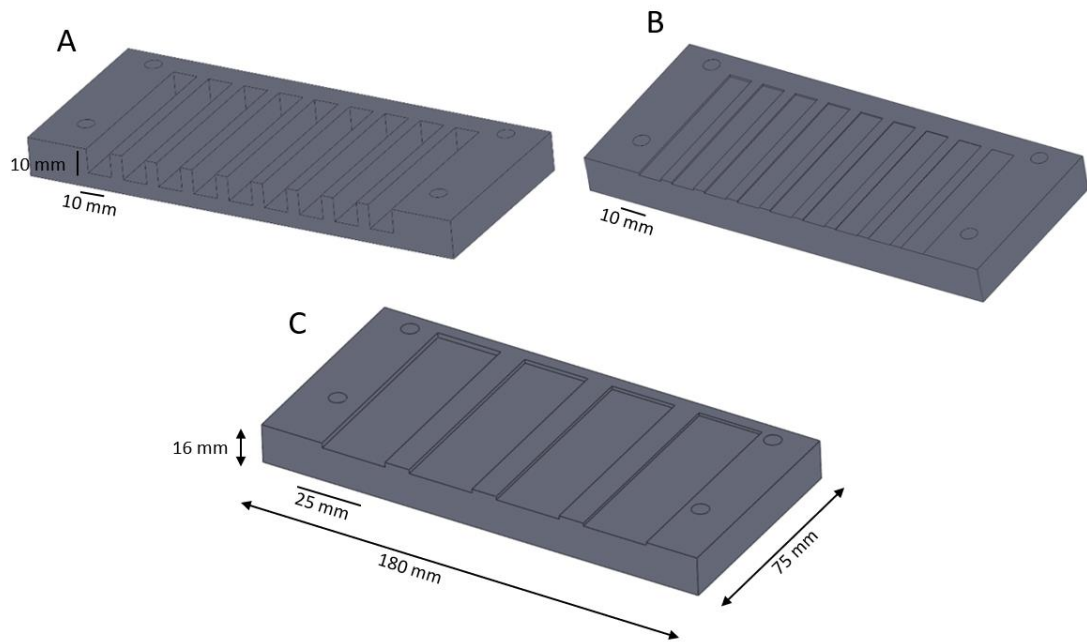


Figure 80 Machined aluminium base plates for DED feasibility studies. A: 10 x 10 x 65 mm voids, B: 10 x 10 x Z mm voids ($Z = 0.9\text{--}0.1$ mm), C: 25 x 5 x 75 mm voids.

The purpose of baseplate A (Figure 80 A) was to accommodate glass powders in cavities of 10 x 5 x 65 mm. The cavities were enclosed by three sides to allow easy removal of contents after processing. Baseplate B (Figure 80 B) was of similar design with varying cavity depths from 0.1 mm to 0.9 mm. Baseplate C (Figure 80 C) was designed to accommodate standard microscope slides of 1 x 25 x 75 mm, similarly with one open side to allow easy removal of slides post process.

6.3.3 Powder Study 1: Feasibility of Processing Different Glass Compositions

Baseplate A was used for the first feasibility test of glass processing by DED. The baseplate was fixed to an x-y coordinate stage, and glass powder (GTS-2: soda lime silica, $DV_{50} = 102 \mu\text{m}$) was spread in the cavities with a flat edge to create a homogenous powder bed. The baseplate was encased in an Argon bag during processing, and the glass powder was irradiated under varying parameters, from 200-1200 W laser power and 200-400 mm/min scan speed (Table 16). The calculated energy densities (described in 2.5) for these parameters ranged between 30-180 J/mm². Post process, the resulting glass structures and remaining powder were carefully removed from the cavities and observed under optical microscopy.

Table 16 Process parameters for investigating the feasibility of processing soda lime silica beads (GTS-2) at varying laser power and scan speed.

Test #	Laser Power (W)	Scan Speed (mm/min)
1	200	400
2	400	400
3	600	400
4	800	400
5	1000	400
6	1200	400
7	200	200
8	400	200
9	600	200

The observations of soda lime silica behaviour, as processed by the defined parameters, informed the process parameters used for other glass compositions. To investigate the feasibility of processing borosilicate (GTS-4) and fused silica (GTS-5), the same baseplate (A) and experimental procedure were used, with laser powers between 600-1800 W, and scan speeds of 500-700 mm/min (Table 17). The calculated energy densities for these parameters were similar to those used for soda lime silica investigations, ranging between 50-180 J/mm². Resulting structures were observed by optical microscopy.

Table 17 Process parameters for feasibility investigation of borosilicate (GTS-4) and fused silica (GTS-5) glass compositions.

Test #	Laser Power (W)	Scan Speed (mm/min)
1	600	500
2	600	600
3	600	700
4	800	600
5	1000	600
6	1200	600
7	1400	600
8	1600	600
9	1800	600

6.3.4 Powder Study 2: Effect of Powder Bed Thickness

To investigate the effect of processing glass powder beds of varying thickness, baseplate B was used. Soda lime silica (GTS-2) was spread into cavities of varying thickness, between 0.1 and 0.9 mm, to create homogenous powder beds. The glass powder was irradiated at

constant parameters of 200 W and 600 mm/min (20 J/mm²). Resulting fused glass was observed under optical microscopy and dimensions were measured using digital callipers.

6.3.5 Powder Study 3: Feasibility of Fusing Glass Powder to Glass Substrates

Baseplate C, designed to accommodate standard microscope slides (soda lime silica, Biosigma), was used to prove the feasibility of fusing glass powder to glass substrates by laser irradiation using the DED system. For the first test with this baseplate, glass powder (GTS-2) was spread on the surface of microscope slides affixed to the baseplate. The glass powder layer had a thickness of 1 mm. Parameters between 150-250 W and 400-500 mm/min were investigated.

The second part of this study involved delivering powder via a side nozzle to the glass substrates and processing by laser irradiation. Microscope slides were affixed to the substrate by a small section of cellophane tape. A further iteration of this study involved modifying the surface of baseplate C by bead blasting and coating with graphite to darken the surface beneath the transparent glass substrates. For the final iteration of this study, a cellophane tape layer was applied to the surfaces of microscope slide substrates.

To investigate powder delivery using alternative methods, glass powder (GTS-2) was delivered via coaxial nozzle to glass substrates coated with a single layer of cellophane tape, mounted on the darkened aluminium base plate. Combinations of parameters between 100-200 W and 500-700 mm/min were tested, with powder feed parameters of 4-8 rpm (wheel speed) and 5-10 L/min (carrier gas pressure).

6.3.6 Feasibility of Glass Fibre Processing

Soda lime silica glass fibres were processed by two methods. In the first method, glass fibres (SLSG-Fibre) were secured to glass substrates attached to the DED base plate, and irradiated at various parameters: (100-200 W, 400 mm/min), within an argon bag.

For the second method, glass fibres were fed through a wire feeder affixed to the DED set-up at a 45° angle to the substrate (Figure 81). The wire feeder, designed to deliver metal wires of 1 mm diameter, was used to deliver soda lime silica drawn glass fibres (SLSG-Fibre)

to glass substrates at various parameters (100-400 W, 200-400 mm/min). Observations were recorded and melted structures were visualised via optical microscopy.

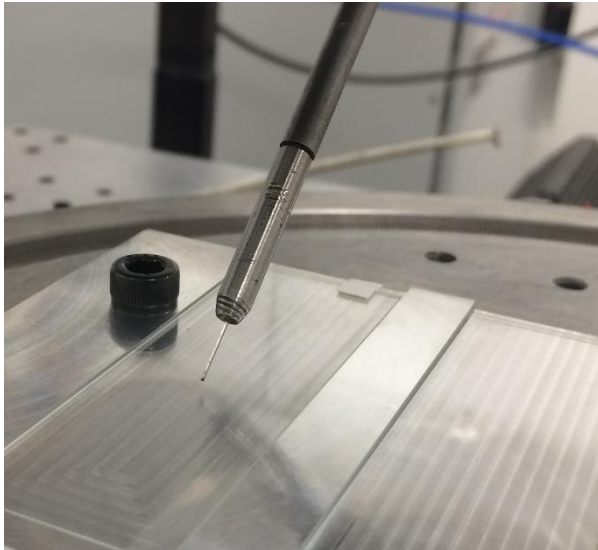


Figure 81 SLSG-Fibre processing trial set up, with 1 mm wire feeder attachment.

6.3.7 Results

6.3.7.1 Feasibility of Processing Different Glass Compositions by DED

Soda lime silica glass powder (GTS-2) consolidated at all energy densities tested, forming solid glass samples of varying thickness depending on energy density (Figure 82). Generally, glass powder melted more consistently at higher energy densities, with some samples showing limited consolidation at lower energy densities (Figure 82, Sample 1). At higher energy densities the powder consolidated to form glass rods with some observed transparency (Figure 82; Sample 9). These results showed the first indication of a difference in glass melting behaviour at different parameter combinations, despite having the same calculated energy density. For example, sample 2 was processed at parameters of 400 W and 400 mm/min, with a calculated energy density of 60 J/mm². Sample 7 was also processed at 60 J/mm², however, used a lower laser power of 200 W and slower scan speed of 200 mm/min. Despite being processed at the same energy density, sample 7 showed consistent consolidation of the powder feedstock, whereas sample 2 melted powder inconsistently, forming multiple discrete sections of melted glass.



Figure 82 Effect of energy density on DED of soda lime silica glass powder (GTS-2). Sample numbers indicate the process parameters defined in Table 1. Calculated energy densities: 1= 30 J/mm², 2= 60 J/mm², 3= 90 J/mm², 4=120 J/mm², 5= 150 J/mm², 6= 180 J/mm², 7= 60 J/mm², 8= 120 J/mm², 9= 180 J/mm².

Each solid glass part was surrounded by a layer of unfused powder, obscuring the optical transparency to varying degrees. The glass rods were examined under optical microscopy,

including a cross section of the part (Figure 83). Bubbles were seen throughout the melted glass samples, suggesting porosity within the melted glass. This porosity further reduced transparency.

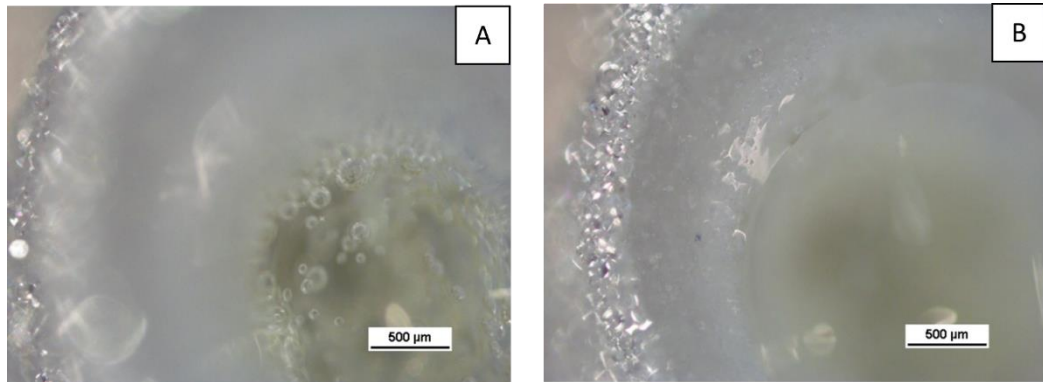


Figure 83 Optical microscopy of soda lime silica (GTS-2) melted by DED irradiation at 1200 W and 400 mm/min.

In the feasibility investigations into DED processing of other glass compositions, glass melting was observed at varying energy densities (as described in Table 17). As expected, borosilicate and fused silica compositions required greater energy to achieve full melting than soda lime silica glass compositions. Borosilicate and fused silica glass powders behaved similarly to soda lime silica, with powder generally requiring higher energy densities to achieve consistent glass melting and consolidation. This is due to the differences in chemical composition and related thermal properties, i.e., Borosilicate and fused silica have higher processing temperatures than soda lime silica (Softening points (viscosity = $10^{6.6}$ PaS): soda lime silica = $\sim 700^{\circ}\text{C}$, fused Silica = $\sim 1600^{\circ}\text{C}$, Borosilicate = $\sim 1220^{\circ}\text{C}$)³⁰. Sufficient energy density to create glass rods of borosilicate (GTS-4) was only achieved above energy densities of 80 J/mm^2 (800 W laser power, 600 mm/min scan speed). For fused silica (GTS-5), all but one of the parameter combinations tested resulted in the formation of melted globules of glass, forming small sections of melted glass. Only at the highest energy density tested (180 J/mm^2 , at parameters of 1800 W, 600 mm/min) did the fused silica glass powder fully consolidate to form a continuous, solid glass rod.

6.3.7.2 The Effect of Powder Bed Thickness on DED Glass Processing

The effect of variation of powder bed thickness on laser irradiation of soda lime silica (GTS-2) was observed in this feasibility study. Evidence of fusion of glass powder was seen for each powder bed thickness (Figure 84). Processing of powder beds below 0.3 mm thickness resulted in formation of very small globules of transparent glass. Glass fusion was more prominent at increasing powder bed thickness, forming more regular structures of fused glass.



Figure 84 Fused soda lime silica glass powder in powder beds of varying thickness (left to right: 0.1-0.9 mm).

With powder bed thickness below 0.3 mm, glass fusion was minimal, with small, transparent globules of glass forming on absorption of laser energy. Optical microscopy of these small structures revealed small segments of transparent fused glass, surrounded by unfused glass powder (Figure 85), similar to the results of the 10 mm powder bed thickness trials. Bubbles of gas present inside the melted glass were visible and slightly obscured transparency. The dimensions of fused glass samples varied significantly depending on powder bed thickness, as observed under microscopy and as measured by digital callipers (Figure 86). As the powder bed thickness increased, so too did the average thickness of fused glass pieces. In general, the variation in the dimensions of fused glass samples also increased with increasing powder bed thickness. These results showed evidence of conduction of heat through glass powder adjacent to scan tracks, highlighting a drawback of processing glass powder beds.

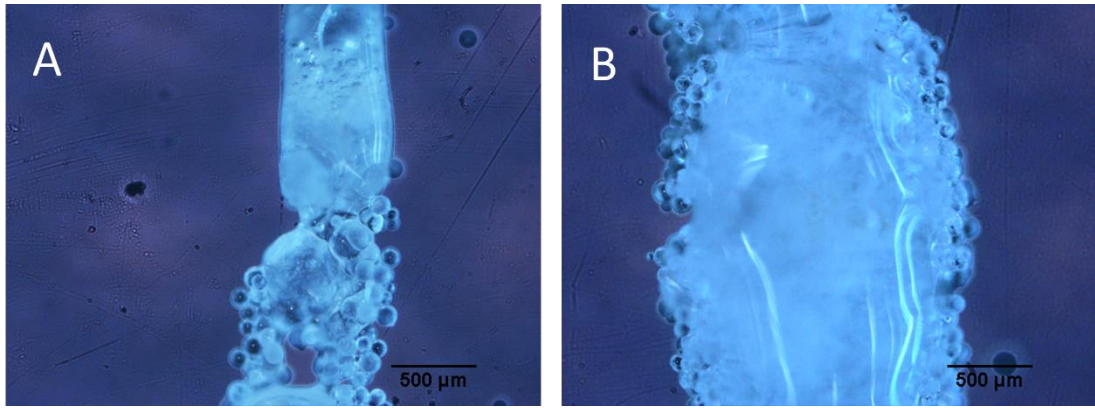


Figure 85 Fused soda lime silica glass samples processed in powder bed thickness of A: 0.1 mm and B: 0.9 mm.

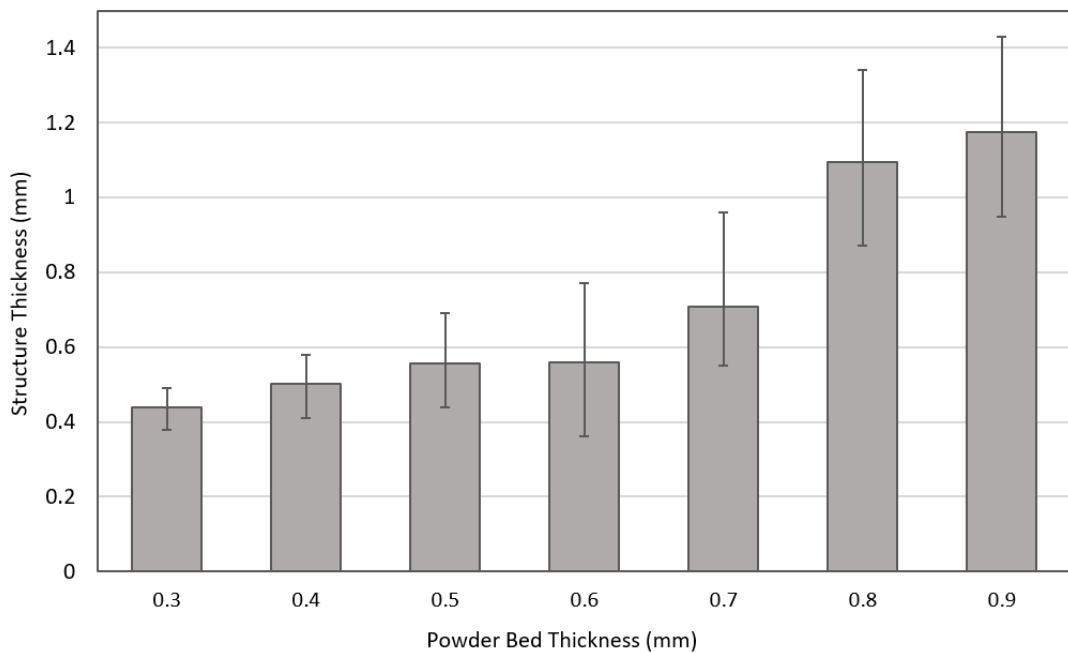


Figure 86 Dimensions of fused soda lime silica glass segments by powder bed thickness, with error bars indicating the minimum and maximum measured values.

Observations made when processing glass of varying powder bed thickness (as well as during the first feasibility study using a 10 mm powder bed) suggested that the powder bed method suffered limitations due to the high surface tension of glass powders. During laser irradiation at sufficient energy densities, glass powder would melt and consolidate, and high surface tension would cause the melted glass to contract and form globules/beads. Excess energy would be imparted to surrounding powder, causing un-melted powder to attach to the surface of the melted glass. The same effect was observed during powder bed fusion of glass by SLM at high energy densities. This highlighted the need for alternative methods of

feedstock delivery, in order to obtain dimensional accuracy of processed parts, leading to the third feasibility study investigating powder delivery by lateral and coaxial nozzles.

6.3.7.3 Methods of Powder Feedstock Delivery

Initial trials with baseplate C were generally unsuccessful. 1 mm powder beds that were spread on microscope slide surfaces suffered the same limitations as seen in the earlier powder feasibility studies. During processing of GTS-2, at sufficient energy density ($\sim 30 \text{ J/mm}^2$), the glass powder absorbed the laser energy and formed small glass segments as expected (Figure 87). Melted glass feedstock did not adhere to the glass substrate beneath the powder bed.

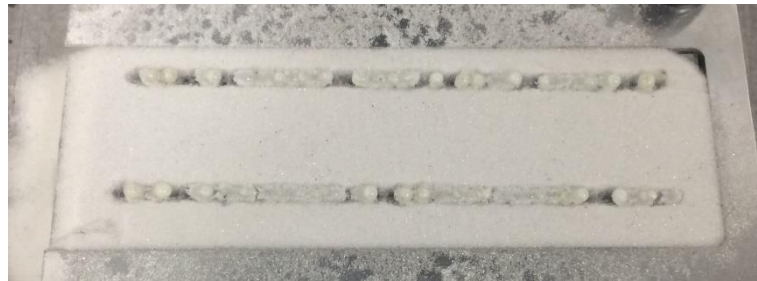


Figure 87 Evidence of fusion of soda lime silica glass in a 1 mm powder bed atop a glass substrate.

For the first investigation into feedstock delivery by powder nozzle, little glass melting was seen. This was the result of various factors: the reflectivity of the aluminium baseplate, the high transmissivity of the transparent glass slides and glass feedstock, and inconsistencies in powder delivery. Owing to this, laser absorption was insufficient for melting to occur. A combination of bead blasting and darkening of aluminium surfaces, as well as coating of glass microscope slides with a single layer of cellophane tape resulted in the successful melting, consolidation, and adhesion of glass powder to glass microscope slides.

At parameters of 200 W laser power and 550-650 mm/min scan speed, and powder flow rate of 4 rpm, consistent deposition of melted soda lime silica glass on glass substrates was achieved with this set-up (Figure 88). The glass slides remained intact, with no significant cracking. The glass deposits appeared opaque to the naked eye, and the effect of processing on the adhesive tape layer was visible. The adhesive tape surrounding the glass deposit was degraded, leaving behind a black carbon residue. When viewing from the underside, micro-cracks could be seen along the process track, but these did not penetrate to the bottom surface of the substrate.

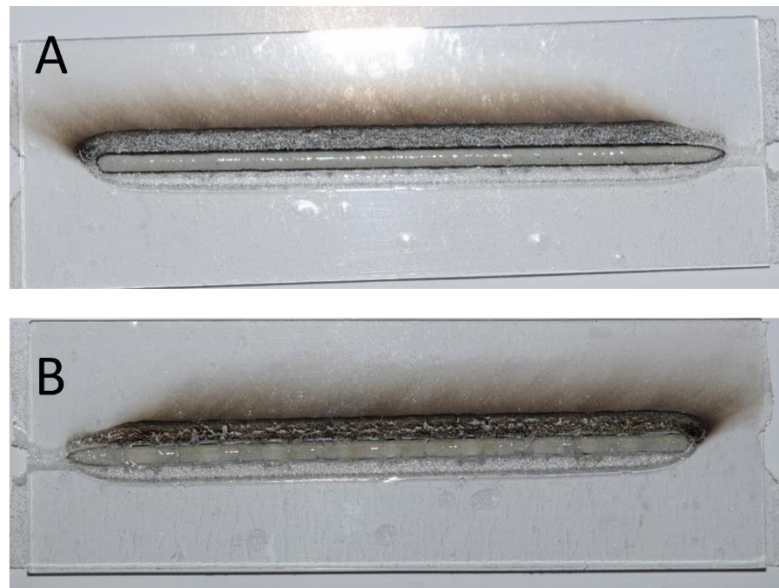


Figure 88 Soda lime silica (GTS-2) melted and deposited onto glass substrate of the same composition, using parameters of 200 W laser power and 650 mm/min scan speed with powder delivery by coaxial nozzle. A: Top surface of glass substrate B: Bottom surface of glass substrate.

The positive effect of baseplate darkening on laser absorption is explained by the increased absorptivity of the graphite layer, causing a localised heating of the substrate when irradiated by the laser. Conduction of this heat through the glass substrate raised the temperature of the glass powder feedstock and substrate, increasing its absorptivity, allowing melting of glass powder to occur.

A similar effect could be attributed to the cellophane tape layer. During processing, the tape absorbed some of the laser radiation, causing localised heating on the surface of the glass substrate, aiding glass melting as described above. Consequently, when glass powder was melted and deposited onto the glass slide, the tape layer surrounding the glass deposit was affected, leaving a black (carbon) residue behind (a product of melting the organic polymer and adhesive layers of the tape). The degradation of the adhesive tape layer was investigated by FTIR spectroscopy (Perkin Elmer, US), to confirm the degradation of the polymer layers on laser irradiation (see appendix).

6.3.7.4 Compatibility of Glass Fibre Delivery for DED Processing

Glass fibres that were attached to glass substrates for processing showed evidence of melting and deposition. Glass melting and fusion occurred at 150 W, 400 mm/min, and 200 W, 400 mm/min. However, the soda lime silica glass substrates cracked due to thermal stress, and fusion was inconsistent.

In some instances, fibres broke as soon as processing commenced. SLSG-Fibre feedstocks were not completely regular, with slight variations in dimension due to the nature of manual fibre drawing, leading to the fibres not being perfectly flat to the glass substrate. This could explain some of the inconsistencies observed during processing, and the failure to achieve melting of glass fibre feedstocks.

Glass fibres suffered from a lack of flexibility and their brittle nature, making manual feeding of glass fibres through the wire feeder challenging. Glass fibres snapped and broke during the feeding process, and manual delivery was inconsistent when compared to the automatic feeding of flexible metal wires. The increased transparency of glass fibres compared with powder material was suspected to reduce laser absorption, causing a lack of melting. During this trial it was observed that laser energy was transmitted through the transparent glass feedstock (fibres) and transparent glass substrates (microscope slides) to the reflective aluminium surface, with little to no absorption of energy at the feedstock-substrate interface. From this observation, further optimisation of baseplates was undertaken to reduce the reflection of laser energy. When laser energy was successfully absorbed by the glass fibres, melting occurred with evidence of adhesion to glass substrates. In these cases, glass substrates suffered from thermal shock and cracked. Under optical microscopy transparency of melted glass was confirmed, with internal porosity visible (Figure 89).

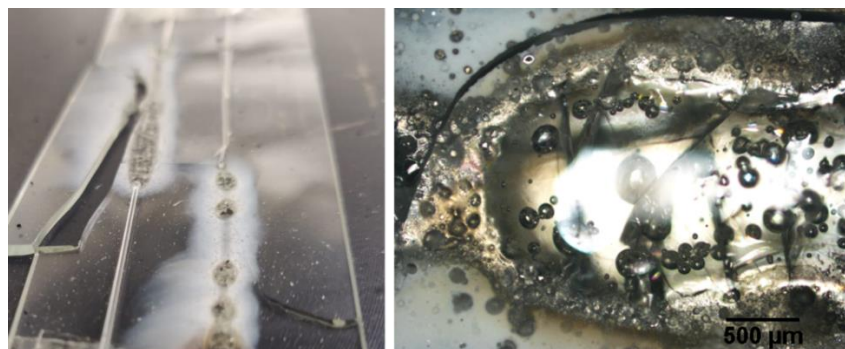


Figure 89 Glass fibres (SLSG-Fibre) processed onto a glass substrate at 150 W laser power, and 400 mm/min scan speed.

6.3.8 Discussion and Conclusions for Feasibility Studies

Glass fibre trials confirmed that melting of glass fibres by DED was possible, however with the available set-up, the brittle nature of the drawn glass fibres, and the manual feeding of the material to the nozzle and substrate, fibre trials resulted in frequent cracking and failure of effective processing. This challenge was also reported in literature, overcoming it by using thicker glass filaments/rods (1 mm \varnothing) in conjunction with a custom designed filament feeder¹⁵⁶, or coating 0.5 mm \varnothing quartz glass fibres with a polymer to protect fibres from breaking during delivery¹⁶⁰. Fibre trials were discontinued due to the incompatibility of the DED system and the glass fibre feedstocks. It was also considered that the fibre fed deposition method would be less able to create complex geometries than the powder deposition method, this being an aim of this work.

Feasibility studies confirmed the possibility of melting glass powders through DED processing. The trials showed evidence that the DED set-up was capable of melting and consolidating glass powders by laser irradiation. Glass powder spread on a substrate to create a powder bed suffered expected limitations, with laser energy transferring to surrounding powder, and causing structures to expand and deform. From this observation, further investigation into the method of powder delivery was a particular focus going forwards, with emphasis on automatic powder delivery by coaxial and side nozzle powder feeders. The results of feasibility studies investigating laser irradiation of thin powder bed layers were reminiscent of the investigations by Luo et al. who observed the discontinuity of processed tracks when processing a powder bed¹⁵⁵. This effect was somewhat overcome by Luo et al. through the focusing of the laser beam to a smaller spot size of 70 μm . Another similar observation in the work by Luo et al. was the fusion of glass powder surrounding the melt pool, increasing the dimensions of parts.

The feasibility studies presented an initial investigation into the effect of energy density on glass processing by DED. The results indicated a general trend of glass materials requiring sufficient energy density to melt and consolidate consistently. Additionally, evidence showed an independent effect of laser power and scan speed, with differences in glass melting behaviours observed despite processing with process parameters producing the same calculated energy density. This observation suggested that for glass the energy density can only offer estimations of laser absorption by feedstock materials, and in itself is a unique measure of processability.

A significant discovery during the feasibility study was the effect of a cellophane tape layer on glass processing by DED. The implementation of a cellophane tape layer aided adhesion of the melted glass powder to the glass substrates. The most likely explanation is a localised heating effect caused by the cellophane tape layer absorbing laser radiation. The exothermic release of energy during tape degradation heated the glass substrate and glass powder as it was delivered to the substrate surface. The increase in absorptivity of the glass powder feedstock caused by an increase in temperature allowed sufficient laser absorption for the glass to melt and caused thermal degradation in the organic cellophane and adhesive. A cellophane tape layer was applied to every glass substrate going forward.

The following conclusions were drawn:

- Processing of glass by the available DED set-up was possible, with clear evidence of consolidation and melting of glass powder and fibres in the feasibility studies.
- Laser irradiation of powder beds suffered limitations due to the high surface tension of glass causing transference of energy to powder beds and causing expansion of melted zone into the surrounding powder.
- Glass fibres were brittle and lacked the flexibility required for automatic feeding through the 1 mm wire nozzle.
- Substrate properties had a large impact on the absorption of laser energy by feedstock materials.
- Darkening of substrates, the use of an adhesive tape layer, and the utilisation of an automatic powder feeder aided glass melting by DED.

The results of the feasibility studies informed the experimental methods going forwards. The importance of substrate properties and feed method were highlighted and addressed in future DED experiments. The investigations following on from the feasibility studies focused on parameter investigation, and the processing of different glass designs on glass substrates of varying thickness.

6.4 Adaptation of Machine Set-Up

6.4.1 Introduction

Machine set-up was adapted to allow processing of glass powders by DED. Based on the results of the feasibility studies detailed in 6.2, automatic powder delivery was considered superior to powder bed set-ups. Investigation into powder delivery via two different nozzles was carried out to determine an efficient method of delivering a constant quantity of glass powder consistently. Different glass powders (e.g., different morphology, particle size distribution, or composition) were considered for DED processing, as well as substrate thickness/type, and the effect of moderate heating. Process parameters were investigated, as well as the effect of design geometry on DED processing and thermal shock (cracking). Multi-layer processing was considered, as well as processing onto bottle substrates for glass packaging décor applications.

6.4.2 Investigation of Powder Feedstock Delivery

Multiple feed attachments were tested for automatic delivery of glass powder for effective DED processing. Feasibility studies verified the incompatibility of glass wire feeding for DED processing in these investigations, and so glass powder delivery was the focus going forward. The two powder nozzle attachments were A) a 1 mm coaxial nozzle and B) a 2 mm lateral (side fed) nozzle. The coaxial nozzle was affixed to the laser head on the z axis. The lateral nozzle was affixed to the machine at an angle of 27.5° to the laser. Nozzle height was determined by the calibrated height of the laser head for processing with a 1 mm spot size, and was positioned 10 mm above substrates. Feed rate was measured to determine suitable feed parameters for effective glass processing.

A Teflon tube delivered glass powder from an automatic powder feeder (Model 1264, Miller Thermal inc, US) to a confined pot via a copper side nozzle or coaxial nozzle, using a volumetric feed principle. Delivery parameters of Argon (carrier gas) pressure (L/min), and flow rate determined by wheel speed (rpm) were varied between 5-10 L/min and 2-8 rpm, and glass delivered was measured by mass (g) over a 10 second period, repeated up to 15 times. Powder was heated to ~50°C prior to delivery. The materials used to measure feed rate were soda lime silica beads of varying particle size distribution ($Dv_{50} = 44, 102$ and $258 \mu\text{m}$ (GTS-6, GTS-2, GTS-1 respectively)). For side nozzle powder delivery, measurements were taken for delivery of feedstock through an uncoated 2 mm copper nozzle, and a copper nozzle lined with 2 mm Teflon tubing. Observations were made as to the effectiveness of delivering

powder by these means, and measurements of mass delivered over time were used to inform suitable parameters for processing different glass powders. The results of feed rate measurement are described in 6.5.

Single tracks of soda lime silica (GTS-2) were processed onto a microscope slide of the same composition at two flow rates: 1 rpm (slow rotation – limited quantity) and 12 rpm (fast rotation – larger quantity), to observe the effect of powder wheel speed on glass processing. Control parameters were used for each test, using energy densities of 11, 12, and 13 J/mm². Resulting samples were observed under SEM, and track height was measured using digital callipers.

6.4.3 The Importance of Substrates and Baseplates

Feasibility studies described in Section 6.2 highlighted the importance of baseplates and substrate properties for laser absorption. The transparent nature of glass substrates allowed laser energy to transmit through the substrate surface and reach the surface of the baseplate beneath. Feasibility studies concluded that reflective baseplates (e.g., machined aluminium) beneath glass substrates reduced the absorption of energy at the substrate surface by reflecting the laser radiation. Additionally, an increase in absorptivity of the glass powder was observed after two modifications: darkening of the base plate surface, and applying a cellophane tape layer to the glass substrate.

A black anodised stage was created to mount glass substrates onto directly, eliminating the potential reflection of laser radiation by the stage. Another critical factor for processing glass powder onto the glass substrates was adhesion of melted glass powder at the substrate surface. This was only achieved through using an adhesive cellophane tape layer. When irradiated during processing, the cellophane layer created a heated zone as it vaporized, allowing glass powder particles to adhere to the glass surface and melt.

Initial experimental trials were carried out on standard microscope slides (Biosigma) of 70 x 25 x 1 mm dimensions. Once successful processing was achieved on 1 mm substrates, a thicker soda lime silica substrate of 100 x 100 x 4 mm (supplied by GTS), was used. These substrates were produced by the float glass process (floating on a tin bath). Finally, glass bottle substrates were used to demonstrate the potential for glass décor application by powder fed DED.

For all glass substrates, a layer of cellophane tape was adhered to the surface before processing. Substrates were fixed to the black anodised base plate and secured with adhesive tape to ensure a stable, flat processing surface was achieved.

Two bottle substrates, both soda lime silica composition, were used to investigate processing of glass powder onto a transparent bottle surface. The first bottle substrate (Bottle A) was irregular in shape, with two large, sloped sides. Bottle B was a regularly shaped square bottle, with decorative striations on multiple sides to varying degrees (Figure 90). Dimensions were measured approximately using digital callipers. Bottle A measured 100 x 75 mm at the base, with a height of 225 mm, and bottle B measured 75 x 75 x 250 mm.

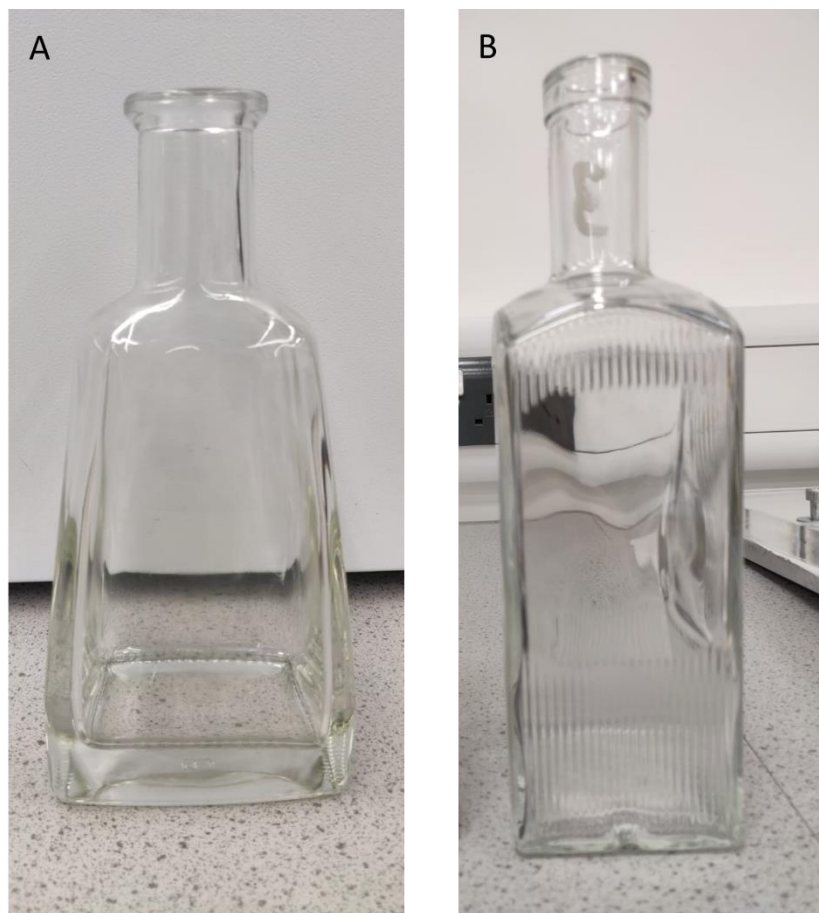


Figure 90 Bottle substrates used for investigations into DED of glass on substrates of different thickness/dimensions.

Consideration of the empty space between bottle surfaces was necessary to account for the potential loss of laser radiation through the transparent surfaces. Various different options were considered to counter this: filling the bottle with a dark powder to absorb excess energy, such as black PA12 (black nylon 12 powder), or a high melting temperature material

like sand; and applying a coat of multi-purpose, matt black paint on the inside surfaces of the bottle.

Bottles were prepared according to the options above, and coated with a single layer of cellophane tape, to emulate the process conditions of the other flat glass substrates. Bottle substrates were affixed to the DED base plate and surrounded by an Argon bag for processing. Processing parameters were informed by experimental investigations on other glass substrates. Design geometries included single tracks, straight and curved features, and text design.

6.4.4 Investigation of Experimental Variables

Other variables were investigated for their effect on processing glass powder by this method, such as laser focal length, and the use of a substrate heater. To investigate the effect of laser focal length on processing, the height of the laser head was altered by movement in the z direction. For processing at focus, the stage was positioned 10 mm below the powder feed nozzles, and 192 mm below the laser head (focal length as calibrated), corresponding to a spot size of 1 mm ($F=0$). Adjustment of the stage position in relation to the laser head was carried out in order to bring the focal point above and below the substrate surface: $F<0$ for focus below the substrate surface, and $F>0$ for focus above the substrate surface (Figure 91). Variation of the z height between -3 and +3 mm was explored and the results observed when processing a single track at energy densities of 10 J/mm^2 and 11 J/mm^2 . Average glass deposit height was measured using digital callipers.

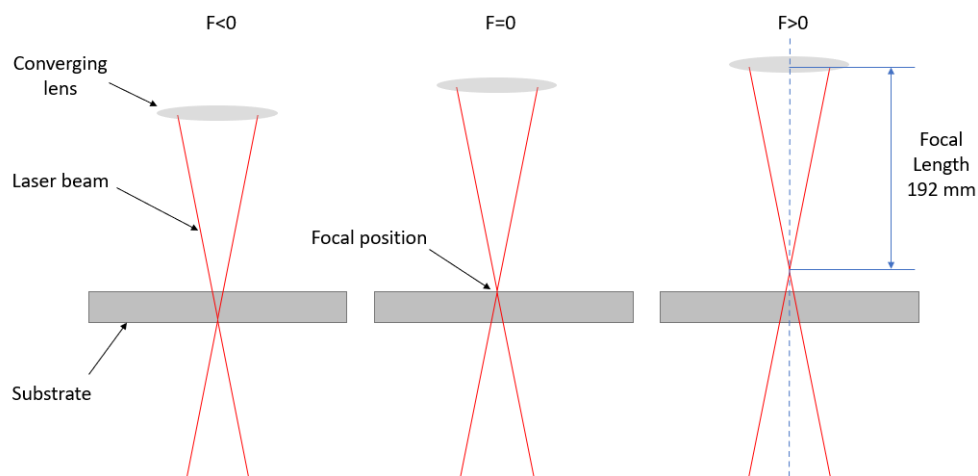


Figure 91 Laser focal position in relation to substrate surface as determined by laser head height.

Adjustment of the z height was also used to explore multi-layer processing of soda lime silica glass powder on 1 mm glass substrates. Glass powder (GTS-6: $DV_{50} = 44 \mu\text{m}$) was processed at a constant energy density of 16.7 J/mm^2 (feed parameters 12 rpm, 10 L/min), and the laser head height was adjusted vertically in 0.8 mm increments (an approximation of the deposited track) and processed to create a multi-layer glass structure. Deposit height was measured using digital callipers and compared for 1, 2, and 5 layer processing.

A stage heater was employed to investigate the effect of substrate pre-heating on glass powder processing by DED. The aluminium baseplate described in Section 6.2 (Figure 80 C), with a bead blasted and graphite darkened surface, was mounted to the stage heater. Glass microscope slides were affixed to the baseplate and coated with a single layer of cellophane tape to aid adhesion and improve laser absorption at the glass substrate surface. Glass powder was fed via lateral powder nozzle to the substrate at the laser interface.

The heated stage was ramped up to 100°C (measured by infra-red thermometer) before glass powder was processed at 125 W laser power and 450 mm/min (16.7 J/mm^2). Resulting glass tracks were investigated by SEM, and the occurrence of sub-surface lateral cracks were considered.

6.5 Optimisation of DED Process Parameters

Process parameter investigations primarily focused on laser power, and scan speed, with the measurement of Energy Density used to relate the two. The equation used to calculate energy density for DED processing was described in section 2.6, assuming a layer thickness of 1 mm.

The Ytterbium doped, continuous wave (CW) fibre laser (IPG Photonics Ltd, USA) was restricted to an upper limit of 2kW laser power, operating at a wavelength of 1070 nm. Scan speed was dictated by the translation stage (X-LRQ-E Series, Zaber, Canada), and was restricted to an upper limit of 6000 mm/min (100 mm/s). Scan speed was controlled via GCode and operation of the laser and the stage were independent of each other, requiring manual control.

Initial feasibility studies (described in Section 6.2) helped to narrow parameters down to an appropriate range. Laser power and scan speed were varied between 95-130 W and 500-700 mm/min respectively in order to populate a process map. Feasibility studies also concluded that energy density calculations could be used to estimate energy absorption for different parameter combinations but may not offer a complete representation of total energy absorption during processing.

During this process parameter investigation, energy density was calculated for each combination of parameters to assess any correlation. Other set-up variables were kept constant: microscope slides of 1 mm thickness with a single layer of cellophane tape coating were used as substrates, processing took place inside an Argon bag for shielding, soda lime silica powder (GTS-6) was delivered through a Teflon lined, 2 mm side nozzle, feed parameters were kept constant at 2 rpm and 5 L/min, and processing was carried out at focus with a 1 mm spot size. Cameras (Logitech, CHE) were used to monitor the process remotely. The stage movement was controlled by a simple incremental GCode to process a single track of 60 mm length on each substrate. A delay of 2 seconds was utilised between switching on of laser power and stage movement to allow for laser dwell time and initial absorption of laser energy by the powder at the substrate surface.

To investigate the effect of scan design on glass DED, a number of different GCodes were generated to illustrate different geometric features. The GCode format was necessary for the Zaber (translation stage) software to successfully translate the code to a stream of

commands. Different geometry designs were used during experimental trials, with four main designs demonstrating the different features studied (Figure 92)

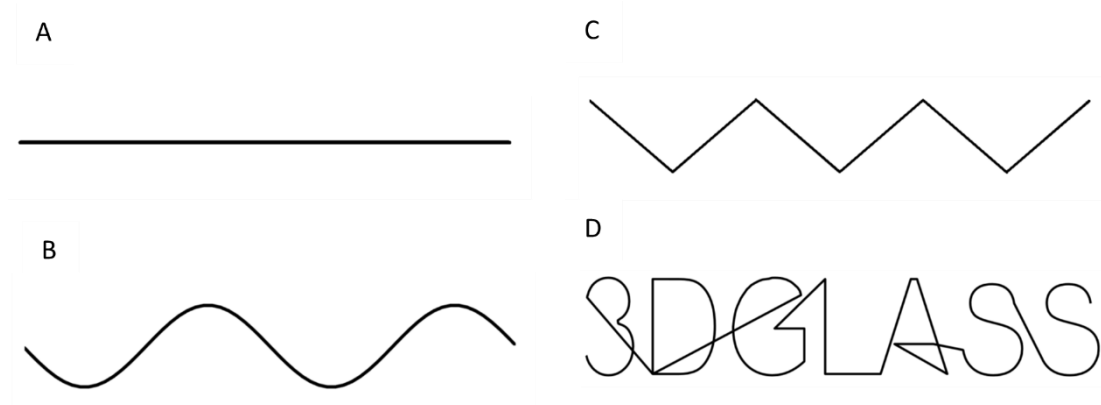


Figure 92 Four main design geometries showing features of interest. A: Single tracks, B: Curved Features, C: Straight Features, D: Combination Features (text).

Each design was confined to 60 x 20 mm to accommodate processing onto glass substrates of 70 x 25 x 1 mm dimensions. A simple track was designed for the purpose of process parameter investigation (Design A). This scan design was simply written using an incremental GCode format (G91), instructing the stage to move 60 mm in one axis at a specified speed (eg F600 for 600 mm/min). The design was positioned in the centre of the substrates, as far from the edges as possible. The curved features design (Design B) was created using coordinates of a sine wave with the absolute coordinate GCode (G90). The total number of points written in the curved features GCode was 60.

A straight features scan design (Design C) was written using incremental GCode, similar to the single track design, but requiring simultaneous movement in the x and y axes, with 6 points of movement. Finally, a design combining curved and straight features was created to process a text design. The initial design was created in STL format using a 3D CAD package (Solidworks, Dassault, FR), and converted to a GCode format (Repetier Host). The generated GCode was then edited using a text editor (Sublime), in order to be translated by the x-y stage software (Zaber). Absolute coordinate GCode was used for every feature in this design, with approximately 344 points. Scan speed was decided based on feature type, with the maximum scan speed (F6000 = 100 mm/s) used for transition between letters in order to cease material consolidation.

Designs were processed onto glass substrates of various dimensions. Initially, 1 mm thick microscope slides were used to evaluate process parameters based on material deposition (melting, consolidation, and adhesion). Substrate cracking was also assessed for 1 mm microscope slides, particularly for single tracks, however, for the other designs, cracking was expected due to the increased concentration of energy applied during processing, liable to cause thermal shock in parts and substrates. The required energy densities for processing designs B, C, and D onto 1 mm substrates were investigated, with the incidence and severity of cracking recorded. The energy densities required for successful processing of these designs were then used for processing on thicker substrates, with the understanding that resistance to thermal shock would be greater than the 1 mm substrates.

6.6 Experimental Results

6.6.1 Measurement of Feedstock Delivery Rate

6.6.1.1 Effect of Particle Size Distribution

Particle size distribution had a significant effect on the mass of glass beads delivered through a copper side nozzle. Results showed that delivery of glass beads through a 2 mm copper nozzle varied depending on average particle size. The average mass of GTS-6 ($\sim 44 \mu\text{m}$) delivered was measured as 23 mg/s, GTS-2 ($\sim 102 \mu\text{m}$) as 45 mg/s, and GTS-1 ($\sim 258 \mu\text{m}$) as 69 mg/s (Figure 93). As the average particle size increased, the average mass delivered over a 10 second period increased.

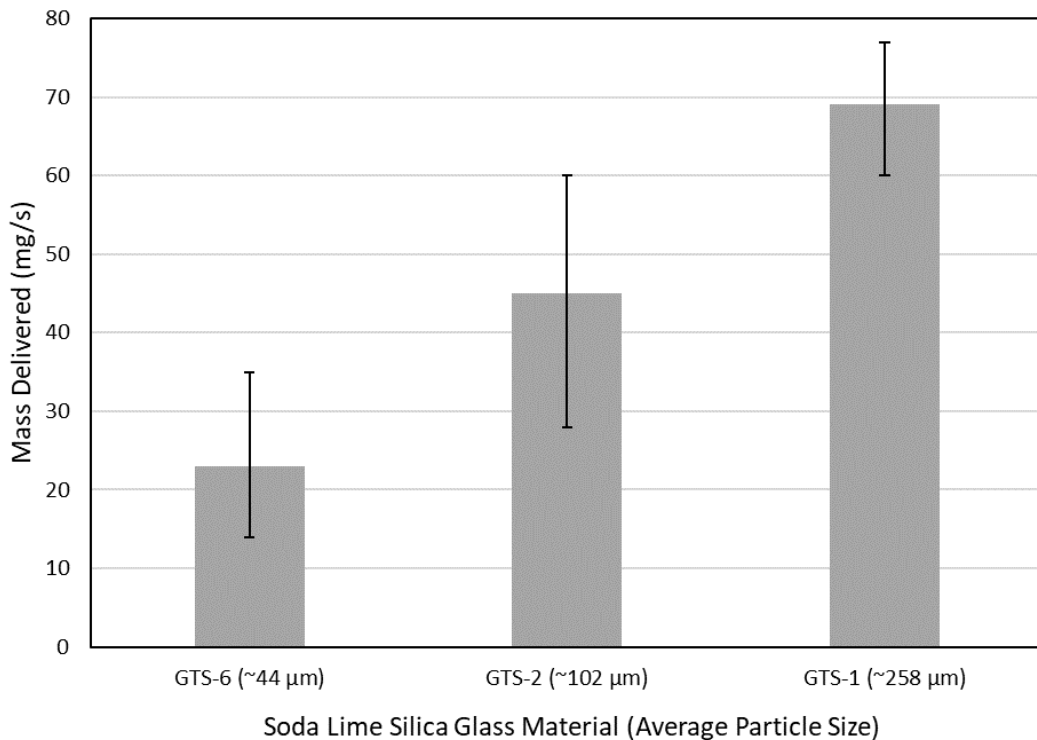


Figure 93 Average glass powder delivery (mg/s) by copper side nozzle of soda lime silica feedstocks of varying particle size distribution. Error bars indicate the minimum and maximum values of mass delivery measurements.

6.6.1.2 Effect of Nozzle Type

A significant difference was seen between the powder feed rate through a side nozzle and a coaxial nozzle (Figure 94). For soda lime silica spheres of $\sim 44 \mu\text{m}$ (GTS-6), powder flow was severely impeded by the coaxial nozzle. It is suspected that the smaller average particle size of GTS-6 caused increased cohesivity due to increased electrostatic interaction between fine

particles in comparison to the larger particle size soda lime silica feedstocks (GTS-1 and GTS-2). The smaller particle size also may have led to increased moisture content in the feedstock, reducing flowability, however, efforts were made to dry all glass powder feedstocks by vacuum oven at 100°C for 12 hours before processing^{114,230}. The reduced flowability measured in powder rheology testing (Section 4.3) was attributed to this property, and subsequently caused a reduced feed rate through coaxial nozzle feeding (3.3 mg/s). Another explanation for this reduction in feed rate is electrostatic interaction between the copper nozzle and the glass material, causing material to collect in the nozzle and block the smaller, annular orifice (effectively 0.25 mm wide) of the coaxial nozzle. This was hypothesised due to the observation of material build-up inside the coaxial nozzle, and attachment of powder particles to the outside of the nozzle. The positive interaction between the glass powder and copper nozzle was thought to have severely reduced the flow of powder to the substrate, making the coaxial nozzle ineffective for delivery of GTS-6.

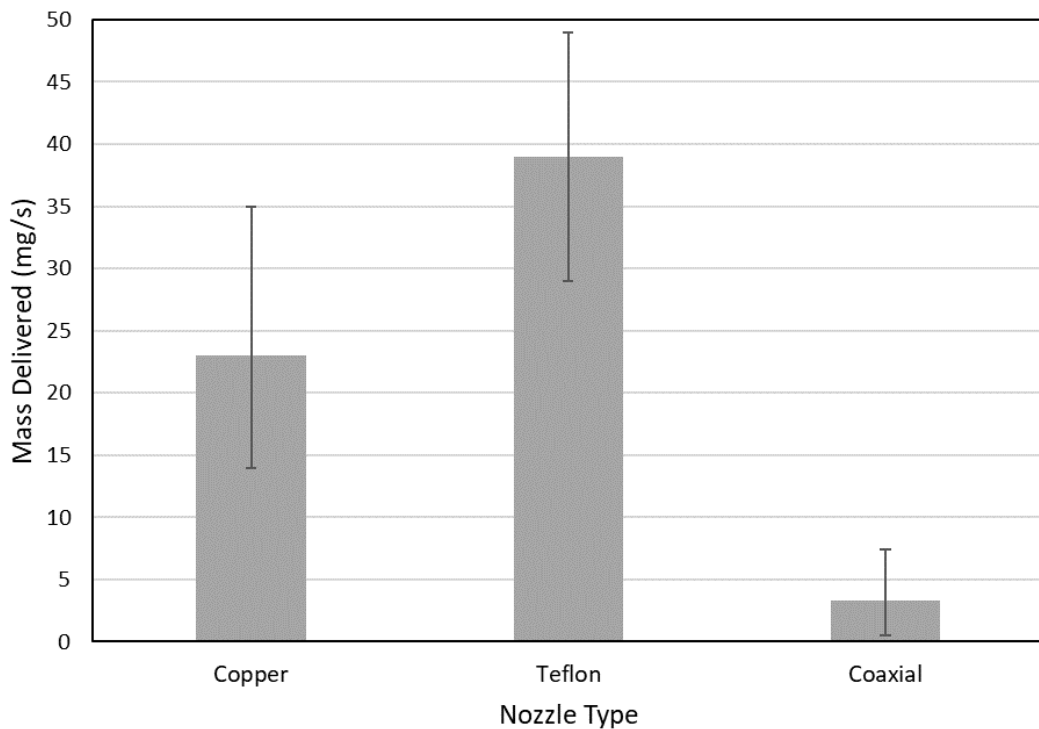


Figure 94 Feed delivery rate (mg/s) of GTS-6 through a copper nozzle, Teflon lined nozzle, and coaxial nozzle. Error bars indicate the minimum and maximum values of mass delivered.

The copper side nozzle achieved an average powder flow of 23 mg/s for GTS-6. Although this was an acceptable rate of powder delivery for the intended processing, the copper material of the nozzle was observed to attract glass particles to the inside of the nozzle, restricting the

flow of powder over time. This was combated by blowing compressed air through the nozzle at regular intervals, however this was inefficient for processing over a long period. A Teflon tube was used to line the side nozzle to prevent the attraction of powder particles to the nozzle surface by electrostatic forces. The measured average feed rate of powder through the Teflon nozzle was 39 mg/s, a significant increase compared to the copper nozzle.

6.6.1.3 Effect of Powder Wheel Speed (RPM)

Powder feed rate was measured at varying powder wheel speed (RPM). Powder wheel speed was controlled at 2 rpm and 4 rpm, and the average mass of soda lime silica (GTS-6) delivered was recorded. Wheel speed determined the quantity of glass powder metered through the feed system, and therefore average mass of GTS-6 delivered increased with rpm as expected (Table 18).

Table 18 Average powder feed rate of GTS-6 at 2 rpm and 4 rpm powder wheel speeds.

Wheel Speed	Mass Delivered (mg/s)	
	Range	Average
2 rpm	14-35	23
4 rpm	23-34	27

6.6.1.4 The Effect of Powder Feed Rate on Glass Processing

Despite a small difference between mass delivered at 2 rpm and 4 rpm of GTS-6 powder, comparison of processed glass tracks at two extremes - 1 rpm and 12 rpm - revealed the significant impact feed rate had on glass processing (Figure 95).

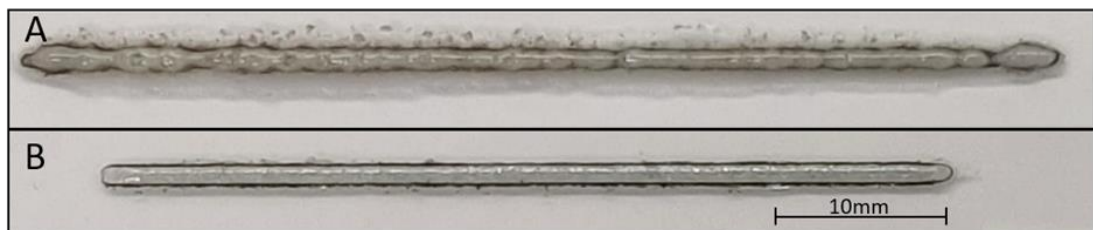


Figure 95 Processed tracks of GTS-6 using energy density = 11 J/mm² at different powder wheel speeds. A: 12 rpm, B: 1 rpm.

Processed tracks were visibly distinct, with a higher feed rate resulting in an obvious variation in track height and width. Measurement of average track height confirmed that glass deposit height was significantly increased at 12 rpm compared to lower flow rates. At process parameters of 11 J/mm², the average track height at 12 rpm was 0.9 mm, at 1 rpm, the average track height was measured at 0.2 mm. Results were compared at three different energy densities, 11, 12, and 13 J/mm², with average track height remaining consistent across these parameters (Figure 96). Error bars show higher variance in measurements of 12 rpm deposit heights compared to 1 rpm deposit heights, suggesting powder delivery was more consistent at lower flow rates. This could be due to differences in powder capture rate at varying wheel speeds.

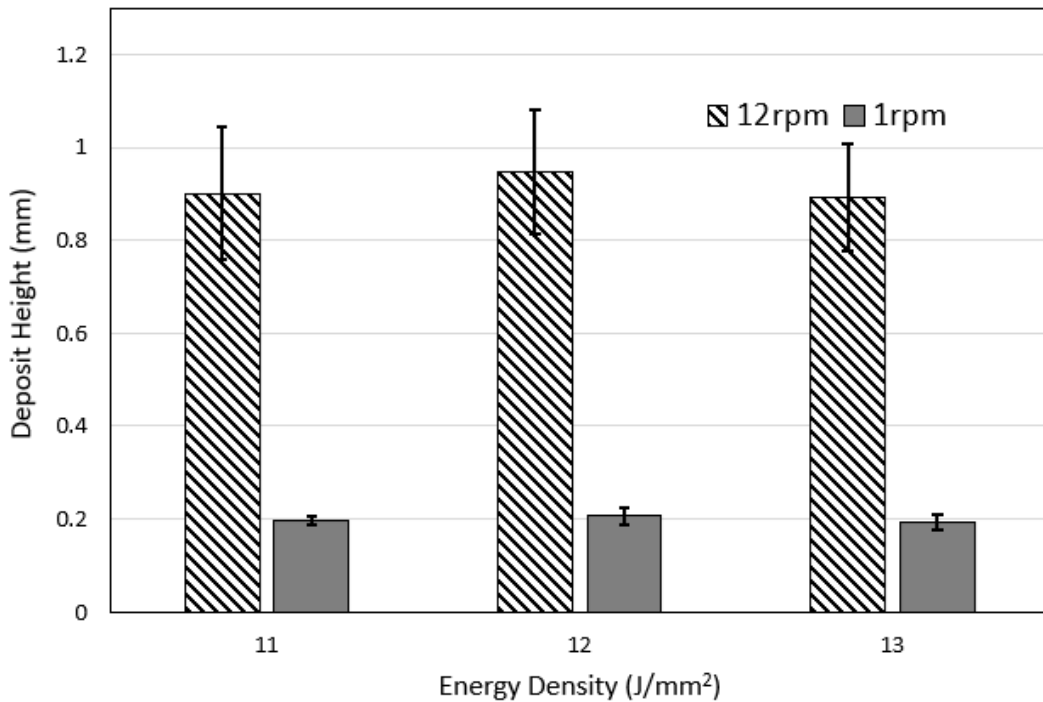


Figure 96 Comparison of average glass deposit height (mm) at 1 rpm and 12 rpm powder wheel speeds, at 11-13 J/mm² energy density. Error bars indicate minimum and maximum measured values.

The glass deposits were observed under SEM to provide a more detailed view of the deposit variations at the two extremes of feed rate (Figure 97). At 1 rpm feed rate, glass tracks showed consistent and regular boundaries compared to the significant variation in track height and width observed at 12 rpm. This variation in dimension for higher feed rate was attributed to the greater mass of glass powder delivered, and therefore melted and deposited by the laser. The area surrounding deposited glass tracks showed blackening in the SEM images. This is likely explained by the combustion of the organic layer of the cellophane

tape on laser irradiation, leaving behind a carbon residue. Cracks were seen in structures processed at both powder wheel speeds tested.

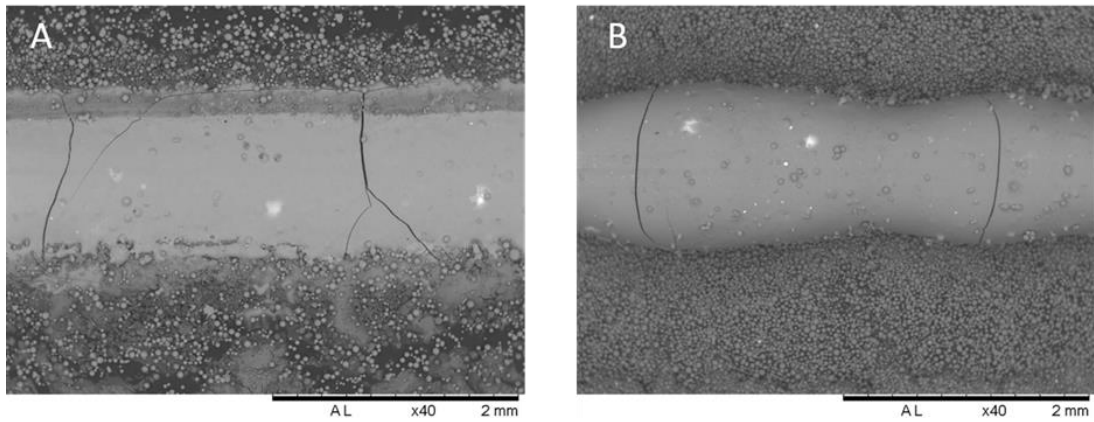


Figure 97 SEM images of deposited glass tracks at $ED= 11 J/mm^2$. Powder wheel speeds of A: 1 rpm, B: 12 rpm.

Variation in track height would negatively impede multi-layer processing, so a high rpm was avoided. Surface roughness also increased for high rpm feed rates, which is undesirable for décor applications. In order to achieve consistent and accurate tracks of deposited glass, a low rpm was selected for future testing, with 2 rpm selected as the experimental constant. Another benefit of low feed rate was the reduced quantity of glass used during each build, and therefore reduced material cost for single layer builds.

6.6.2 Experimental Variables

6.6.2.1 Laser Focal Length

Out of focus processing was carried out at two energy densities: 10 and 11 J/mm² (Scan speed: 11.3 mm/s, laser powers: 115 W, 125 W). For control processing, substrates were placed at focus position (F=0). To investigate out of focus processing, substrates were placed at F<0 and F>0 at 1 mm increments up to +/- 3 mm.

At F<0 consistent fusion of glass powder was not observed. At F=0, and F>0, fusion of glass was successful, and average deposit height was measured (Table 19) (Figure 98). Deposit height was largest at focus (F=0), and generally decreased with increasing substrate distance (F= 1-3). The corresponding spot sizes can be estimated from previous beam profiling of the laser system. D86 values for the laser beam were estimated as 0.9 mm at F=0, increasing to 0.956 mm at F=2, and 1.068 mm at F=4 (see appendix). Therefore, energy density decreases with increasing focal length and spot size.

Table 19 Results of the investigation into the effect of laser focal position on glass deposition.

F<0	F=0	F>0
 F= -1		 F= +1
 F= -2		 F= +2
 F= -3		 F= +3

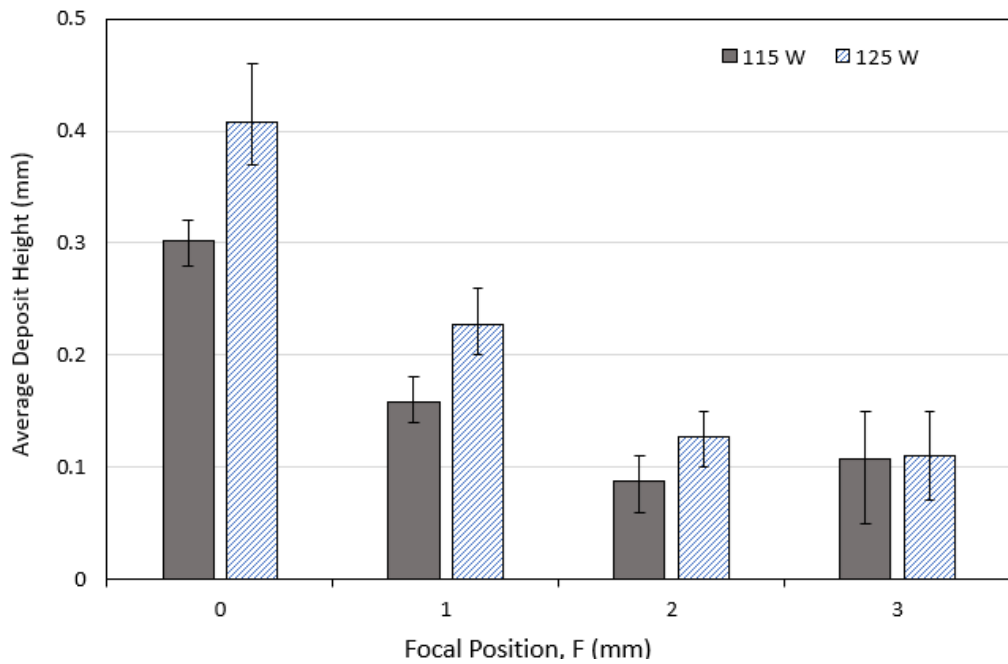


Figure 98 Average glass deposit height by laser focal position (at varying laser power). Scan speed = 680 mm/min. Error bars indicate minimum and maximum measured values.

As the substrate was incrementally moved below the focal point of the laser, deposit height generally decreased. This is likely explained by the laser spot becoming more diffuse at the substrate surface as it is moved further away, reducing the energy density. The powder feed remained unchanged, and so deposit thickness did not vary significantly between samples. As the spot size increased, the mass of material receiving a critical energy density to become molten was reduced, meaning deposit height was lower, while deposit thickness remained the same as the powder stream remained constant. The effect of energy density on deposit height is demonstrated at two laser powers, 115 W and 125 W. A higher energy density ($\sim 11 \text{ J/mm}^2$: 125 W, 11.3 mm/s) generally resulted in a larger average deposit height than the lower energy density trial ($\sim 10 \text{ J/mm}^2$ – 115 W, 11.3 mm/s), due to the increased mass of material reaching a molten state.

There are multiple possible explanations for the lack of fusion observed at $F < 0$. Even very small misalignments in the laser beam angle can have a large effect on the processing of material out of focus. Any error in the laser angle would be exacerbated by vertical movement of the substrate, changing the expected energy density during processing. The volume of interaction can change significantly with each mm alteration of focal position, as this would change the volume of powder entering the laser beam, particularly when using a lateral powder feed nozzle.

At $F < 0$, the laser is transmitted through the glass slide and focused on the black anodised base plate beneath. Theoretically, the spot size diameter should be equivalent when out of focus by the same amount above or below the substrate, therefore providing the same energy density. Despite this, the results show a distinct difference during processing. This phenomenon could be caused by differences in the interaction of glass powder and laser energy in the two different scenarios, as illustrated in Figure 99. The image represents powder delivery, and the location of the laser focal point in relation to the substrate. Glass powder delivered laterally to the laser beam during $F > 0$ processing occurs below the focal point of the laser, allowing glass particles to enter a higher energy density during deposition. In contrast, during $F < 0$ processing, powder is introduced above laser focal point, meaning the material delivered has no opportunity to enter an area of high energy density during deposition, resulting in a reduction in laser absorption by the glass powder.

Additionally, for $F > 0$ focal position, the laser beam is diverging, whereas at $F < 0$ focal position the beam is converging. For the diverging beam, the area of laser irradiation is smaller and more focused, experiencing a higher energy density. Conversely, for $F < 0$ focal position, the converging beam results in a larger area of laser radiation, and an effectively lower energy density, explaining the significant differences observed when altering these conditions.

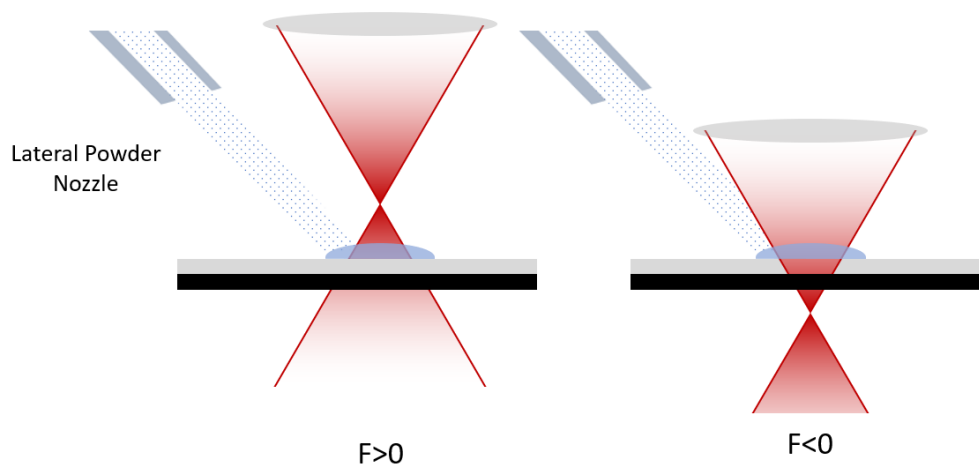


Figure 99 Image showing powder irradiation at $F > 0$ and $F < 0$.

6.6.2.2 Multi-Layer Processing

When processing in multiple layers, glass substrates suffered from thermal stress, cracking in every instance. Deposit height was measured by digital calliper, and an average taken. With each additional layer, the deposit height increased, as expected (Figure 100). With

increasing number of layers (and therefore average deposit height), variance also increased. Structures also exhibited curling at the two ends of the process track. This effect was likely the result of a build-up of internal stresses. Due to the prevalence of substrate cracking, single layer processing was the research focus going forward. For the application considered in this work, the customised décor of bottles, this is not a serious limitation, however, it does question the applicability of this process to true 3D printing.

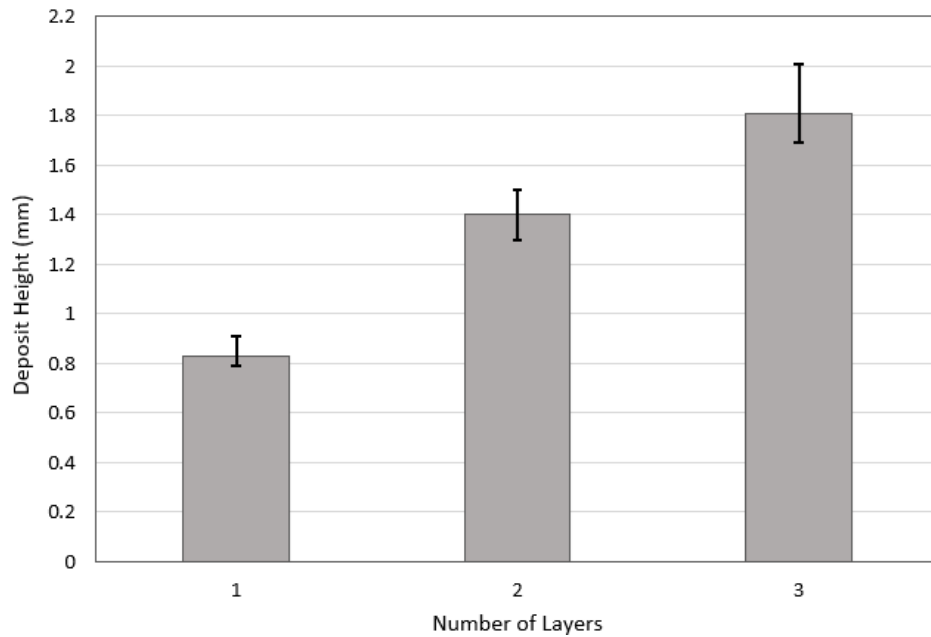


Figure 100 Average deposit height of 1, 2, and 5 layers of processed soda lime silica (GTS-6) on a glass microscope slide (1 mm). Error bars indicate minimum and maximum measured values.

6.6.2.3 The Effect of Moderate Heating on Glass Powder Processing

The experimental set-up used in the DED investigations was modified in this investigation to include a stage heater module. Under normal conditions, processing occurred inside an Argon bag for shielding purposes, and to contain blown powder. The stage heater module prevented the use of an Argon bag (the plastic would melt). Another important factor considered during these heated trials was the melting temperature of cellophane tape (~93°C).

At 16 J/mm² ED, glass powder melted and deposited onto the heated glass substrates, forming melted glass tracks. By SEM, deposited tracks under heated conditions were compared to tracks deposited at room temperature using the same processing parameters.

The track boundaries of heated and room temperature deposited tracks differed in regularity, with heated trials causing a variation in the melted glass boundaries (Figure 101). This is likely due to the initiation of cellophane tape layer degradation, causing variation in the substrate surface during heated trials.

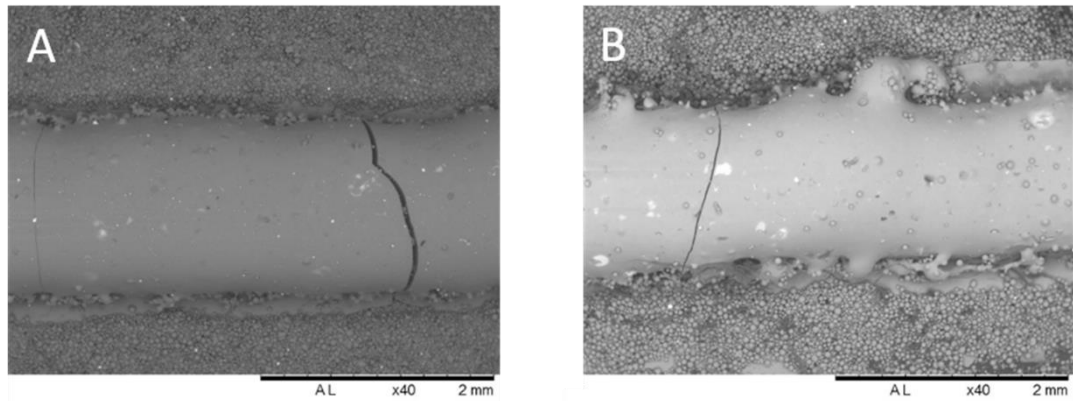


Figure 101 SEM images of processed glass tracks on 1 mm glass substrates at A: room temperature and B: moderate heating ($\sim 100^{\circ}\text{C}$).

Cracking was observed in the SEM images of both heated and room temperature deposited tracks. This is evidence of thermal shock. It has been reported that heating of substrates and/or process chambers for Additive Manufacturing of glass reduces the thermal gradients and therefore can reduce the incidence of thermal shock/cracking in parts^{158,231}. Cracking was observed in the built structures of deposited glass tracks under SEM and micro-cracks could also be seen penetrating the glass substrates a small distance the glass substrates along the deposited track. Cracks propagated in line with the deposit but did not result in fracture of parts.

6.6.3 Laser Processing Parameters for Glass DED

The investigation of process parameters for single track processing of soda lime silica glass (GTS-6) on 1 mm substrates of the same material was collated into a process map (Figure 102). The results were evaluated by three observations and recorded on a graph. Produced parts were inspected for fracture of the glass substrate, consistency of deposited glass material, and the evidence of successfully melted glass structures. Combinations of parameters that resulted in substrate failure were recorded with a red cross, those which resulted in the inconsistent deposition and melting of glass powder were recorded with a blue diamond, and the combinations of parameters which successfully built a continuous

track of melted glass on a substrate that survived with no fracture were recorded as green circles.

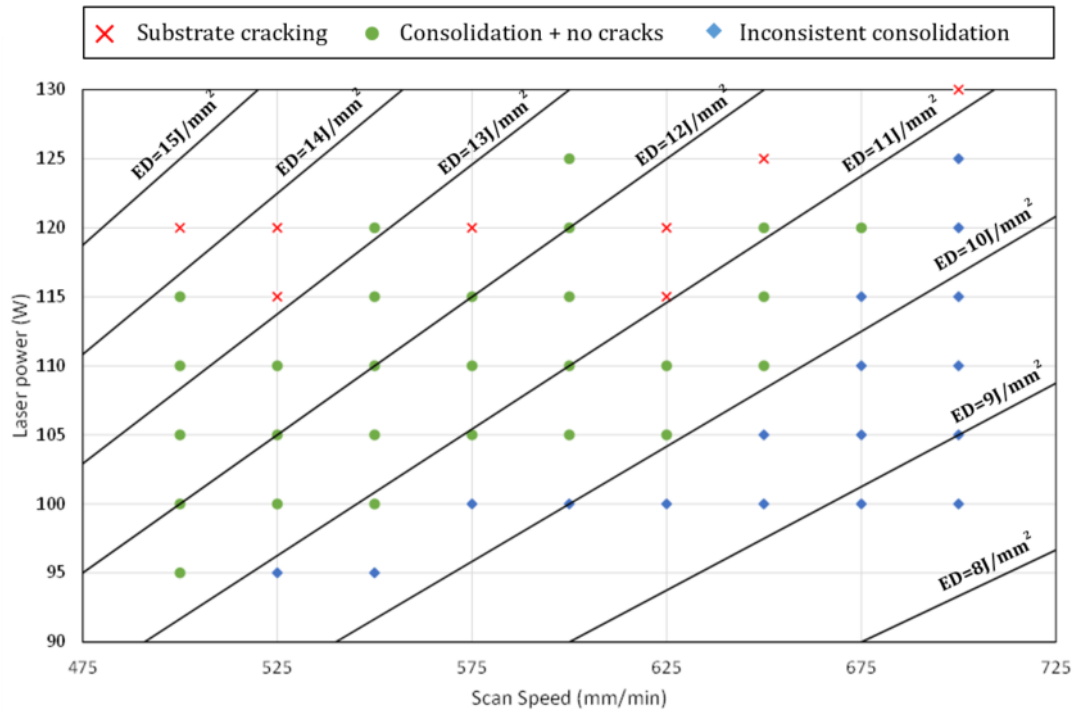


Figure 102 Process map for single tracks of soda lime silica (GTS-6) on a 1 mm substrate of the same composition. Trendlines depict the energy density at different combinations of laser power and scan speed.

The results show a relationship between Energy Density and inconsistent consolidation of glass, as this only occurred at energy densities below 11 J/mm^2 , as shown in the process map; with every combination of parameters below 10 J/mm^2 resulting in inconsistent consolidation of glass. This suggests that a minimum energy density was required for successful consolidation and melting of glass to occur to form a consistent track.

Cracking of substrates generally occurred at higher laser powers, regardless of energy density. For example, the combination of 130 W laser power and 700 mm/min scan speed resulted in substrate fracture despite relating to a moderate energy density (11.1 J/mm^2). Substrate cracking only occurred at or above 115 W. However, there are several cases where fracture did not occur despite laser powers greater than 115 W employed, e.g., combinations of 125 W, 600 mm/min, and 120 W, 675 mm/min.

Despite the limitations to using energy density to describe processing windows, recommendations can be made based on the results of this parameter investigation. For

example, parameter combinations that have a calculated energy density above 11 J/mm^2 , specifically with a laser power below 115 W all resulted in consistent consolidation of glass, without significant cracking. This could be used to guide DED processing parameters to a suitable “processing window”.

Processing of soda lime glass filaments was reported by Luo et al¹⁵⁶. The optimal parameters reported for melting of filament feedstocks was 20 W laser power, and 0.25 mm/s scan speed, with a layer thickness of 0.5 mm. The calculated energy density is 160 J/mm^2 . These parameters differ significantly from the range of laser powers and scan speeds used in this work for DED processing of soda lime silica glass powder (95-125 W laser power, 8.3-11.7 mm/s scan speed). In comparison, soda lime silica powder melting was achieved at energy densities above 11 J/mm^2 in this work. A heated substrate was also utilised for fibre fed DED processing, maintaining the substrate temperature at elevated temperatures (530°C). As substrate cracking was an important factor when assessing the laser processing parameters for soda lime silica powder, the use of a high temperature substrate heater could allow for a wider processing window by lowering thermal gradients and thus reducing the risk of substrate cracking at higher energy densities. Investigation into the effect of high temperature substrate heating for powder fed DED of soda lime silica glass is recommended for future work.

6.6.4 The Effect of Scan Design on Glass DED

6.6.4.1 Single Track

The single track design was successfully processed onto glass substrates of 1 mm, with a range of parameters, as demonstrated during process mapping. Under ideal parameters, this design did not result in substrate cracking, and produced a consistent deposit of glass, adhered to the substrate surface (Figure 103).



Figure 103 An example of a single track of processed soda lime silica (GTS-6) on a 1 mm glass substrate ($ED= 11 \text{ J/mm}^2$).

Post processing involved the removal of cellophane tape, aided by the use of acetone. Substrate cracking was visible from the under-side of the microscope slide, but cracking did

not penetrate the whole 1 mm thickness. This was further visualised by micro-XCT (Nikon MCT 225, Nikon, JP) (Figure 104).

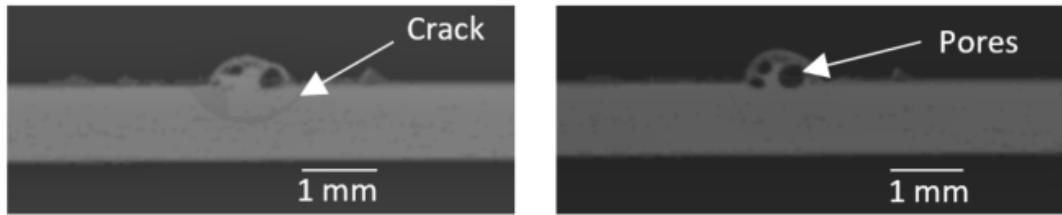


Figure 104 XCT images of a cross section of DED processed glass (GTS-6) on glass substrate. Images show crack formation and internal porosity. Sample was processed at 12 J/mm² (feed parameters: 2 rpm, 5 L/min).

The surface of the glass substrate appears to be melted during processing, aiding adhesion and melting of feedstock powder. Cracks developed laterally along the laser scan track, penetrating approximately 0.5 mm through the thickness of the substrate, before propagating in the reverse of the scan direction. These micro-cracks did not cause failure of the part. Cracks were also seen in the processed track by SEM (see Figure 101). XRD analysis confirmed the deposited glass remained amorphous after DED processing (Figure 105).

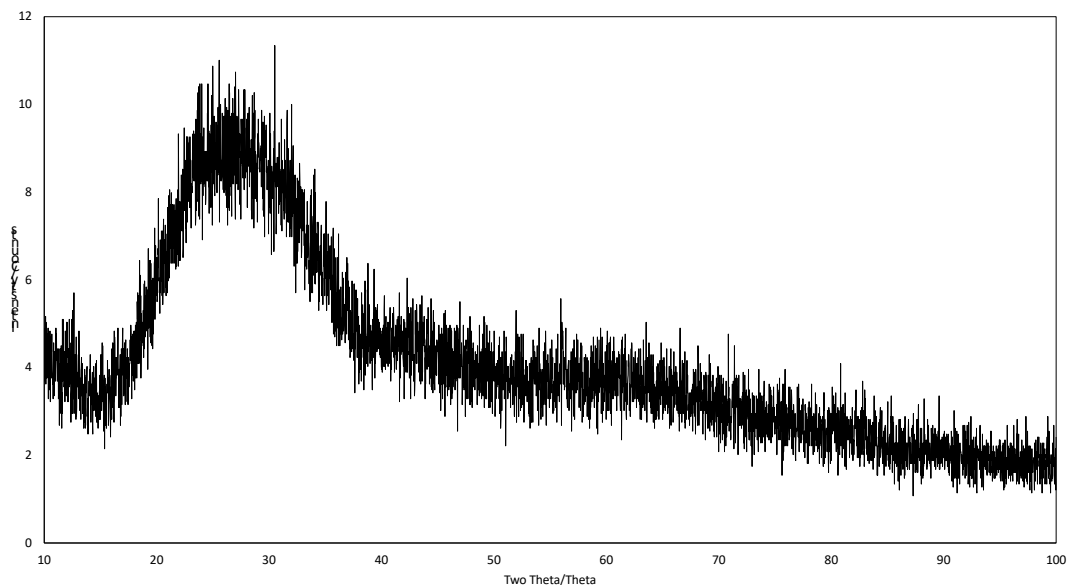


Figure 105 XRD analysis of DED processed GTS-6 glass showing no crystallinity.

6.6.4.2 Curved Features

When processing a curved design on 1 mm substrates, cracking occurred due to thermal stresses. For a curved design, compared to a single track, a larger area of the substrate surface was irradiated, meaning substrates experienced a higher concentration of energy, and was more likely to crack. Although substrate fracture occurred in these investigations, parameters were varied to find suitable energy densities for consistent melting and deposition of feedstock onto the substrates (Figure 106). At the lowest energy density (8.8 J/mm^2), glass was not deposited consistently onto the substrate, suggesting an insufficient energy density for successful processing and deposition of melted glass feedstock onto the glass substrate. As the energy density increased, processing of glass powder was achieved. Processing GTS-6 at energy densities of $9.24\text{--}10.12 \text{ J/mm}^2$ resulted in consistent deposits of glass feedstock, melted and adhered to the substrate. Cracking was observed to increase with increasing energy density as expected.

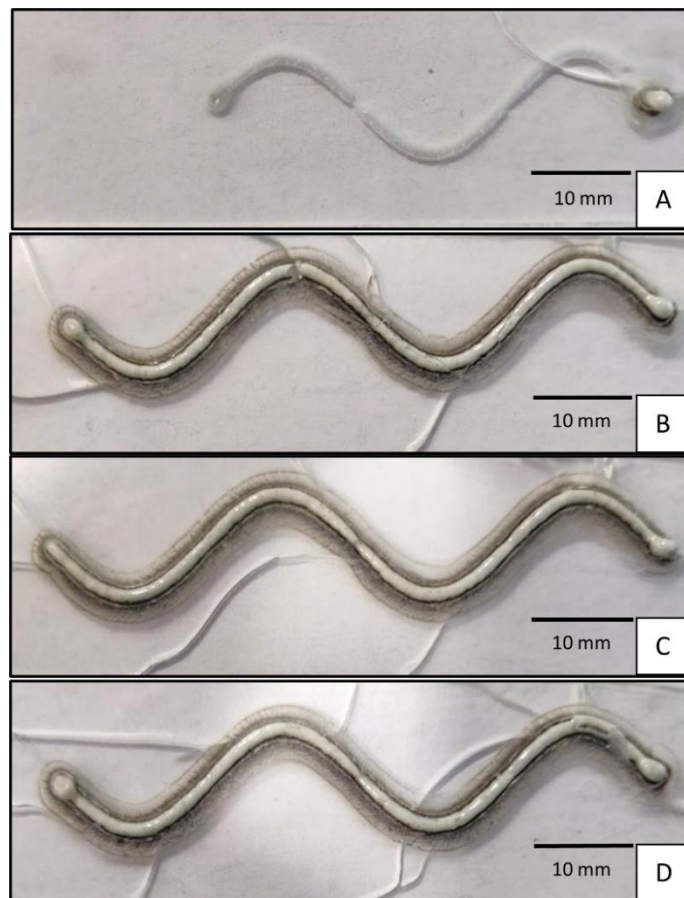


Figure 106 Curved features design of GTS-6 processed onto 1 mm glass substrates at varying energy density. A: 8.8 J/mm^2 , B: 9.24 J/mm^2 , C: 9.68 J/mm^2 , D: 10.12 J/mm^2 .

Cracking was observed to initiate from the apex of curves, corresponding with a sharp change in geometry or scan direction (and therefore increased stress concentrations). These features are also situated closer to the edges of substrates, which are expected to require less stress for fracture (edges are more susceptible to imperfections/damage and therefore are weaker)^{3,232}.

Processing of the curved feature design on a 4 mm thick plate at 9.24 J/mm^2 , as informed by the investigation on 1 mm substrates, resulted in the successful deposition of melted glass (Figure 107). The substrate remained intact, with no evidence of catastrophic thermal fracture. Internal micro-cracks were visible to the naked eye, penetrating into the substrate beneath the processed track.



Figure 107 GTS-6 glass feedstock processed onto a 4 mm glass substrate at 9.24 J/mm^2 in the curved features design.

For processing the curved features design onto a glass bottle surface, with a thickness varying between 5-7 mm, the chosen energy density was 9.68 J/mm^2 . This energy density was selected over 9.24 J/mm^2 (used for the 4 mm plate processing) as it did not show a significant increase in cracking, and a higher energy density was expected to be tolerated on thicker substrates. Deposition and adhesion of glass feedstock to the glass bottle substrate was successful, resulting in a consistent curved structure (Figure 108).

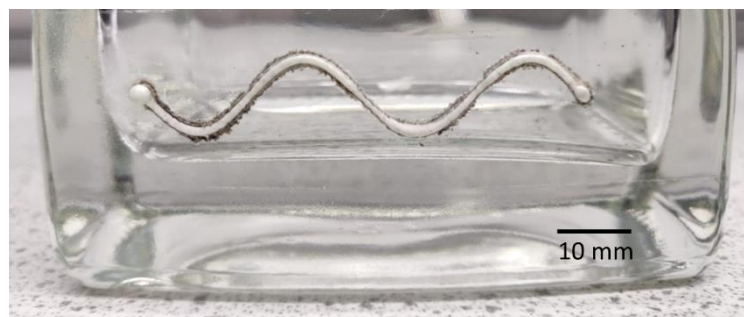


Figure 108 Curved feature design of GTS-6 successfully processed onto a glass bottle substrate at 9.68 J/mm^2 by powder fed DED.

During glass bottle processing, the black paint coating on the inside surface of the bottle absorbed laser irradiation, and melted/vaporized (gas fumes were produced, and liquid paint pooled inside). This suggests that the paint acted as an energy sink, and likely aided the glass processing by the exothermic release of heat, increasing the absorptivity of glass feedstock at the substrate surface by conduction. An area of reduced deposit dimension was observed particularly in areas where travel was positive in the y direction. A possible explanation for this is the direction of stage movement in relation to lateral powder delivery causing variation in powder capture rate. Also, slight misalignments of the powder nozzle and laser spot could favour a particular travel direction. Another possible explanation is variation in powder feed consistency, but this is unlikely as it was repeatedly observed in the same location when processing this design.

6.6.4.3 Straight Features

On 1 mm substrates, the straight features design was expected to cause cracking and fracture due to thermal stresses. On these thin substrates, the straight features design (much like the curved features design) covered a larger area on the substrate than a single track. The straight features design also incorporated sharp alterations in geometry (at the peaks of the design), causing high stress concentrations, therefore making thermal cracking more likely. Results showed the successful consolidation of glass feedstock and deposition on 1 mm substrates at a range of parameters, although cracking was evident on these thin substrates (Figure 109).

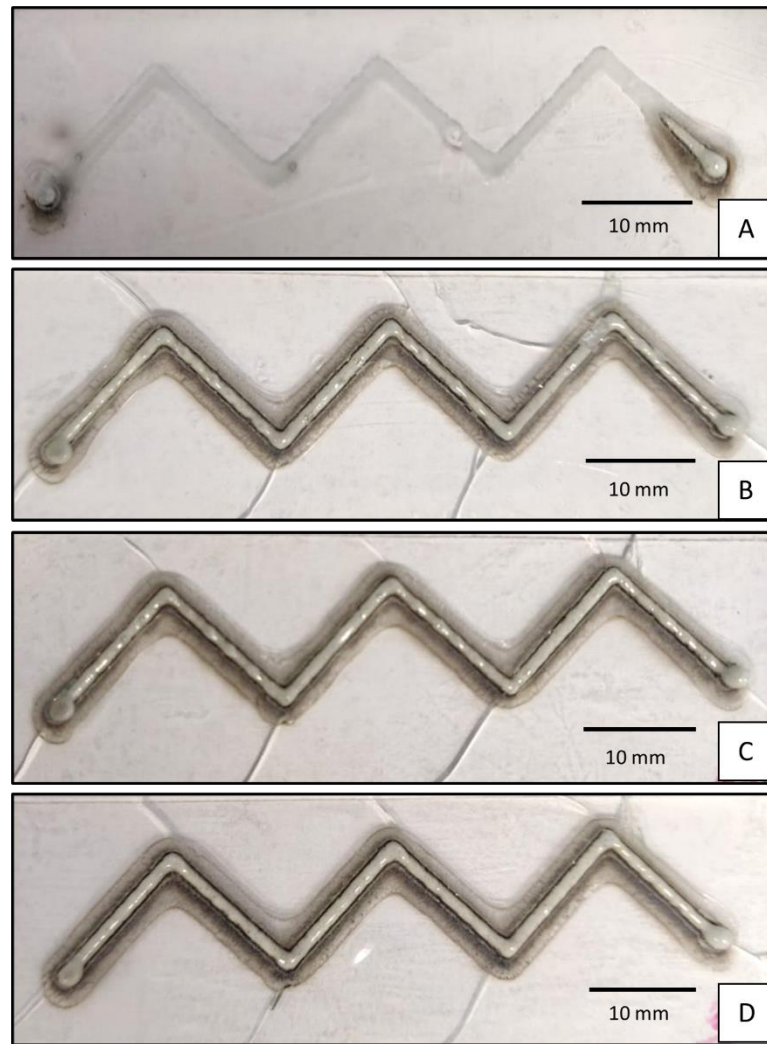


Figure 109 GTS-6 glass processed onto 1 mm glass substrates using the straight features design at different energy densities A: 10.12 J/mm², B: 12.0 J/mm², C: 12.6 J/mm², D: 13.2 J/mm².

At the lowest energy density (10.12 J/mm²), glass was not melted and deposited consistently onto the glass substrate, suggesting there was insufficient energy to successfully process the glass feedstock. A small area of consolidation and deposition can be seen on the right-hand side of 29 A, as this is where the laser dwell time is accounted for in processing (scan speed =0), therefore this small area is not representative of the process parameters tested.

At increasing energy density, (12.0-13.2 J/mm²) glass feedstock was melted and deposited onto the substrate to produce the straight features design. Cracking was seen for all of these parameter combinations, initiating from areas of directional change/geometric alteration as expected, and propagating to the edges of the substrates. Areas of inconsistent powder deposition can be seen in certain areas, such as on positive travel in y, characterised by variation in deposit height. This is likely caused by slight variation in the angle of the powder nozzle in relation to the laser focus, causing a difference in the processing dependent on

direction of travel. This could also be caused by inconsistent powder delivery during processing.

When GTS-6 powder was processed on 4 mm plates in the straight features design, an energy density of 12.6 J/mm^2 was selected. This energy density was chosen as it produced well defined, consistent tracks on 1 mm substrates, with no observed increase in substrate cracking from lower energy densities. A consistent deposit of consolidated glass in the straight features geometry was successfully processed, with the absence of thermal cracking (Figure 110). The thicker substrate resisted thermal shock that was seen on 1 mm substrates with the same energy density. Furthermore, this structure was built on the same 4 mm substrate that the curved features design was processed on.

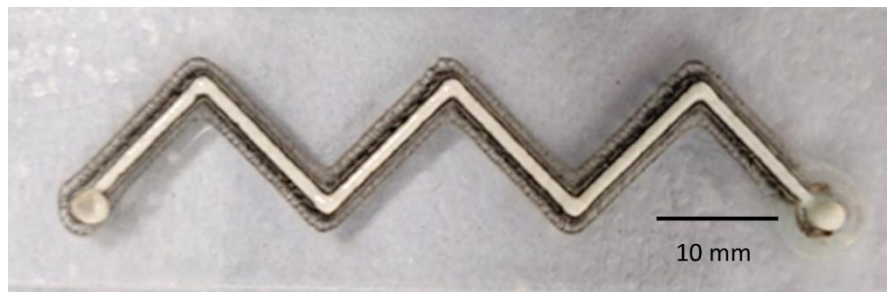


Figure 110 GTS-6 feedstock processed onto a 4 mm glass substrate using the straight features design, at 12.6 J/mm^2 .

Processing of the straight features design onto a bottle substrate was carried out at 13.2 J/mm^2 , as a higher energy density was expected to be tolerated on thicker substrates. Processing of the design was mostly successful, and did not appear to suffer from thermal cracking (Figure 111).

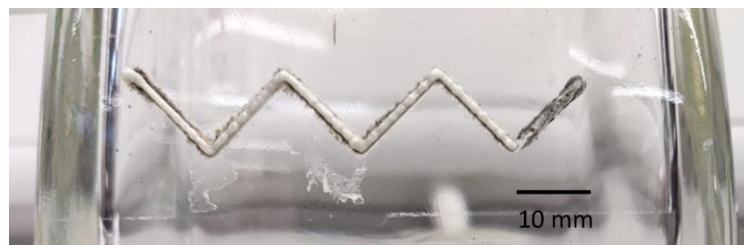


Figure 111 GTS-6 Glass processed by the straight features design onto a bottle substrate. Energy density = 13.2 J/mm^2 .

Areas of inconsistent dimension were observed. Possible explanations are inconsistent powder feed and misalignment of the powder nozzle with the laser focus. The latter is a more likely explanation, especially when considered alongside the bottle substrate shape, as the processing surface was not completely flat and had a slight convex shape, which may have further exacerbated the effect of misalignment. Another observation made is seen on the right-hand side of Figure 111, where the glass has not adhered to the bottle surface. Instead, the inside surface of the bottle has absorbed the laser energy, and etched along the scan track. The top surface of the glass remains un-affected. For this effect, it is possible that powder feed delivery was inconsistent, and for this area of the scan track, insufficient feedstock was delivered to the laser. The black paint coating the inside surface of the bottle absorbed the laser energy, with excess energy causing this etching/micro-cracking on the inside surface of the glass bottle.

6.6.4.4 Combined Features/Text Design

The combined features design incorporated both curves and straight lines to process a text structure "3DGLASS". This design featured more geometric complexity than the other designs investigated and therefore the most stress concentrations.

1 mm substrates cracked during processing at every investigated combination of parameters for the text design, as expected. Despite this, due to the low cost and good availability of microscope slides, these were used to optimise the GCode and parameters for consistent deposition of each design feature, before processing on thicker substrates.

During processing of the text features, laser power was kept constant at 100 W, and scan speed was varied depending on the feature. Parameters were altered iteratively to achieve a consistent deposition of the combined features geometry. Scan speed was increased to max travel speed (100 mm/s) to inhibit deposition of glass between features where deposition was not required. Pauses of 0.5-0.7 s were incorporated into the GCode at the beginning of the structure and immediately after maximum travel speed to allow for laser dwell and successful processing of features. Scan speeds between 450-650 mm/min were used, with slower scan speeds utilised for straight features, and faster scan speeds for curved features. Energy densities used during processing were therefore between 9.2 and 13.3 J/mm². The complete geometry was processed at these parameters on 1 mm substrates with consistent deposition (Figure 112).



Figure 112 GTS-6 processed on 1 mm substrates by the combined features (text) design at 100 W and scan speeds between 450-650 mm/min.

Processing of the structure on a 4 mm plate allowed successful deposition of each geometry feature, without substrate fracture (Figure 113). The larger dimension of the 4 mm thick substrate (100 x 100 mm) allowed processing to take place further away from more fragile edges, reducing the likelihood of cracking. Surrounding tape was removed with acetone, however a black residue (carbon) was left surrounding the deposited glass.



Figure 113 Text features processed on a 4 mm substrate between 9.2-13.3 J/mm².

6.7 Discussion and Conclusions for DED Investigations of Glass Processing

6.7.1 Experimental Results

Process parameter investigation revealed two significant correlations. Firstly, a sufficient energy density was required to raise the temperature of glass feedstocks, increasing absorption, and allowing glass melting to occur. Energy densities below 11 J/mm^2 often resulted in inconsistent consolidation of glass powder and thus unsuccessful glass processing. Secondly, on the other end of the spectrum, substrate cracking was observed to occur only above a laser power of 115 W. This cracking is possibly related to the volume of molten glass deposited and the substrate thickness. As the laser power (energy) increased, the mass of molten material deposited onto the substrate increased, which in turn increased the magnitude of transient thermal strains generated due to differential shrinkage as the molten glass deposit solidified and cooled. Above a certain laser power, the amount of material solidified, and hence level of thermal strain generated in the substrate, reached a critical value required to cause cracking in the substrate. However, the explanation for cracking seeming to be related to laser power and not energy density is still unclear, and further work is necessary to fully characterise this relationship.

To reduce the likelihood of substrate cracking a number of potential measures could be employed. A thicker substrate would reduce the strain, and indeed it is shown elsewhere in this work that increasing substrate thickness reduces the likelihood of cracking for a particular set of processing conditions. Literature has suggested that other glass compositions with a lower coefficient of thermal expansion, such as fused quartz (CTE = $0.5 \times 10^{-6}/^{\circ}\text{C}$), would be more resistant to thermal shock during DED processing^{160,161}. Investigations into DED processing of fused quartz glass powder on glass substrates of the same composition may show a reduced likelihood of cracking from thermal shock. Other potential measures include reducing transient thermal gradients, e.g., by substrate heating, or by reducing stress concentrations, e.g., by changing the geometry of the deposit, again the effectiveness of these measures are demonstrated elsewhere in this work.

These two relationships were taken into consideration when selecting laser power and scan speed parameters for effective glass powder DED processing. While energy density was used to represent combinations of laser power and scan speed, the independent effect of each must be considered. The most successful combination of parameters for processing a single

track of soda lime silica (GTS-6) glass onto 1 mm substrates was found to be between 11.5 - 12.5 J/mm², with laser powers below 115 W. The parameters differ significantly from those reported by Luo et al., which had a calculated energy density of 160 J/mm² for melting of soda lime silica filaments by DED processing¹⁵⁶.

Processing onto thicker glass substrates (4 mm and bottles substrates), and processing of more complex geometrical designs was successful to varying degrees. When processing curved and straight features, a significant difference was observed in the required energy density for successful processing. This is explained by the acceleration and deceleration of the motors in the translational stage required for sharp changes in direction. Curved features required less acceleration/deceleration of the stage motors compared to the straight features design, which incorporated more severe changes in travel direction. This is why a higher energy density was required for successful processing of the straight features design (12.0 J/mm²), than for curved features (9.24 J/mm²). A geometry designed with both straight features and curved features (ie text design) required fine tuning of scan speed to achieve successful processing of each feature. The complex designs cracked 1 mm microscope slides but were successfully processed onto thicker substrates.

Thicker substrates tolerated higher energy density processing compared to 1 mm thick microscope slide substrates, as expected. This allowed processing of multiple geometry designs on the same substrate, without fracture. Processing onto bottle substrates was achieved by applying a coat of matt-black paint to the inside surface of the bottle.

Substrate heating was utilised in literature for the purpose of reducing thermal stresses in parts and substrates, with soda lime silica and borosilicate filaments processed on substrates heated to 530°C, and 450°C respectively^{156,158}. The addition of a heated stage showed potential for decreasing thermal stresses when processing glass on glass by DED but requires further investigation. The necessity of a cellophane tape layer for DED processing limited substrate heating due to the lower melting temperature of the tape. In order to achieve high temperature substrate heating, an adhesive tape with a higher melting temperature may prove useful. Processing of multiple layers was considered. Glass was successfully deposited onto previously processed layers, increasing the deposit thickness. Unfortunately, substrate cracking (of 1 mm substrates) was unavoidable in these investigations. With further optimisation of process parameters and set up, multi-layer processing could be achieved.

6.7.2 DED Set-Up and System

Various adaptations were made to the DED system over the course of the experimental investigation, allowing for more efficient and effective processing of glass powder by this method. Powder feed nozzles made of copper suffered from the effects of electrostatic interaction with glass powders, causing material build up inside the nozzle, and thus impeded powder delivery. It was therefore not possible to use the copper coaxial nozzle in conjunction with glass powders, limiting powder delivery to the copper side nozzle. The introduction of a Teflon powder feed hose helped to alleviate this problem allowing for more consistent powder delivery, however, the lateral nozzle was subject to potential alignment errors and also limited processing to single layer structures as expected from literature¹⁵. It is expected that further development of equipment and methods could overcome these issues.

The CNC stage was upgraded to allow greater automated control of design geometry and scan speed through the Zaber translation stage and software; however this suffered some limitations. Translation of GCode carried out by the Zaber software required simplified GCode, meaning that GCode generated from 3D CAD software had to be carefully edited to ensure processing would be accurate and successful.

The modular DED set-up lacked the automation required for reliable processing, meaning the potential for errors with timing and coordination of laser processing, powder feed, and stage movement was significant and difficult to account for in the results. Independent control of translation stage, laser operation, and powder feed caused inconsistencies during processing. Furthermore, laser beam profiling was carried out three years prior to this research, measuring the power loss of the 600 μm laser fibre as 10.5% (see appendix). Without relevant data for measured power loss this must be estimated from previous beam profiling.

The DED system used during these investigations lacked some of the sophistication of other commercially available DED systems. For example, some commercial DED systems can achieve an inert atmosphere, as opposed to the rudimentary Argon bag utilised in this investigation, to provide shielding and containment of powder. Many commercial systems allow integrated and automatic control of laser, stage (often with rotational capability), and powder feed²³³. With this capability, investigations of glass powder processing by DED would be more accurate, avoiding the potential errors associated with manual coordination of laser, stage, and feedstock delivery. The results of these investigations provide insight into the

system requirements for processing glass by DED, despite the challenges and limitations discussed.

6.7.3 Conclusions

The outcomes of these investigations into DED processing of glass powder include:

- Feasibility studies proved that glass powders could be melted by DED laser irradiation with careful consideration of process set-up including powder delivery and the substrates and baseplates used.
- Soda lime silica glass powder was successfully deposited onto glass substrates of the same composition, with various geometric designs demonstrated.
- The effects of laser processing parameters, substrate properties, and powder feed parameters on glass processing were reported.
- Ideal experimental conditions were found for processing GTS-6 glass feedstock. An automatic powder feed via Teflon side nozzle (with a powder wheel speed of 2 rpm), darkened baseplates beneath glass substrates, and a cellophane tape layer to aid laser absorption were found to be essential for glass processing.
- A processing window for soda lime silica glass (single tracks on 1 mm substrates) was identified: energy density above 11 J/mm² to achieve glass melting, and below 115 W laser power to avoid substrate fracture.
- Processing of glass on bottle substrates without cracking was demonstrated, showing potential for application of glass packaging décor by DED.

The findings described in this chapter outline the potential for processing glass powder by this method, and with further optimisation could be used for applying customisable container décor for high value glass packaging in industry.

Chapter 7

General Discussion and Conclusions

7.1 Introduction

The overall aim of this work was to assess the feasibility of processing glass powders by SLM and DED. These two AM methods were selected as laser processing provides high energy densities suited for processing high temperature materials. The literature presented some promising preliminary studies into SLM processing of glass but mostly demonstrated rudimentary geometries and was limited to a few compositions of glass. Initial results for processing glass filaments by DED have been described, but until now, processing of glass powder by DED, which could offer greater geometric freedom and resolution, has not been reported.

Various factors affecting glass processing by DED and SLM were explored. In particular, the influence of machine set-ups and processing parameters for achieving consolidation of glass powder were investigated, with a focus on processing structures on glass substrates. As the field of glass processing by AM is still emerging, assessment of glass powder processing by the two different techniques was worthwhile. DED and SLM lend themselves to different applications, for example, DED is useful for processing on large or irregular substrates, while SLM offers fine control over processing parameters and is capable of greater geometric complexity. As the two techniques shared common features, such as material consolidation by laser irradiation, and processing of powder feedstocks, SLM and DED were equally explored.

7.2 Evaluation of Glass Processing by SLM

The novelty of glass processing by SLM in this work is characterised by parameter investigations for on-glass processing. Initial work identified processing windows for soda lime silica glass on alumina substrates, fabricating structures with complex geometries. Further refinement of processing windows to allow on-glass processing was carried out with the aim of achieving accurate glass structures on 1 mm glass substrates, whilst avoiding cracking from thermal shock. A process map was generated for glass-on-glass processing of soda lime silica, taking substrate cracking and adhesion into account. Building on the work by Fateri and Gebhardt¹³², who observed the effect of scan strategy on SLM of glass squares, this work considered the effect of scan rotation on glass processing for non-cubic structures, showing an effect on the dimensional accuracy of parts. 90° rotation of scan direction between layers resulted in distorted geometry, focussing energy density in the x and y axes, whereas a 67° rotation showed a more even melting of glass feedstocks.

A delay between layer processing was also found to be beneficial for processing glass powder feedstocks, as described in literature for other materials processed by laser powder bed fusion (LPBF)^{125,126,234}. This delay allowed dissipation of heat in processed parts before spreading of subsequent powder layers, preventing distortion of geometries in the build direction and reducing the risk of delamination as a consequence. Mohr et al. reported a short inter-layer time (layer delay) increased the melt pool depth over the build height by up to 20% during LPBF of 316L stainless steel¹²⁶. This phenomenon is comparable to the observations of balling and brightly glowing glass powder beds during SLM of glass when processed with a short inter-layer time. A reduction in hardness of up to 20%, an increase in porosity, and increase in grain size was also reported for a short inter-layer time. Further characterisation of glass parts with regards to these findings is required for full evaluation of the benefits of a layer delay. Literature suggests that the effect of a layer delay is dependent on the material used, with some materials benefiting from a longer delay during AM than others²³⁴. The results of these investigations into glass powder processing by SLM suggests that layer delay is an important factor to consider, with further characterisation of a suitable layer delay for different compositions of glass recommended for future work.

Energy density was used to assess the effect of laser processing parameters on glass processing (particularly on glass substrates). This was an effective way of relating these parameters and assigning a single value to each combination of parameters for the glass samples produced for process maps. While energy density helped to visualise the total

energy absorbed by each sample, the results suggested that laser power and scan speed had an independent effect on glass processing, as samples showed differences despite having the same calculated energy density. This was also the case for DED processing. Additionally, the geometric design of parts, or the volume of parts on the build platform, resulted in different energy density requirements, and as such needed to be accommodated for by alteration of hatch spacing, scan speed, or laser power. The reliability of energy density as a design parameter for AM processing has also been criticised in literature, with certain publications reporting limitations to energy density calculations for AM processing^{168,235}. The findings of this work generally agree with the consensus in literature that energy density is not an accurate description of the SLM process, and that these calculations should only be used as guidelines and estimations of energy density for different combinations of process parameters.

One significant factor highlighted during this study, was the porosity and opaque appearance of SLM glass structures when processed within the parameter windows described. Transparency of glass parts was generally not achieved in other research describing glass processing by LPBF^{87,88,92,94,130–132}. These factors raise the question of glass consolidation, and if complete melting occurs during processing at these energy densities. When compared to the appearance of structures processed at higher energy densities (with the consequence of balling), and at higher substrate temperatures, structures were less glassy in appearance. It is speculated that SLM of glass at the recommended parameters (without substrate heating) consolidated glass powder via sintering rather than melting. While the recommended parameters allowed formation of 3D glass structures, parts could be brittle and porous, limiting their applications. For example, leak tight performance as glass CFRs is unlikely without consolidating glass feedstocks by complete melting (e.g., with the utilisation of a high temperature substrate heater).

High temperature substrate heating explored in this research showed promise for fully melting glass powder, without distortion of geometry due to the high surface tension of glass. Only single layer structures were processed due to machine restrictions, and further work is needed to evaluate the full potential of processing glass by SLM at high substrate/chamber temperatures.

Investigation into SLM of different glass compositions was of interest in this study; however, the low flowability of custom glass powders with irregular morphologies limited the progress of these experiments. Spheroidisation by flame and plasma was considered to improve the

flowability of these powders to allow processing by SLM. This case study demonstrated the potential to improve the flowability of glass powders by these processes, however, further work is needed to evaluate SLM processing of these bespoke compositions.

Ultimately, this work presents a process map for processing of soda lime silica glass powder onto glass substrates of the same composition, whilst avoiding cracking from thermal shock. Recommendations are made for processing set-ups, including darkening of base plates to reduce reflection, consideration of substrate temperatures and consideration of feedstock properties. Additionally, suitable processing parameters (laser power, scan speed, hatch spacing, and scan strategies) are suggested.

7.3 Evaluation of Glass Processing by Powder-Fed DED

Soda lime silica glass powder was successfully processed by DED using a lateral powder nozzle. The research described in this work presents novel processing of glass powder by DED, so challenges associated with powder delivery had to be overcome. This involved characterisation of glass powder feedstocks and investigations into delivery of glass powder to find suitable parameters for consistent delivery. There are many powder delivery methods used for DED processing, with several variables described by Singh et al. The experimental set-up used in these investigations was limited to the nozzles and powder feed methods described, with certain drawbacks highlighted in literature. For example, delivery of powder via carrier gas is known to be sensitive to particle velocity, with high velocity resulting in decreased powder capture, and powder particles adhering to the nozzle surface after rebounding on the substrate surface¹⁵⁰. This was observed during processing of glass powders. Powder wheel speed (RPM) and carrier gas pressure (L/min) were varied to find suitable parameters for delivery of glass powder, and the nozzle material was modified to prevent interaction with glass powder by using a 2 mm Teflon tube to line the copper nozzle. The same modification could not be applied to the coaxial nozzle, which suffered from similar limitations due to the low flowability of feedstocks.

Another limitation that was found common in literature is the use of lateral nozzles for powder delivery. Powder capture rate was reportedly less efficient for lateral nozzles compared to coaxial nozzles²³⁶, and the scanning direction had an impact on powder capture and surface finish²³⁷. The lateral nozzle was selected due to the ease of set up and compatibility with the available glass feedstocks (glass powders flowed easily through the lateral nozzle), however, alignment with the substrate and laser beam was carried out manually, so accuracy and reliability between machine set-ups was compromised¹⁵⁴. The lateral nozzle allowed easy analysis of the feasibility of glass powder processing, however, a coaxial nozzle would have been preferable for multi-layer processing¹⁵.

The success of glass processing was sensitive to multiple factors, including the delivery of powder, the laser focal length, and the process parameters (laser power and scan speed). A process map was created assessing the effect of laser power and scan speed on processing a single track of soda lime silica on a microscope slide (Section 6.5.3). Cracking of substrates was used as a key indication of excessive energy density. Instances where substrates cracked were classified as unsuitable. There are other factors to consider that could have contributed to the initiation and propagation of cracking within substrates. Firstly, the delay between

laser initiation and powder melting at the start of a track was variable. This delay was attributed to laser dwell time, and the time taken for sufficient powder capture within the laser beam to initiate melting. During the delay, glass substrates were stationary and subjected to laser power in the absence of feedstock deposition; absorption of laser energy prior to feedstock consolidation and deposition could have caused changes within the thermal profile of the substrates. This could have led to absorption of excess energy density above what was calculated during processing, causing cracking, and therefore misrepresenting certain combinations of parameters. Similarly, variations in the powder feed rate could have caused inconsistencies in powder capture, resulting in excess laser power absorption by the glass substrates, increasing thermal shock. Additionally, as a cellophane tape layer was applied manually to the substrate surface, variations in the tape layer could have caused an effect on processing. Finally, any defects within the 1 mm glass microscope slides could have facilitated cracking from thermal shock. Repeat tests for each combination of parameters was carried out to account for these factors. The process map indicates the suitable process parameters found during these experiments, presenting the first parameter recommendations for glass powder DED processing.

Geometric designs for DED investigations required multiple steps to generate a simplified GCode that was recognisable by the stage software. The GCode controlled translational stage movement by x and y coordinates, but did not instruct laser control or material feed rate. The lack of integrated control of the different modules restricted automation and increased the risk of human error. Glass processing was affected by the designed geometry – depending on whether scan tracks were straight or curved. This is due to the associated movements of the stage, the direction of travel, and the alignment of the feed nozzle. For straight features, stage movement was unidirectional in one axis, whereas for curved features, stage motion required simultaneous movement in both x and y axes, with directional changes. The increased acceleration and deceleration of motors required for curved features is speculated to have an effect on scan speed and therefore energy density. For this reason, a reduction in scan speed is recommended to compensate for the reduced energy density of curved features, and the potential reductions in powder capture rate from directional changes. For geometries combining straight and curved features for a single build, laser power was kept constant and scan speed was altered accordingly. Different geometries were built in single layers on glass substrates of different thickness. As expected, cracking was reduced in thicker glass substrates, and glass bottles were able to be used as substrates when inside surfaces

were coated in removable black paint. This work ultimately demonstrates the potential for imparting décor onto glass packaging by powder-fed DED.

7.4 SLM vs DED for Glass Processing

Comparison of DED and SLM as techniques for glass processing was not the overall aim of this research; however, evaluation of the challenges and limitations faced during this research allows some technical comparisons to be made. Specification wise, the DED set-up boasted a higher power laser (2 kW) than the laser equipped in the Realiser SLM-50 (100 W). Laser power limits the achievable energy density during processing, therefore glass compositions and their melting temperatures should be considered when selecting the technique. Other commercial SLM systems are capable of higher laser powers and may therefore be suitable for glass compositions with higher melting temperatures than tested in this work. Consideration of base plates and substrates was essential to both processing techniques. As transparent glass substrates were used for processing glass structures onto, base plate modification was necessary to improve laser absorption at the substrate surface by reducing reflection and acting as a heat source. For SLM, glass substrates had to be reduced in size to be accommodated on the SLM build platform. For DED, glass substrates of varying size and form, from microscope slides to large bottles, could be accommodated on the build platform.

Both SLM and DED showed sensitivity to feedstock properties, which are therefore necessary to consider when selecting a laser processing method. For powder-fed DED, nozzle selection was limited due to the flowability (and cohesion) of the glass powder material. The feedstock used in these experiments only achieved suitable and consistent delivery through a lateral nozzle, with inter-particle cohesion preventing delivery by coaxial nozzle. For single layer processing, the performance of a side nozzle was sufficient, however, a coaxial nozzle offers certain benefits over side nozzle feeding, particularly for multi-layer processing. With this in mind, processing 3D glass structures on glass substrates by DED is likely to require a well flowing glass powder feedstock that is compatible with a coaxial nozzle. To achieve this, a spherical glass powder with a smaller particle size range than used in this study is recommended, and nozzle material should be considered to prevent electro-static interaction between the feedstock and nozzle.

While SLM was also sensitive to the flowability of glass powder feedstocks, a homogenous powder bed was easily achieved with each of the spherical powders used¹¹⁷. Particle size distribution affected the layer height and therefore overall resolution of parts, but feedstocks with various particle size ranges flowed sufficiently for powder bed formation. Fine glass powder feedstock was used to give satisfactory resolution but did demonstrate lower

flowability than larger average particle size feedstocks. This is a common trade-off in SLM processing¹¹⁵. Glass powders with angular or irregular morphologies were unable to form homogenous single layers within a powder bed due to the low flowability. SLM of various glass powder feedstocks can be easily optimised for processing, as long as the feedstock has sufficient flowability.

While the processing of soda lime silica powder was successfully achieved by both SLM and DED techniques, delivery of glass via nozzle systems introduced additional challenges during DED processing. Powder-fed DED required optimisation of feed parameters to achieve a consistent delivery of glass to substrate, whereas the wiper system utilised in SLM allowed convenient and consistent delivery of powder bed layers. Nozzle alignment was important for delivering a powder flow to a precise location, and this was subject to human error. Powder feed parameters had an impact on powder delivery, including wheel speed (RPM) and carrier gas pressure (L/min). Additional steps were required to investigate suitable powder feed parameters for each glass feedstock used.

The resulting glass structures achieved by SLM and DED were significantly different. SLM produced opaque and porous structures when processed within the recommended process window, while DED produced melted glass structures with a level of transparency. The differences in appearance could be caused by the different glass melting/consolidation mechanisms of the two techniques. When processing onto glass substrates, glass melted by DED resulted in strong adhesion to substrates, whereas SLM structures were easily removed. This is because in SLM the glass powder was processed in discontinuous tracks on the glass substrate, while in DED glass powder was processed continuously by laser irradiation. For this reason, DED may be considered superior for applications requiring strong adhesion of glass powder to glass substrates, such as for glass packaging décor, and SLM may be considered superior for applications requiring individual parts designed with removal from substrates in mind.

For the experimental set-ups described in this work, glass powder was easily accommodated by the Realizer SLM-50, whereas the modular nature of the powder DED set-up required consideration of nozzle attachments, delivery and containment of powder, and alignment of all parts. Conversely, incorporation of substrate heaters was difficult to achieve in the confines of the Realizer-SLM 50, whereas the DED set-up was less restricted in terms of space, and therefore allowed easier access to install extra modules (such as a substrate heater).

One attractive trait of SLM is the recyclability of unused powder. In SLM, glass powder was selectively fused along scan tracks, building parts within a powder bed. On removal of parts, remaining glass powder could be recycled by simply sieving the material. For many materials, the effect of repeated recycling and SLM processing of feedstocks has been reported, such as increased particle size distribution, altered particle morphology, and altered flowability^{185,238}. Work has not yet shown the effect of recycling glass powders for SLM. Future investigations are recommended to assess changes to SLM of glass feedstocks as a result of recycling. For DED, feedstock powder travelled through various tubes and nozzles during delivery to the substrate. Capture rate was less than 100%, and therefore excess glass powder remained unfused despite being delivered to the build area. While unfused glass powder was contained within the argon bag surrounding the build platform, recycling was not recommended due to the potential for contamination during delivery, as well as during processing due to the vaporisation of organic cellophane tape. In this regard, SLM wasted less feedstock material than powder-fed DED processing.

Geometric complexity was demonstrated during SLM of glass feedstocks. For DED, only single layer structures were formed, with complexity in 2D but not 3D demonstrated. The degree of complexity achievable in SLM is in part due to the discontinuous laser processing allowed by the automatic control of laser scanning, rapidly turning the laser on and off as directed by CAD data. Lattices and channels could be easily formed thanks to this. In this work, DED processing was directed by GCode, without integrated control of the laser. The laser was manually switched on at the beginning of the process, and switched off at the end of the GCode (stage movement). Discontinuous processing was achieved with limited success by altering stage speed to inhibit glass melting. The lack of integrated laser control with CAD data prevented high degrees of complexity for DED parts. For the set-ups described in this work, SLM processing allowed greater geometric freedom than DED, however this may not apply to more sophisticated/commercial DED set-ups that use integrated systems.

In summary, when comparing the two AM techniques for glass processing, this work presents SLM as more capable for forming complex geometries of high resolution, while DED presented benefits for processing on a variety of glass substrates with potential to achieve fully melted structures and possibly transparency. Experimental set-ups play a large role in assessing the suitability of glass processing, and this work compares a commercially available SLM system with a modular DED laser set-up. While the DED system lent itself to easy modification, it is not representative of the capabilities of other DED systems.

7.5 Energy Density as a Measurement for SLM and DED

Energy density was used to represent the absorption of laser energy by glass feedstocks for both SLM and DED investigations. The purpose of energy density calculations was to combine two or more processing parameters into one value, in order to represent different combinations of parameters and make comparisons. Process maps were generated using these calculated values, however, making assessments of the effect of parameters based on energy density suffers certain limitations.

For DED, the energy density calculations considered only two varying factors: laser power and scan speed. As described in 2.6, layer thickness was defined as 1 mm for DED experimental tests. This simplified energy density calculation allowed easy observation of the effects of these parameters on DED glass samples. For SLM, two energy density calculations were used, one for “2D” representations, where laser power, scan speed, and layer thickness were considered, and one for “3D” representations, which also accounted for hatch spacing. General trends were identified based on calculated energy density and observations made during DED and SLM, with resulting process maps offering guidelines for suitable processing parameters.

The benefits of using energy density to analyse glass processing by SLM and DED stop there. For laser processing of glass, there are many additional factors that are not taken into consideration for energy density calculations, such as temperature, laser spot size, and time; these can all influence the energy absorption of powder feedstocks. The limitations of using energy density to define processing windows were described in literature and encountered in this work^{168,235}. When mapping the effect of laser power and scan speed on DED processing, general trends were found, however, there were multiple cases that deviated from the trend, or appeared anomalous. For example, high laser power often resulted in substrate cracking regardless of calculated energy density. For combinations of parameters that shared the same calculated energy density, assumptions could be made that resulting observations would be equivalent, however, this was not always the case. Laser power and scan speed appeared to have independent effects on glass processing by DED, indicating that other factors play a significant role in glass laser melting.

For SLM, the energy density calculations for “3D” representations of multi-layer glass processing are potentially flawed. While laser power, scan speed, hatch spacing, and layer thickness are all taken into account for these energy density calculations, the overall 3D dimensions are not considered. This calculation fails to account for build height, and arguably

only describes the energy density per layer. As glass parts are built, residual energy within previous layers undoubtedly affects the absorption of laser energy by subsequent powder layers. The absence of time and temperature considerations in the energy density calculations arguably leads to an inaccurate representation of the overall energy requirements for glass processing.

While energy density has been used throughout these investigations to assess SLM and DED of glass, this method does not provide a complete picture of laser processing of glass. The parameters stated for processing windows should be considered independently to the calculated energy density, and additional factors acknowledged. These figures should be used as an indication of energy requirements for glass processing, while understanding the limitations. A more comprehensive approach to assessing energy density during laser processing is required for an accurate representation of AM systems and glass absorption of laser energy. Until a suitable alternative is proposed, energy density offers a simple method for estimating energy absorption in SLM and DED.

7.6 Conclusions

In this work, glass material was processed by SLM and powder fed DED. Section 4.6 reported the results of feedstock investigations, Section 5.8 discussed the results of SLM investigations, and Section 6.6 discussed the results of DED investigations. The following conclusions for this research were made:

- Glass powders were characterised for AM processing, with flowability highlighted as a key factor for successful processing by SLM and powder-fed DED.
- A case study was carried out to assess the feasibility of spheroidising custom glass compositions for improved powder flowability. Flame and plasma spheroidisation showed promising results for morphology modifications, however a similar improvement in flowability may be achieved by reducing the particle size distribution through sieving.
- The feasibility of processing glass powder by DED was proven, achieving melting and consolidation of soda lime silica glass feedstock.
- Powder-fed DED was demonstrated for glass décor applications, imparting single layer structures onto glass bottles without causing thermal shock.
- Process parameter investigations for DED of soda lime silica identified a suitable processing window where energy density was greater than 11 J/mm^2 and laser power was below 115 W.
- Soda lime silica glass was successfully processed onto substrates of the same composition, without fracturing from thermal shock.
- A processing window for SLM of glass (on ceramic substrates) was identified as 80-110 J/mm^3 , while glass-on-glass SLM generally showed most success above 76 J/mm^3 .
- Modifications were made to the Realizer SLM-50 to incorporate a high temperature substrate heater, with investigations showing promising initial results for glass processing at high temperatures.
- Energy density was used to relate different parameters (particularly laser power and scan speed) for populating process maps for SLM and DED of glass, however these parameters appeared to have independent effects on glass processing.

The results of this work further inform glass processing by laser AM techniques. Processing windows have been presented for SLM and DED of soda lime silica glass powders providing guidance for future parameter investigations. This work demonstrates the potential for glass processing by DED and SLM, as well as the challenges and limitations, and suggests certain applications that may interest research and industry. With further work, these AM

technologies could become reliable methods for manufacturing customised glass products in a one-step process.

Chapter 8

Recommendations for Future Work

The recommendations for future work are made based on experimental investigations described in this thesis. In general, this work contributes insight into glass processing by SLM, particularly on substrates of the same composition, and has described novel processing of glass powder by DED. The results of this work provide a good foundation for further work, with processing set-ups and processing windows reported for successful processing of soda lime silica glass feedstocks onto glass substrates. Recommendations for future work are made to help establish SLM and DED as valid methods for processing glass powder feedstocks for various applications.

8.1 Recommendations for SLM of Glass

This work described the experimental set-ups and process parameters for processing soda lime silica glass beads by SLM. Ideal processing parameters have been suggested, including assessments of laser power, scan speed, hatch spacing, and scan strategy. There is still scope to further characterise the effects of SLM parameters on glass processing. Recommendations for future work includes thorough investigation into different scan strategies, as well as any optimal layer delays or energy density gradients to allow dissipation of residual heat between layers. As optimal parameters differ for varying geometries, further investigation is required to quantify the different parameter requirements by geometry. This work suggests suitable processing parameters that serve as a good foundation for glass processing by SLM, however future work will help to provide a more complete picture for optimal glass processing.

Many of the demonstrated SLM glass parts were opaque and porous. In Chapter 5 and 7, speculations into the mechanism of fusion were raised due to the difference in appearance of the parameters used for “optimal” processing, and parts processed at high substrate temperature. As these parts appeared more glassy and melted, it is possible that complete melting and consolidation of glass powder could be achieved through optimisation of parameters at high substrate temperatures. For a comprehensive investigation into SLM processing of glass at high substrate temperatures, certain machine limitations must be overcome. With the SLM hardware described in this work, space is confined to a small processing chamber, making accommodation of heating equipment challenging. Additionally, the substrate heater described reduced the possible build height, and relied on conduction of heat through insulating materials to the substrate surface. Alternative heating methods may be more effective than the substrate heater used in this work, such as infrared chamber heaters. Additionally, accurate monitoring of powder bed temperature was not achieved through the use of K-Type thermocouples, and alternative methods should be considered to improve this.

In order to achieve multi-layer processing of glass by SLM at high temperatures, the powder bed temperature must be optimised to allow effective spreading. As the powder bed temperature increased towards the glass transition temperature, particles began to consolidate by sintering, and flowability reduced, preventing the formation of a homogenous powder bed. Additionally, adaptation to spreading materials (e.g. rubber wiper blades) is necessary for automated powder spreading, avoiding the risk of melting wiper materials.

On implementation of machine recommendations, the effect of heating on glass powder SLM should be assessed by carrying out a parameter optimisation by Design of Experiments (DoE). As many of the reported parameter investigations processed at substrate temperatures $\sim 250^{\circ}\text{C}$, new process maps would need to be populated to view the effect of parameters on glass SLM at high powder bed temperatures.

For fabrication of customised GCFR structures by SLM, additional work is needed to demonstrate the potential for leak-tight flow of liquids through structures. Parts must be fabricated with ports and valves to allow fluid pressure testing. This could be achieved through incorporation of ports and valves in the CAD files prior to processing, or additional parts fixed to channel structures post-process. For the former, further optimisation of parameters for these varying geometries would be required. From analysis of glass SLM part porosity, leak-free flow of fluids is unlikely to be achieved with the presented parameters. Investigations into reducing part porosity (e.g. by processing high temperature powder beds) would be necessary to demonstrate the potential suitability of glass SLM for GCFR applications.

8.2 Recommendations for Powder-Fed DED of Glass

Power-fed DED of glass was demonstrated for single-layer structures on glass substrates. While this is appropriate for the application of décor onto glass packaging, it does not demonstrate the level of geometrical freedom promised by AM processing. Multi-layer processing was explored in brief during this work, encountering significant thermal shock as a result. Further investigations into multi-layer processing of glass materials would help to define optimal processing parameters to avoid thermal shock and could inspire future applications for 3D fabrication of glass parts by this method.

One recommendation for achieving multi-layer processing by powder-fed DED is the utilisation of a coaxial nozzle. This feedstock delivery method is more suited for 3D processing, and is likely to achieve consistent feedstock deposition regardless of scan direction when compared to a single, lateral nozzle. For glass powder processing via coaxial nozzle, feedstock flowability is a significant concern. During this work, the cohesive forces present in feedstocks characterised with a large proportion of fine particles prevented sufficient flow of powder through a coaxial nozzle and resulted in blockages within the feed system. A reduced particle size distribution, and therefore increased flowability, is recommended for use with the coaxial nozzle. Nozzle material is also worth considering, as soda lime glass feedstocks were observed to adhere to the inside and outside surfaces of copper nozzles, reducing the consistency of powder feed to substrates. Different materials may offer reduced interaction with glass feedstocks, as demonstrated with the Teflon lining of the lateral nozzle described in 8.4.

Cracking of substrates was a key factor for assessing the DED parameters for glass processing. As cracking is recognised as the result of high temperature gradients causing thermal shock, a substrate heater was considered to reduce the thermal gradients. As a layer of cellophane tape was required on the glass substrate to aid glass processing, the substrate temperature was limited by the melting temperature of the tape (~100°C). This prevented substrate heating to the glass transition temperature of soda lime silica, and therefore 100°C was considered “mild” heating. A potential reduction in crack frequency was reported during mild heating compared to processing at ambient temperatures and substrate heating is therefore of interest for future work. Higher temperature adhesive tapes are available and may provide the same beneficial effect of the cellophane tape layer to glass processing by DED, whilst allowing substrate heating at higher temperatures (avoiding the degradation of the adhesive tape layer). Process parameter investigations

would be required to define processing windows at various substrate temperatures. These investigations would help to define the effect of substrate heating on DED of glass on glass substrates and would confirm any reductions in crack frequency as a result of increased substrate temperature.

8.3 Additional Recommendations

The experimental investigations described in this work focussed on AM processing of soda lime silica glass. This material was readily available in bead form providing ideal flow characteristics for SLM and DED processing. Investigations into AM of other glass compositions is of interest, as glass properties are known to differ depending on composition. Different glass compositions were created in the interest of exploring SLM and DED processing of these materials. Two methods of spheroidisation were assessed for processing these custom angular glass materials to produce powder feedstocks with suitable flowability. However, investigation into laser processing of these glasses was beyond the scope of this work, and is yet to be explored. Providing the flowability of these glass feedstocks is sufficient for forming a powder bed in SLM, or consistent delivery by powder-fed DED, investigations into process parameters required for melting these materials is recommended.

Compositions of particular interest for SLM and DED are Fe-doped glass compositions, including soda lime silica, 13-93 bioactive glass, and borosilicate glass. As Fe dopants are expected to reduce the energy required to melt the glass (compared to the virgin composition), melting may be achieved at lower energy density, reducing thermal gradients and therefore stresses. Virgin borosilicate glass is also of interest for SLM processing to produce GCFR structures from this highly durable composition. Processing borosilicate by SLM is likely to require higher energy densities than demonstrated for soda lime silica, and a higher power laser (>100 W) is therefore recommended.

For SLM and DED, part inspection was carried out visually, either through optical microscopy, SEM, or XCT. Further characterisation is recommended to provide a comprehensive picture of achievable glass structures by these AM techniques. For SLM glass parts, flexural strength has been measured, yet there is more scope for further characterisation, for example quantifying compressive and tensile strength.

For DED glass samples, inspection by polariscope to assess thermal stresses would be of interest for glass parts/substrates processed by DED, as these showed a degree of transparency. Inspection of processed parts by polarised light would provide information on the residual stresses imparted into substrates and deposited glass, and would allow further understanding of the effect of DED laser irradiation on glass parts. Evaluation of porosity is also recommended for DED glass samples, as XCT revealed pores/gas bubbles within melted glass structures. Mechanical properties have not yet been investigated for DED glass parts.

Fabrication of stand-alone glass parts of specific dimensions would allow evaluation of flexural strength by three-point bend testing and comparison with measurements for SLM glass parts.

8.4 Summary

The work described in this thesis provides solid foundations for developing glass processing by SLM and powder-fed DED. The experimental investigations focussed on parameter optimisation for soda lime silica glass, and present recommendations for processing set-ups, processing parameters, and glass compositions of interest. The drive to improve AM processing of glass comes from various industries and research, aspiring towards customisation of glass products with a degree of geometric freedom unobtainable by traditional glass processing. Further work will help to identify the possibilities and limitations of glass processing by SLM and DED, inspiring new applications and securing these AM methods as valid glass processing techniques for industry and beyond.

References

1. Vogel W. *Structure and Crystallization of Glasses*. Oxford: Pergamon, 1971.
2. Rawson H. *Glasses and Their Applications*. CRC Press, 1991.
3. Rune Persson H. *Glass Technology*. Cheong Moon Gak Publishing co., 1983.
4. Abou Neel EA, Pickup DM, Valappil SP, et al. Bioactive functional materials: A perspective on phosphate-based glasses. *J Mater Chem* 2009; 19: 690–701.
5. Ahmed I, Collins CA, Lewis MP, et al. Processing, characterisation and biocompatibility of iron-phosphate glass fibres for tissue engineering. *Biomaterials* 2004; 25: 3223–3232.
6. *International Commission on Glass, Towards an International Year of Glass in 2022 Toward a United Nations Year of Glass 2022 Glass for a Sustainable Society*. 2020.
7. Grand View Research. *Flat Glass Market Size, Share & Trends Analysis Report By Application (Architectural, Automotive & Transportation), By Product (Tempered, Laminated, Insulated, Basic), By Region, And Segment Forecasts, 2020 - 2027*. 2020.
8. NSG. Pilkington and the Flat Glass Industry. *Glas Ind* 2010; 64.
9. Pilkington LAB. Review Lecture. The Float Glass Process. *Proc R Soc London* 1969; 314: 1–25.
10. McGee W, Newell C, Willette A. Glass cast: A reconfigurable tooling system for free-form glass manufacturing. In: *ACADIA 2012 - Synthetic Digital Ecologies: Proceedings of the 32nd Annual Conference of the Association for Computer Aided Design in Architecture*. 2012, pp. 287–294.
11. Thompson K. The Corning Museum of Glass Partners on Glass Competition Show Blown Away [Internet]. Behind the Glass. 2021 [cited 2021 Mar 23]; Available from: <https://blog.cmog.org/2019/02/13/the-corning-museum-of-glass-partners-on-glass-competition-show-b>.
12. The Float Process [Internet]. Pilkington.com. 2021 [cited 2021 Mar 23]; Available from: <https://www.pilkington.com/en/us/architects-page/glass-information/the-float-process>.
13. Atzeni E, Salmi A. Economics of additive manufacturing for end-usable metal parts. *Int J Adv Manuf Technol* 2012; 62: 1147–1155.
14. Atzeni E, Iuliano L, Minetola P, et al. Redesign and cost estimation of rapid manufactured plastic parts. *Rapid Prototyp J* 2010; 16: 308–317.
15. Gibson I, Rosen D, Stucker B. *Additive Manufacturing Technologies*. Second. New York, NY: Springer New York, 2015.
16. ISO/ASTM. Additive Manufacturing - General Principles Terminology (ASTM52900). *Rapid Manufacturing Association* 2013; 10–12.
17. Wohlers Report 2014 Wohlers Associates.

18. Hideo Kodama. Automatic method for fabricating a three- dimensional plastic model with photo- hardening polymer. *Rev Sci Instrum* 1998; 52: 2–6.
19. Deckard C. *Method And Apparatus For Producing Parts By Selective Sintering*. US Patent 4,863,538, <https://patents.google.com/patent/US4863538> (1986).
20. Meiners W, Wissenback K, Gasser A. *Shaped Body Especially Prototype or Replacement Part Production*. European Patent DE 19649865C1, 1996.
21. Reddy K, Dufera S. Additive Manufacturing Technologies. *IJMITE* 2016; 4: 89–112.
22. *Wohlers Report 2019 - 3D Printing and Additive Manufacturing State of the Industry, Annual Worldwide Progress Report*, Wohlers Associates. 2019.
23. Vigneshwaran T. Metal Additive Manufacturing : A road to Future. *Int J Sci Res Eng Trends* 2020; 6: 3118–3121.
24. Thomas D. Costs, benefits, and adoption of additive manufacturing: a supply chain perspective. *Int J Adv Manuf Technol* 2016; 85: 1857–1876.
25. Frazier WE. Metal additive manufacturing: A review. *J Mater Eng Perform* 2014; 23: 1917–1928.
26. Holmström J, Partanen J, Tuomi J, et al. Rapid manufacturing in the spare parts supply chain: Alternative approaches to capacity deployment. *J Manuf Technol Manag* 2010; 21: 687–697.
27. Wong K V., Hernandez A. A Review of Additive Manufacturing. *ISRN Mech Eng* 2012; 2012: 1–10.
28. Zhang D, Liu X, Qiu J. 3D printing of glass by additive manufacturing techniques: a review. *Front Optoelectron*; 2020.
29. Zachariasen WH. The Atomic Arrangement In Glass. *J Am Chem Soc* 1932; 54: 3841–3851.
30. Holloway DG. *The Physical Properties of Glass*. London: Wykeham Publications Ltd, 1973.
31. Mozzi RL, Warren BE. The structure of vitreous silica. *J Appl Crystallogr* 1969; 2: 164–172.
32. Hasanuzzaman M, Rafferty A, Sajjia M, et al. Properties of Glass Materials. In: *Reference Module in Materials Science and Materials Engineering*. Elsevier, pp. 1–12.
33. Le Bourhis E. *Glass*. Weinheim, Germany: Wiley-VCH Verlag GmbH & Co. KGaA, 2007.
34. Shelby JE. *Introduction to Glass Science and Technology*. 2nd ed. Royal Society of Chemistry, 2005.
35. Adams LH, Williamson ED. The Annealing of Glass. *J Franklin Inst* 1920; 190: 597–631.
36. Tool AQ, Valasek J. *Concerning the Annealing and Characterstics of Glass*. Washington D.C.: Scientific Papers of the Bureau of Standards, 1920.
37. Larsen AW, Merrild H, Christensen TH. Recycling of glass: Accounting of greenhouse gases and global warming contributions. *Waste Manag Res* 2009; 27: 754–762.
38. Keller D. Social and Economic Aspects of Glass Recycling . *Theor Rom Archaeol J* 2005; 0: 65.

39. Freestone IC. The recycling and reuse of Roman glass: Analytical approaches. *J Glass Stud* 2015; 57: 29–40.
40. Godfrey L. Waste plastic, the challenge facing developing countries—Ban it, change it, collect it? *Recycling* 2019; 4: 2–7.
41. UK Statistics on Waste, Department for Environment Food & Rural Affairs, Government Statistical Service. 2021; 1–25.
42. Du K, Shi P. Subsurface precision processing of glass substrates by innovative lasers.pdf. *Glass Science and Technology* 2003; 76: 95–98.
43. Jones GO. *Glass*. 2nd Editio. Chapman and Hall Ltd, 1971.
44. Stair R, Faick CA. Glasses Containing Rare Earth and Other Oxides. *J Res Natl Bur Stand (1934)* 1947; 38: 95–101.
45. Narottam P, Bansal RHD. *Handbook of Glass Properties*. Academic Press Inc, 1986.
46. Greaves GN, Sen S. Inorganic glasses, glass-forming liquids and amorphizing solids. *Adv Phys* 2007; 56: 1–166.
47. Vogel W. *Glass Chemistry*. 2nd Editio. Berlin, Heidelberg: Springer Berlin Heidelberg. Epub ahead of print 1994. DOI: 10.1007/978-3-642-78723-2.
48. Fu Q, Rahaman MN, Bal BS, et al. Preparation and bioactive characteristics of a porous 13–93 glass, and fabrication into the articulating surface of a proximal tibia. *J Biomed Mater Res Part A* 2007; 82A: 222–229.
49. Brink M. The influence of alkali and alkaline earths on the working range for bioactive glasses. *J Biomed Mater Res* 1997; 36: 109–117.
50. El-Rashidy AA, Roether JA, Harhaus L, et al. Regenerating bone with bioactive glass scaffolds: A review of in vivo studies in bone defect models. *Acta Biomater* 2017; 62: 1–28.
51. Brink M, Karlsson K, Yli-Urpo A. *Novel Bioactive Glasses and Their Use*. European Patent, EP 0 802 890 B1, 2001.
52. Pitkänen V, Tikkanen J, Paaajanen M, et al. Processing of spherical bioactive glass particles. *J Aerosol Sci* 1995; 26: S831–S832.
53. Fagerlund S, Hupa L. Melt-derived Bioactive Silicate Glasses. In: *RSC Smart Materials*, pp. 1–26.
54. Pirhonen E, Niiranen H, Niemelä T, et al. Manufacturing, mechanical characterization, and in vitro performance of bioactive glass 13-93 fibers. *J Biomed Mater Res - Part B Appl Biomater* 2006; 77: 227–233.
55. Fu Q, Rahaman MN, Sonny Bal B, et al. Mechanical and in vitro performance of 13-93 bioactive glass scaffolds prepared by a polymer foam replication technique. *Acta Biomater* 2008; 4: 1854–1864.
56. Fu Q, Saiz E, Rahaman MN, et al. Bioactive glass scaffolds for bone tissue engineering: State of the art and future perspectives. *Mater Sci Eng C* 2011; 31: 1245–1256.
57. Coon E, Whittier AM, Abel BM, et al. Viscosity and crystallization of bioactive glasses from 45S5 to 13-93. *Int J Appl Glas Sci* 2021; 12: 65–77.

58. Klein J, Stern M, Franchin G, et al. Additive Manufacturing of Optically Transparent Glass. *3D Print Addit Manuf* 2015; 2: 92–105.
59. Klein J. *Additive Manufacturing of Optically Transparent Glass*. Masters Thesis, Massachusetts Institute of Technology, 2014.
60. Zaki RM, Strutynski C, Kaser S, et al. Direct 3D-printing of phosphate glass by fused deposition modeling. *Mater Des* 2020; 194: 0–8.
61. Baudet E, Ledemi Y, Larochelle P, et al. 3D-printing of arsenic sulfide chalcogenide glasses. *Opt Mater Express* 2019; 9: 2307.
62. Nguyen DT, Meyers C, Yee TD, et al. 3D-Printed Transparent Glass. *Adv Mater* 2017; 29: 1701181.
63. Dylla-Spears R, Yee TD, Sasan K, et al. 3D printed gradient index glass optics. *Sci Adv*; 6. Epub ahead of print 18 November 2020. DOI: 10.1126/sciadv.abc7429.
64. Sasan K, Lange A, Yee TD, et al. Additive Manufacturing of Optical Quality Germania–Silica Glasses. *ACS Appl Mater Interfaces* 2020; 12: 6736–6741.
65. Nan B, Gołębiewski P, Buczyński R, et al. Direct Ink Writing Glass: A Preliminary Step for Optical Application. *Materials (Basel)* 2020; 13: 1636.
66. Lei J, Hong Y, Zhang Q, et al. Additive Manufacturing of Fused Silica Glass Using Direct Laser Melting. *2019 Conf Lasers Electro-Optics, CLEO 2019 - Proc* 2019; 4–5.
67. Chen Q, Roether JA, Boucaccini AR. Tissue Engineering Scaffolds from Bioactive Glass and Composite Materials. *Top Tissue Eng*; 2008; 4.
68. Tesavibul P, Felzmann R, Gruber S, et al. Processing of 45S5 Bioglass by lithography-based additive manufacturing. *Mater Lett* 2012; 74: 81–84.
69. Thavornnyutikarn B, Tesavibul P, Sitthiseripratip K, et al. Porous 45S5 Bioglass[®]-based scaffolds using stereolithography: Effect of partial pre-sintering on structural and mechanical properties of scaffolds. *Mater Sci Eng C* 2017; 75: 1281–1288.
70. Elsayed H, Zocca A, Schmidt J, et al. Bioactive glass-ceramic scaffolds by additive manufacturing and sinter-crystallization of fine glass powders. *J Mater Res* 2018; 33: 1960–1971.
71. Elsayed H, Schmidt J, Bernardo E, et al. Comparative Analysis of Wollastonite-Diopside Glass-Ceramic Structures Fabricated via Stereo-Lithography. *Adv Eng Mater* 2019; 21: 1–8.
72. Kotz F, Plewa K, Bauer W, et al. Liquid Glass: A Facile Soft Replication Method for Structuring Glass. *Adv Mater* 2016; 28: 4646–4650.
73. Kotz F, Arnold K, Bauer W, et al. Three-dimensional printing of transparent fused silica glass. *Nature* 2017; 544: 337–339.
74. Kotz F, Risch P, Arnold K, et al. Fabrication of arbitrary three-dimensional suspended hollow microstructures in transparent fused silica glass. *Nat Commun* 2019; 10: 1439.
75. Kotz F, Quick AS, Risch P, et al. Two-Photon Polymerization of Nanocomposites for the Fabrication of Transparent Fused Silica Glass Microstructures. *Adv Mater* 2021; 33: 2006341.
76. Doualle T, André J-C, Gallais L. 3D printing of silica glass through a multiphoton

- polymerization process. *Opt Lett* 2021; 46: 364–367.
77. Cooperstein I, Shukrun E, Press O, et al. Additive Manufacturing of Transparent Silica Glass from Solutions. *ACS Appl Mater Interfaces* 2018; 10: 18879–18885.
 78. Shukrun Farrell E, Schilt Y, Moshkovitz MY, et al. 3D Printing of Ordered Mesoporous Silica Complex Structures. *Nano Lett* 2020; 20: 6598–6605.
 79. Liu C, Qian B, Ni R, et al. 3D printing of multicolor luminescent glass. *RSC Adv* 2018; 8: 31564–31567.
 80. Moore DG, Barbera L, Masania K, et al. Three-dimensional printing of multicomponent glasses using phase-separating resins. *Nat Mater* 2020; 19: 212–217.
 81. Yap CY, Chua CK, Dong ZL, et al. Review of selective laser melting: Materials and applications. *Appl Phys Rev* 2015; 2: 041101.
 82. Kruth JP, Mercelis P, Van Vaerenbergh J, et al. Binding mechanisms in selective laser sintering and selective laser melting. *Rapid Prototyp J* 2005; 11: 26–36.
 83. Dewidar MM, Lim JK, Dalgarno KW. Comparison between direct and indirect laser sintering of metals. *J Mater Sci Technol* 2008; 24: 227–232.
 84. Kruth JP, Wang X, Laoui T, et al. Lasers and materials in selective laser sintering. *Assem Autom* 2003; 23: 357–371.
 85. Prado MO, Zanotto ED, Müller R. Model for sintering polydispersed glass particles. *J Non Cryst Solids* 2001; 279: 169–178.
 86. Prado MO, Zanotto ED. Glass sintering with concurrent crystallization. *Comptes Rendus Chim* 2002; 5: 773–786.
 87. Kolan KCR, Leu MC, Hilmas GE, et al. Effect of material, process parameters, and simulated body fluids on mechanical properties of 13-93 bioactive glass porous constructs made by selective laser sintering. *J Mech Behav Biomed Mater* 2012; 13: 14–24.
 88. Kolan KCR, Leu MC, Hilmas GE, et al. Fabrication of 13-93 bioactive glass scaffolds for bone tissue engineering using indirect selective laser sintering. *Biofabrication*; 2011; 3.
 89. Liu J, Gao C, Feng P, et al. Selective laser sintering of β -TCP / nano-58S composite scaffolds with improved mechanical properties. *JMADE* 2015; 84: 395–401.
 90. Liu J, Hu H, Li P, et al. Fabrication and Characterization of Porous 45S5 Glass Scaffolds via Direct Selective Laser Sintering. *Mater Manuf Process* 2013; 28:6: 610–615.
 91. Gao C, Liu T, Shuai C, et al. Enhancement mechanisms of graphene in nano-58S bioactive glass scaffold: mechanical and biological performance. *Sci Rep* 2015; 4: 4712.
 92. Kolan KCR, Huang Y, Semon JA, et al. 3D-printed Biomimetic Bioactive Glass Scaffolds for Bone Regeneration in Rat Calvarial Defects. *Int J Bioprinting*; 2020; 6.
 93. Lin K, Sheikh R, Romanazzo S, et al. 3D Printing of Bioceramic Scaffolds—Barriers to the Clinical Translation: From Promise to Reality, and Future Perspectives. *Materials (Basel)* 2019; 12: 2660.
 94. Klocke F, McClung A, Ader C. Direct laser sintering of borosilicate glass. In: *Proceedings*

of the 15th Annual Solid Freeform Fabrication Symposium 2004, pp. 214–219.

95. Varshneya AK, Mauro JC. *Fundamentals of Inorganic Glasses*. Elsevier, 2019. Epub ahead of print 2019. DOI: 10.1016/C2017-0-04281-7.
96. Fluegel A. Glass viscosity based on a global statistical modeling approach. *Glas Technol Eur J Glas Sci Technol A* 2007; 48: 13–30.
97. Kruth JP, Levy G, Klocke F, et al. Consolidation phenomena in laser and powder-bed based layered manufacturing. *CIRP Ann - Manuf Technol* 2007; 56: 730–759.
98. Zocca A, Colombo P, Günster J, et al. Selective laser densification of lithium aluminosilicate glass ceramic tapes. *Appl Surf Sci* 2013; 265: 610–614.
99. Gmeiner R, Deisinger U, Schönherr J, et al. Additive Manufacturing of Bioactive Glasses and Silicate Bioceramics. *J Ceram Sci Technol* 2015; 86: 75–86.
100. Rieper H. *Systematic parameter analysis for selective laser melting (SLM) of silver-based materials*. PhD Thesis, University of Louisville, Kentucky, 2013.
101. Dhanawade DA, Bhatwadekar S. A Review on Types of Powder Bed Fusion Process in Additive Manufacturing Technology. *Int J Eng Technol Sci Res* 2017; 4: 2394–3386.
102. Dev Singh D, Mahender T, Raji Reddy A. Powder bed fusion process: A brief review. *Mater Today Proc* 2020; 2–7.
103. Kamath C. Data mining and statistical inference in selective laser melting. *Int J Adv Manuf Technol* 2016; 86: 1659–1677.
104. Catchpole-Smith S, Aboulkhair N, Parry L, et al. Fractal scan strategies for selective laser melting of ‘unweldable’ nickel superalloys. *Addit Manuf* 2017; 15: 113–122.
105. Leicht A, Yu CH, Luzin V, et al. Effect of scan rotation on the microstructure development and mechanical properties of 316L parts produced by laser powder bed fusion. *Mater Charact* 2020; 163: 2–10.
106. Pakkanen JA. *Designing for Additive Manufacturing-Product and Process Driven Design for Metals and Polymers*. PhD Thesis, Polytechnic University of Turin, Turin, 2018.
107. Jia H, Sun H, Wang H, et al. Scanning strategy in selective laser melting (SLM): a review. *Int J Adv Manuf Technol* 2021; 113: 2413–2435.
108. Promoppatum P, Yao SC. Influence of scanning length and energy input on residual stress reduction in metal additive manufacturing: Numerical and experimental studies. *J Manuf Process* 2020; 49: 247–259.
109. Kruth JP, Badrossamay M, Yasa E, et al. Part and material properties in selective laser melting of metals. *16th Int Symp Electromachining, ISEM 2010* 2010; 3–14.
110. Criales LE, Arisoy YM, Lane B, et al. Laser powder bed fusion of nickel alloy 625: Experimental investigations of effects of process parameters on melt pool size and shape with spatter analysis. *Int J Mach Tools Manuf* 2017; 121: 22–36.
111. Parry L, Ashcroft IA, Wildman RD. Understanding the effect of laser scan strategy on residual stress in selective laser melting through thermo-mechanical simulation. *Addit Manuf* 2016; 12: 1–15.
112. Sutton AT, Kriewall CS, Leu MC, et al. Powders for Additive Manufacturing Processes:

- Characterization Techniques and Effects on Part Properties. In: *Solid Freeform Fabrication 2016: Proceedings of the 27th Annual International Solid Freeform Fabrication Symposium*. 2016, pp. 1004–1030.
113. Spierings AB, Herres N, Levy G. Influence of the particle size distribution on surface quality and mechanical properties in AM steel parts. *Rapid Prototyp J* 2011; 17: 195–202.
 114. Muñoz-Lerma J, Nommeots-Nomm A, Waters K, et al. A Comprehensive Approach to Powder Feedstock Characterization for Powder Bed Fusion Additive Manufacturing: A Case Study on AlSi7Mg. *Materials (Basel)* 2018; 11: 2386.
 115. Tan JH, Wong WLE, Dalgarno KW. An overview of powder granulometry on feedstock and part performance in the selective laser melting process. *Addit Manuf* 2017; 18: 228–255.
 116. Cordova L, Bor T, de Smit M, et al. Measuring the spreadability of pre-treated and moisturized powders for laser powder bed fusion. *Addit Manuf* 2020; 32: 101082.
 117. Brika SE, Letenneur M, Dion CA, et al. Influence of particle morphology and size distribution on the powder flowability and laser powder bed fusion manufacturability of Ti-6Al-4V alloy. *Addit Manuf* 2020; 31: 100929.
 118. Mussatto A, Groarke R, O’Neill A, et al. Influences of powder morphology and spreading parameters on the powder bed topography uniformity in powder bed fusion metal additive manufacturing. *Addit Manuf* 2021; 38: 101807.
 119. Tran HC, Lo YL. Systematic approach for determining optimal processing parameters to produce parts with high density in selective laser melting process. *Int J Adv Manuf Technol* 2019; 105: 4443–4460.
 120. Masamune S, Smith JM. Thermal conductivity of beds of spherical particles. *Ind Eng Chem Fundam* 1963; 2: 136–143.
 121. Wischeropp TM, Emmelmann C, Brandt M, et al. Measurement of actual powder layer height and packing density in a single layer in selective laser melting. *Addit Manuf* 2019; 28: 176–183.
 122. Abu-Lebdeh T, Dampney R, Lamberti V, et al. Powder Packing Density and Its Impact on SLM-Based Additive Manufacturing. pp. 355–367.
 123. Liu B, Wildman R, Tuck C, et al. Investigation the effect of particle size distribution on processing parameters optimisation in selective laser melting process. In: *22nd Annual International Solid Freeform Fabrication Symposium*. 2011, pp. 227–238.
 124. Sofia D, Granese M, Barletta D, et al. Laser sintering of unimodal distributed glass powders of different size. *Procedia Eng* 2015; 102: 749–758.
 125. Pavan M, Faes M, Strobbe D, et al. On the influence of inter-layer time and energy density on selected critical-to-quality properties of PA12 parts produced via laser sintering. *Polym Test* 2017; 61: 386–395.
 126. Mohr G, Altenburg SJ, Hilgenberg K. Effects of inter layer time and build height on resulting properties of 316L stainless steel processed by laser powder bed fusion. *Addit Manuf* 2020; 32: 101080.
 127. Yadollahi A, Shamsaei N, Thompson SM, et al. Effects of process time interval and heat treatment on the mechanical and microstructural properties of direct laser deposited

- 316L stainless steel. *Mater Sci Eng A* 2015; 644: 171–183.
128. Torries B, Shao S, Shamsaei N, et al. Effect of inter-layer time interval on the mechanical behavior of direct laser deposited Ti-6Al-4V. *Solid Free Fabr 2016 Proc 27th Annu Int Solid Free Fabr Symp - An Addit Manuf Conf SFF 2016* 2016; 1272–1282.
 129. Goodridge RD, Tuck CJ, Hague RJMM. Laser sintering of polyamides and other polymers. *Prog Mater Sci* 2012; 57: 229–267.
 130. Fateri M, Gebhardt A, Thuemmler S, et al. Experimental Investigation on Selective Laser Melting of Glass. *Phys Procedia* 2014; 56: 357–364.
 131. Fateri M, Gebhardt A. Jewelry Fabrication via Selective Laser Melting of Glass. In: *Proceedings of the ASME 2014 12th Biennial Conference on Engineering Systems Design and Analysis. Volume 1: Applied Mechanics; Automotive Systems; Biomedical Biotechnology Engineering; Computational Mechanics; Design; Digital Manufacturing; Education; Mar.* American Society of Mechanical Engineers. Epub ahead of print 25 July 2014. DOI: 10.1115/ESDA2014-20380.
 132. Fateri M, Gebhardt A. Selective Laser Melting of Soda-Lime Glass Powder. *Int J Appl Ceram Technol* 2015; 12: 53–61.
 133. Khmyrov RS, Grigoriev SN, Okunkova AA, et al. On the possibility of selective laser melting of quartz glass. *Phys Procedia* 2014; 56: 345–356.
 134. Khmyrov RS, Protasov CE, Grigoriev SN, et al. Crack-free selective laser melting of silica glass: single beads and monolayers on the substrate of the same material. *Int J Adv Manuf Technol* 2016; 85: 1461–1469.
 135. Protasov CE, Khmyrov RS, Grigoriev SN, et al. Selective laser melting of fused silica: Interdependent heat transfer and powder consolidation. *Int J Heat Mass Transf* 2017; 104: 665–674.
 136. Vernerová M, Kloužek J, Němec L. Reaction of soda-lime-silica glass melt with water vapour at melting temperatures. *J Non Cryst Solids* 2015; 416: 21–30.
 137. Kamarudin K, Wahab MS, Shayfull Z, et al. Dimensional Accuracy and Surface Roughness Analysis for AlSi10Mg Produced by Selective Laser Melting (SLM). *MATEC Web Conf* 2016; 78: 01077.
 138. Holländer A, Cosemans P. Surface technology for additive manufacturing. *Plasma Process Polym* 2020; 17: 1–13.
 139. Wegner A, Harder R, Witt G, et al. Determination of Optimal Processing Conditions for the Production of Polyamide 11 Parts using the Laser Sintering Process. *Int J Recent Contrib from Eng Sci IT* 2015; 3: 5.
 140. Fateri M. *Selective laser melting of glass powders*. Doctoral Thesis, RWTH Aachen University, Germany, 2017.
 141. Gan MX, Wong CH. Properties of selective laser melted spodumene glass-ceramic. *J Eur Ceram Soc* 2017; 37: 4147–4154.
 142. Wang WH, Dong C, Shek CH. Bulk metallic glasses. *Mater Sci Eng R Reports* 2004; 44: 45–89.
 143. Li HF, Zheng YF. Recent advances in bulk metallic glasses for biomedical applications. *Acta Biomater* 2016; 36: 1–20.

144. Calin M, Gebert A, Ghinea AC, et al. Designing biocompatible Ti-based metallic glasses for implant applications. *Mater Sci Eng C* 2013; 33: 875–883.
145. Deng L, Wang S, Wang P, et al. Selective laser melting of a Ti-based bulk metallic glass. *Mater Lett* 2018; 212: 346–349.
146. Miedzinski M. *Materials for Additive Manufacturing by Direct Energy Deposition*. Masters Thesis, Chalmers University of Technology, Gothenburg, 2017.
147. Dass A, Moridi A. State of the Art in Directed Energy Deposition : From. *Coatings*.
148. Svetlizky D, Das M, Zheng B, et al. Directed energy deposition (DED) additive manufacturing: Physical characteristics, defects, challenges and applications. *Mater Today*; xxx. Epub ahead of print 2021. DOI: 10.1016/j.mattod.2021.03.020.
149. Yamazaki T. Development of A Hybrid Multi-tasking Machine Tool: Integration of Additive Manufacturing Technology with CNC Machining. *Procedia CIRP* 2016; 42: 81–86.
150. Singh A, Kapil S, Das M. A comprehensive review of the methods and mechanisms for powder feedstock handling in directed energy deposition. *Addit Manuf* 2020; 35: 101388.
151. Zekovic S, Dwivedi R, Kovacevic R. Numerical simulation and experimental investigation of gas-powder flow from radially symmetrical nozzles in laser-based direct metal deposition. *Int J Mach Tools Manuf* 2007; 47: 112–123.
152. Fessler J, Merz R, Nickel A, et al. Laser deposition of metals for shape deposition manufacturing. In: *Solid Freeform Fabrication Symposium Proceedings*. 1996, pp. 117–124.
153. Mazzucato F, Tusacciu S, Lai M, et al. Monitoring Approach to Evaluate the Performances of a New Deposition Nozzle Solution for DED Systems. *Technologies* 2017; 5: 29.
154. Saboori A, Biamino S, Lombardi M, et al. How the nozzle position affects the geometry of the melt pool in directed energy deposition process. *Powder Metall* 2019; 62: 213–217.
155. Luo J, Pan H, Kinzel EC. Additive Manufacturing of Glass. *J Manuf Sci Eng Trans ASME* 2014; 136: 1–6.
156. Luo J, Gilbert LJ, Qu C, et al. Additive Manufacturing of Transparent Soda-Lime Glass Using a Filament-Fed Process. *J Manuf Sci Eng Trans ASME* 2017; 139: 1–8.
157. Luo J, Bender T, Bristow DA DA, et al. Bubble formation in additive manufacturing of borosilicate glass. In: *Solid Freeform Fabrication 2016: Proceedings of the 27th Annual International Solid Freeform Fabrication Symposium - An Additive Manufacturing Conference, SFF 2016*. 2016, pp. 998–1003.
158. Luo J, Hostetler JM, Bristow DA, et al. Heat transfer in additive manufacturing of glass. In: *ASME 2017 Heat Transfer Summer Conference, HT 2017*. 2017, pp. 1–5.
159. Pohl L, von Witzendorff P, Chatzizyrl E, et al. CO2 laser welding of glass: numerical simulation and experimental study. *Int J Adv Manuf Technol* 2017; 90: 397–403.
160. Von Witzendorff P, Pohl L, Suttman O, et al. Additive manufacturing of glass: CO2-Laser glass deposition printing. *Procedia CIRP* 2018; 74: 272–275.

161. Capps NE, Johnson JE, Landers RG, et al. Comparison of volumetric to surface heating for filament-fed laser heated additive manufacturing of glass. In: *ASME 2019 Heat Transfer Summer Conference, HT 2019*. 2019, pp. 1–7.
162. Rettschlag K, Hohnholz A, Jäschke P, et al. Laser glass deposition of spheres for printing micro lenses. *Procedia CIRP* 2020; 94: 276–280.
163. Luo J. *Additive manufacturing of glass using a filament fed process*. Doctoral Thesis, Missouri University of Science and Technology, 2017.
164. Campanelli SL, Contuzzi N, Angelastro A, et al. Capabilities and Performances of the Selective Laser Melting Process. *New Trends Technol Devices, Comput Commun Ind Syst*. Epub ahead of print 2010. DOI: 10.5772/10432.
165. Tang X, Zhang S, Zhang C, et al. Optimization of laser energy density and scanning strategy on the forming quality of 24CrNiMo low alloy steel manufactured by SLM. *Mater Charact* 2020; 170: 110718.
166. Carter LN, Wang X, Read N, et al. Process optimisation of selective laser melting using energy density model for nickel based superalloys. *Mater Sci Technol (United Kingdom)* 2016; 32: 657–661.
167. Kluczyński J, Śniezek L, Grzelak K, et al. The influence of exposure energy density on porosity and microhardness of the SLM additive manufactured elements. *Materials (Basel)*; 11. Epub ahead of print 2018. DOI: 10.3390/ma11112304.
168. Prashanth KG, Scudino S, Maity T, et al. Is the energy density a reliable parameter for materials synthesis by selective laser melting? *Mater Res Lett* 2017; 5: 386–390.
169. Mirkoohi E, Seivers DE, Garmestani H, et al. Heat source modeling in selective laser melting. *Materials (Basel)* 2019; 12: 1–18.
170. Lumay G, Fiscina J, Ludewig F, et al. Influence of cohesive forces on the macroscopic properties of granular assemblies. In: *AIP Conference Proceedings*. 2013, pp. 995–998.
171. Li Q, Rudolph V, Weigl B, et al. Interparticle van der Waals force in powder flowability and compactibility. *Int J Pharm* 2004; 280: 77–93.
172. Freeman R. Measuring the flow properties of consolidated, conditioned and aerated powders - A comparative study using a powder rheometer and a rotational shear cell. *Powder Technol* 2007; 174: 25–33.
173. Strondl A, Lyckfeldt O, Brodin H, et al. Characterization and Control of Powder Properties for Additive Manufacturing. *JOM* 2015; 67: 549–554.
174. Nan W, Ghadiri M, Wang Y. Analysis of powder rheometry of FT4: Effect of particle shape. *Chem Eng Sci* 2017; 173: 374–383.
175. Olakanmi EO, Cochrane RF, Dalgarno KW. A review on selective laser sintering/melting (SLS/SLM) of aluminium alloy powders: Processing, microstructure, and properties. *Prog Mater Sci* 2015; 74: 401–477.
176. Gu YW, Yap AUJ, Cheang P, et al. Spheroidization of glass powders for glass ionomer cements. *Biomaterials* 2004; 25: 4029–4035.
177. Lakhkar NJ, Park JH, Mordan NJ, et al. Titanium phosphate glass microspheres for bone tissue engineering. *Acta Biomater* 2012; 8: 4181–4190.
178. Gupta D, Hossain KMZ, Ahmed I, et al. Flame-Spheroidized Phosphate-Based Glass

- Particles with Improved Characteristics for Applications in Mesenchymal Stem Cell Culture Therapy and Tissue Engineering. *ACS Appl Mater Interfaces* 2018; 10: 25972–25982.
179. Hossain KMZ, Patel U, Ahmed I. Development of microspheres for biomedical applications: A review. *Prog Biomater* 2015; 4: 1–19.
 180. Kelkar RM. *High quality spherical powders for Additive Manufacturing Processes along with methods of their formation*. US Patent US 2019/0061005, 2019.
 181. Sreekumar KP, Saxena SK, Kumar Y, et al. Studies on the preparation and plasma spheroidization of yttrium aluminosilicate glass microspheres for their potential application in liver brachytherapy. *J Phys Conf Ser* 2010; 208: 0–5.
 182. Kriewall CS, Newkirk JW. Plasma Spheroidization of Vitreloy 106A Bulk Metallic Glass Powder. *Metall Mater Trans* 2019; 50: 4791–4797.
 183. Li Q, Zhang L, Wei D, et al. Porous Nb-Ti based alloy produced from plasma spheroidized powder. *Results Phys* 2017; 7: 1289–1298.
 184. Wei WH, Wang LZ, Chen T, et al. Study on the flow properties of Ti-6Al-4V powders prepared by radio-frequency plasma spheroidization. *Adv Powder Technol* 2017; 28: 2431–2437.
 185. Powell D, Rennie AEWW, Geekie L, et al. Understanding powder degradation in metal additive manufacturing to allow the upcycling of recycled powders. *J Clean Prod* 2020; 268: 122077.
 186. Murray JW, Simonelli M, Speidel A, et al. Spheroidisation of metal powder by pulsed electron beam irradiation. *Powder Technology* 2019; 350: 100–106.
 187. Volf MB. *Chemical Approach to Glass (Glass Science & Technology)*. 1984.
 188. Vercamer V. *Spectroscopic and Structural Properties of Iron in Silicate Glasses*. PhD Thesis, Pierre and Marie Curie University, Paris, 2017.
 189. Donald SB, Swink AM, Schreiber HD. High-iron ferric glass. *J Non Cryst Solids* 2006; 352: 539–543.
 190. Shi C, Ermold ML, Oulundsen GE, et al. CO₂ and CO laser comparison of glass and ceramic processing. In: Kaierle S, Heinemann SW (eds) *High-Power Laser Materials Processing: Applications, Diagnostics, and Systems VIII*. SPIE, p. 20.
 191. Karazi SM, Ahad IU, Benyounis KY. Laser Micromachining for Transparent Materials. In: *Reference Module in Materials Science and Materials Engineering*. Elsevier. Epub ahead of print 2017. DOI: 10.1016/B978-0-12-803581-8.04149-7.
 192. ABRISA Technologies. Specialty Glass Materials Products & Specifications. 2014; 1–35.
 193. Belardi W, Sazio PJ. Borosilicate based hollow-core optical fibers. *Fibers* 2019; 7: 1–8.
 194. Hoppe A. *Bioactive Glass Derived Scaffolds with Therapeutic Ion Releasing Capability for Bone Tissue Engineering*. Doctoral Thesis, University of Erlangen-Nuremberg, 2014.
 195. Luo J, Gilbert L, Qu C, et al. Wire-Fed additive manufacturing of transparent glass parts. *Proc ASME 2015 Int Manuf Sci Eng Conf* 2015; 1: V001T02A108.
 196. Velez M, Kolan KCR, Leu MC, et al. Selective laser sintering fabrication of 13-93

- bioactive glass bone scaffolds. *Ceram Trans* 2011; 228: 185–193.
197. Liu H, Jiang Q, Huo J, et al. Crystallization in additive manufacturing of metallic glasses: A review. *Addit Manuf* 2020; 36: 101568.
 198. Liu Y, Li T, Ma H, et al. 3D-printed scaffolds with bioactive elements-induced photothermal effect for bone tumor therapy. *Acta Biomater* 2018; 73: 531–546.
 199. Capel AJ, Wright A, Harding MJ, et al. 3D printed fluidics with embedded analytic functionality for automated reaction optimisation. *Beilstein J Org Chem* 2017; 13: 111–119.
 200. Gutmann B, Köckinger M, Glotz G, et al. Design and 3D printing of a stainless steel reactor for continuous difluoromethylations using fluoroform. *React Chem Eng* 2017; 2: 919–927.
 201. Leclerc M, Gauvin R. *Functional Materials - For Energy, Sustainable Development and Biomedical Sciences*. De Gruyter, 2014.
 202. Zhang H, Bai Y, Zhu N, et al. Microfluidic reactor with immobilized enzyme-from construction to applications: A review. *Chinese J Chem Eng* 2021; 30: 136–145.
 203. Capel AJ, Edmondson S, Christie SDR, et al. Design and additive manufacture for flow chemistry. *Lab Chip* 2013; 13: 4583–4590.
 204. Dragone V, Sans V, Rosnes MH, et al. 3D-printed devices for continuous-flow organic chemistry. *Beilstein J Org Chem* 2013; 9: 951–959.
 205. Mathieson JS, Rosnes MH, Sans V, et al. Continuous parallel ESI-MS analysis of reactions carried out in a bespoke 3D printed device. *Beilstein J Nanotechnol* 2013; 4: 285–291.
 206. Kitson PJ, Glatzel S, Chen W, et al. 3D printing of versatile reactionware for chemical synthesis. *Nat Protoc* 2016; 11: 920–936.
 207. Okafor O, Weilhard A, Fernandes JA, et al. Advanced reactor engineering with 3D printing for the continuous-flow synthesis of silver nanoparticles. *React Chem Eng* 2017; 2: 129–136.
 208. Wirth T. *Microreactors in Organic Chemistry and Catalysis*. 2nd ed. John Wiley & Sons, Incorporated, 2013.
 209. Smith RK. Laboratory Ware. In: *Water and Wastewater Laboratory Techniques*. WEF, 1995.
 210. Ronggui S, Righini GC. Characterization of reactive ion etching of glass and its applications in integrated optics. *J Vac Sci Technol A Vacuum, Surfaces, Film* 1991; 9: 2709–2712.
 211. Gugger H. *Laser Marking of Ceramic Materials, Glazes, Glass Ceramics and Glasses*. United States Patent 4769310. United States Patent 4769310, 1988.
 212. Iliescu C, Chen B, Miao J. Deep wet etching-through 1mm Pyrex glass wafer for microfluidic applications. In: *Proceedings of the IEEE International Conference on Micro Electro Mechanical Systems (MEMS)*. 2007, pp. 393–396.
 213. Li PM. *Study of the FT4 powder rheometer: comparison of the test methods and optimization of the protocols*. PhD Thesis, University of Technology of Compiègne, Compiègne, 2017.

214. Freeman T. *An introduction to Powders*. 2008.
215. Maher Boulos, Plasma power can make better powders, *Metal Powder Report*, Volume 59, Issue 5, 2004, Pages 16-21.
216. Datsiou KC, Saleh E, Spirrett F, et al. Additive manufacturing of glass with laser powder bed fusion. *J Am Ceram Soc* 2019; 1–5.
217. Datsiou KC, Spirrett F, Ashcroft I, et al. Laser powder bed fusion of soda lime silica glass: Optimisation of processing parameters and evaluation of part properties. *Addit Manuf*; 39. Epub ahead of print March 2021. DOI: 10.1016/j.addma.2021.101880.
218. Moulijn JA, Kapteijn F. Monolithic reactors in catalysis: Excellent control. *Curr Opin Chem Eng* 2013; 2: 346–353.
219. Kapteijn F, Moulijn JA. Structured catalysts and reactors – Perspectives for demanding applications. *Catal Today*. Epub ahead of print 2020. DOI: 10.1016/j.cattod.2020.09.026.
220. Song JL, Li YT, Deng QL, et al. Rapid prototyping manufacturing of silica sand patterns based on selective laser sintering. *J Mater Process Technol* 2007; 187–188: 614–618.
221. De Focatiis DSA, Buckley CP. Determination of craze initiation stress in very small polymer specimens. *Polym Test* 2008; 27: 136–145.
222. Li D, Li W, Wang R, et al. Temperature dependence of the three-point bending fracture behavior of soda – lime – silica glass with surface scratch. *J Non Cryst Solids* 2015; 409: 126–130.
223. Barton JL, Caurant D. The oxidation of ferrous iron in glass at high temperatures II. *Fundam Glas Sci Technol - ESG 1993* 1993; 193–198.
224. Washburn EW, Shelton GR, Libman EE. The viscosities and surface tensions of the soda-lime-silica glasses at high temperatures. *Bull* 1924; 140: 71 pp.
225. Liu J, Zhang B, Yan C, et al. The effect of processing parameters on characteristics of selective laser sintering dental glass-ceramic powder. *Rapid Prototyp J* 2010; 16: 138–145.
226. Tong A. Improving the accuracy of temperature measurements. *Sens Rev* 2001; 21: 193–198.
227. Yadroitsev I, Smurov I. Selective laser melting technology: From the single laser melted track stability to 3D parts of complex shape. *Phys Procedia* 2010; 5: 551–560.
228. Kandasami RK, Murthy TG. Effect of particle shape on the mechanical response of a granular ensemble. *Geomech from Micro to Macro - Proc TC105 ISSMGE Int Symp Geomech from Micro to Macro, IS-Cambridge 2014* 2015; 2: 1093–1098.
229. Medrano Tellez AG. *Fibre Laser Metal Deposition with Wire : Parameters Study and Temperature Control*. PhD Thesis, University of Nottingham, Nottingham, 2010.
230. Bodhmag A. Correlation between physical properties and flowability indicators for fine powders. *Univ Saskatchewan* 2006; 1–122.
231. Hostetler JM, Johnson JE, Goldstein JT, et al. Fiber-Fed Printing of Free-Form Free-Standing Glass Structures. In: *Solid Freeform Fabrication 2018: Proceedings of the 29th Annual International Solid Freeform Fabrication Symposium*. 2018, pp. 994–1002.

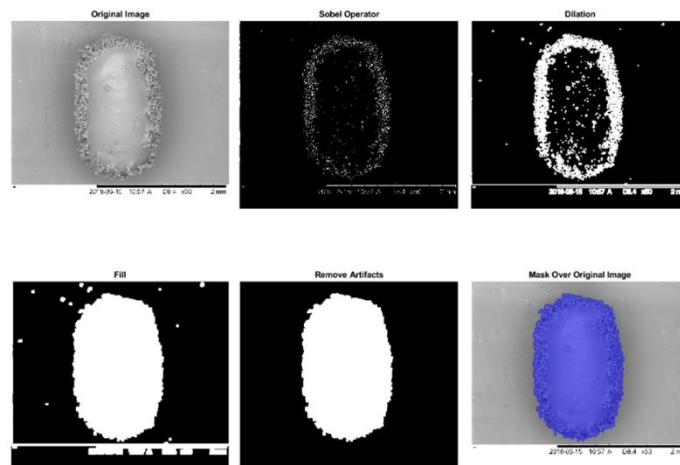
232. Veer FA, Zuidema J. The Strength of Glass , Effect of Edge Quality. *Glas Process Days* 2003; 106–109.
233. BeAM Directed Energy Deposition, Commercial Booklet.
234. Denlinger ER, Heigel JC, Michaleris P, et al. Effect of inter-layer dwell time on distortion and residual stress in additive manufacturing of titanium and nickel alloys. *J Mater Process Technol* 2015; 215: 123–131.
235. Scipioni Bertoli U, Wolfer AJ, Matthews MJ, et al. On the limitations of Volumetric Energy Density as a design parameter for Selective Laser Melting. *Mater Des* 2017; 113: 331–340.
236. Dias Da Silva M, Partes K, Seefeld T, et al. Comparison of coaxial and off-axis nozzle configurations in one step process laser cladding on aluminum substrate. *J Mater Process Technol* 2012; 212: 2514–2519.
237. Li Y, Yang H, Lin X, et al. The influences of processing parameters on forming characterizations during laser rapid forming. *Mater Sci Eng A* 2003; 360: 18–25.
238. Cordova L, Campos M, Tinga T. Revealing the Effects of Powder Reuse for Selective Laser Melting by Powder Characterization. *Jom* 2019; 71: 1062–1072.

Appendix

Geometrical Accuracy of SLM Glass Elements

Two SLM glass samples were visualised by SEM. The overall geometrical accuracy in the x-y plane was estimated as the maximum deviation from the intended part geometry (defined by CAD). The SEM images were processed by an inbuilt edge function (Matlab, Mathworks) using a Sobel operator to detect part edges. Image dilation emphasised the edges, and an image fill function was used to identify enclosed regions by creating a bounding box. Artifacts were removed, and the total area was measured and compared to CAD defined dimensions.

Sample 1



Sample 2

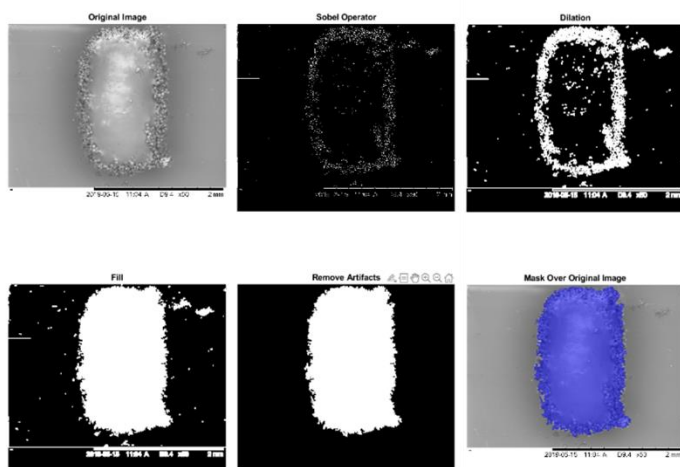
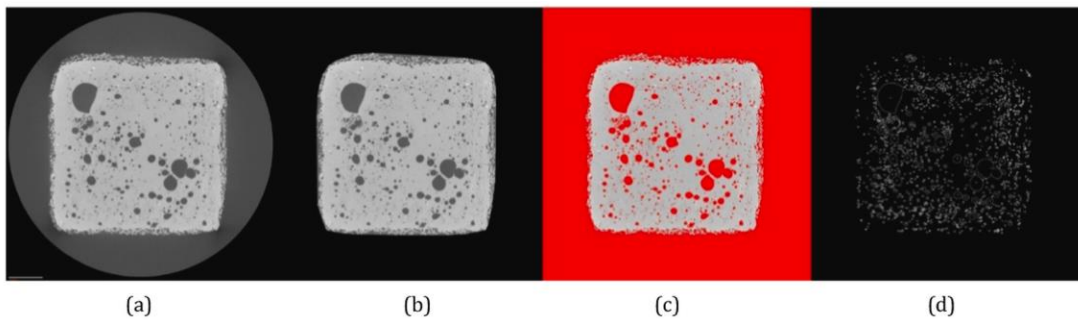


Image Processing for Porosity Measurements of Cubic SLM glass structures (ImageJ)

XCT cross sectional images were analysed using the open-source software ImageJ. Background information was removed from cross sectional images to isolate the sample geometry. A segmentation algorithm was used to convert pixels to binary: assigning black pixels "0" and white pixels "1". Porosity was calculated as a ratio of porous area over total area by ImageJ.

Example of ImageJ processing for SLM cubic glass sample



a: Cross sectional XCT image of glass cube, b: removal of background, c: image segmentation, d: pore extraction.

Three Point Bend Testing of Glass Samples

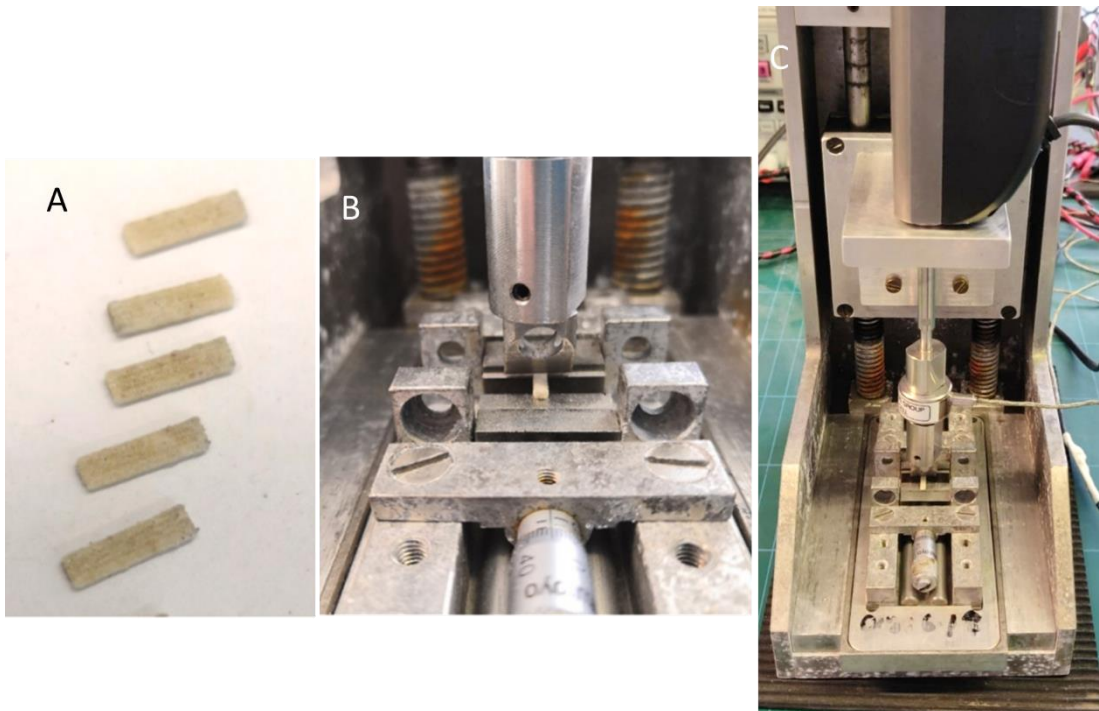
1 x 2 x 8 mm SLM samples of GTS-6 were fabricated vertically on the build platform (8 mm high in the z direction). Four sets of processing parameters were used to fabricate the samples, with 24 samples in each category. The support span was 5.35 mm and the strain rate was 0.0005 s⁻¹. The failure stress was calculated with:

$$\sigma_f = \frac{(3 \cdot P_f \cdot l_s)}{(2 \cdot b \cdot d^2)}$$

P_f = failure load, l_s (support span) = 5.35 mm, b (width) = 2 mm, d (height) = 1 mm. The ramp stress history of each sample was converted to constant stress over 60 s and data was analysed and fitted to a 2-parameter Weibull distribution.

- 1: Energy density: 79 J/mm³, scan direction: x axis (short dimension, 1 mm)
- 2: Energy density: 93 J/mm³, scan direction: x axis (short dimension, 1 mm)
- 3: Energy density: 108 J/mm³, scan direction: x axis (short dimension, 1 mm)
- 4: Energy density: 108 J/mm³, scan direction: y axis (long dimension, 2 mm)

Samples were annealed at 560°C for two hours at a heating and cooling rate of 2°C/min.



A: Image of glass test samples, B-C: three-point bend test rig.

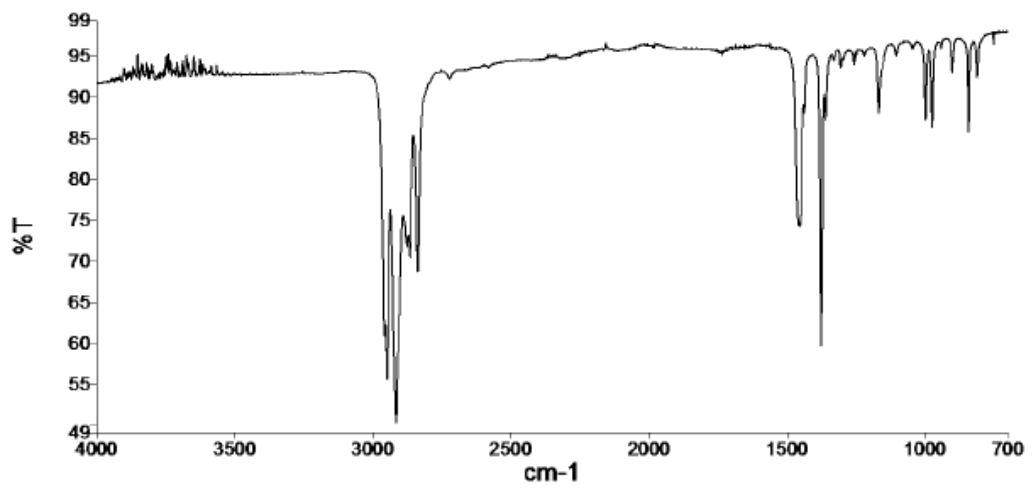
FTIR of DED Samples

FTIR was carried out on different areas of a laser processed DED glass sample using a (Frontier FTIR, Perkin Elmer, UK).

Sample	Description	Peaks (cm ⁻¹)
1	Cellophane tape on glass slide	1375, 1455, 2838, 2866, 2917, 2949, 2959
2	Cellophane tape layer, irradiated (white)	751, 940, 1158, 1375, 1454, 1729, 2956
3	Cellophane tape layer, irradiated (black)	841, 1062, 1158, 1376, 1454, 1729, 2874, 2957
4	Glass fibre – irradiated tape (black)	1436, 1731, 2321
5	Glass fibre – irradiated tape	750, 880, 1027, 1434, 1727
6	Glass deposit	998, 1368, 1741
7	Cellophane tape (adhesive)	738, 840, 942, 1064, 1159, 1242, 1377, 1455, 1729, 2874, 2958
8	Cellophane tape (top layer)	840, 972, 1167, 1357, 1455, 2838, 2866, 2917, 2949

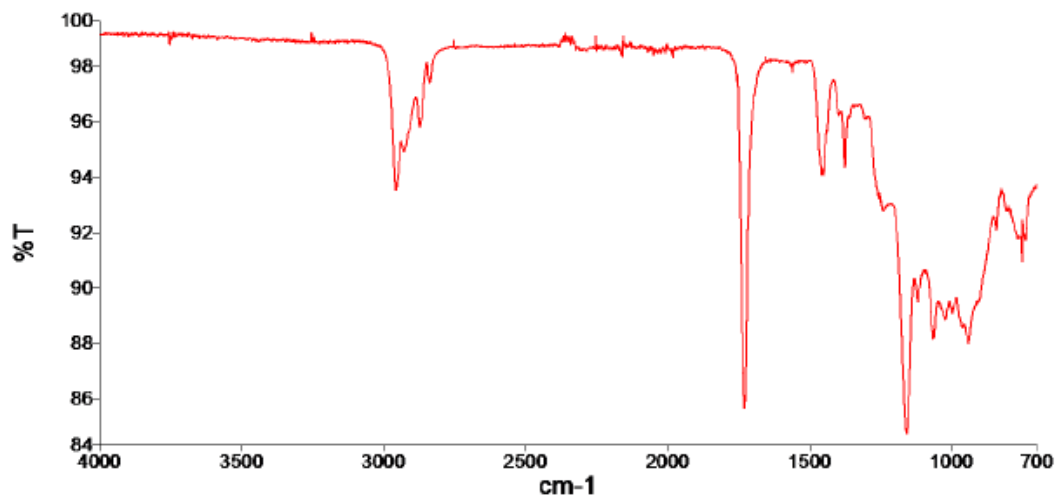
Sample 1

Spectrum



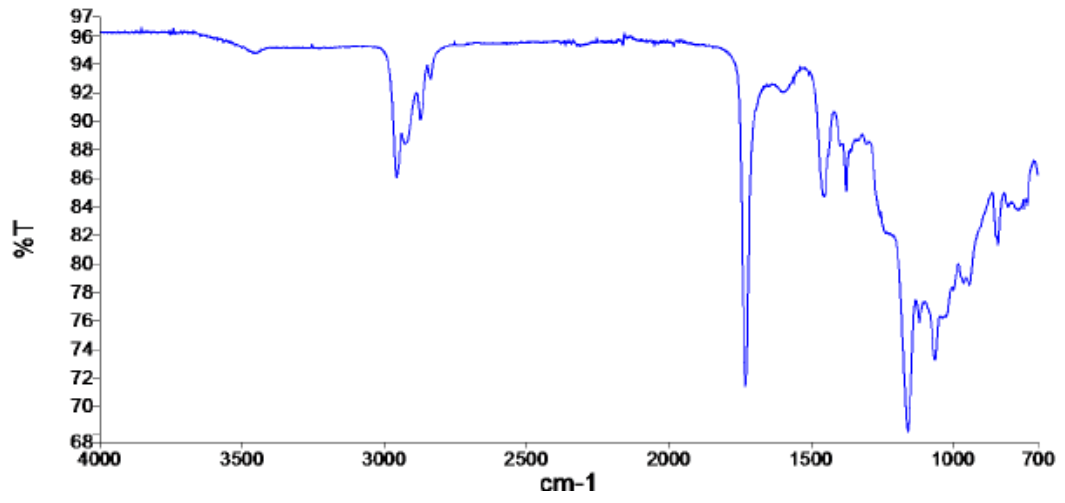
Sample 2

Spectrum



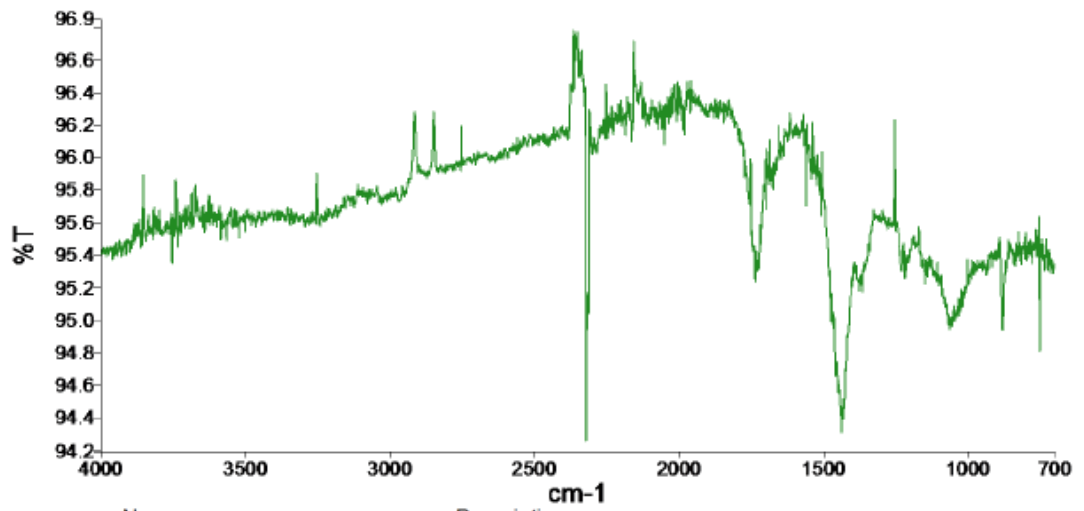
Sample 3

Spectrum



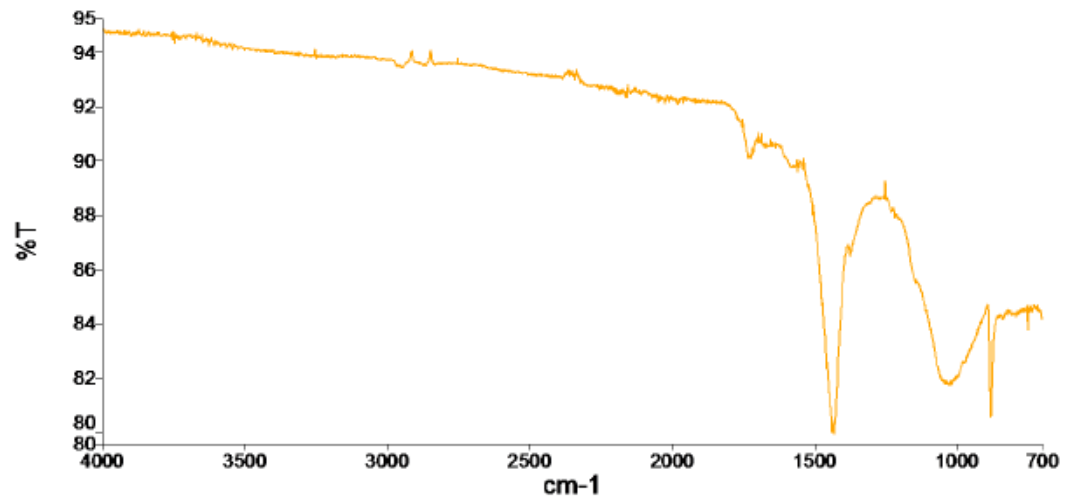
Sample 4

Spectrum



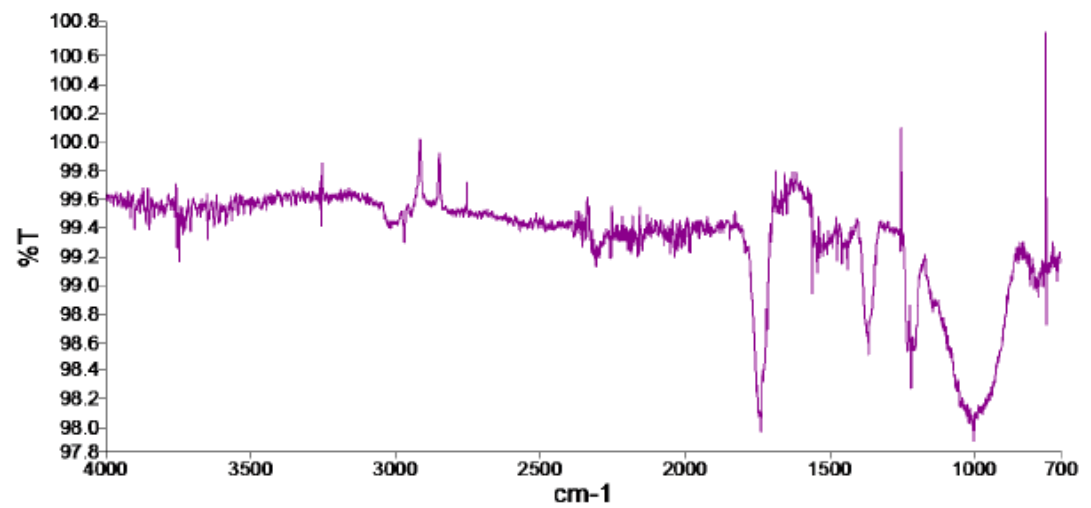
Sample 5

Spectrum



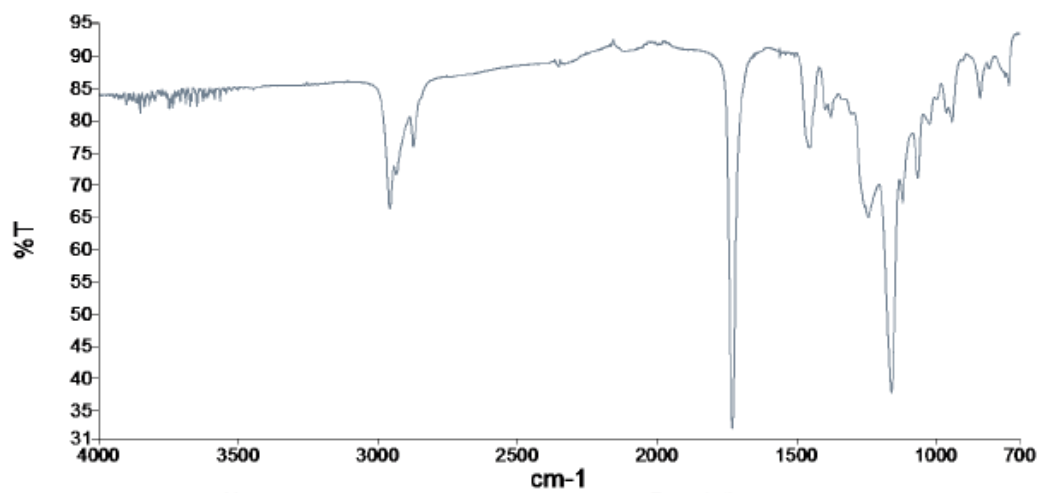
Sample 6

Spectrum



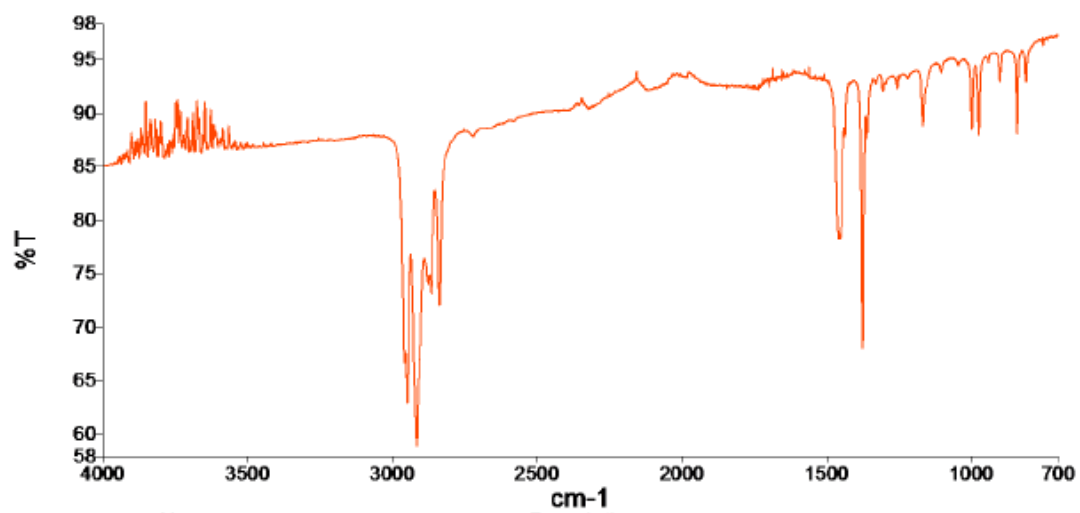
Sample 7

Spectrum



Sample 8

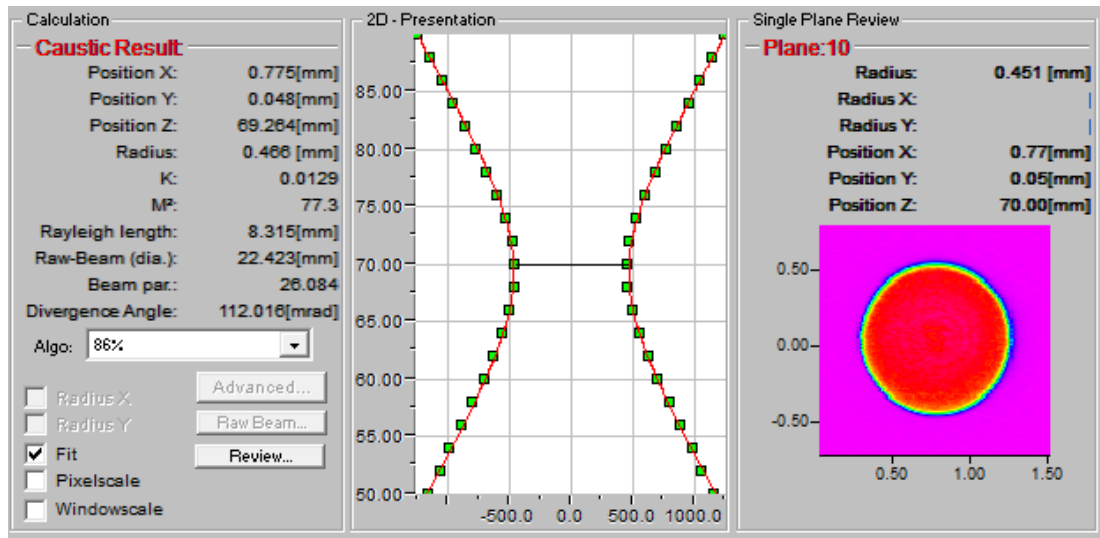
Spectrum



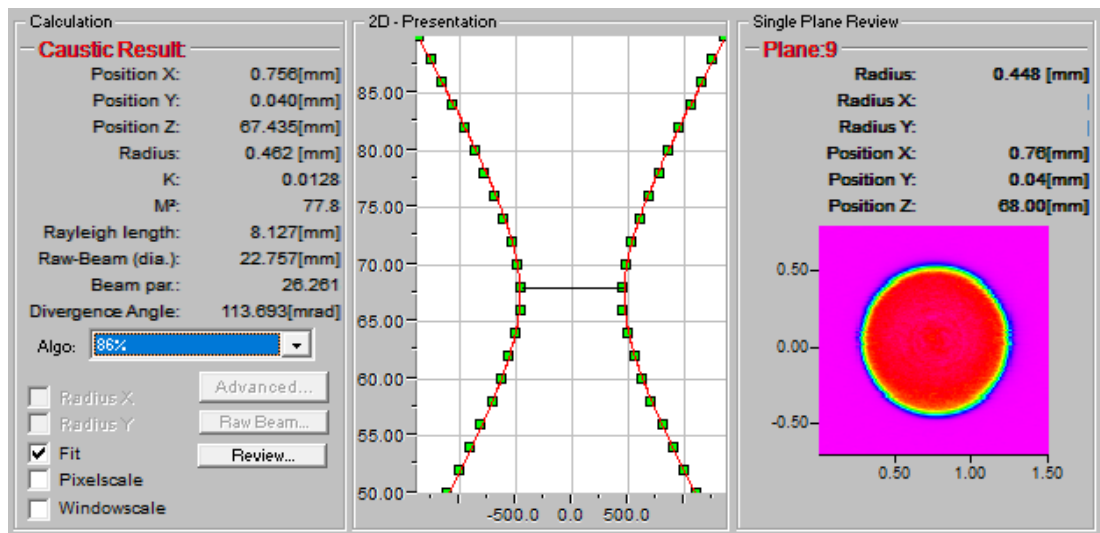
Power Loss and Beam Profiling of IPG 2 kW Laser

The DED IPG laser was profiled in October 2017 using PRIMES Monitor. Measurement set-up: PRECITEC YW50 WELDING HEAD (Lens = 200mm / Coll = 125mm / Fibre = 600um diameter). Values in brackets indicate the laser power recorded on PRIMES Monitor.

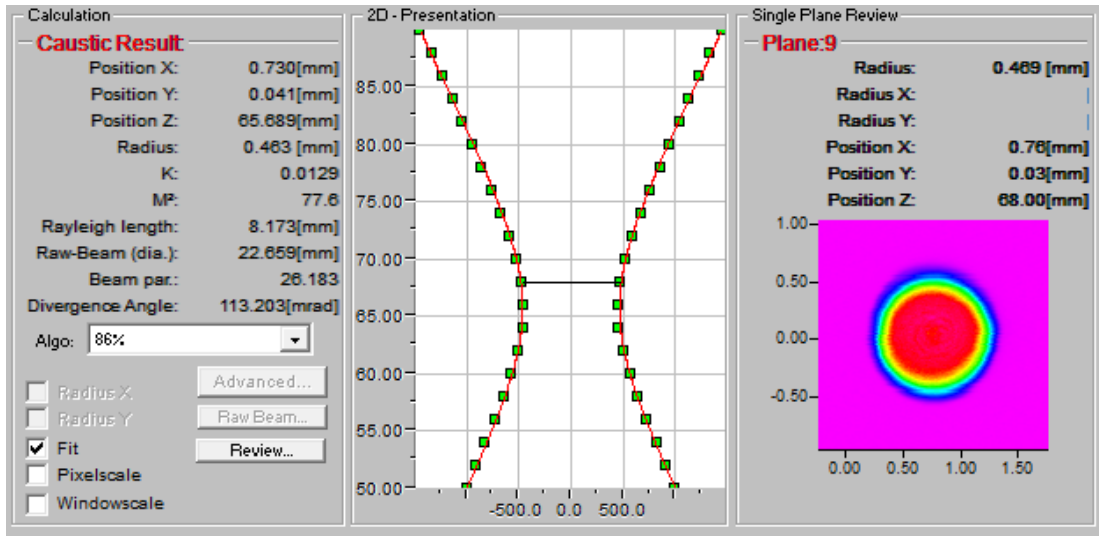
NU-02-FL200-FC125-FD600um-500W (433W on PM)



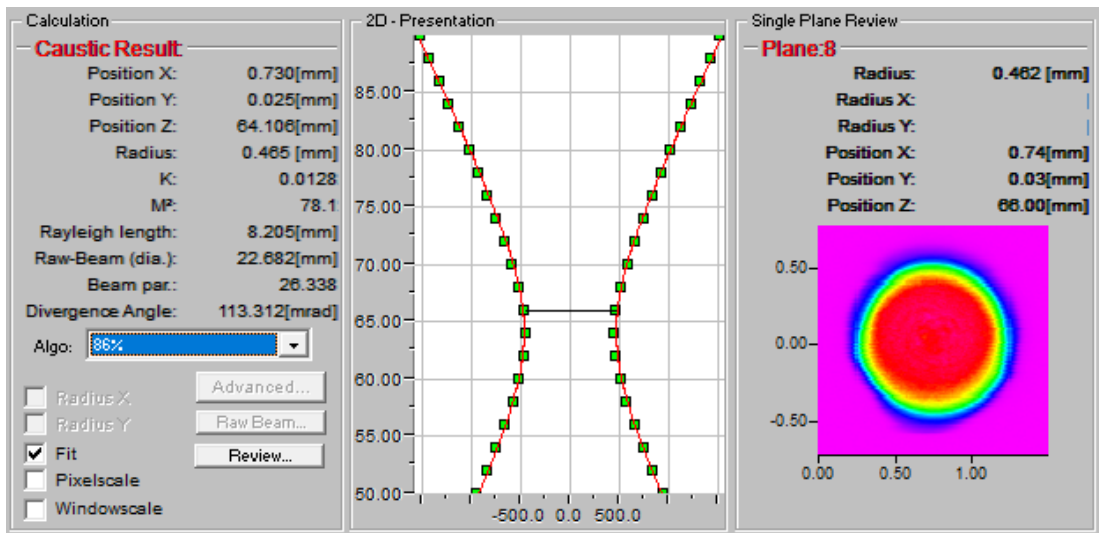
NU-03-FL200-FC125-FD600um-1000W (880W on PM)



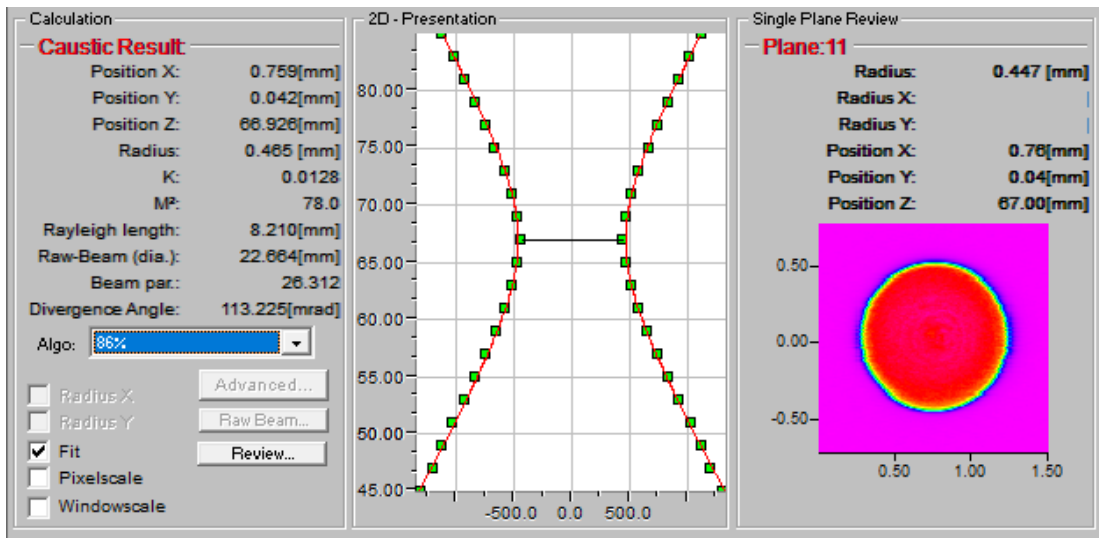
NU-04-FL200-FC125-FD600um-1500W (1334W on PM)



NU-05-FL200-FC125-FD600um-2000W (1792W on PM)



NU-06-FL200-FC125-FD600um-1200W (1075W on PM)



NU-07-FL200-FC125-FD600um-1800W (1610W on PM)

